Production of the Biodegradable Plastic PHB (Poly-3-hydroxybutyrate) using Recombinant *Escherichia coli* Bacteria.

by

Richard van Wegen

Department of Chemical Engineering
University of Adelaide

July 2000

Abstract

Disposal of plastic, in particular packaging, is a serious problem confronting many countries. Part of a solution lies in using biodegradable plastics such as poly-hydroxyalkanoates (PHAs), which can be produced by bacterial fermentation. Substantial developmental work is required to achieve economically-attractive PHA production.

The aim of this thesis is to improve the understanding of PHA production by recombinant *Escherichia coli*, with a view to guiding future developmental work. Such understanding is an important aid to achieving economic improvements.

This aim is achieved via the following methodology:

- Several experimental techniques are developed and tested. Quantitative, repeatable fermentation profiles are obtained for acetyl-CoA and 3-hydroxybutyryl-CoA concentration, and the production and consumption of major extracellular metabolites.
- An economic description of PHA production by *E. coli* is formulated, highlighting areas where significant cost reductions are possible and setting the direction for the remainder of the thesis.
- A quantitative analytical framework is developed for the cellular metabolism of XL1-Blue(pSYL107) during PHB production. Metabolic flux analysis techniques are used to quantify the major fluxes.
- The *in-vitro* kinetics of the PHB pathway are adapted for use with *in-vivo* fermentation data. Likely ranges of concentration are established for enzymes, cofactors, and intermediates of the PHA pathway. The sensitivity of PHB production rate to a variety of metabolic changes is established using metabolic control analysis.
- The effects of different oxygen-supply regimes and different nutrient feeding strategies are also examined and explained using the metabolic and kinetic models.

The models are used to explain the underlying factors influencing the progress of a typical PHB fermentation. The thesis also suggests numerous areas where further improvements to PHB production are possible, and proposes ways in which they could be implemented.

Acknowledgements

There have been many people who have helped me bring the saga to a satisfying conclusion and I am indebted to them all:

My supervisors: Dr Anton Middelberg, whose helpful advice, guidance, and eye for opportunities have been invaluable. Dr Connor Thomas, who gave me technical assistance with microbiology and helped me through a difficult crossroads when my project was foundering. Dr David Williams, who provided support in numerous miscellanous ways.

Chris Mansell who provided endless pun-full entertainment, stimulating conversation, useful advice and ideas about experiments and equipment, a sympathetic ear for my frustrations, and generally unlimited assistance. On my behalf he sacrificed many nights of sleep to help with marathon experiments, putting in ridiculous overtime far beyond the call of duty and even friendship. Without his help it would have been so much harder.

The guys in the workshop Jason Peake, Brian Mulcahy and Peter Kay, who were sources of much practical advice and were never too busy to make some gadget I needed for my experiments.

The secretaries Elaine Minerds, Mary Barrow and Lynette Kelly, always helpful despite my often-inconvenient requests.

Andrew Wright, for his ceaseless willingness to help solve my problems despite his own heavy workload.

Sanh Tran for his patience with my outlandish computer requests.

Jennifer Critchley for her efforts to improve the department and her willingness to be helpful.

Eric Dunlop, for his numerous long meetings and support during periods of PhD crisis.

Many lecturers in the department, and also Dr Brian Saunders (Chemistry Dept), Dr Grant Booker (Biochemistry Dept), Dr John Wallace (Biochemistry Dept), and Dr Alistair Anderson (Uni of Hull, England), who patiently answered my many questions and requests with no thought of gain for themselves.

Dr Sang Yup Lee at KAIST in Korea, who allowed me to utilise the strain of bacteria featured in most of my experiments.

Greg Zadow from the Dairy Research & Development Corporation for his help and advice.

The fellow sufferering students at the Microbiology department, who gave endless guidance with my microbiology problems: Rebecca Pinyon, Mark Webster, and especially Shuguang Zhang who also helped me enormously during my attempts at molecular biology.

Andrew Berry at the Department of Biotechnology, Flinders University, who spent numerous hours helping me use his experimental equipment, and provided invaluable technical guidance as well.

Many postgrads past and present at the Dept of Chemical Engineering, all good friends and many mentors as well.

My parents who have supported me in many ways throughout all these years of study.

My wife Cathy who provided endless help and support, and without whom I probably wouldn't have made it this far.

Thanks very much to you all, you have helped me beyond measure.

----> Richard

My work was made possible by the generous financial support of the Commonwealth Government APA scheme, the Dairy Research and Development Corporation, and the Frank Perry Scholarship.

Contents

Chapter 5 - Effects of Oxygen Supply

Chapter 6 - Effects of pH-stat Glucose Feeding

Chapter 7 - Conclusions

Declaration of Consent

I, Richard van Wegen, hereby certify that this work contains no material which has been accepted for the award of any other degree or diploma in any University or other tertiary institution. Furthermore, to the best of my belief and knowledge the thesis contains no material previously published or written by someone else, except where I have duly acknowledged him or her in the text.

I give my consent and enthusiastic encouragement to people wishing to borrow or photocopy this copy of my thesis from the University Library.

(Signed & Dated)

Chapter 1

1.1. Introduction

1.1.1. Why Biodegradable Plastics?

The Environmental Problem

In 1990, about 100 000 000 tons of plastic material were produced worldwide (Doi (1990b)). Plastics have considerable advantages relative to metals, woods, and glasses (Guillet (1995)). In particular they exhibit:

- far lower manufacturing costs;
- higher strength-to-weight ratio;
- far lower requirements for energy and water during production.

One of the major uses for plastic is for packaging, which is discarded after a short period of use. Unfortunately, typical commodity plastics degrade in the environment only at very slow rates. Poly-Ethylene-Terepthalate (PET), for example, has an expected lifespan of at least one hundred years. Items which find their way into natural watercourses and the ocean cause the death of millions of marine animals each year, by ingestion or entanglement (Environmental Protection Agency (1991)). Plastic also forms a large proportion of highly visible pollution, i.e. litter. On average beaches, the litter is around 66% by weight (90% by number) plastic (Environmental Protection Agency (1991)). This is presumably why two thirds of surveyed Americans believe that plastics are the single greatest threat to the environment, due to their non-biodegradability (Brandl *et al.* (1995)).

In the US, the Municipal Solid Waste (MSW) stream sent to landfill has composition as given by Table 1.1.

Table 1.1: Composition of Municipal Solid Waste sent to landfill in the US (Environmental Protection Agency (1991)).

	MSW (% by weight)	Further breakdown (% by weight)
BIODEGRADABLE		
Organic (food scraps, yard waste, etc)	11.8	20.0
Paper Products	47.3	80.0
	59.1	100.0
NON-BIODEGRADABLE		
Plastics	7.4	18.0
Rubber	0.6	1.5
Metal	9.3	22.6
Glass	3.8	9.2
Unidentified	15.0	36.4
Others	5.1	12.4
	41.2	100.0

Although plastic comprises only 8% by weight, this waste is recalcitrant, unlike (e.g.) garden waste which will compost and quite rapidly decrease in volume. Thus, it is more relevant to observe that plastic constitutes 18% of the non-degradable waste by weight. Furthermore,

plastic occupies more volume per weight than other types of waste: several studies have estimated the volume% as 2-3 times the weight% (Environmental Protection Agency (1991)). Hence plastic constitutes 35 - 55 % by volume of the non-degradable waste, and is therefore a major culprit in tying up large areas of land for long periods. In addition, some studies have shown that the biodegradation of materials wrapped in plastic bags is significantly impaired (Environmental Protection Agency (1991)), although other researchers report conflicting results. The plastic proportion of US MSW was predicted to reach 9.2% by 2000 (Environmental Protection Agency (1991)).

Landfilling is a large waste of valuable land, especially near major cities. In many states and countries, the available landfill space is almost exhausted. One way of addressing this problem has been to introduce recycling schemes. Recycling can work well for large items such as chairs, crates, and car parts. However recycling schemes pose a number of significant problems, especially for packaging. The plastic items must be sorted into the different polymer types, and then they must be transported back to a central depot. Both of these processes are expensive. Contamination by food and other chemicals, and degradation caused by the cleaning procedures used, results in severe reductions in polymer physical properties. Thus, the recycled plastic can only be used to make items for which inferior polymer is acceptable, and there are only a limited number of these (e.g. insulation, wheelie bins, plant stakes) In addition, many types of plastic are unable to be recycled. There are currently massive stockpiles of unwanted recycled plastic in many countries (Germany in particular), because there is simply insufficient demand for them. Recycling does make some useful contribution, but is not the final answer.

Part of A Solution

The problems mentioned above would be significantly less severe if plastics did not have such a long lifetime. A number of plastics exist which do degrade rapidly, generally classified into three main types:

- biodegradable plastics, which "mineralise" completely to carbon dioxide, salts, water and biomass;
- disintegrable plastics, which disintegrate into small fragments but do not degrade further;
- "others", which lie between these two extremes.

Biodegradable plastics would therefore be a significant improvement over conventional polymers for producing packaging. At the end of their useful life they could be composted and would not require landfill space. Any items which inadvertantly found their way into waterways or other natural environments would rapidly decompose and no longer pose a pollution problem.

Biodegradable polymers would not be suitable for making most other items (such as car components and garden chairs) (Scott and Gilead (1995)). However these larger goods could easily be recycled due to reduced contamination and ease of sorting. This strategy is already being followed by many car manufacturers, who are labelling plastic components according to polymer type.

1.1.2. Types of Biodegradable Plastic

There are a wide variety of polymers which rapidly biodegrade (Karlsson and Albertsson (1995)). Some of the most important types are:

- polyhydroxyalkanoates (Page (1995));
- starch and starch blends (Maddever (1992); Bastioli (1995); Soest and Vliegenthart (1997));
- cellulose acetate and blends (Mayer *et al.* (1995));
- polycaprolactone (Bastioli *et al.* (1995));
- polylactate (Vert *et al.* (1995));
- chitin and chitosan (Peter (1995));
- poly(ethylene-carbon monoxide) (Harlan and Kmiec (1995)).

The two types that show greatest promise are polylactate and polyhydroxyalkanoates:

- Polylactate production is about to achieve commercial productions levels, with Cargill currently manufacturing a 140 000 ton-per-annum plant in the US. A similar size plant is to be constructed in Europe in the near future.
- Polyhydroxyalkanoates (PHAs) also have significant potential because they possess a number of desirable properties that many other biodegradable polymers lack. The most promising type of PHA is poly(hydroxybutyrate-co-hydroxyvalerate): it is strong, tough, transparent with good clarity and has very low gas permeability (Holmes (1988)). Unlike many other types of biodegradable polymer, it also possesses excellent moisture resistance. It decomposes quite rapidly in nearly all natural environments but doesn't degrade in air regardless of the humidity (Brandl *et al.* (1995); Cox (1993)). These properties make it highly suitable as a packaging material. However as described in Section 1.2.3, commercialisation efforts to date have not succeeded in achieving economically viable production.

1.1.3. Polyhydroxyalkanoates

Poly-hydroxyalkanoate (PHA) is the name given to types of polyester with the following general structure:

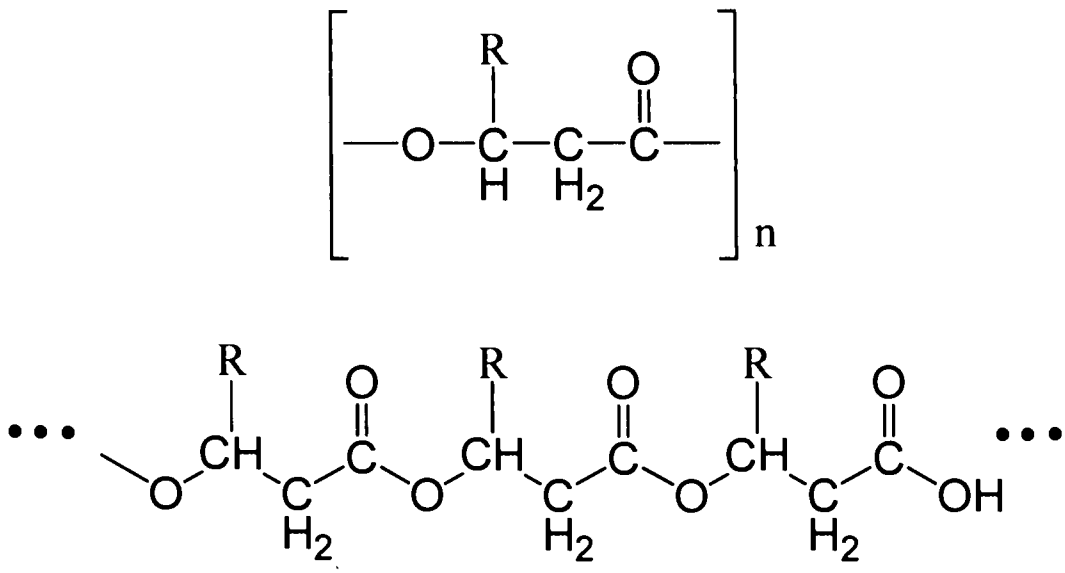

Figure 1.1: Generic molecular structure of polyhydroxyalkanoates (PHA).

In naturally occurring PHAs, the R group is a straight-chain alkane containing between 0 and 11 carbons. PHAs are stereospecific, with all monomers in the D(-) configuration. By far the most common type of PHA is polyhydroxybutyrate (PHB) with the structure shown in Figure 1.2.

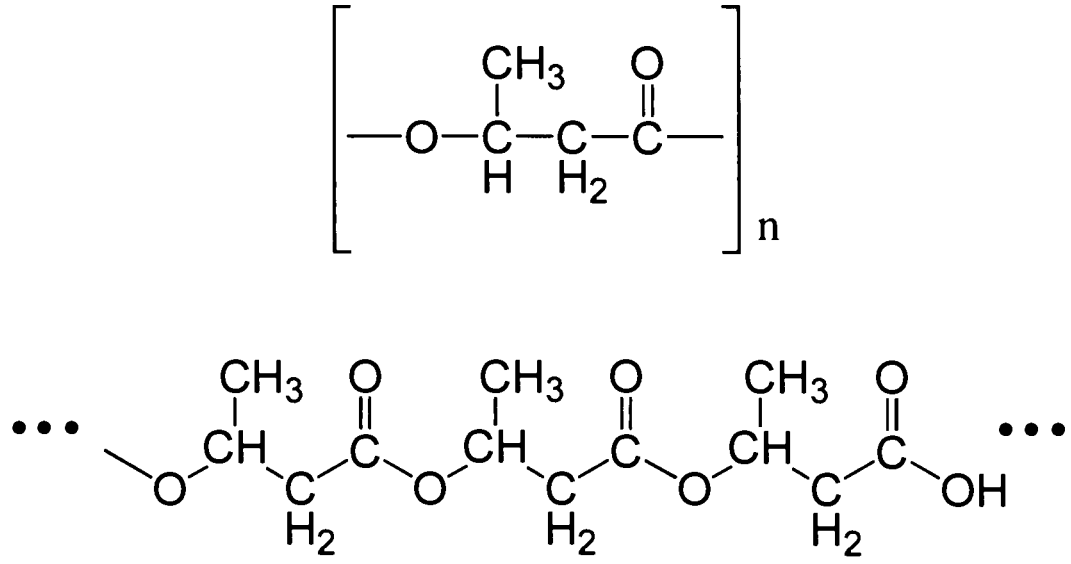

Figure 1.2: Molecular structure of polyhydroxybutyrate (PHB).

Pure PHB is completely crystalline, and as a result has good strength. Unfortunately, its toughness is poor (Barham (1990)). In addition, it exhibits severe aging (i.e. marked deterioration in properties with time) over a period of only several days (de Koning (1995)). When freshly moulded, PHB typically has a tensile strength of 80 MPa, and will strain by 60% before failure. After only three or four days at ambient temperature, the tensile strength drops to around 10 MPa and the specimen fails after a mere 2% extension. This brittle behaviour is due to the formation of many small cracks which join up under stress, causing premature failure. Annealing procedures can partially overcome aging, but not entirely (de Koning (1995)). A further problem with PHB is its low degradation temperature. Pure PHB melts at 177 °C, and decomposes rapidly at only 200 °C. This limits its usefulness for moulding applications. For these reasons (among others) considerable interest has been generated in a different type of PHA, poly(3-hydroxybutyrate-co-3-hydroxyvalerate), which is a random copolymer with molecular structure as shown in Figure 1.3.

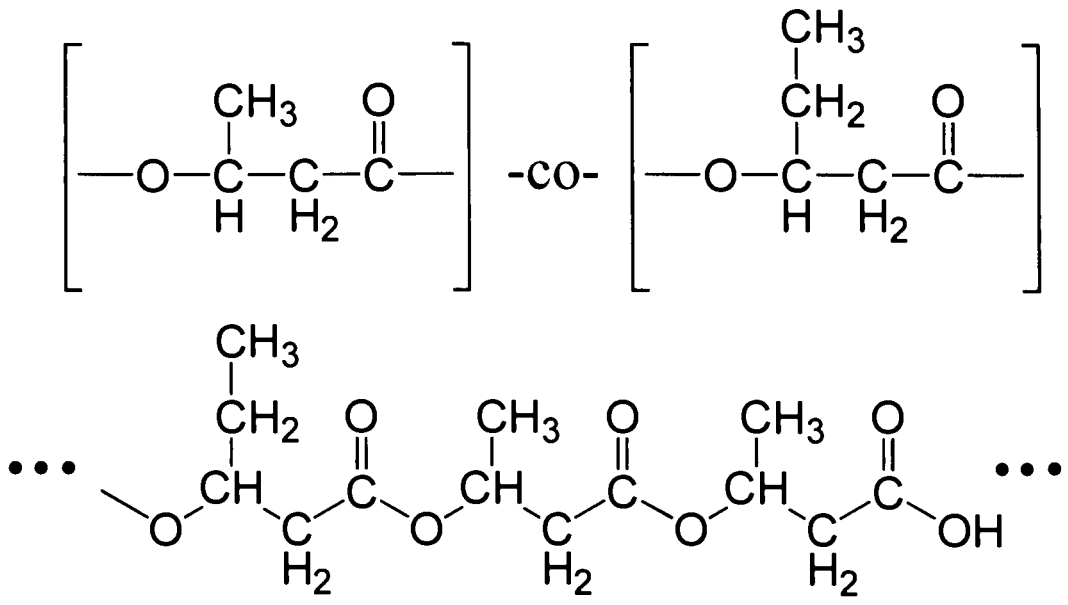

Figure 1.3: Molecular structure of poly(hydroxybutyrate-co-hydroxyvalerate) (PHBV). The momomers are arranged in random order.

The presence of the valerate units lowers the crystallinity of the polymer and improves its properties significantly: ductility and toughness are improved, and the aging phenomenon is eliminated (Barham *et al.* (1992)). Furthermore, the melting temperature of the polymer is reduced but the degradation temperature is unaffected. This allows the polymer to be injection- and blow-moulded. The slower crystallisation rate of P(HB/HV) means longer residence times are required, although they can be reduced by adding nucleating agents (de Koning (1995)). The mechanical properties of P(HB/HV) are comparable to conventional polymers, lying between polyethylene and polyethylene terepthalate.

Table 1.2: Comparison of PHA properties with those of conventional commodity plastics (Byrom (1994); Doi (1990b)).

	Melting Point °C	Tensile Strength MPa	Flexural Modulus GPa	Extension to break %	Notched Izod J/m	Water uptake wt%
PHB	177	40	3.5	3	35	0.2
P(HB / 10%HV)	150	25	1.2	20	100	
P(HB / 20%HV)	135	20	0.8	100	300	
Polypropylene	170	35	1.7	400	45	0.0
Polyethylene-terepthalate	262	56	2.2	7300	3400	0.4
High density polyethylene	135	29	0.9	-	32	
Polystyrene	110	50	3.1	-	21	

Table 1.3: Mechanical and gas barrier properties of biaxially drawn polymer films (Doi (1990b)).

	Draw Ratio	Flexural Modulus (GPa)	Stress at break (MPa)	Extension to break (%)	Oxygen Permeability ($cm^3 m^{-2}$ $atom^{-1} day^{-1}$)
PHB	4x4	4.0	100	75	45
P(HB / 17%HV)	5x5	1.9	54	50	60
Polyethylene terepthalalate	4x4	4.4	200	120	70
Polypropylene	7x7	2.0	160	140	1700
Low density polyethylene		0.3	10	700	7000

Table 1.4: Typical properties of commercially available BIOPOL resins (Byrom (1994)).

	Melting Point °C	Young's Modulus GPa	Tensile Strength MPa	Flexural Modulus GPa	Extension to break %	Notched Izod $J.m^{-1}$
low HV copolymer	162	1.0	31	2.7	8	60
plasticised low HV copolymer	151	0.8	28	1.8	16	161
medium HV copolymer	153	0.9	28	2.0	15	98
plasticised medium HV copolymer	144	0.7	25	1.0	20	198
high HV copolymer	144	0.5	23	1.4	35	200
plasticised high HV copolymer	136	0.4	20	0.8	42	360

Table 1.5: Thermal and mechanical properties of P(3HB-co-3HV) copolymers (Doi (1990b)).

Composition (mol %HV)	Melting Temperature (°C)	Young's Modulus (GPa)	Tensile Strength (MPa)	Notched Izod Impact Strength ($J.m^{-1}$)
0	179	3.5	40	50
3	170	2.9	38	60
9	162	1.9	37	95
14	150	1.5	35	120
20	145	1.2	32	200
25	137	0.7	30	400

Table 1.6: Mechanical properties at 23 °C for solution-cast films of P(3HB) with different stereoregularities (Abe *et al.* (1994)).

isotactic diad fraction	Young's Modulus (Gpa)	Tensile Strength (MPa)	Extension to break (%)
1.00 (isotactic)	1560	38	5
0.84	1190	15	7
0.76	310	11	10
0.68	90	11	740
0.30	20	13	1020

The crystallinity and hence mechanical properties of pure PHB can also be modified by altering its stereoregularity (Abe *et al.* (1995)), however this has implications for its biodegradability. Longer chain PHAs are generally not useful for packaging applications because they are elastomeric, amorphous and somewhat sticky. However they may be more suitable for latex products such as coatings (de Koning *et al.* (1997)).

1.1.4. Biodegradation of PHA

A number of microorganisms have evolved the ability to excrete enzymes which depolymerise extracellular PHB (and hence PHA) and allow its utilisation as a growth substrate. In particular, many fungi (such as *Aspergillus fumigatus*, *Paecilomyces marquandii*, *Acremonium sp.*) appear to play a major role in environmental PHA degradation. Among the other microorganisms that have demonstrated the ability to grow on PHB as a sole carbon source are actinomycetes (*Streptomyces*), and various gram-positive and gram-negative bacteria such as *Bacillus megaterium*, *Varivorax sp.*, *Arthrobacter viscosus* and *Acidovorax sp.* (Byrom (1994)).

The rate of biodegradation of PHAs depends on a number of factors (Holmes (1988)), including:

- polymer composition, molecular weight, percentage crystallinity and stereoregularity;
- the use of plasticisers (addition of degradable plasticiser increases the surface area of the degrading polymer, and hence increases biodegradation rate) (Cox (1993));
- thickness and surface area of the item (e.g. bottles vs film);
- environmental conditions, in particular:
  - pH;
  - temperature (higher temperature causes more rapid degradation);
  - oxygen concentration (anaerobic conditions accelerate degradation);
  - ionic strength;
  - the microbial flora present.

Table 1.7: Time for substantially complete biodegradation of PHB (weeks) (Holmes (1988)).

	film (75 μm)	moulding (1 mm)
anaerobic sewage	1	6
well-watered soil (25 °C)	12	75
estuarine sediment (25 °C)	8	40
bovine rumen (cow stomach)		25

Table 1.8: In-situ biodegradation of PHA, weight loss after half a year (Mergaert *et al.* (1995)).

	PHB	P(HB-10%HV)	P(HB-20%HV)
freshwater pond	4-7%	4-7%	4-7%
freshwater canal	17%	38%	80%
seawater	25%	35%	30%

Table 1.9: Percentage biodegradation of PHA film after 14 days (Cox (1993)).

	PHB	P(HB/18%HV)
anaerobic sewage	36%	100%

PHB and P(HB/HV) will degrade essentially under all conditions in a microbially active environment. This is in contrast to many other 'biodegradable' plastics which require exposure to sunlight or particular environments. Under ideal conditions, thin films of PHA (70 μm) degrade in as little as a week and 1 mm bottles in six weeks. In simulated landfill, 60% weight loss occurred over 50 weeks. Turned stack composting produced 80% weight loss in 15 weeks (Byrom (1994)). Even in extremely unfavourable environments degradation still occurs, albeit slowly (lifetime extrapolated to 10 years for a shampoo bottle at a depth of 80 m in a freshwater lake) (Brand and Puchner (1990)).

There is some conflict as to whether P(HB/HV) degrades more rapidly than PHB or not. Experiments in soils indicated more rapid degradation of P(HB/HV) than PHB (Byrom (1994)), and similarly in water (Mergaert *et al.* (1995); Cox (1993); Mergaert *et al.* (1992)). However it was reported in another study that P(HB-71%HV) degraded six times more slowly than PHB at 37 °C pH 7.5 (Doi (1990a)). A copolymer of 3-hydroxybutyrate and 4-hydroxybutyrate showed the most rapid degradation rate of all, far faster than either PHB or P(HB/HV) (Doi *et al.* (1989)).

The PHB stereoregularity and degree of crystallinity are interdependent, but have opposite effects on the biodegradation rate of the polymer (Abe *et al.* (1994); Abe *et al.* (1995); Hocking *et al.* (1995); Shimamura *et al.* (1994b); Doi *et al.* (1993)):

- When the level of crystallinity is reduced, the biodegradation rate increases: the rate is 20 times faster on amorphous PHB than on crystalline PHB (Shimamura *et al.* (1994a));
- As the S monomer content increases, the biodegradation rate decreases. Isotactic (S)PHB does not appear to biodegrade.

However, since decreasing the stereoregularity causes a reduction in crystallinity, the two effects offset one another to a certain extent, such that atactic racemic PHB shows a higher degradation rate than isotactic (R) PHB.

An important point to note is that the degradation of isotactic (R) PHB forms a mixture of monomeric and dimeric units. However, degradation of racemic PHB additionally produces trimers and tetramers. This is because most PHA depolymerases are unable to hydrolyse bonds to (S) monomeric units.

In general, as the molecular weight of the polymer increases, its speed of biodegradation decreases (Hiramitsu and Doi (1993)).

1.1.5. Potential Uses for PHB and PHBV

The main uses for PHB and PHBV will be based on its biodegradability and biocompatibility (i.e. it is non-toxic and non-antigenic). Some applications which have been seriously proposed are: (Brandl *et al.* (1995))

- single-use disposable items and packaging (film wrap, bottles, plastic lined milk cartons). Currently, PHBV (tradename BIOPOL) is used to make (among other things) disposable razors and food trays in Japan and shampoo bottles in Germany, Japan and the USA;
- biomedical products, for example implants, wound care products, and slow release pharmaceuticals (Yagmurlu *et al.* (1999));
- slow release agricultural pellets, e.g. fertilisers, plant growth hormones, pesticides;
- supporting matrices for de-nitrifying bacteria in sewage treatment plants;
- optically active substrate for chiral drug synthesis;
- biodegradable reinforced composites, when used with cellulosic fibres. A bike helmet produced from such material retained its mechanical properties indefinately in normal outdoor environments, yet completely biodegraded within 40 days when buried in soil;
- credit cards, phonecards and similar items (Editor (1998)).

It was proposed to use PHA for fishing nets, which are a major hazard to marine life once they are discarded. Unfortunately, PHA rapidly loses its tensile strength once biodegradation starts, due to surface degradation of the polymer. This makes such an application unlikely.

The number and range of applications to which PHAs will be put depends on how far their cost can be reduced. Unless the price per kg is brought down to a level comparable with petroleum based plastics, only the more exotic low-volume applications are likely to be viable.

1.2. Occurrence and Production of PHAs

A number of reviews on PHA production have been published (Poirier *et al.* (1995); Anderson and Dawes (1990); Steinbuchel and Valentin (1995); Byrom (1987); Steinbuchel and Schlegel (1991); Brandl *et al.* (1995); van der Leij and Witholt (1995); Dawes (1990); Doi (1990b); Lee (1996d); Jendrossek *et al.* (1996)).

1.2.1. Natural Occurrence

A wide variety of bacteria accumulate PHA intracellularly as inclusion bodies, especially members of the classes *Alcaligenes*, *Methylobacterium*, *Pseudomonas*, *Rhodospirillum*, *Rhodococcus*, *Azotobacter*. (See Steinbuchel (1991) for a more comprehensive list). PHB inclusion bodies were first observed in bacteria by Lemoigne in 1925 (Dawes (1990); Fuller (1990)). Research in the 1960s (by Dawes, Doudoroff & Schlegel in particular) elucidated the metabolic pathways involved in PHB synthesis and the mechanisms of regulation (Dawes and Senior (1973); Oeding and Schlegel (1973)). PHB is the most common naturally-occurring type of PHA. Typically between 8 and 12 granules are present per cell (Dawes (1990)), and they grow in size as the polymer level increases. In some cases the polymer has been observed at levels greater than 90% of dry cell weight (Lee *et al.* (1994c)), causing gross distortion of cell shape.

PHB and P(HB/HV) are normally crystalline, however a considerable body of evidence exists to suggest that they are present intracellularly in amorphous form (Bonthrone *et al.* (1992)), and do not crystallise until subjected to purification procedures (solvents, heating, or water removal). Several postulates have been proposed to explain this:

- the polymer is plasticised by water or a lipid;
- the polymer is present in an enolic rather than a ketonic state;
- the crystallisation rate of pure, un-nucleated PHB is extremely slow. (The argument is that once the polymer is extracted from the cells, small foreign particles contaminate the granules and act as nucleants, causing rapid crystallisation). This third explanation has been given the most support (de Koning (1995)).

Several studies have shown that in native producers (e.g. *Pseudomonas oleovorans*) inclusion bodies of PHB are enclosed in organised structures called phasins. This structure consists of a highly ordered, double protein array with associated phospholipids (Stuart *et al.* (1995); Mayer *et al.* (1996)). It has been shown that in recombinant *E. coli*, many proteins bind to the granule surface via both specific and non-specific interactions (Steinbuchel *et al.* (1995)) Other studies (Horowitz and Sanders (1995)) confirm that granules are about 98% PHB with small amounts of protein and lipid. In the presence of these surfactants, the nucleation rate of the amorphous polymer is extremely low. Once the surfactants are removed however, granules in solution aggregate and the polymer crystallises rapidly.

The fact that microbial synthesis of PHA is widespread indicates the survival advantage conferred upon those bacteria able to accumulate it. In the 1950s, Macrae and Wilkinson demonstrated that nitrogen limitation affected the level of PHB accumulation (Macrae and Wilkinson (1958)). The main function of high molecular weight bacterial PHB appears to be carbon and energy storage. During balanced growth, only low levels of PHB accumulate in the cell. However, under conditions where growth is limited by some nutrient (e.g. nitrogen, oxygen, phosphorus, or magnesium) whilst carbon is in plentiful supply, PHB is synthesised in large amounts. Once the (non-carbon) nutrient limitation is alleviated, the granules of PHB are re-metabolised and used to support growth. As demonstrated in a series of experiments

(Dawes and Senior (1973)), this gives an advantage over cells which must rely on other carbon sources. The advantage to the cell of storing carbon as a polymer rather than as small molecules is that PHA has negligible effect on the cell's osmotic potential.

In the sixties and seventies it was discovered that PHB is not the only type of PHA accumulated by bacteria (Davis (1964); Wallen and Rohwedder (1974)). In some organisms (e.g. *Pseudomonas oleovorans*), the PHB synthesis pathway is extremely versatile. By altering the feed substrates, a wide variety of monomers with different side groups can be incorporated into the polymer chain, including linear and branched chains, and functional groups (Steinbuchel and Valentin (1995); Steinbuchel (1991); Anderson *et al.* (1990)). In general however, the levels of polymer accumulation are low for all except the smallest side groups. As the side group chain length increases, PHA becomes too soft and thermoplastic to be of much practical application. Furthermore, as the bulkiness of the side group increases the polymer molecular weight decreases, and the biodegradability of the plastic is also impaired. In many cases, two phase reactors are required and the substrate is quite expensive. Despite these drawbacks, it is possible that some niche markets will become apparent for the more unusual PHAs and justify the cost of their production. Perhaps the three most promising areas are:

1. the production of Poly(3-hydroxybutyrate- co- 3-hydroxypropionate) or Poly(3-hydroxybutyrate- co- 4-hydroxybutyrate). Both these polymers exhibit significantly increased biodegradation rate, presumably due to reduced crystallinity and because PHA synthase has easier access to the ester sites (Shimamura *et al.* (1994a));
2. the production of PHA with unsaturated side chains. Such PHAs can be crosslinked to form rubber, without destroying their biodegradability (de Koning (1995); Dekoning *et al.* (1994));
3. use of long-chain PHAs for latex-based coatings (de Koning *et al.* (1997)).

In the future it may be possible to improve production of novel PHAs by engineering metabolic pathways or using site-directed mutagenesis for the production of new enzymes.

1.2.2. PHA Enzymes

PHA production in *R. eutropha* is achieved by three gene products (see Figure 1.4),

- phaA, substrate-specific 3-ketothiolase (β-ketothiolase);
- phaB, NADPH-linked 3-ketoacyl reductase (acetoacetyl-CoA reductase);
- phaC, PHA synthase.

The genes are all situated on a single operon in the order phbC, phbA, phbB (Janes *et al.* (1990); Steinbuchel and Schlegel (1991)) The total operon is 5.2 kb long (Lee *et al.* (1994c)), with a 307 bp leader sequence before the first gene.

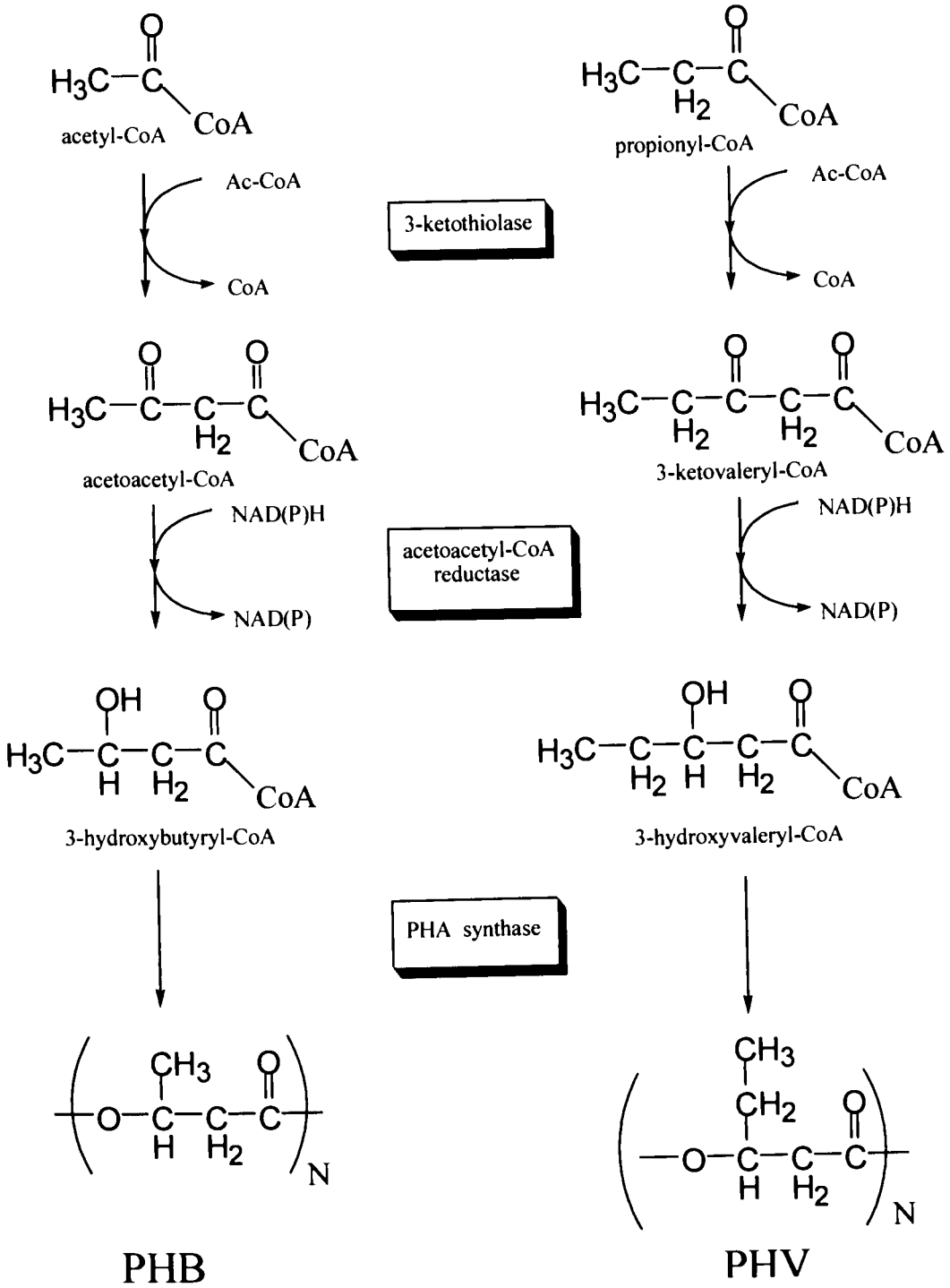

Figure 1.4: Enzymatic pathway to PHB and PHV.

- Two distinct types of 3-ketothiolase have been isolated from different organisms (Slater *et al.* (1998)). The first is relatively substrate specific, and will only produce four- and five-carbon 3-ketoacyl-CoAs. The other will produce 3-ketoacyl-CoAs with a carbon chain length between four and ten. In some organisms, 3-ketothiolase is also used for fatty acid degradation (Mansfield *et al.* (1995)).
- There are two main types of reductase: NADH linked and NADPH linked (Haywood *et al.* (1988)):
  - The NADPH linked acetoacetyl reductase is the more important in PHB synthesis. It acts to form a D(-) product. The substrate must have a carbon chain length of between four and six;
  - The NADH linked reductase has been found to be non-essential for PHB synthesis: its primary function appears to be fatty acid degradation (Mansfield *et al.* (1995)). It generates an L(+) product from substrates with carbon chain length up to ten. Because PHA synthase will only act on D(-) substrates, this forward path does not appear useful for PHB production. However, when supplied with an L(+) hydroxyacyl-CoA, the reaction proceeds in reverse to form acetoacetyl-CoA. The acetoacetyl-CoA could then be used by the NADPH-linked reductase to form the D(-) 3-hydroxyacyl-CoA substrate for PHB synthase. Conceivably, the NADH-linked enzyme may thus allow usage of L(+)-3-hydroxyacyl-CoA from fatty acid metabolism (β oxidation) for PHB production (Eggink *et al.* (1992)).
- A variety of PHA synthases have been discovered but the predominant one is D(-) specific and only accepts four- and five- carbon substrates (Haywood *et al.* (1989)). Unlike the other two enzymes, several forms of PHB synthase have been discovered which are functionally equivalent but differ somewhat in their genetic sequence. In *Ralstonia eutropha* there is only one synthase. The enzyme is present in a soluble form while no PHB synthesis is occurring, however once PHB production commences the enzyme binds to the growing PHB granules. Some work suggests that PHA synthase may be unstable in the absence of substrate (Peoples and Sinskey (1989a); Kidwell *et al.* (1995)).

1.2.3. Industrial Production

In 1976, in response to expected oil prices of greater than $100 a barrel, Zeneca (a subsidiary of ICI) began to conduct research into the production of plastic from non-petrochemical sources: such a plastic would be relatively immune to the envisaged oil price fluctuations. Contrary to predictions however, the price of oil dropped dramatically, and thus PHA's biodegradability became the focus of research effort instead.

Zeneca commenced industrial production of PHBV in 1990, marketed under the tradename BIOPOL. In 1996 the rights for the process were transferred to Monsanto. The bacteria used are a mutant strain, *Ralstonia eutropha* H16 (formerly *Alcaligenes eutrophus* and before that *Hydrogenomonas eutropha*), able to utilise glucose as a growth substrate. When propionic acid is fed to the cells, a random copolymer of hydroxybutyrate and hydroxyvalerate is produced. A typical production run consists of several stages (Byrom (1992); Byrom (1990)):

1. Inoculation: at this point, the minimal medium consists of glucose, an amount of phosphate calculated to produce a desired dry cell weight, and an excess of other nutrients;
2. Cell growth: over 40-60 hours, the cells are grown to a high density with glucose feeding, and no PHB accumulation occurs;
3. Polymer production: once phosphate limitation occurs, cell growth stops and polymer accumulation commences. During the stationary phase, propionic acid (the precursor for

the HV monomer) is fed in addition to glucose. The ratio of propionic acid to glucose is controlled according to the desired level of HV in the polymer;

4. Harvest: after a further 60 hours, fermentation is stopped and the cells are harvested by heat shock and flocculation. The plastic is recovered from the cells by a series of enzyme and hydroxide washes, then formed into chips for commercial use;

Fermenter capacity is up to 220 kl. Total dry cell weight is consistently in excess of 100 $g.l^{-1}$, of which typically 70% -80% is polymer. The PHBV yield on glucose is approximately 0.3 grams of PHA per gram of glucose. The level of HV is generally between 5% and 30%: HV content greater than this cannot be achieved because propionic acid is toxic to the cells. (Propionic acid is used commercially to inhibit mould growth (Lewis and Yang (1992)), and inhibits the growth of *A. eutrophus* at concentrations as low as 0.1 % w/w) (Kim *et al.* (1994)). Culture stability is excellent, because PHA production only occurs during the stationary phase and hence there is no selection pressure during the growth phase.

R. eutropha was chosen from among a number of other PHB-producing bacteria for several reasons:

- the polymer produced has high molecular weight, which is necessary for good physical properties;
- extraction of the granules is comparatively easy;
- no polysaccharide (e.g. glycogen) granules are produced, thus PHA production is more efficient and recovery is simplified.

With the original production strain, the efficiency of propionate utilisation was low (30%). Instead of being incorporated as HV monomers, most of the propionate was metabolised to acetate and then either converted to HB or catabolised for energy. Since propionic acid is more than three times as expensive than glucose, Zeneca developed an auxotrophic mutant that lacked the ability to convert propionate to acetate. Using this improved strain, the propionate efficiency rose to around 80%, significantly reducing substrate costs. In 1995 Zeneca's maximum production capacity was between 500-1000 tonnes per year (Page (1995)). The 1995 potential market for PHA was estimated at around 1.5 million tonnes per year (Page (1995)).

Unfortunately the price of BIOPOL is very high, around $15/kg (US 1995) (Poirier *et al.* (1995)). At a production rate of 10000 t/yr, economy of scale could (optimistically) lower this to $5/kg. However, this obviously cannot compete with commodity plastics produced from petroleum, which are typically less than $1/kg.

1.2.4. Production in Recombinant *Escherichia coli*

Wild type *E. coli* possesses chromosomal PHB synthesis genes, however these are only expressed under special conditions e.g. during the development of competence (Lee *et al.* (1994c)). Hence, various plasmids have been created to allow expression of pha genes in *E. coli*. The earliest such plasmids (derived from *R. eutropha*) were produced by three groups acting independently (Schubert *et al.* (1988); Slater *et al.* (1988); Peoples and Sinskey (1989b)). Following from this, a more effective plasmid with a higher copy number (designated p4A) was created by deleting 400 basepairs of non-essential information (Janes *et al.* (1990)). Many other derivative plasmids have been constructed by adding various useful genes, the most important of which are:

- parB(hok-sok) locus. One of the earliest problems encountered with PHB production in recombinant *E. coli* was plasmid segregative instability. Because *E. coli* produce PHB during growth, unlike *R. eutropha* they are subject to strong selection pressure against PHB

production. The parB locus employs a post-segregational killing mechanism that lyses cells which have lost the plasmid (Gerdes (1988)). Plasmids containing the locus are stable for at least 120 generations (Lee *et al.* (1994c); Lee and Chang (1995));

- High copy-number replicons. It has been shown repeatedly that a high copy number (100-500) is essential for good PHB production (Lee and Chang (1995); Lee *et al.* (1995b));
- Inducible promoters. Many plasmids use the native *R. eutropha* promoter, which works well in *E. coli* (Lee *et al.* (1994d)). The operon is well expressed, because of its good transcriptional homology with *E. coli* genes (Slater *et al.* (1988)). Also, the promoter closely matches the native *E. coli* σ_{70} consensus sequence. However the native promoter leads to constitutive expression of the pha genes, which slows growth, increases selection pressure, and broadens the distribution of polymer age (and hence material properties). Inducible promoters have been used, with varying success (Kidwell *et al.* (1995));
- ftsZ, a protein involved in septum formation. A phenomenon observed in many PHB-producing *E. coli* is severe filamentation, particularly in defined media. This is presumably caused by a heat shock response to the over-expression of PHA enzymes (Lee *et al.* (1994d)). Overexpression of ftsZ overcomes this problem (Lee (1994)).

The pha genes from numerous other bacteria have also been cloned into *E. coli* (Zhang (2000)). Of particular interest is the *Alcaligenes latus* operon, which appears to be better at PHBV production than the *R. eutropha* operon (Choi *et al.* (1998); Choi and Lee (1999)).

PHB has been shown to accumulate to extremely high levels in *E. coli* (80-90%), at which point the cell shape is severely distorted by polymer granules (see Figure 1.5). Cells which have accumulated PHB to a high level cannot form colonies (Lee *et al.* (1994a)), and after extented culturing periods they tend to lyse spontaneously (Lee *et al.* (1994d)). As previously mentioned, severe filamentation often occurs.

Figure 1.5: Transmission electron micrograph of *E. coli* containing high levels of PHB (Lee *et al.* (1994d)). Cell is approximately 1 μm wide by 4 μm long.

E. coli has a number of advantages over other bacteria for the production of PHAs (Lee *et al.* (1994c); Lee and Chang (1995)):

- rapid growth, on simple media;
- ease of recovery (cells with high PHA levels are rather fragile);
- lack of depolymerase activity, hence intracellular polymer degradation is negligible and the polymer is of higher molecular weight;
- availability of many useful plasmids & mutants;
- well established high-cell-density culture techniques;
- high levels of PHA accumulation.

Many factors significantly affect the level of PHB production by recombinant *E. coli*:

- plasmid type and copy number (Lee *et al.* (1994c); Lee and Chang (1995));
- strain. Several studies have examined PHB production in different strains of *E. coli*, ranging from cloning strains such as XL1-Blue to protein-overproduction strains like Topp1 (Lee *et al.* (1995b); Lee *et al.* (1994d); Lee and Chang (1995); Ling *et al.* (1997));
- growth medium, especially complex vs minimal media. In general, complex media give higher PHB levels although this is not always the case (Lee *et al.* (1995b); Lee and Chang (1995); Lee and Chang (1994); Kalousek and Lubitz (1995); Dennis (1991); Yim *et al.* (1995)). Defined supplements such as amino acids also increase PHB yield, the most effective being:
  - the amino acids cysteine, isoleucine, methionine and proline;
  - oleic acid.
- The amino acids above require more NADPH for their synthesis than the others. Thus, if the need to synthesise them is removed, more NADPH is available for use by acetoacetyl-reductase, the second enzyme in the PHA synthesis pathway. Similarly, oleic acid can both provide extra acetyl-CoA for PHB production and reduce NADPH cost for fatty acid synthesis (Lee *et al.* (1995b));
- feeding method. In general, fed batch methods with pH-stat feeding of glucose give the best yields of PHB (Kim *et al.* (1992); Cutayar and Poillon (1989));
- bioreactor type. Large differences in PHB yield are often observed when comparing fermenters with shake flasks (Lee and Chang (1994));
- other fermentation conditions such level of dissolved oxygen. The effects of oxygen limitation are not clear, but both excess and insufficient oxygen supply lead to reduced PHB yield (Wang and Lee (1997)).

1.2.5. PHBV Production in *E. coli*

Unlike *R. eutropha*, most strains of *E. coli* will not make PHBV from propionate. In order to use medium-supplied propionate, the cells must first transport it into the cell, then activate it to propionyl-CoA. These processes could conceivably occur in a number of ways:

Transport into the cells may occur via:

- passive diffusion. Acetate and other short-chain-fatty-acids (SCFAs) will freely cross the outer membrane via porins or by diffusion, then diffuse across the inner cell membrane (Clark and Cronan (1996); Diez-Gonzalez and Russell (1997));
- atoAD, part of the ATO operon for SCFA utilisation (atoA, atoB, atoC, atoD, atoE, atoS). It has highest activity for acetoacetate and butyrate. Expression of atoC is induced by acetoacetate, which in turn induces production of the other four ATO genes;
- atoE, an open reading frame in the ATO operon. Its putative function is to transport SCFAs across the inner membrane (Clark and Cronan (1996)).

Once in the cytoplasm, propionate may be converted to propionyl-CoA by:

- ack-Pta (Rhie and Dennis (1995a); Brown *et al.* (1977)). The enzymes (acetate kinase(2.7.2.1) and phosphotransacetylase(2.3.1.8)) are constitutively expressed, and are used by *E. coli* to grow on acetate and propionate. Their levels vary little with substrate or aerobic vs anaerobic conditions. They don't exhibit acetate induction or glucose repression (Clark and Cronan (1996)). Overexpression of ackA increases both the level of PHBV accumulated and its HV content;

- acs, an inducible acetyl-CoA synthetase (6.2.1.1). This enzyme has been poorly studied, but is known to be active on propionate and to be repressed by glucose (Clark and Cronan (1996)).

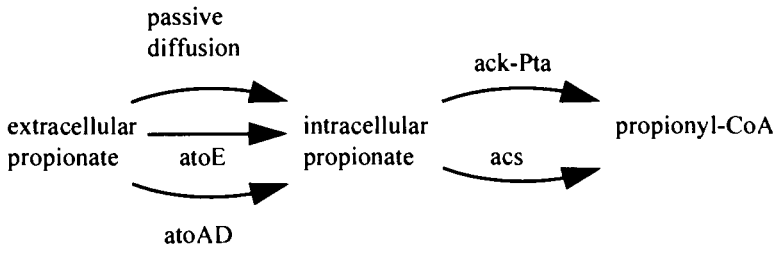

Figure 1.6: Possible pathways for production of propionyl-CoA from extracellular propionate during PHBV production by recombinant *E. coli*.

Successful PHBV production has been achieved in *E. coli* in two ways, as described in the following sections.

fadR atoC mutants

PHBV has been produced from propionate in *E. coli* strains which contain the fadR atoC(con) mutations (Rhie and Dennis (1995b); Slater *et al.* (1992)). The proposed mechanisms of action are (DiRusso and Nunn (1985); Nunn (1986)):

- the fadR mutation (fatty acid degradation repressor) causes constitutive expression of the fadAB ketothiolase, which supplements the activity of phaA (i.e. 3-ketothiolase) See Table 1.10;
- the atoC(con) mutation gives constitutive expression of the atoAD gene product. atoAD purportedly acts to increase the transport rate of propionate across the cell membrane by a factor of 10. However it should be noted that the uptake rate was measured by assuming negligible passive diffusion of propionate, which may not be justified. If passive diffusion was appreciable, then the measured difference in propionate uptake must instead reflect different rates of conversion to other compounds, e.g. propionyl-CoA. The ATO operon also codes for the atoB enzyme (3-ketoacyl-CoA thiolase II) which has its highest specificity for short chain 3-ketoacyl-CoA compounds (C4, C5).

The atoC(con) mutation alone results in slow P(HB/HV) production and growth, possibly because the intracellular propionate concentration reaches toxic levels. When combined with fadR however, the two mutations have a synergistic effect (Rhie and Dennis (1995b)). It is not clear whether catabolite repression by glucose affects the action of the fadR atoC(con) mutations.

Table 1.10: Relative activities of the *Ralstonia eutropha* PHA synthesis enzymes with substrates of different chain length and stereochemistry (Haywood *et al.* (1988); Steinbuchel and Schlegel (1991); Doi (1990b)).

Chain length and stereoisomer of substrate	3-ketothiolase A	3-ketothiolase B	NADPH linked acetoacetyl reductase	NADH linked acetoacetyl reductase	PHA synthase
D(-) C_4	100	100	100	9.7	100
D(-) C_5	3	30	48*	31	7.5
D(-) C_6	0	17	3.6	17	0
D(-) C_7	0	19	0	14	0
L(+) C_4	-		0	100	0
L(+) C_5	-		0	35	0
L(+) C_6	-		0	50	0
L(+) C_7	-		0	99	0
Metabolic Function	PHB synthesis	fatty acid catabolism	PHB synthesis	fatty acid catabolism	PHB synthesis

* Steinbuchel and Schlegel (1991) lists 18 but is a misprint, Doi (1990b) and Haywood *et al.* (1988) list 48

Addition of 1 $g.l^{-1}$ oleate (cis-9-octadecanoic acid) during PHBV production caused a threefold increase in HV mol% (Yim *et al.* (1995)), suggesting that either:

- oleate induces enzymes which assist HV production but are not induced by the fadR atoC(con) mutations; or
- oleate somehow alleviates catabolite repression of the fad operon; or
- an indirect effect is occurring, for example oleate is being metabolised and affecting levels of intracellular metabolites such as acetyl-CoA.

Pre-induction/supplementation

Several studies have examined the ability of acetate, propionate and oleate to stimulate PHBV production, in the absence of the fadR atoC mutations (Slater *et al.* (1992); Yim *et al.* (1996); Choi and Lee (1999)):

- Acetate induction: Two studies have grown *E. coli* on 10-30 mM acetate to OD 0.8 then added between 10-30 mM propionate and 10-20 $g.l^{-1}$ glucose. *E. coli* HMS174 did not produce PHBV under this regime, however JM109, HB101, and XL1-Blue all yielded 7 to 10 mol% HV. Presumably the enzymes induced in some strains of *E. coli* during growth on acetate have sufficient activity on propionate to allow HV production.
- Propionate induction: *E. coli* has also been grown on 10-30 mM propionate with addition of glucose at OD 0.8. With HMS174 this gave production of PHBV for 2-4 hours, after which only PHB was produced. In XL1-Blue however this regime allowed sustained production of PHBV with 20-30 mol% HV depending on propionate concentration.
- Oleate: For both acetate-induced and -uninduced cultures of XL1-Blue, 1 $g.l^{-1}$ oleate supplementation during growth on glucose and propionate gave 15 mol% HV. Cell mass and PHA content were also enhanced.

In each case above it appears that enzymes were induced which assist in HV production. The enzymes involved may or may not be the same as for fadR atoC(con) mutants, possible candidates are:

- the ace operon, which encodes the enzymes of the glyoxylate shunt for growth on fatty acids. Previous work (Maloy and Nunn (1981)) showed a fivefold increase in acetate utilisation when the ace operon was induced during growth on succinate. This may also be influencing propionate usage;
- the fad operon for oleate supplementation;
- unstudied inducible systems, such as atoE for acetate transport (Clark and Cronan (1996)) or the prp operon for propionate utilisation, discovered in *E. coli* and *Salmonella typhimurium* (Horswill and Escalante-Semerena (1997); Hammelman *et al.* (1996)).

When *Alcaligenes latus* pha genes were used instead of the *R. eutropha* pha genes, PHBV accumulation by these methods was greatly improved. High accumulation of PHBV in a fed-batch fermenter was achieved, viz up to 160 $g.l^{-1}$ of 10%(mol/mol) PHBV in 55 h (Choi and Lee (1999)).

1.3. Summary of Thesis Structure

1.3.1. Overall Structure

The aim of this thesis is to improve understanding of PHA production by recombinant *E. coli*, with a view to guiding future developmental work. Such understanding is an important aid to achieving improvements in an economic sense. The three major steps in such a process are:

1. Identifying aspects of PHA production where improvements will bring the most economic benefits.
2. Focussing quantitative experiments in these areas, to analyse and understand the underlying mechanisms involved.
3. Using this understanding to make process improvements on a rational basis.

The major contributions made by this thesis are as follows:

- Providing an economic description of PHA production by *E. coli*, highlighting areas where significant cost reductions are possible.
- Developing a quantitative analytical framework for the cellular metabolism during PHA production.
- Adapting the *in-vitro* kinetics of the PHB pathway for use with *in-vivo* fermentation data.
- Designing appropriate experimental techniques and conducting repeatable experiments to verify the suitability of the models.
- Applying the metabolic and kinetic models to address several previously unanswered questions, including:
  - Which environmental and/or metabolic factors trigger the onset of PHB production in *E. coli*?
  - What are the underlying metabolic changes that occur during various stages of the fermentation, and how can they be exploited to improve PHA production?
  - What are the short-term and long-term effects of oxygen deprivation on PHB production?
  - Does the nutrient-feeding strategy used have an appreciable effect on PHB production?
  - What further improvements to PHB production are possible and how can they be implemented?

1.3.2. Detailed Structure

Chapter 2 is used to provide detailed fermentation performance data for use in the Chapter 3 economic analysis. Detailed mathematical analysis ("Metabolic Flux Analysis") is conducted on the data to elucidate the activities of key enzymatic pathways during fermentation. Several key areas of uncertainty are identified for further study.

Chapter 3 describes an economic analysis for a PHA production process. It gives an estimate for the net-present-cost of PHB produced by recombinant *E. coli* fermentation. The sensitivity of the cost to numerous process variables is investigated, identifying several fermentation variables as highly influential. These variables are selected for further study.

The aim of Chapter 4 is to develop and analyse a repeatable "base-case" fermentation, against which the effects of process variables can be contrasted. Several experimental techniques are developed for this purpose. Metabolic flux analysis is applied to the data and used to draw several conclusions about the factors influencing the onset of PHB production. A numerical study is conducted based on literature kinetic data and measurements of intracellular acetyl-

CoA and 3-hydroxybutyryl-CoA concentrations. This investigation yields useful information on variables affecting PHB synthesis rate.

Following on from the results of Chapters 3 and 4, two fermentations in Chapter 5 examine the effects of oxygenation on PHB production, viz
1. increased oxygen supply rate for the entire duration of the first fermentation.
2. a sudden drop in oxygen supply rate halfway through the second fermentation.
Metabolic flux analysis is again used to quantify the observed changes in underlying metabolic pathways. Several areas for further manipulation are highlighted.

Chapter 6 investigates the effect of pH-stat nutrient feeding on fermentation performance. The potential short-term and long-term effects on PHB production are studied.

Chapter 7 provides a summary of the contributions made by the thesis.

Chapter 2

2.1. Summary

There are three main purposes to this chapter:

- to develop a quantitative analytical framework for the metabolism of XL1-Blue(pSYL107) during PHB production;
- to apply the model to high-cell-density fermentation data, for three reasons:
  - as a preliminary test of the model;
  - to glean insights into the regulatory mechanisms occurring at high cell density, and suggest possible improvements;
  - to guide the development of later experiments: more rigorous verification and analysis of the model is described in Chapters 4, 5 and 6;
- to gain the necessary fermentation data for an economic analysis (Chapter 3).

A single 52 h glucose-minimal-medium fed-batch fermentation was carried out in a 6.6 l bioreactor. Aeration was by an air/oxygen mixture adjusted as necessary to avoid oxygen limitation. The production rates of PHB, residual cell mass, carbon dioxide, acetic acid, formic acid, lactic acid, and ethanol were measured. The consumption rates of glucose and ammonium ion were also measured.

The fermentation achieved 78% PHB with 227 $g.l(broth)^{-1}$ dry cell weight. Peak PHB production rate was 0.14 $gPHB.gRCM^{-1}h^{-1}$. PHB yield on glucose was 0.74 $mol(PHB).mol(Glc)^{-1}$. Formic acid, acetic acid, and lactic acid were excreted to moderate levels (maximum 8 $g.l^{-1}$, 4.6 $g.l^{-1}$, and 12 $g.l^{-1}$ respectively). Ethanol was not detected. Typical two-phase production of PHB was observed: initially residual cell mass synthesis was high with low PHB production. After a transition period of approximately 10 h, RCM synthesis ceased and PHB synthesis reached a maximum. There was a gradual, exponential decline in all fluxes over the second half of the fermentation but PHB yield on glucose was constant at 85% $mol(PHB).mol(Glc)^{-1}$.

A brief period of oxygen limitation occurred. This coincided with the cessation of RCM synthesis, and rapid excretion of acetic and lactic acid.

A metabolic network model was developed and applied to the data. Mass-balance closure was excellent (105%) although some systematic error was indicated.

The data suggest that PHB production may be improved in several ways, as outlined in the conclusions. Several improvements to the experimental methods are also described.

2.2. Introduction

High-PHB-yielding fermentations of *E. coli* and *R. eutropha* have been achievable for several years (Lee (1996c)). Levels of 160 g(PHB).l^{-1} or more are possible (Wang and Lee (1997)). However, thorough study of the metabolism of *E. coli* during high-cell-density PHB synthesis has not yet been performed. If further advances are to be made, analysis and modelling of the fermentation process will become increasingly important, for several reasons:

- "blind" techniques such as mutation-selection yield diminishing returns once the straight-forward genetic modifications have occurred, and it is impractical to test all the possible variations in fermentation parameters on a pilot scale;
- improvements in an economic sense may require tradeoffs, for example sacrificing cell density for PHB yield on glucose;
- co-ordinated changes in fermentation protocol and strain properties may be required.

Metabolic engineering techniques are finding increasing use for improving the performance of industrial microorganisms. Examples of theoretical and practical applications of metabolic engineering are described in the following references: (Bailey (1991); Stephanopolous and Vallino (1991); Nielsen and Villadsen (1994); van der Heijden *et al.* (1994a); Delgado and Liao (1997); Sauer *et al.* (1997); Stephanopolous and Simpson (1997); Mauch *et al.* (1997)).

Metabolic flux analysis is a useful first step to quantifying the behaviour of *E. coli* during PHB production. The technique is finding widespread application as an aid to the metabolic engineering of such diverse microorganisms as *E. coli* (Varma *et al.* (1993b)), hybridomas (Zupke and Stephanopolous (1995); Bonarius *et al.* (1997)), *Penicillium chrysogenum* (Jorgensen *et al.* (1995)), yeasts (van Gulik and Heijnen (1995)), and *Corynebacterium glutamicum* (Vallino and Stephanopolous (1993); Hammelman *et al.* (1996)). Even a simple metabolic model can reveal much information about the performance of the cells. Resolving the experimental data into metabolic fluxes yields several advantages for PHB production by *E. coli*:

- the validity of the experimental data can be checked and errors rectified by utilising degrees of redundancy in the system, for example an overall carbon balance and overall NAD(P)H balance ("redox balance");
- the flux through several key internal fluxes can be quantified, in particular TCA cycle flux, fluxes for NADPH generation, and total ATP generation;
- the network can provide a basis for determining the maximum possible production capabilities and minimum possible metabolic requirements (Varma *et al.* (1993b)).

The major components of this chapter are:

1) Development of a metabolic flux model for PHB production by XL1-Blue(pSYL107);
2) Collection and analysis of high-cell-density fermentation data for the purposes of:
   - preliminary verification of the flux model;
   - providing a guide for developing the more rigorous experimental protocols used in Chapters 4, 5, and 6;
   - elucidating how the major fluxes change during PHB production, and gaining an understanding of the underlying mechanisms at work;
   - suggesting areas where improvements in PHB production can be made;
   - providing sufficient mass balance data to perform an economic analysis of an industrial PHB production process (Chapter 3).

2.3. Modelling and Theoretical Aspects

Biochemical Network

PHB production by *E. coli* is quite simple from a metabolic-network standpoint. An overall view of the metabolic network is shown in Figure 2.1.

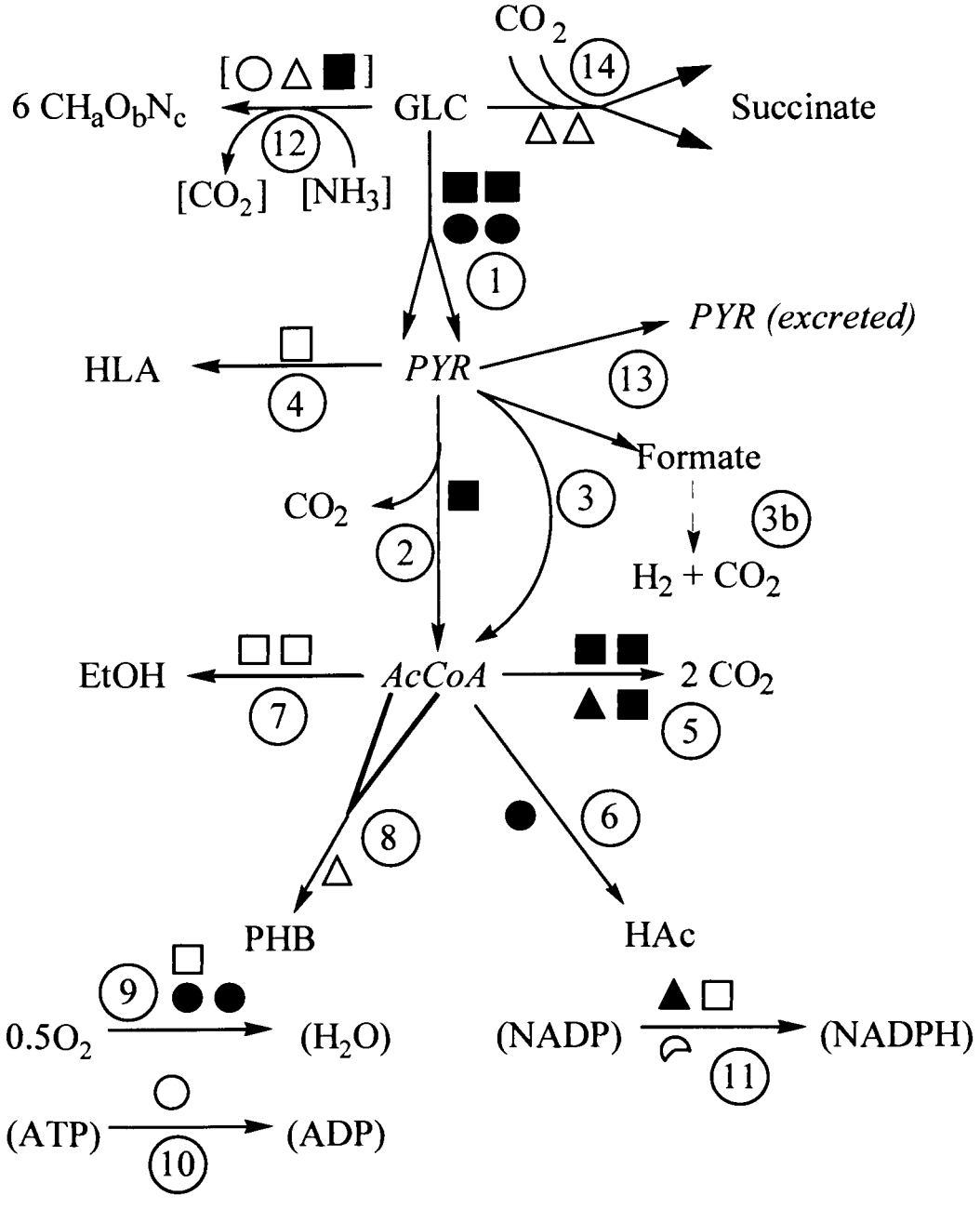

Figure 2.1: Pictorial representation of the flux network , with flux labels shown in open circles. Cofactor requirements are indicated by ○ = ATP, □ = NADH, △ = NADPH. Open shapes indicate consumption (of ATP, NADH, or NADPH); filled shapes indicate production. ᔓ indicates consumption of 2/3 ATP. [] indicate variable cofactor requirements.

The reactions in the network are described in more detail below.

Glycolysis

Glucose is imported via the phosphotransferase system and converted to pyruvate. Although glucose can also pass through the pentose phosphate pathway (PPP), this is not treated separately. The function of the PPP is primarily to provide precursors for biomass synthesis (for example ribose-5-phosphate and NADPH) (Varma and Palsson (1993a)). Hence

- production of NADPH is lumped into flux 11 (see below) and the carbon flux incorporated into flux 1;
- production of carbon precursors for biomass synthesis is lumped into flux 12.

Hence glycolysis is represented by Flux 1.

$$Glc + 2ADP + 2NAD^{+} \rightarrow 2PYR + 2NADH + 2ATP \qquad \text{(Flux 1)}$$

Pyruvate Catabolism

E. coli possesses two key enzymes for pyruvate conversion to acetyl-coA (accoA) (Bock and Sawers (1996); Kessler and Knappe (1996)). Oxidative decarboxylation by the pyruvate dehydrogenase complex (PDH) generates NADH and is the major pathway under aerobic conditions. Under anaerobic conditions, pyruvate is converted to accoA by pyruvate-formate lyase (PFL), with the co-formation of formate. At a medium redox potential between true aerobic and anaerobic, both enzymes may be functional in metabolising pyruvate (Bock and Sawers (1996)). As this study intentionally employs very low oxygen concentrations during PHB formation, both pathways are included in the network:

$$PYR + NAD^{+} \xrightarrow{PDH} AccoA + CO_2 + NADH \qquad \text{(Flux 2)}$$

$$PYR \xrightarrow{PFL} AccoA + Formate \qquad \text{(Flux 3)}$$

Pyruvate-formate-lyase production is enhanced under anaerobic conditions. It can alternate between an oxygen-labile active form, and an oxygen-stable but inactive form. The conversion is enzymatic, with formation of active PFL stimulated by pyruvate and NADH.

The formic acid produced by PFL is either excreted to the medium or decomposed to CO_2. Under anaerobic conditions, the formate-hydrogen lyase system (FHL) accomplishes this by generating H_2, viz

$$Formate \xrightarrow{FHL} H_2 + CO_2 \qquad \text{(Flux 3b)}$$

The FHL complex is synthesised at very low levels at neutral pH. When the pH drops due to acid product secretion, formate is reimported into the cell to offset the pH. Upon reaching a critical internal concentration, it induces FHL production. In addition to FHL, there may also be an active aerobic formate dehydrogenase. This enzyme converts formate to CO_2 by exporting two protons and oxidising one molecule of ubiquinone, which is subsequently used to generate ATP. Thus this enzyme is approximately equivalent to PDH with oxidation of NADH to ATP, and hence is not explicitly included in the network.

Production of lactic acid from pyruvate is also observed during anaerobic fermentation. In general lactic acid is observed to appear last during batch culture, when acid secretion has significantly lowered the pH and (presumably) the production of other organic acids is inhibited by end products. During pH-controlled batch fermentation the amount of lactic acid formed should be minimal, although this is very dependent on environmental conditions. High PFL activity is the primary reason that the route to lactate is completely bypassed at neutral or basic pH. LDH activity is enhanced by pyruvate.

$$PYR + NADH \xrightarrow{LDH} HLA + NAD^{+} \qquad \text{(Flux 4)}$$

Under some conditions of metabolic imbalance, *E. coli* has been demonstrated to excrete pyruvic acid into the medium (Neijssel *et al.* (1996)). This probably arises from excessive internal concentrations. To account for this possibility, flux 13 must be incorporated into the network.

$$PYR \xrightarrow{excretion} PYR(excreted) \qquad \text{(Flux 13)}$$

Acetyl-coA catabolism

Acetyl-coA (accoA) can flow into the tricarboxylic acid (TCA) cycle, where it is converted to NAD(P)H:

$$AccoA + 3NAD^{+} + NADP \rightarrow 2CO_2 + 3NADH + NADPH \qquad \text{(Flux 5)}$$

The stoichiometry has been simplified by treating $FADH_2$ as NADH, and GTP as ATP. Since $FADH_2$ enters the oxidative phosphorylation network directly at the quinone pool (Nielsen and Villadsen (1994)), it generates approxiately one ATP per molecule whereas NADH generates two (see "Oxidative Phosphorylation" below). Consequently, $FADH_2$+GTP≅NADH. Contrary to early belief, most TCA cycle enzymes are inducible in *E. coli*, governed by the Crp (cAMP receptor protein) and ArcAB (aerobic respiration control) gene products (Cronan and LaPorte (1996)). Several studies have confirmed that during rapid fully-aerobic growth on glucose, only the branched biosynthetic form of the cycle is present. Most of the cellular energy is obtained from substrate level phosphorylation. Likewise the TCA cycle is not utilised during anaerobic growth. Its highest activity is obtained during aerobic growth on acetate or fatty acids. Hence it is uncertain whether the TCA cycle will be functioning at all during PHB production.

AccoA may also be converted to acetate (HAc) and excreted, via the acetate-kinase and phosphotransacetylase (ack-pta) enzymes:

$$AccoA + ADP \leftrightarrow HAc + ATP \qquad \text{(Flux 6)}$$

The ack-pta pathway is enhanced by pyruvate, and repressed by NADH, ADP and ATP (Bock and Sawers (1996)). Acetate excretion can occur in *E. coli* even when oxygen supply is plentiful (The "Crabtree" effect). Various studies have suggested this to be caused by a mismatch between glycolytic and TCA fluxes, which in turn leads to excessive intracellular acetyl-CoA concentrations (Goel *et al.* (1995a)).

Under conditions of low oxygen, NADH regeneration may also occur via ethanol formation (Kessler and Knappe (1996)):

$$AccoA + 2NADH \xrightarrow{ADH} EtOH + 2NAD^{+} \qquad \text{(Flux 7)}$$

ADH expression increases in response to a rise in intracellular NADH/NAD ratio, in an attempt to restore internal redox balance by producing highly-reduced ethanol.

Finally, poly(3-hydroxybutyrate) (PHB) is formed in recombinant *E. coli* from accoA according to the stoichiometry in Flux equation 8, via three enzymes originally isolated from *Ralstonia eutropha* (Lee (1996c)):

$$2AccoA + NADPH \rightarrow PHB + NADP^{+} \qquad \text{(Flux 8)}$$

Several fatty oxidation enzymes can supplement enzymes in this pathway however their activity is probably negligible compared to the recombinant enzymes and they have been ignored.

Succinic acid production

Although there are several likely pathways to succinic acid, both Lee *et al.* (1994b) and Bock and Sawers (1996) indicate that the route used during anaerobic fermentation of *E. coli* is as follows:

1. Glucose is converted to phosphoenolpyruvate.
2. Phosphoenolpyruvate is to oxaloacetate via the anaplerotic enzyme PEP carboxylase.
3. The TCA cycle is operated in reverse to generate succinate (via malate dehydrogenase, fumarase, and fumarate reductase).
4. The succinate is then excreted.

If this reaction sequence is lumped together as a single flux, we obtain

$$Glc + 2CO_2 + 2NADPH \rightarrow 2Succinate + 2NADP^{+} \qquad \text{(Flux 14)}$$

The literature does not mention why succinate is excreted during anaerobic growth but not during aerobic growth. Possibly a membrane transport mechanism is induced during

anaerobiosis, or alternatively the intracellular concentration of succinate may reach high levels.

Oxidative phosphorylation

E. coli has a flexible oxidative phosphorylation network consisting of two dehydrogenases (NDHI and NDHII) and two cytochrome ubiquinol oxidases (*bo*$_3$-type and *bd*-type). The rates of proton translocation per electron transferred to O_2 for NDHI, NDHII, *bd*-oxidase and *bo*$_3$-oxidase are 2, 0, 2, and 1, respectively, giving a maximum of 8 H^+ exported per NADH oxidised. A figure of 6 H^+ exported per electron is reasonable, giving approximately 2 ATP per NADH molecule based on 3 H^+/ATP (Harold and Maloney (1996)):

$$NADH + \frac{1}{2}O_2 + 2ADP \rightarrow NAD^+ + 2ATP \qquad \text{(Flux 9)}$$

Clearly, this stoichiometry will vary depending on the relative flux through the components of the OP network, and will probably change throughout the course of the fermentation.

ATP usage for maintenance and futile cycling is represented by flux equation 10:

$$ATP \rightarrow ADP \qquad \text{(Flux 10)}$$

Unlike NADP(H) and NAD(H), it is not generally possible to construct a meaningful balance on ATP. The reasons for this are variable production efficiency by oxidative phosphorylation, and poorly quantified requirements for biosynthesis and cellular maintenance. Flux 10 is introduced primarily to open the ATP balance and prevent it from influencing estimates of other fluxes. Experimental values for the flux should be interpreted with this fact in mind.

Anabolic Reactions

Anabolic reactions generally require NADPH rather than NADH. NADPH is principally generated in three ways by *E. coli*, viz the TCA cycle, the Pentose Phosphate pathway, and the energy-linked NAD(P)H transhydrogenase. It is not readily possible to distinguish between the latter two pathways by stoichiometric analysis, hence for this network they have been lumped together in a single equation:

$$NADH + NADP^+ + \tfrac{2}{3}ATP \longrightarrow NAD^+ + NADPH + \tfrac{2}{3}ADP \qquad \text{(Flux 11)}$$

Mutants in either the PP or transhydrogenase pathways do not exhibit significant changes in growth (Ingraham *et al.* (1983); Varma and Palsson (1993b)). Evidence also suggests that the split of glycolytic flux through the PP pathway is highly variable. Hence it is not possible to say which of these two fluxes will be the most significant fraction of flux 11.

Biomass formation in minimal media requires the uptake of ammonia and substrate. There is a net consumption of ATP and NADPH, but net production of NADH and CO_2:

$$(1+\alpha)\mathrm{Glc} + \alpha_N \mathrm{NH_3} + \gamma_N \mathrm{NAD} + \gamma_P \mathrm{NADPH} + \gamma_A \mathrm{ATP}$$
$$\downarrow \qquad \text{(Flux 12)}$$
$$6\mathrm{CH_aO_bN_c} + 6\alpha_C \mathrm{CO_2} + \gamma_N \mathrm{NADH} + \gamma_A \mathrm{ADP} + \gamma_P \mathrm{NADPH}$$

where a, b and c are determined from an elemental analysis of the biomass. The ATP, NAD, and NADPH requirements can be expressed in terms of yield coefficients:

$$\gamma_A = 6[12 + a + 16b + 14c]Y_{xATP} \qquad (2.1)$$

$$\gamma_N = 6[12 + a + 16b + 14c]Y_{xNAD} \qquad (2.2)$$

$$\gamma_P = 6[12 + a + 16b + 14c]Y_{xNADPH} \qquad (2.3)$$

where Y_{xATP} is 35.7×10^{-3} mol ATP per g RCM of biomass, Y_{xNAD} is 20.5×10^{-3} mol NAD per g RCM biomass, and Y_{xNADPH} is 14.6×10^{-3} mol NADPH per g RCM biomass (Ingraham *et al.* (1983)). These yield coefficients are based on *E. coli* B/r cells growing in minimal glucose medium at 37 °C, with a 40 minute doubling time.

Anabolic carbon dioxide production is difficult to quantify, because it arises from many different reactions. The carbon dioxide requirement for biomass synthesis in this model is calculated from tables of biomass composition in Ingraham *et al.* (1983). The assumption is made that synthesis of 1 mole of ribose-5-phosphate, erythrose-4-phosphate, or acetyl-CoA produces 1 mole of CO_2, and that synthesis of 1 mole of oxaloacetate requires 1 mole of CO_2. This yields an estimate of 2.3 mmol of CO_2 produced per g of biomass, and hence

$$\alpha_C = [12 + a + 16b + 14c] \times 0.0023 \qquad (2.4)$$

Unfortunately the coefficients in the biomass equation (γ_A, γ_N, γ_P, and α_C) are subject to significant uncertainty, because the average macromolecular composition of the cells is likely to change during the fermentation.

Comments on Biochemical Network

The network as described above has effectively three degrees of freedom, viz an NAD(P)H balance, an overall carbon balance, and a nitrogen balance. However because of several practical limitations the actual network used for flux analysis in this chapter is a subset of the equations described above:

- the rate of oxygen consumption was not accurately measured, and therefore was calculated from the NAD(P)H balance instead;
- the flux through formate-hydrogen-lyase (if any) cannot be accurately quantified unless the rate of hydrogen production is measured. If oxygen consumption had been measured, FHL quantification would theoretically be possible via an NAD(P)H balance, but in practice this would be very sensitive to errors in the rate measurements. Furthermore, as described earlier, the flux is likely to be negligible at neutral pH. Therefore it is not included in the network;
- ammonia uptake was not explicitly excluded in the network because of uncertainty in the biomass nitrogen content;
- extracellular pyruvic acid concentration was not measured, hence flux 13 is not included;
- succinic acid concentration was not measured, hence flux 14 is not included.

Thus the metabolic network diagram used to analyse the fermentation in this chapter is as shown in Figure 2.2.

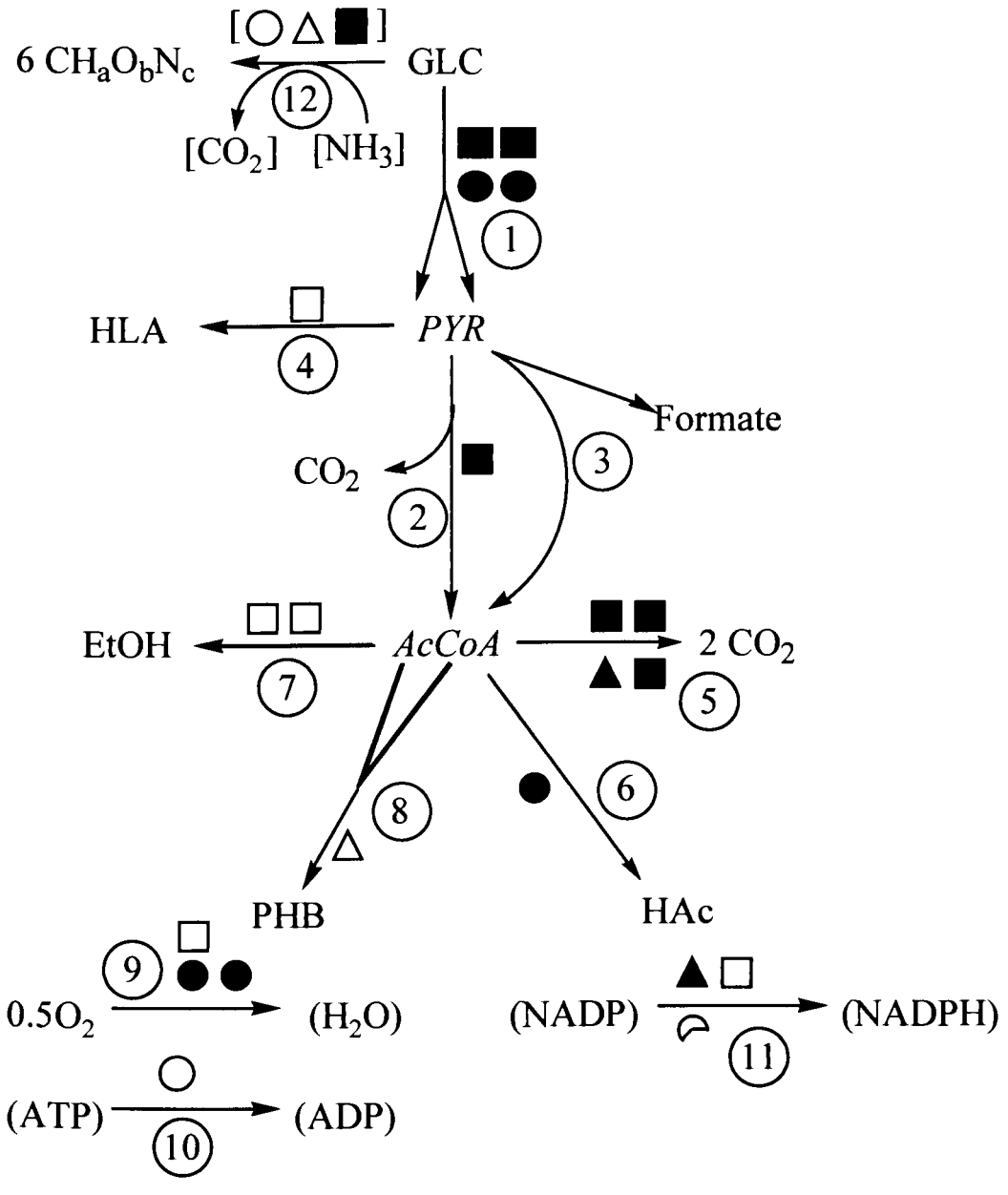

Figure 2.2: Pictorial representation of the flux network used for the high-cell-density fermentation, with flux labels shown in open circles. Cofactor requirements are indicated by ○ = ATP, □ = NADH, △ = NADPH. Open shapes indicate consumption (of ATP, NADH, or NADPH); filled shapes indicate production. ⌒ indicates consumption of 2/3 ATP, [] indicate variable cofactor requirements.

2.4. Materials and Methods

2.4.1. Flux Analysis

As described in Appendix D, the reaction network and stoichiometry may be written in standard matrix notation for flux analysis (Nielsen and Villadsen (1994)):

$$\underline{\mathbf{A}}\underline{\mathbf{x}} = \underline{\mathbf{r}} \tag{2.5}$$

where

$\underline{\mathbf{A}}$ = the stoichiometric matrix embodying a mass balance on each metabolite

$\underline{\mathbf{x}}$ = column vector of fluxes

$\underline{\mathbf{r}}$ = a column vector of metabolite accumulation rates.

For the network in this study, the pseudo-steady state approximation for intracellular species has been applied and all other metabolites in the model except O_2 are measured. $\underline{\mathbf{A}}$ is thus firstly partitioned into rows corresponding to measured (m), calculated (c), and pseudo-steady-state intracellular (p) metabolites. The pseudo-steady state approximations lead to linear dependencies amongst the fluxes, hence row reduction is used on $\underline{\mathbf{A}}_p$ to obtain Equation 2.6:

$$\begin{pmatrix} \underline{\mathbf{A}}_{md} & \underline{\mathbf{A}}_{mi} \\ \underline{\mathbf{A}}_{cd} & \underline{\mathbf{A}}_{ci} \\ \underline{\mathbf{I}} & \underline{\mathbf{A}}_{pi} \\ \underline{\mathbf{0}} & \underline{\mathbf{0}} \end{pmatrix} \begin{pmatrix} \underline{\mathbf{x}}_d \\ \underline{\mathbf{x}}_i \end{pmatrix} = \begin{pmatrix} \underline{\mathbf{r}}_m \\ \underline{\mathbf{r}}_c \\ \underline{\mathbf{0}} \\ \underline{\mathbf{0}} \end{pmatrix} \tag{2.6}$$

where A has also been columnwise partitioned into "dependent" and "independent" fluxes. $\underline{\mathbf{A}}_{pi}$ is the matrix relating the "dependent" and "independent" fluxes, viz

$$\underline{\mathbf{I}}.\underline{\mathbf{x}}_d + \underline{\mathbf{A}}_{pi}.\underline{\mathbf{x}}_i = \underline{\mathbf{0}} \tag{2.7}$$

Estimates of the reaction fluxes may be obtained by least squares regression for the overdetermined system:

$$\underline{\mathbf{x}} = \begin{pmatrix} \underline{\mathbf{x}}_d \\ \underline{\mathbf{x}}_i \end{pmatrix} = \begin{pmatrix} -\underline{\mathbf{A}}_{pi}\left(\underline{\mathbf{T}}^T\underline{\mathbf{F}}_m^{-1}\underline{\mathbf{T}}\right)^{-1}\underline{\mathbf{T}}^T\underline{\mathbf{F}}_m^{-1}\underline{\mathbf{r}}_m \\ \left(\underline{\mathbf{T}}^T\underline{\mathbf{F}}_m^{-1}\underline{\mathbf{T}}\right)^{-1}\underline{\mathbf{T}}^T\underline{\mathbf{F}}_m^{-1}\underline{\mathbf{r}}_m \end{pmatrix} \tag{2.8}$$

where

$$\underline{\mathbf{T}} = \underline{\mathbf{A}}_{mi} - \underline{\mathbf{A}}_{md}\underline{\mathbf{A}}_{pi} \tag{2.9}$$

$\underline{\mathbf{F}}_m$ is the variance-covariance matrix of the measured accumulation rates.

Calculated rates (in particular oxygen consumption) are obtained from

$$\underline{\mathbf{r}}_C = \underline{\mathbf{A}}_C \underline{\mathbf{x}} \tag{2.10}$$

Estimates of the flux errors are given by the flux variance-covariance matrix:

$$\underline{\mathbf{F}}_X = \left(\underline{\mathbf{C}}_i - \underline{\mathbf{A}}_{pi}\underline{\mathbf{C}}_d\right)\underline{\mathbf{F}}_{Xi}\left(\underline{\mathbf{C}}_i - \underline{\mathbf{A}}_{pi}\underline{\mathbf{C}}_d\right)^T \tag{2.11}$$

where

$$\underline{\mathbf{F}}_{Xi} = \left(\underline{\mathbf{T}}^T \underline{\mathbf{F}}_{\mathbf{m}}^{-1} \underline{\mathbf{T}}\right)^{-1} \tag{2.12}$$

$$\underline{\mathbf{x}} = \begin{pmatrix} \underline{\mathbf{x}}_d \\ \underline{\mathbf{x}}_i \end{pmatrix} = \underline{\mathbf{C}}_i \underline{\mathbf{x}}_i + \underline{\mathbf{C}}_d \underline{\mathbf{x}}_d \tag{2.13}$$

$$\underline{\mathbf{C}}_i = \begin{pmatrix} \underline{\mathbf{0}} \\ \underline{\mathbf{I}} \end{pmatrix} \tag{2.14}$$

$$\underline{\mathbf{C}}_d = \begin{pmatrix} \underline{\mathbf{I}} \\ \underline{\mathbf{0}} \end{pmatrix} \tag{2.15}$$

Gross errors, in either the stoichiometry or the measured rates, are indicated if h_δ does not follow the $\chi^2_{rank(\mathbf{F}_{Xi})}$ statistic (van der Heijden *et al.* (1994b)), where:

$$h_\delta = \underline{\boldsymbol{\delta}}^T \left(\underline{\Delta \mathbf{F}}_{\mathbf{m}} \underline{\Delta}^T\right)^{-1} \underline{\boldsymbol{\delta}} \tag{2.16}$$

$$\underline{\Delta} = \underline{\mathbf{I}} - \underline{\mathbf{T}}\left(\underline{\mathbf{T}}^T \underline{\mathbf{F}}_{\mathbf{m}}^{-1} \underline{\mathbf{T}}\right)^{-1} \underline{\mathbf{T}}^T \underline{\mathbf{F}}_{\mathbf{m}}^{-1} \tag{2.17}$$

$$\underline{\boldsymbol{\delta}} = \underline{\Delta \mathbf{r}}_{\mathbf{m}} \tag{2.18}$$

2.4.2. Experimental Methods

The experimental work for this chapter was performed by Heng Ho Wong at the Department of Chemical Engineering and Bioprocess Engineering Research Centre, Korea Advanced Institute of Science and Technology (KAIST). Analysis was subsequently performed by the author at the University of Adelaide. The flux model was developed by the author in conjunction with Dr Anton Middelberg during his sabbatical from the University of Adelaide, and Dr Sang Yup Lee at the Department of Chemical Engineering and Bioprocess Engineering Research Centre, Korea Advanced Institute of Science and Technology (KAIST).

Bacterial strain and plasmid

Recombinant *Escherichia coli* (*E. coli*) strain XL1-Blue (*supE44 hsdR17 recA1 endA1 gyrA96 thi relA1 lac F'(proAB+ lacIq lacZΔM15Tn10(tet^r))*) harbouring pSYL107 was used in this study (Wang and Lee (1997)). The plasmid pSYL107 contains the *R. eutropha* PHA biosynthesis genes, an *E. coli ftsZ* filamentation-suppression gene, the *parB* locus for plasmid stability, and an ampicillin resistance gene (Lee (1994)).

Medium and culture conditions

A single fed-batch high-cell-density fermentation was conducted with no deliberate oxygen restriction. Stock culture was stored in 20% (v/v) glycerol at −70 °C before being used to inoculate two 1 l shake flasks. Each shake flask contained 0.2 l MR-medium (Wang and Lee (1997)) supplemented with separately-sterilised 20 $g.l^{-1}$ glucose, 0.1 $g.l^{-1}$ ampicillin and 0.01 $g.l^{-1}$ thiamine. The MR medium contained the following per litre: 22 g KH_2PO_4, 3 g $(NH_4)_2HPO_4$, 0.7 g $MgSO_4.7H_2O$, 0.8 g citric acid, 5 ml of trace-metals solution. The trace-metals solution contained the following per litre of 5 M HCl: 10.0 g $FeSO_4.7H_2O$, 2.0 g $CaCl_2$, 2.2 g $ZnSO_4.7H_2O$, 0.5 g $MnSO_4.4H_2O$, 1.0 g $CuSO_4.5H_2O$, 0.1 g $(NH_4)_6Mo_7O_{24}.4H_2O$, 0.02 g $Na_2B_4O_7.10H_2O$.

Following incubation for 30 h at 30 °C and 250 rpm, the culture (total of 0.4 l) was used to inoculate a 6.6 l Bioflo 3000 bioreactor (New Brunswick Scientific Co., Edison, NJ, USA) containing 1.2 l of initial medium with the same composition as the seed culture. Culture temperature was controlled at 30.0±0.5 °C. Automatic feeding of 25%(v/v) ammonia water occurred when pH fell below 6.90. The amount added was measured using an electronic mass balance. Foam was controlled by manually adding 30%(v/v) antifoam 289 (Sigma Chemical Co., St. Louis, MO, USA) as required. Where possible dissolved oxygen was maintained above 20% by automatically varying agitation speed (maximum 1000 rpm). The inlet gas consisted of a mixture of air and bottled oxygen. During the fermentation, gas flowrate was held constant at 4.0 $l.min^{-1}$ and its oxygen concentration was increased in discrete steps as required. The bioreactor was not pressurised. Volumetric oxygen mass-transfer coefficient (k_La) varied between 5 min^{-1} and 9 min^{-1} depending on broth volume.

Batch cultivation was employed until the initial glucose charge was depleted. Thereafter, nutrient feeding solution (700 $g.l^{-1}$ glucose; 15 $g.l^{-1}$ $MgSO_4.7H_2O$, 0.25 $g.l^{-1}$ thiamine) was added using a pH-stat feeding strategy (Lee (1996b)). When the pH rose above 7.00, an appropriate amount of feeding solution was added automatically to restore the glucose concentration in the culture medium to 20 $g.l^{-1}$. This feeding volume was calculated on-line using computer software (AFS3.42, New Brunswick Scientific Co.).

Analytical procedures

Cell growth was monitored by measuring the optical density at 600 nm (OD_{600}) using a spectrophotometer (BECKMAN DU®650, CA, USA). The composition of outlet gas from the bioreactor was measured using a mass spectrometer (HAL Quadrupole mass spectrometer, Warrington, England). Cell concentration, defined as dry cell weight (DCW), was determined as follows: culture broth (2-20 ml) was collected in a preweighed tube, pelleted by centrifugation, washed twice with distilled water, then dried to constant weight in a vacuum oven. PHB concentration was determined using a gas chromatograph (HP5890, Hewlett-Packard, Wilmington, DE, USA) with n-butyric acid as internal standard (Braunegg *et al.* (1978)). Residual Cell Mass (RCM) is defined as DCW ($g.l^{-1}$) minus PHB concentration ($g.l^{-1}$). PHB content (%) is defined as the ratio of PHB concentration to cell concentration.

The elemental composition of the sample was determined as follows: 25 ml of culture broth was centrifuged at 2100 g for 40 min, and the supernatant discarded. The pellet was resuspended in distilled water and centrifuged again (2x). The final pellet was dried to constant weight in an oven at 60 °C and ground into powder. The carbon, hydrogen, oxygen,

nitrogen and sulfur contents were then analysed using an elemental analyser (CE Instruments, Italy).

Concentrations of formic acid, lactic acid and acetic acid in the culture medium were measured by HPLC (Hitachi L-3300 RI monitor, L-600 pump, D-2500 chromato-integrator, Tokyo, Japan) using an ion exchange column (Aminex® HPX-87H, 300 mm × 7.8 mm, Hercules, CA USA) with 0.01 N H_2SO_4 mobile phase. Enzymatic test kits were used to measure the concentrations of glucose (Yeongdong Pharmaceutical Corp, Korea), ethanol (Boehringer Mannheim, Germany), ammonia (Boehringer Mannheim) and carbon dioxide (Sigma Diagnostics, USA) in the culture medium.

2.4.3. Analysis of Data

Gas CO_2 composition was calculated from the ratio of measured CO_2 and Ar abundances (peak 44 / peak 40), using previously-generated standards. Given the measured inlet flowrate and measured inlet composition the production of CO_2 could be calculated.

Mass balance calculations

The net production of each analyte during a given sample period was calculated as follows:

$$\Delta r = m_{after}.C_{after} - m_{before}.C_{before} + \gamma.\dot{r}_{measured} \tag{2.19}$$

where

Δr	= mass of analyte produced (g)
m	= mass of broth on a no-sampling basis (kg)
C	= concentration of analyte (g.kg(broth)$^{-1}$)
γ	= average mass-sampling factor over the sample period
$\dot{r}$	= external addition of analyte (g), for example glucose feed

This equation yields a non-sampling basis, viz the values that would be observed if no samples were taken from the bioreactor. Conceptually this corresponds to taking the sample and placing it in another "imaginary" bioreactor with the same operating conditions. Hence the definition of mass-sampling factor

$$m_{no-sampling-basis(k)} = m_{actual(k)}.\gamma_k \tag{2.20}$$

where

γ_k	= mass-sampling factor at sample k.

The factor is calculated using the approximation

$$\gamma_{n+1} = \gamma_n \left(1 + \frac{S_{actual}}{m_{actual}} \right) \tag{2.21}$$

where

S_{actual} = actual mass withdrawn from bioreactor between samples n and n+1 (g)

m_{actual} = actual mass of broth in bioreactor (g)

Conceptually this represents taking (for example) 5% from the real bioreactor and each imaginary bioreactor, then placing this into yet another imaginary bioreactor. A consequence of the no-sampling basis is the need to apply the mass-sampling factor to any measured analyte additions, i.e. the final term in Equation 2.19.

The mass of material in the bioreactor at any time was calculated by mass balance from the known addition and removal of material (including gas flows).

The mass-production rates were converted to molar production rates and then processed using flux analysis methods as described in Section 2.4.1. The covariance matrix for each sample was estimated from measured errors in concentrations, assuming zero correlation between different rate measurements.

For all graphs in this thesis which present rate data or flux data, the lines have been smoothed by central difference in order to improve visual clarity, i.e. given a flux datapoint at hr 12, hr 13, and hr 14, this would be smoothed to produce a flux value at hr 12.5 and a flux value at hr 13.5. This smoothing was performed because the rate data exhibit a high negative correlation from one point to the next, i.e. if the calculated flux at hr 12 is higher than the true value then the flux at hr 13 will tend to be lower, as can be seen from Equation 2.19. The datapoints themselves are not smoothed.

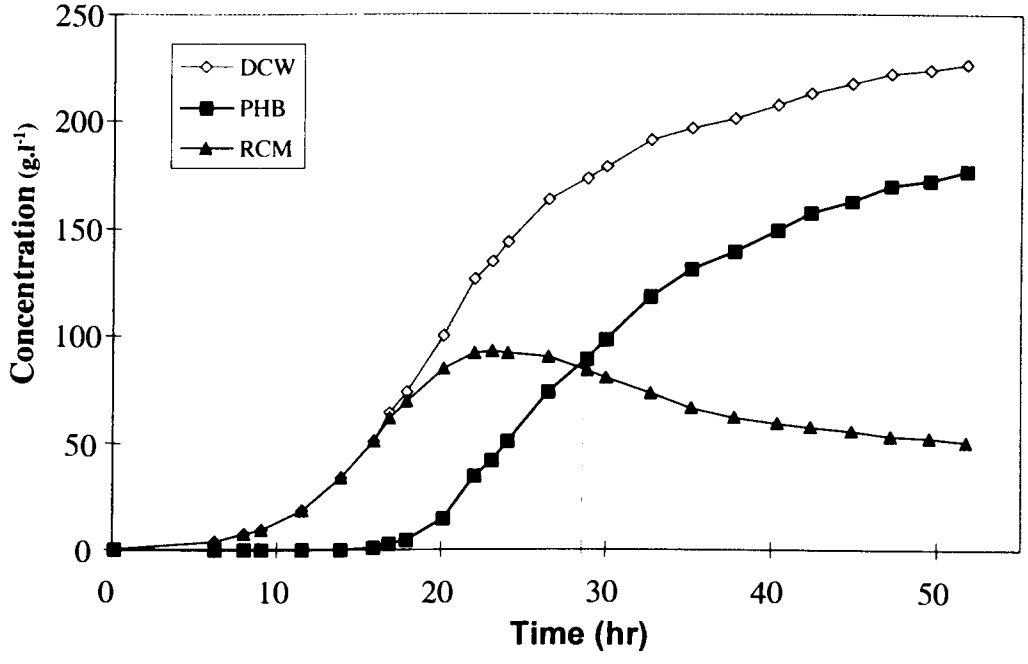

Figure 2.3: Concentrations of dry-cell-weight (DCW), PHB, and residual-cell-mass (RCM).

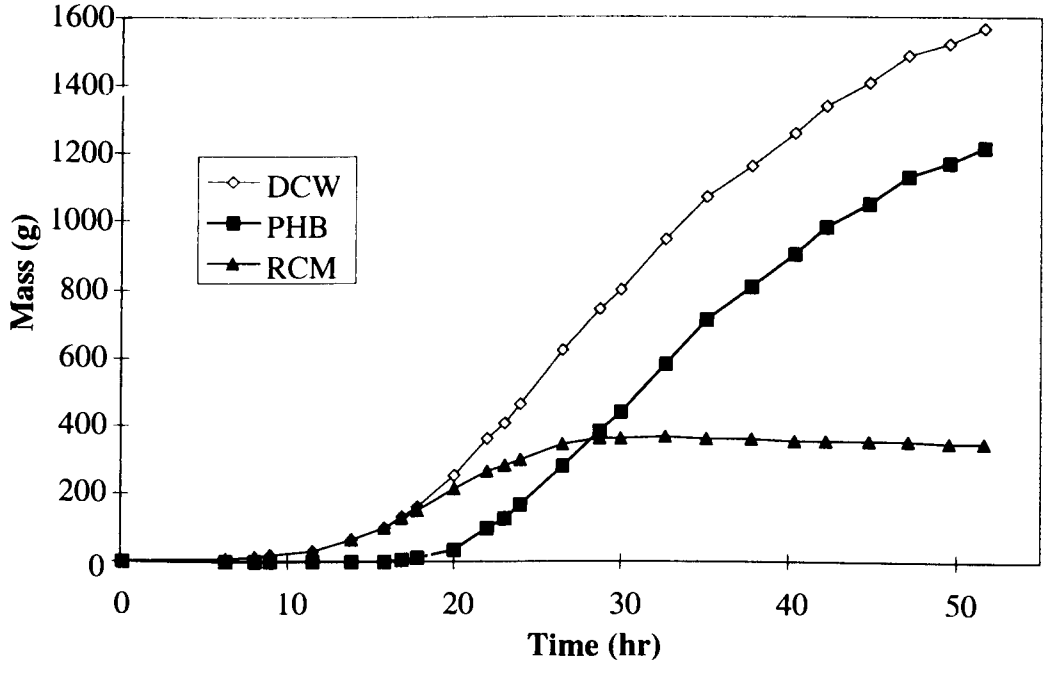

Figure 2.4: Profiles of dry-cell-weight, PHB, and residual-cell-mass on a no-sampling basis.

Figure 2.3 shows that once PHB production commences the residual cell mass (RCM) production halts almost completely. RCM concentration appears to decline from hr 22 onwards but this is due to dilution of the broth by nutrient feed. Figure 2.4 shows the data on a total-mass, no-sampling basis, demonstrating that from hr 27 onwards RCM production stops completely. There is a very slow decline in RCM over the next 24 h (4%). The final dry cell weight achieved was 227 $g.l^{-1}$ with a final PHB content of 177 $g.l^{-1}$ (78%). These figures are extremely high. Overall reactor productivity was 3.39 $g(PHB).L(broth)^{-1}h^{-1}$ on minimal medium, which is also extremely high.

Figure 2.5 shows more clearly the previous observation that once PHB accumulation commences, RCM production rapidly drops to zero. The initial growth rate is 0.3 h^{-1}, which is slow for *E. coli*. Wild types are readily capable of specific growth rates between 0.7 to 1.0 h^{-1} in minimal media at 30 °C (Ingraham *et al.* (1983)). There are numerous possible explanations, including:

- the use of high ampicillin concentration (100 $mg.l^{-1}$);
- the presence of a high-copy-number constitutive plasmid overexpressing PHA enzymes and ftsZ filamentation-suppression protein;
- the *E. coli* strain used (XL1-blue) has been extensively selected, firstly for good DNA cloning ability, and secondly for good PHB production with pSYL107. It may therefore contain mutations which enhance plasmid replication and PHB production, but also cause it to grow slowly.

The figure also shows a curious trend in glucose consumption rate. The consumption rate on a gRCM basis is initially steady at approximately 0.65 $gGlc.gRCM^{-1}h^{-1}$. Thereafter it shows a steady decline throughout the entire fermentation. This is probably due to either:

- uptake being limited by another nutrient, e.g. oxygen;
- a decline in the cell's general metabolic activity level. For example this may reflect PHB enzymes increasingly dominating the metabolism and a decline in the activity of glycolysis enzymes.

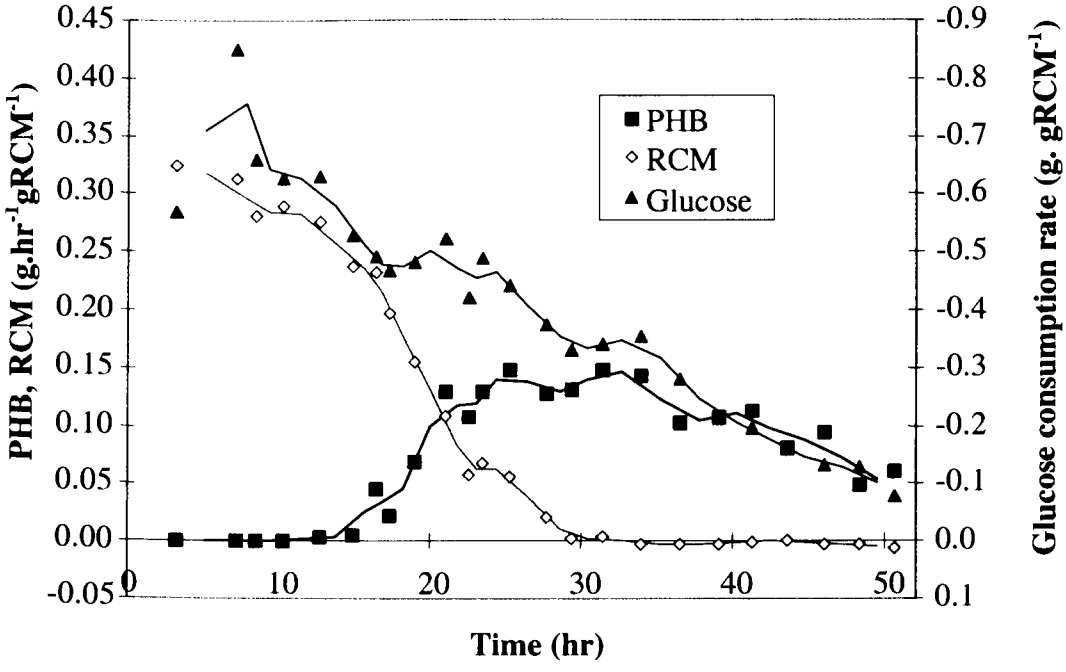

Figure 2.5: Production rates of PHB and residual cell mass (RCM), and consumption rate of glucose.

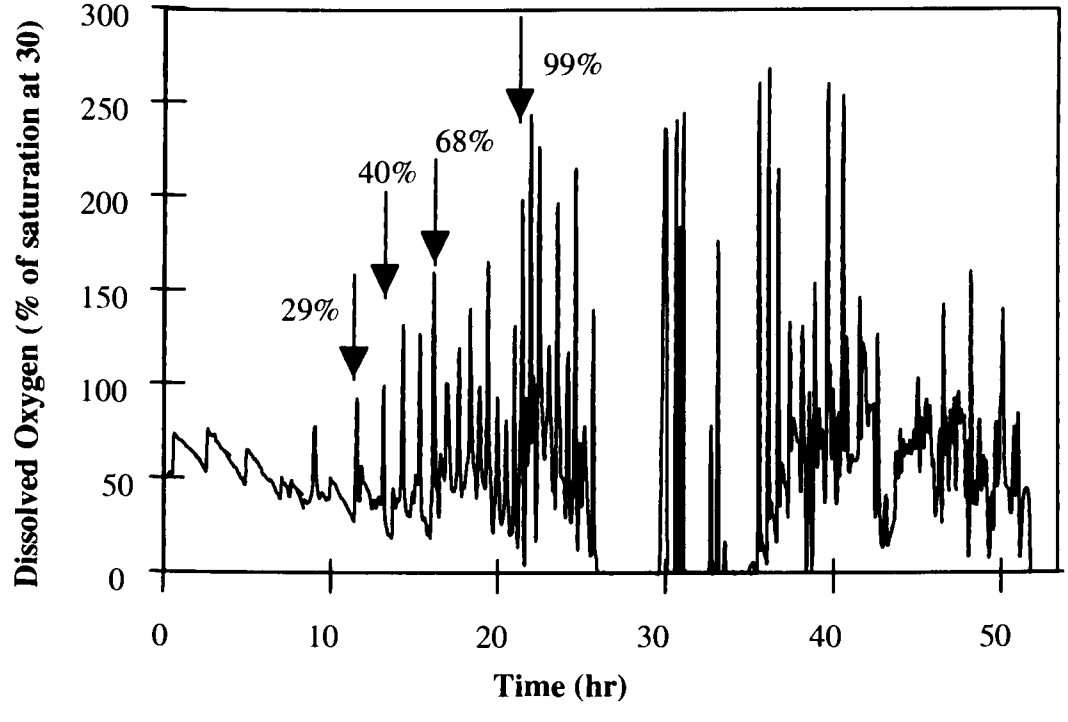

Figure 2.6: Dissolved oxygen profile. Arrows refer to an increase in the oxygen content of the inlet gas, from 21% to 28.8%, 40.4%, 67.5% and 98.5% respectively. Gas flowrate was constant at 4.0 L(STP).min^{-1} and the fermenter was operated at atmospheric pressure.

The dissolved oxygen profile (Figure 2.6) has a number of interesting features. The points marked with arrows indicate changes in the air to oxygen ratio of the feed- from 100:0 to 90:10, 75:25, 40:60 and 0:100 respectively. The large spikes are a result of the pH-stat nutrient feeding used: each time glucose exhausted there was a brief period before the next feeding pulse. During this time cellular oxygen demand is reduced, causing a rise in dissolved oxygen. From 26 h to 30 h oxygen demand was high enough that no spikes were observed.

Accurate quantification of the CO_2 production rate was difficult for several reasons:

- the mass-spectrometer readings drifted during the experiment but no periodic recalibrations were available to correct for it;
- the bottled oxygen contained a different level of inerts (N_2, Ar) than did the air, and during transition periods the levels took a long time to settle;
- the exhaust gas flowrate was not measured.

As a consequence the CO_2 profiles are possibly subject to appreciable systematic error. For the reasons outlined above, combined with insufficiently-accurate measurement of the inlet air-oxygen split, quantification of oxygen consumption was not possible.

Despite these difficulties, the trends in CO_2 production reveal interesting information. Likewise for the O_2 consumption, which can be estimated from flux analysis. These data are shown in Figure 2.7 and Figure 2.8. The total CO_2 production rate is quite noisy, and in particular there is a massive spike at hr 30. This is probably an artefact of some kind, but it is not possible to be certain. Figure 2.8 shows that CO_2 production on a gRCM basis is quite stable at 6 $mmol.gRCM^{-1}h^{-1}$ over hr 10-30, with a small rise at hr 22 corresponding to the switch to 98.5% oxygen feed. This indicates that the cells may have been slightly oxygen limited during this period, because otherwise the CO_2 rate should not have been affected by an increase in O_2 supply. This observation is supported by the O_2 consumption profile (gRCM basis), which shows a gradual decline in oxygen consumption over the period hr 7 - hr 20, despite the high dissolved oxygen concentration (Figure 2.6). Several possible explanations for this are:

- although the average dissolved-oxygen levels are adequate, the cells may be enduring repeated oxygen-limitation for short periods due to anaerobic 'dead zones' in the bioreactor;
- excessive oxygen is toxic to cells through production of oxygen radicals and superoxide ions (O_2^-) (Gennis and Stewart (1996)). The high inlet oxygen concentrations may hence be inhibiting uptake;
- cellular metabolic activity may be declining, as outlined above when discussing glucose consumption.

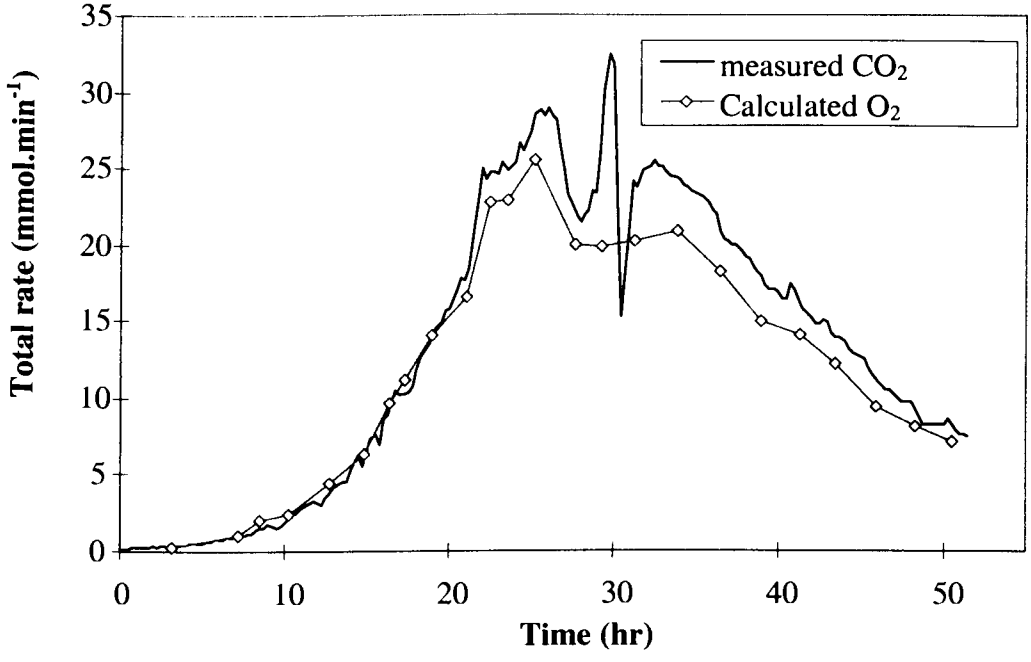

Figure 2.7: Measured CO_2 production rate and estimated O_2 consumption rate.

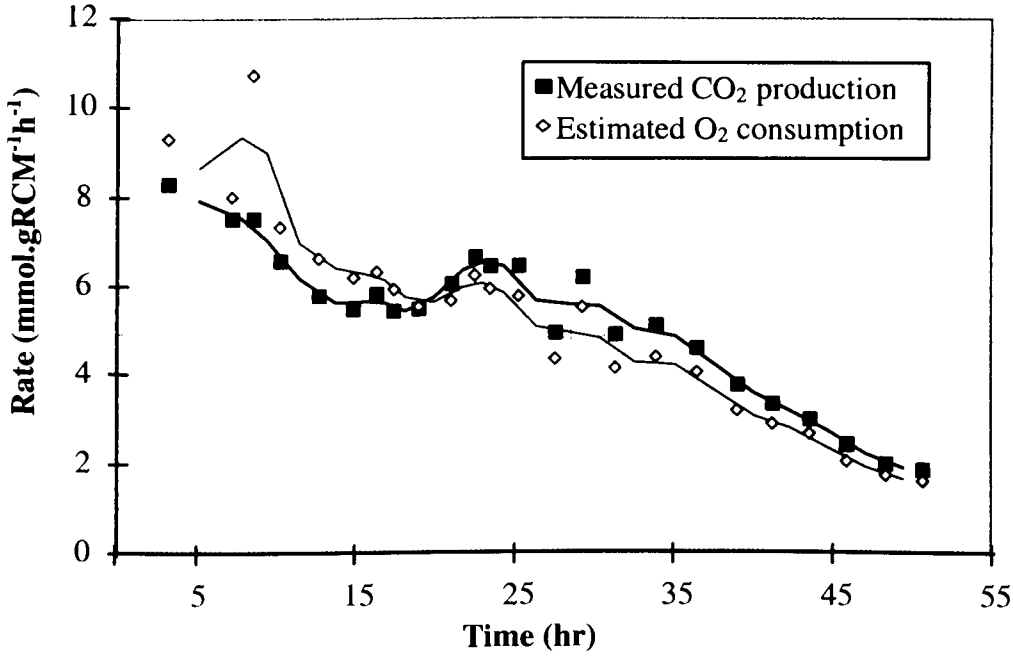

Figure 2.8: Measured CO_2 production rate and estimated O_2 consumption rate on a gRCM basis.

The organic acid profiles in Figure 2.9, Figure 2.10, and Figure 2.11 demonstrate some interesting trends. Formic acid excretion shows a rapid peak at hr 8, but thereafter maintains a low, quite steady production rate. At no point does it appear that reutilisation occurs. In contrast, acetic acid production is low for most of the fermentation. A brief surge occurs at hr 25-30, followed by several hours of reutilisation. Lactic acid shows the greatest variability in production rate. Coinciding with the acetic acid surge was rapid lactic acid production at hr

29, which was then quickly reassimilated. In general, lactic acid production rate appears to correlate quite well with acetic acid rate. There are several possible explanations for the spikiness of the lactic acid profile:

- the error in lactic acid measurements may have been much larger than for acetic acid, although sample replicates do not show this;
- lactic acid may be more sensitive to the fed-batch feeding method used, with lactic acid being produced during glucose-sufficient periods and reutilised upon glucose exhaustion.

It seems likely that the simultaneous rapid excretion of lactic and acetic acids during hrs 27-30 was caused by dissolved oxygen concentration reaching zero. Interestingly there was no apparent effect on formic acid production.

Negligible amounts of ethanol were produced during the fermentation.

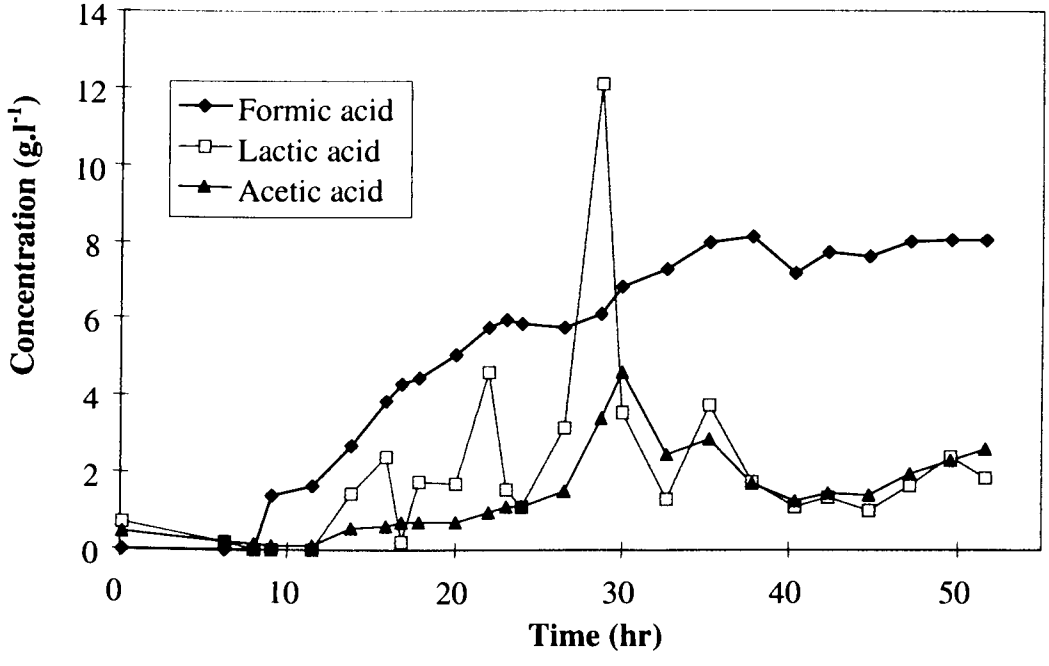

Figure 2.9: Medium concentrations of formic, acetic, and lactic acid.

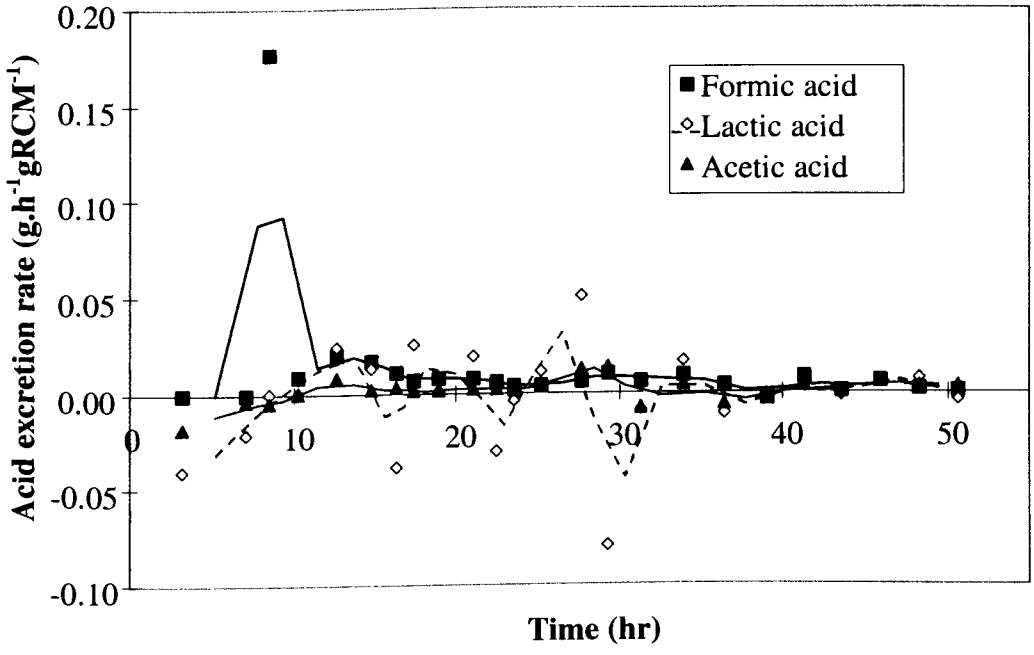

Figure 2.10: Specific production rates of formic, acetic, and lactic acid.

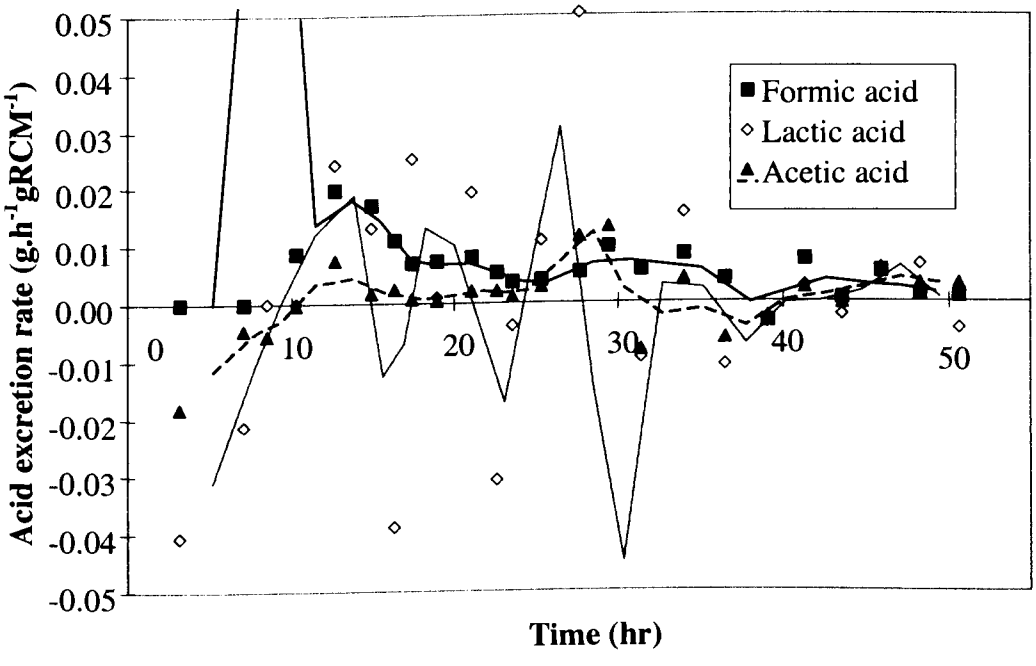

Figure 2.11: Enlarged view of the specific production rates of formic, acetic, and lactic acid.

2.6. Flux Analysis

As formulated, the flux network has one degree of redundancy, viz an overall carbon balance. Closure is excellent (typically 95% on a carbon-mol basis) over the middle period of the fermentation, between hrs 14 and 39. In the earlier stages there is consistent under-detection of products, typically 10% on a carbon-mole basis. Whereas in the final stages, excess carbon is produced (from 20-60%). This may reflect excretion and subsequent re-utilisation of some undetected metabolite, e.g. succinate. An overall mass balance on the fermentation is shown in Table 2.1, indicating some 5% excess carbon production. This must reflect a systematic error in one of the measurements, probably the CO_2 production rate. Closure is also abnormally poor for the two samples over hrs 24 to 29, where about 10% extra carbon is detected. In general the flux most likely to be affected by the poor closure is the TCA flux (5), which is rather sensitive to measured carbon dioxide production.

Glucose conversion to PHB is 49% (mol-C/mol-C), which is approaching the theoretical maximum of 66% (Yamane (1993)). RCM production accounts for most of the wasted 17%.

Table 2.1: Overall mass balance on fermentation.

	mol per 100 mol glucose	mol-C per 100 mol-C glucose
carbon dioxide	265	44
RCM (mol-C-equivalents)	63	10
PHB	74	49
acetic acid	1	0.3
formic acid	7	1.1
lactic acid	1	0.4
ethanol	0	0
	Overall closure:	105%

For the first 23 hours of the fermentation the residual biomass composition was approximately $CH_{1.7}O_{0.50}N_{0.19}$ (excluding PHB). Thereafter it gradually changed to $CH_{2.0}O_{0.65}N_{0.31}$ by the end of the fermentation. This may reflect elevated levels of RNA or plasmid DNA, all of which are high in nitrogen compared with other cellular components. However the error in the final composition is appreciable because of the high level of PHB which must be subtracted from the total cellular composition. The 90% confidence limits for the final RCM composition are $CH_{1.6}O_{0.62}N_{0.28}$ to $CH_{2.4}O_{0.68}N_{0.34}$. The variation in biomass composition is thus quite marked and may lead to moderate systematic flux errors, especially in the early stages when biomass production is rapid.

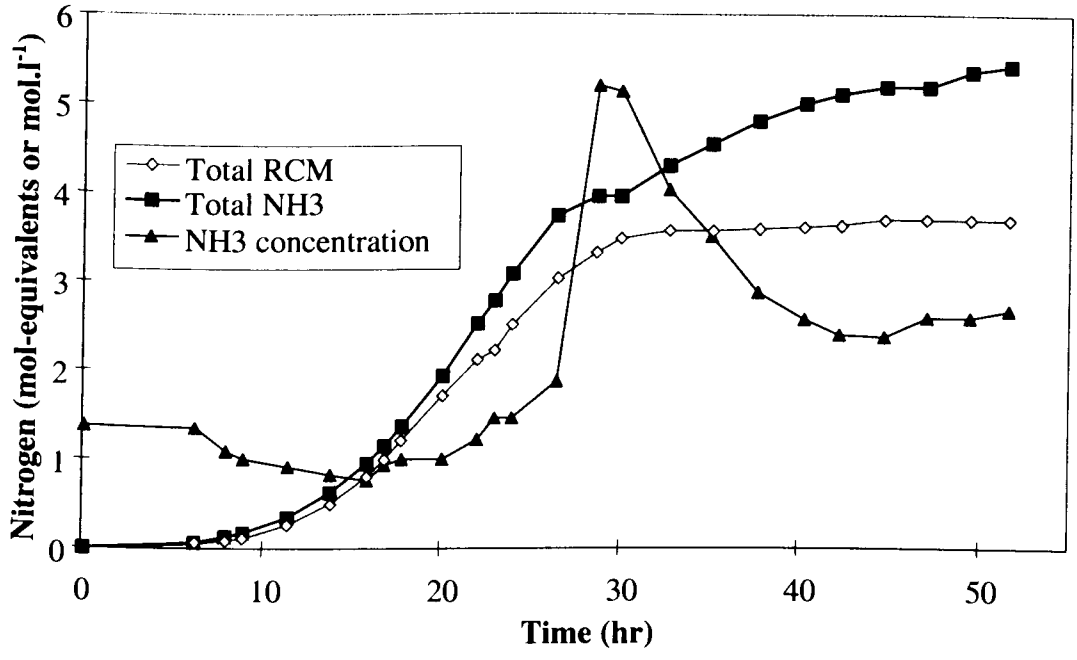

Figure 2.12: Nitrogen balance: broth ammonium ion concentration, total nitrogen present as ammonium ion, and total nitrogen present as residual cell mass.

Figure 2.12 shows that the nitrogen balance is adequate over the first 20 hours while cell growth was rapid (10-20% missing N-products). Interestingly, there is a brief plateau in nitrogen consumption near hr 30, when cell growth almost halted, and ammonia concentration rose from 1.9 $g.l^{-1}$ to 5 $g.l^{-1}$. The rise in broth concentration was caused by the rapid excretion of lactic and acetic acids, since NH_4OH was used for pH control. When cell growth ceased entirely (hr 30) the ammonia consumption rate increased dramatically. Thereafter the consumption rate remained high but the total cell mass nitrogen did not increase appreciably. Stripping of ammonia by the air seems unlikely since this did not occur in the early stages of the fermentation. There is also no evidence of it in the offgas mass-spectrograms. Production of stationary-phase excreted compounds is a possibility. Perhaps the most feasible explanation is that some of the cells are actively growing and hence using nitrogen, whereas other cells are lysing and releasing nitrogen in an undetected form (e.g. proteins). This explanation requires at least 35% lysis (on a mass basis), which is not unreasonable given that previous studies have shown extensive lysis at high cellular PHB content.

Sensitivity tests

In general, the biomass parameters (γ_A, γ_N, γ_P, and α_C) are a cause for concern because they are so poorly defined, and are rather variable due to changes in residual cell mass composition over the course of the fermentation. Several tests were performed to quantify the sensitivity of the fluxes to changes in these parameters, with the following results:

1. The NADPH requirement for biomass production (γ_P) was varied by a factor of two in each direction from the assumed 14.629 mmol per g RCM. During the early stages (hr 0-15), the corresponding variation in transhydrogenase flux (11) was often +/-60% of the glucose flux. The middle (hr 15-35) and late (hr 35-52) stages were less sensitive. The fluxes most

severely affected by changes to the NADPH coefficient are flux 11 and flux 9 (calculated oxygen usage).

2. Halving or doubling the biomass NADH coefficient (γ_N) changes flux 9 by about 100% of glucose flux in each direction, or +/- 25% of the calculated oxygen usage.
3. The ATP coefficient (γ_A) has a large effect on the ATP dissipation flux (10), which varies by about 200% of glucose flux.
4. The CO_2 coefficient (α_C) has negligible on fluxes.

The effect of biomass parameters is (as expected) greatest during the early stages. Thereafter their influence is reduced. In light of these inaccuracies, the ATP dissipation flux (10) and NADPH transhydrogenase flux (10) should be interpreted in a qualitative fashion only, particularly in the early stages.

The main fluxes of interest are the pyruvate-dehydrogenase flux (Flux 2), TCA cycle flux (Flux 5), NADPH transhydrogenase flux (Flux 11), and the ATP dissipation flux (Flux 10), as shown in Figure 2.13 and Figure 2.14. Pyruvate dehydrogenase shows a plateau from hrs 20 to 30, coinciding with the period of maximum PHB production. However both TCA flux and NADPH transhydrogenase flux show a steady decline over the same period. Transhydrogenase flux eventually drops to zero, implying that the NADPH requirement for PHB synthesis is being entirely supplied by the TCA cycle. Changes in oxygen levels, in particular the onset of oxygen limitation at hr 27-30, do not appear to have any effect on TCA cycle flux. This seems strange given the strong dependence of TCA-cycle-gene expression on oxygenation conditions. It may reflect systematic error in the cycle flux, which is quite feasible given that CO_2 measurement was difficult and that the calculated TCA flux is greatly influenced by the measured CO_2 rate. The ATP dissipation flux ranges between 15-30 $mmol.gRCM^{-1}h^{-1}$ from hr 8 - 30. The level of constancy is quite striking given the decline in most other fluxes over the same period. This may reflect an intrinsic demand of the cells for maintenance ATP, which cannot be satisfied from hr 30 onwards. However this is a tentative observation only.

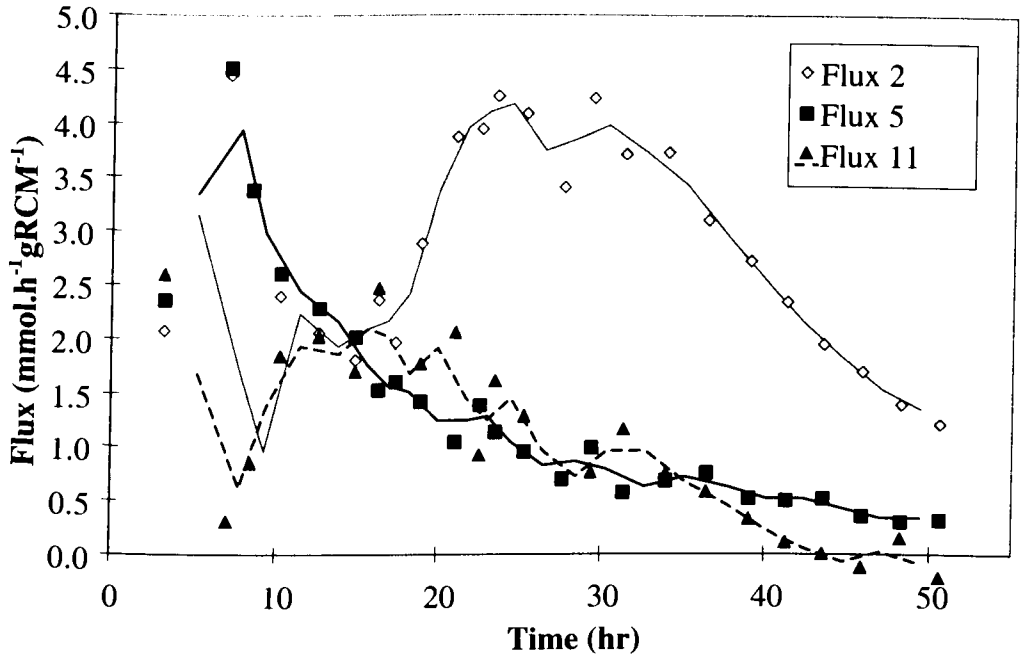

Figure 2.13: Pyruvate dehydrogenase flux (2), TCA cycle flux (5), and NADPH transhydrogeanse flux (11) on a gRCM basis, for the high-cell-density fermentation.

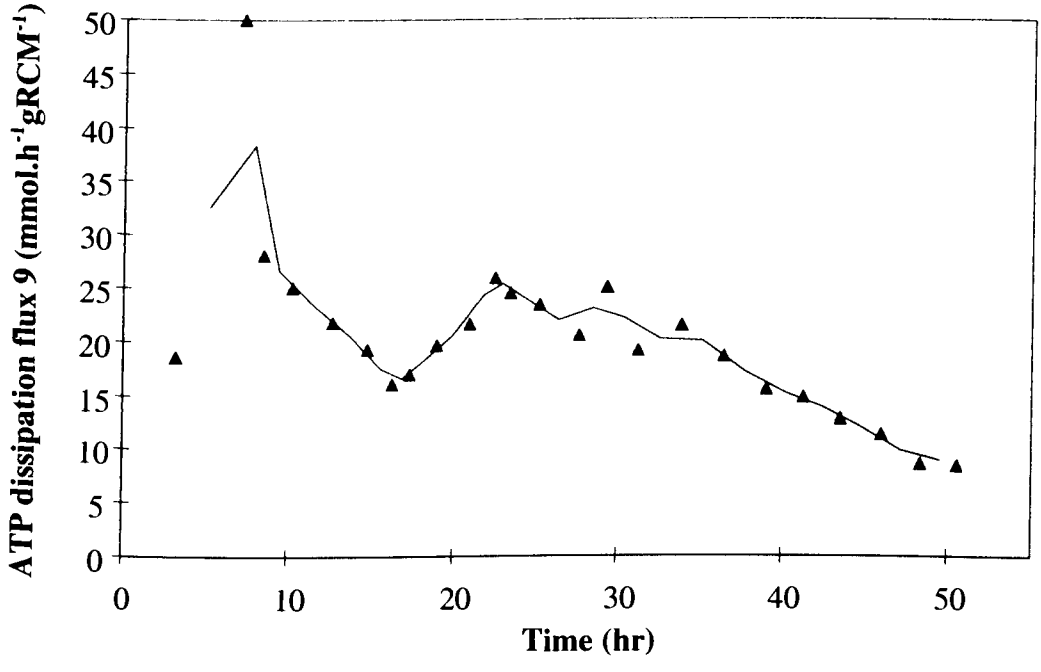

Figure 2.14: ATP dissipation flux (10) on a gRCM basis for the high-cell-density fermentation.

On a glucose basis, the fluxes reveal further information. In particular, PHB production reaches a peak proportion of the glucose uptake flux (about 85% mol/mol) by hr 30 and remains constant for the following 22 hrs. This may represent some maximum possible diversion of glucose to PHB, or conversely the glucose flux may be completely controlled by

the PHB flux. In either case the glucose and PHB fluxes are highly correlated. They are both declining on a gRCM basis from hr 35 onwards, so it seems likely that either:

- glycolysis enzyme activity is declining and preventing adequate supply of carbon for PHB synthesis;
- or PHB enzyme activity is declining, causing reduced glucose uptake.

Interestingly the TCA cycle flux remains fairly constant at 40-50% of the glucose uptake flux for the entire period hr 20 -hr 52. The significance of this is not clear.

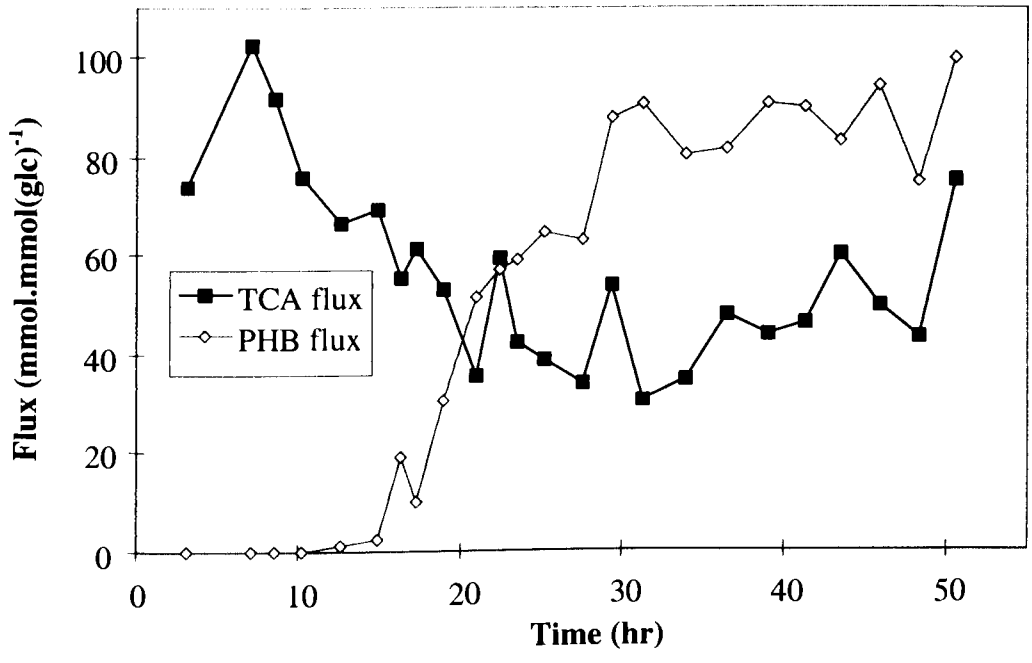

Figure 2.15: PHB flux (8) and TCA cycle flux (5) on a glucose-consumption basis for the high-cell-density fermentation.

2.7. Further Discussion

The fermentation appears to have a number of different phases, which can be roughly delineated as follows:

First phase, hr 0 - 15

Over this initial period, there is no appreciable PHB production. Cell growth is exponential, although it declines gradually from 0.3 $g.gRCM^{-1}h^{-1}$ to 0.25 $g.gRCM^{-1}h^{-1}$ over this period. At approximately hr 8, a surge in formic acid production occurred. This flux was unexpected because formate production is usually restricted to anaerobic conditions. After this initial rapid production, a low basal rate was maintained independent of the conditions. The reasons for these observations are not clear.

Second phase, hr 15 - 22

The start of this phase marks the onset of PHB production. By hr 22 it has reached its maximum of 0.14 $gPHB.gRCM^{-1}h^{-1}$. During the same period, RCM production rapidly declines to only 0.05 $g.gRCM^{-1}h^{-1}$. It is not clear what causes the onset of PHB production. It seems likely that the PHB production increase and RCM decline are related, however the underlying relationship between them is not evident. Several possible explanations are:

- The onset of PHB synthesis drains the supply of cofactors and precursors necessary for RCM synthesis, for example ATP, NADPH or carbon metabolites;
- The decline in RCM synthesis leads to an increase in PHB-enzyme levels, cofactor levels, and/or precursor levels. For example, the copy number of plasmids tends to increase when cell growth is slowed (Brendel and Perelson (1993)), causing the expression of recombinant genes to increase relative to chromosomal genes;
- An unknown third factor gives rise to both the observations, e.g. induction of a global regulation system.

Some excretion of lactic acid is observed during this phase, which was not expected because lactate production is generally observed only at low pH and under oxygen-limited conditions. Formate-hydrogen lyase and lactate dehydrogenase may have been activated by a high pyruvate concentration, caused for example by restricted flux through pyruvate dehydrogenase. There is also a low, constant level of acetic acid excretion which is probably due to overflow metabolism (i.e. the Crabtree effect).

Third phase, hr 22 - 30

Over this period the PHB production rate is constant. CO_2 production and estimated O_2 consumption are relatively constant on a gRCM basis, with a slight surge at hr 22 corresponding to a switch to bottled oxygen. For the first 4 h the RCM production remains approximately constant. However at hr 26, Figure 2.6 shows that oxygen limitation occurs. Simultaneously,

- the RCM production rapidly declines to 0 by hr 30, causing a dip in glucose uptake;
- rapid lactic acid excretion occurs;
- acetic acid production increases.

It therefore seems likely that the oxygen limitation causes rapid excretion of acids. These acids are swiftly reutilised at hr 30 when the oxygen supply becomes less restricted. The absence of ethanol secretion indicates that there is probably sufficient oxygen to maintain a low NADH/NAD ratio.

Fourth phase, hr 30 - 52

Once RCM production reaches zero, oxygen demand is reduced, as shown by the dissolved-oxygen concentration. PHB production remains steady for two hours, but thereafter begins a gradual decline on a gRCM basis. On a glucose basis it remains constant. The CO_2 production and O_2 consumption also decline gradually, despite ample oxygen supply. These observations suggest that the metabolism is in decline over this period. Once RCM synthesis ceases, the cell is no longer able to synthesise sufficient proteins. Hence the enzymes gradually degrade. Nielsen and Villadsen (1994) used the catabolic activity of nitrogen-deprived lactic acid bacteria to estimate the halflife of proteins at 10 h. This corresponds rather well to the observed decline in glucose uptake rate over the period hr 32 - 52. These results suggest that the decline in PHB synthesis during the fourth phase may be due to degradation of cellular enzymes after cellular maintenance of them has ceased. The nitrogen and RCM data suggest that cell lysis may be occurring, which is entirely feasible given the high levels of cellular PHB.

2.8. Conclusions

2.8.1. Improvement of PHB Production

The flux data suggest several ways in which PHB production could be improved:

- The production of formate is undesirable except perhaps under anaerobic conditions. Although it does not directly reduce the efficiency of PHB production, it may inhibit cell function, especially during the growth phase. It may also indicate a restriction through pyruvate dehydrogenase. Lactate excretion should theoretically not be necessary, and is possibly caused by a restricted flux to acetyl-CoA (and hence PHB). If the causes of excessive excretion could be removed, then PHB productivity would likely be improved.
- In the later stages the TCA cycle appears to divert a large proportion of carbon flux from PHB, presumably to supply sufficient ATP for cell maintenance. It would be interesting to test whether PHB productivity could be improved by restricting TCA cycle flux during this period.
- A significant amount of nitrogen "went missing" during the later stages of the fermentation. It would be interesting to restrict the supply of nitrogen in this period. If the nitrogen is being used to generate stationary-phase/stress metabolites then efficiency would be improved if this was prevented. However if cells are lysing and being balanced by continued growth of new cells, then restricting nitrogen would lead to reduced PHB yield. Such a study would help to resolve the question of disappearing ammonia.
- The existing plasmid system for PHB production is poorly controlled. This may be causing the poor efficiency and low initial growth rates, for example due to the metabolic burden imposed by a high copy number plasmid. Use of a vector with controlled copy number may thus improve the fermentation, by reducing the amount of time taken to reach high cell density.
- A significant disadvantage to the current fermentation protocol is the pure oxygen required. Hence using air and allowing the culture to become semi-anaerobic could provide substantial benefits. During this fermentation the dissolved oxygen concentration dropped to zero for four hours, but PHB production did not appear to be significantly impaired. Unfortunately the flux data suggest that the oxygen depletion may have caused rapid lactate and acetate excretion. Although the direct effect on carbon efficiency was negligible, lactate and acetate can inhibit cellular function and thus indirectly reduce PHB production rate and efficiency. Further experiments are required to investigate system performance under more severely oxygen-limited conditions.

2.8.2. Difficulties to be Overcome in Future Experiments

The design of further experiments in this thesis (Chapters 4, 5, and 6) is guided by the results of this chapter. The major difficulties encounted during Chapter 2 are outlined below:

- Neither this experiment nor the literature have identified the cause(s) of the onset of PHB production in *E. coli*. This is a fundamental aspect of the PHB fermentation and as such requires further study.
- Rather poor mass-balance closure was obtained for some samples, indicating that some compounds may be missing from the analysis. They may play a significant role and as such should be identified.
- During some periods of the fermentation, the metabolism was changing too rapidly for the spacing of the sampling periods used. During intervals of rapid change the samples should be taken at least once per hour.

- The problems with offgas analysis need to be overcome, for two reasons. Firstly, the errors in CO_2 production lead to large errors in the estimated TCA cycle flux. Closure of the mass balance was also greatly impaired. Secondly, measuring the oxygen consumption rate would not only directly quantify changes in cellular oxygen demand, but would also provide an extra redundancy check on the data.
- The cells' apparent response to a short period of oxygen limitation (viz cessation of RCM synthesis and rapid excretion of organic acids) does not bode well for future attempts to reduce oxygen supply. The effects of oxygen limitation should be studied in more detail, because the existing data do not show them clearly.

2.8.3. Directions for Remaining Chapters

This chapter has developed a suitable metabolic flux model for PHB production by recombinant *E. coli*, verifying its suitability with preliminary fermentation test data. These fermentation data are used again in Chapter 3 to give the necessary mass-balance data for an economic analysis. Chapters 4, 5, and 6 also use the data as the basis for a more rigorous and repeatable experimental protocol. The metabolic flux model is also refined and applied in more depth to further fermentation data.

Chapter 3

3.1. Summary

The selling price of poly-hydroxyalkanoate (PHA) is near US1995$16 kg^{-1}, compared with less than US1995$1 kg^{-1} for conventional polymers. Significant price improvements are therefore necessary to encourage widespread usage. The aim of this chapter is to estimate the potential production cost of PHA using recombinant *E. coli*, and highlight areas of key sensitivity where research will have the most benefit. The analyses will then be used to set experimental objectives for Chapters 5 and 6.

Based on an annual production of 5000 tonnes of poly-hydroxybutyrate (PHB) from a glucose minimal medium, the break-even selling price per kilogram of plastic is US1995$4.88. A ten year plant life, 40% tax rate, 10% discount rate and a conservative process design based on existing technology are assumed. This cost is highly sensitive to PHB expression level and recovery strategy, and moderately sensitive to medium cost, cell growth yield on glucose, and cellular oxygen demand. Use of oxygen-enriched air is not economically attractive. At the same level of production, the cost can theoretically be reduced to US1995$3.38 kg^{-1} by using dairy whey as a replacement for glucose as the carbon source. However for the seasonal production profile of a typical cheese factory the actual price was only reduced to between US1995$4.54 kg^{-1} and US1995$4.67 kg^{-1}. Further refinements to the process may make modest price improvements, however it seems unlikely that the cost can be reduced to less than US1995$3 kg^{-1} without fundamental modifications. At this price PHB and PHBV are not likely to be competitive with conventional polymers unless strong consumer preference or government legislation fall in their favour.

The economic analysis identifies key directions for further research as:
- investigating the use of inexpensive substitutes for glucose;
- quantifying the differences between poly-(hydroxybutyrate-co-hydroxyvalerate) (PHBV) production and PHB production;
- investigating the cellular response to oxygenation conditions, and reducing the peak cellular oxygen demand;
- improving control of the fermentation, in particular onset of PHA accumulation.

3.2. Introduction

3.2.1. General Introduction

As reviewed in Chapter 1, commercially-produced PHBV is marketed under the name "BIOPOL". It is used to manufacture disposable items such as shampoo bottles, disposable razors and food trays. The market price of BIOPOL is around 1995US$16 per kilogram compared with less than $1 per kilogram for conventional commodity plastics (Poirier *et al.* (1995)). Thus the price difference on a typical 17 μm shopping bag (6.6 g each) is $0.09, and for a 1 mm injection moulded shampoo bottle (60 g) it is $0.84. Obviously, PHA cannot be a serious competitor to more traditional polymers such as polyethylene (PE) and polyethylene terepthalate (PET) or other biodegradable alternatives (e.g., poly-lactic-acid PLA) until its price is substantially reduced. There are many research groups around the world focussing on this goal. However, without due attention to the production process as a whole, efforts to optimise each step individually will waste much effort and result in overall suboptimality. The best approach for reducing PHA cost can only be identified using economic analysis. The purpose of this chapter is therefore to estimate the production cost of PHA using *E. coli*, identify key areas where improvements will have a large impact, and indicate which tradeoffs (e.g., cell density vs fermentation time) will reduce production cost. This is then used to set the direction for the remainder of this thesis.

There are numerous economic analyses of biochemical processes in the literature, for example (Petrides *et al.* (1989); Petrides *et al.* (1995); Middelberg (1996)). In particular, the economics of PHA production have been analysed previously, for PHB/PHBV (Choi and Lee (1997); van Wegen *et al.* (1998)) and for long-chain PHA (de Koning *et al.* (1997)). However in each case the available experimental data for the fermentation were incomplete and of poor quality, leading to uncertainty in the analysis. This chapter draws on data from Chapter 2, which accurately quantifies the performance and requirements of the fermentation step.

3.2.2. Whey and Whey Permeate

Cheese whey is a major byproduct of the dairy industry (Zall (1992)). In 1988 in the US, 26 million metric tons of whey were produced, and only 50% of this was put to useful purpose (mainly human & animal feed). The remaining 50% was disposed of as a pollutant with high BOD, at considerable expense (Hsu and Yang (1991)). Estimated worldwide production of whey is 130 million tonnes and has a growth rate of 3% per year (Zall (1992)). Australian cheese industry produces 1.5 million tonnes per year of dairy whey (Zadow (1992)).

Physically, whey is the watery fluid that remains after removing the coagulum from milk, as in cheese manufacture. There are several major categories of whey, based on the conditions under which it is produced:

- sweet whey, produced by rennet-type enzymes at pH 5.6;
- acid whey, produced by acidification to below pH 5.1;
- salt whey, produced from the manufacture of cheddar cheese, which contains high levels of salt (around 6-8%).

The composition of whey varies quite significantly with a number of factors, especially

- season of the year;
- the species of animal producing the milk;
- the type of cheese being manufactured.

It contains mainly lactose, plus small amounts of lactate, protein, and minerals, with traces of fat. Table 3.1 shows the typical analyses of different types of dairy whey.

Table 3.1: Solids content of whey according to various sources, wt%.

Type of Whey	Source	Lactose	Proteins	Fat	Minerals	Lactate	Other
Sweet	A	4.4%	0.7%		0.5%		
Sweet	B	3-4.5%	<0.05%			0.15-0.42%	
Acid	A	4.1%	0.7%		0.7%		
Acid	B	5%	0.3%			1%	
Acid	C	5%	1%		1%	0.1-0.8%	
Salt	D	4.6%	1.1%	0.7%	7%		ash 2%
Synthetic	E	16 $g.l^{-1}$	5 $g.l^{-1}$ yeast extract		0.25 $g.l^{-1}$ K_2HPO_4 0.05 $g.l^{-1}$ $MnSO_4$		5 $g.l^{-1}$ trypticase

Sources: A = Zall (1992), B = Yang *et al.* (1995), C = Hsu and Yang (1991), D = Zall (1992), E = Lewis and Yang (1992)

One of the uses for dairy whey is production of whey protein concentrate (WPC), often used as a food additive. This is produced by passing the whey through an ultrafiltration unit, giving two fractions:

- the retentate (WPC);
- the permeate, "deproteinised whey".

The whey proteins are too large to pass through the filter membrane, whereas the lactose and salt readily do so. The ratio of lactose to water in each fraction is the same as in the feed. Thus, the deproteinised whey is essentially whey without the proteins, and WPC is effectively whey with increased protein content. WPC can be marketed fairly profitably on its own, however the deproteinised whey must still be disposed of.

3.2.3. Process Description

This section outlines the basic process for PHA production, as described in the literature.

Fermentation

Until several years ago the available strains of PHA-producing recombinant *E. coli* were not suitable for large-scale production. Most literature examples of high yield PHA fermentations were with complex media (e.g. Luria-Bertani broth), which is not economically viable. However the XL1-Blue(pSYL107) system has since been developed by Lee and co-workers (Wang and Lee (1997)), and has high productivity on minimal medium as demonstrated in Chapter 2. The relevant fermentation data from Chapter 2 are used to model the large-scale bioreactor (viz consumption rates of glucose, nitrogen, and oxygen, and production rates of PHB, residual cell mass, and organic acids).

As mentioned in Chapter 1, the PHA of most industrial interest is PHBV. PHBV is generated in the same manner as PHB, except that propanoic acid is added to the medium during the fermentation. The toxicity of propanoic acid causes reduced cell yield and PHA percentage and consequently PHBV will be more costly than PHB. Unfortunately there remains very little large-scale experimental data for PHBV production. For this reason, the following economic analysis focuses on PHB production only. Apart from the fermentation step, all

other process operations are identical for both PHB and PHBV. The PHBV break-even selling price should therefore be similar to PHB selling price in terms of its sensitivity to process variables.

Recovery

After fermentation the contaminating cell components must be separated from the PHA granules. In particular, contaminating proteins and nucleic acids give PHA an offensive odour, cause decolouration during thermal processing, and can be allergenic, limiting the PHA's usefulness. The acceptable levels of these contaminants are listed as 1-2% w/w for protein, 2-4% for RNA, and 0.2-0.3% for DNA (Harrison (1990)). However it should be noted that PHA of this purity would probably not be suitable for use as food packaging, due to the possible allergenic nature of the contaminants, unless their leach rate was very low. No studies in the literature could be found which discuss these requirements.

A number of PHA recovery methods have been suggested which can meet the purity requirements given above. Most of them are restricted to laboratory use, and are technically and economically difficult to scale-up. PHA solubilisation methods such as chloroform extraction can achieve high PHA purity (Doi (1990b)). However, they require large quantities of toxic and volatile solvent, which obviously has adverse environmental consequences and also raises total production cost. Hypochlorite or sodium hydroxide treatments for the digestion of non-PHA cell materials hold promise as cheap recovery methods compared to solvent extraction (Berger *et al.* (1989); Lee *et al.* (1995a)). A chloroform and hypochlorite dispersion method has also been suggested (Hahn *et al.* (1994)). However, extensive work is still required to optimise these processes before large-scale use, particularly with respect to minimising solvent use.

The PHA granules themselves do not contain appreciable amounts of contaminant. Hence high-purity PHA can be produced by processes that wash the granules instead of dissolving them. An industrial method for PHB recovery described by (Harrison (1990)) is based on detergent and enzyme digestion of non-PHB cell materials after PHA release by homogenization, coupled with extensive centrifugation. Hydrogen peroxide is also incorporated into the extraction process to further remove nucleic acids and protein. This causes a reduction of PHB molecular weight to some extent. The complexity and cost of this treatment regime raises total recovery cost. The PHA obtained is also of a relatively low quality.

Homogenization and centrifugation are common unit operations in bioprocessing. A PHA extraction process combining homogenization, disc-stack centrifugation, and sodium hypochlorite treatment has recently been developed (Ling *et al.* (1997); Ling (1999)). It achieves a high PHA recovery and purity, and is well suited to large-scale operation. The main process steps are shown in Figure 3.1.

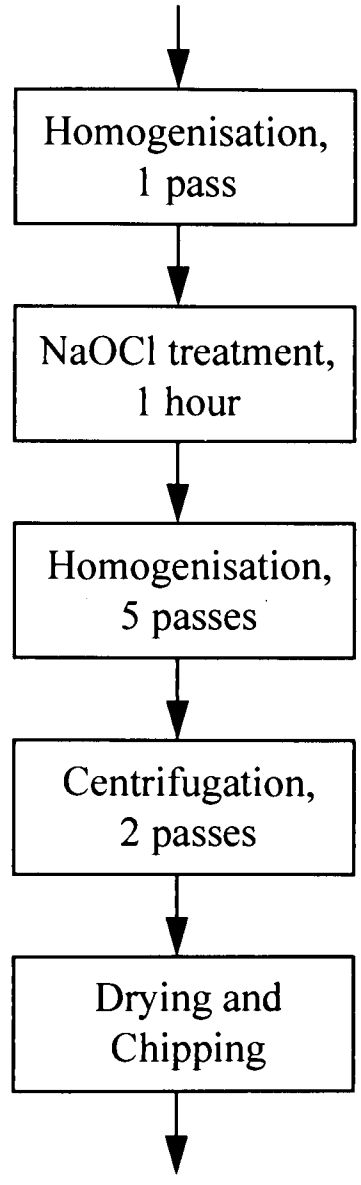

Figure 3.1: Block Diagram for the downstream purification and recovery of PHB.

The recovery process was developed and validated on pilot scale by Ling (1999). As described in the thesis, a low cell concentration (4.3 $g.l^{-1}$ DCW) was employed in the homogeniser feed because only limited material was available (Ling (1999)). However, a higher cell concentration (40 $g.l^{-1}$ DCW) would be employed at production scale because disruption efficiency is relatively insensitive to feed concentration (Kleinig *et al.* (1995)).

The recovery process begins with a single homogenization pass to release PHA granules from the cells. The PHA sludge is then resuspended in buffer, and treated with NaOCl (0.085% w/v active chlorine) for 1 hour at ambient temperature. The major benefit of this step is DNA degradation, giving reduced broth viscosity and enhanced effectiveness of downstream steps (in particular centrifugation). It also enhances protein and RNA removal, by an unknown mechanism.

After digestion, a further five homogeniser passes are performed to micronise cell debris and further reduce broth viscosity, both of which improve centrifuge separation efficiency. Two centrifugation passes are then employed to remove soluble contaminants and cell debris. In developing the process, a low centrifuge feed concentration was again employed because of limited material. In practice, a higher feed concentration would be used, since centrifuge performance decreases only slightly with feed concentration. For example, Wong (1996) concluded that "diluting homogenate at a fixed feedrate can slightly improve (protein) inclusion body recovery, but not its purity". The maximum centrifuge feed concentration for the first pass is 50 $g.l^{-1}$ DCW. The subsequent pass can tolerate a higher solids loading (estimated at 70 - 75 $g.l^{-1}$) because most of the nucleic acids have been removed and hence broth viscosity is greatly reduced.

The experimentally determined PHA recovery and purification after each centrifuge pass are detailed in Table 3.2 An analysis of the final PHA purity confirmed low contaminant levels following this recovery process (protein = 0.32% w/w, DNA = 0.06% w/w, 95.3% w/w cell debris removal).

Table 3.2: Results of PHB fractionation from the optimised recovery process (Ling (1999)).

Process Step	Cumulative		Per pass	
	Cell debris removal	PHB recovery	Cell debris removal	PHB recovery
NaOCl treatment and homogenisation	3.5%	98.7%	3.5%	98.7%
First pass centrifugation	88.4%	93.3%	88.0%	94.5%
Second pass centrifugation	95.3%	91.8%	59.5%	98.4%

The final recovery step is drying using a drum-dryer. Other processes have used spray-dryers (Harrison (1990)) however this is not necessary because unlike many pharmaceuticals PHB is not thermally sensitive below 180 °C. An extruding chipper is then used to create polymer chips for use in conventional injection-moulding machines.

3.3. Process Design and Costing

3.3.1. Process Flowsheet

Figure 3.2 shows the Process Flow Diagram for the PHB production plant used in this economic analysis. The five main sections are feed pretreatment, fermentation, homogenisation, centrifugation, and drying. In order to reduce equipment cost, two bioreactors operate in parallel and several storage tanks are used. The simplified batch schedule diagram is given as Figure 3.8 in Section 3.4.1.

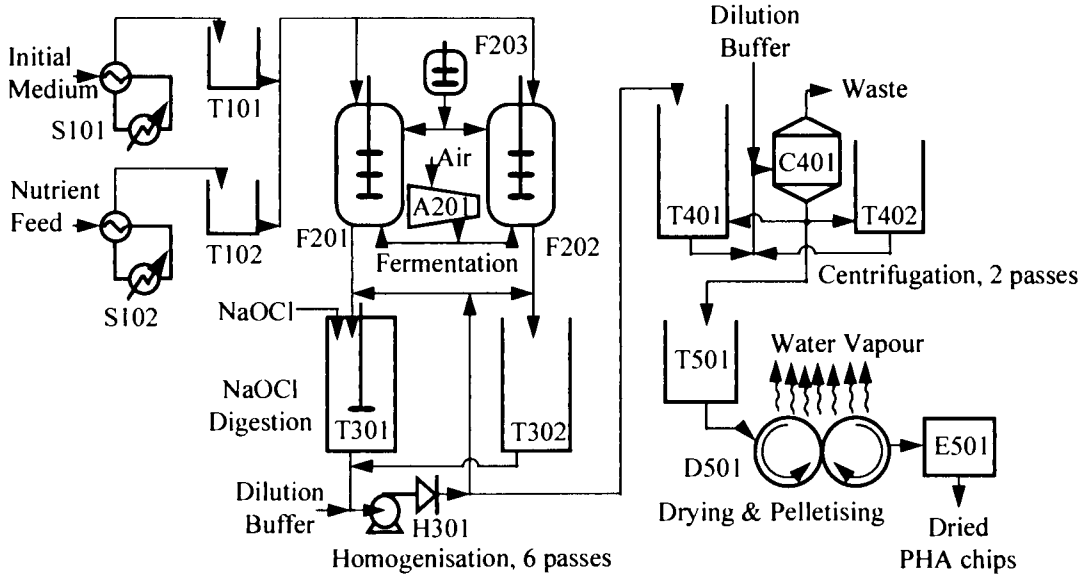

Figure 3.2: Process flow diagram for the PHA production plant employed in this analysis.

The initial batch of medium (20 $g.l^{-1}$ glucose, 22 g KH_2PO_4, 3 g $(NH_4)_2HPO_4$, 0.7 g $MgSO_4.7H_2O$, 0.8 g citric acid plus trace elements) is continuously sterilised by S101 and stored until needed in Tank T101. Similarly the nutrient feed (700 $g.l^{-1}$ glucose + 15 $g.l^{-1}$ $MgSO_4.7H_2O$) is continuously sterilised by S102 and stored in Tank T102. Over a two hour period, bioreactor F201 is filled from T101 and then inoculated from the inoculum bioreactor F203 to an initial cell density of 2 $g.l^{-1}$. The temperature is 30 °C. Air is supplied by compressor A201. F201 is fed with pulses of nutrient solution from Tank T102 as necessary to maintain carbon source concentration above zero. Ammonia gas is used for pH control. After 46 hours the cell density is 82 $g.l^{-1}$ and the cells contain large PHB granules, amounting to 78% of total dry cell mass. F201 is drained into T302 over two hours. After a two hour cleaning period, the fermentation cycle begins again. F202 undergoes the same batch cycle as F201, offset by 26 hours.

The broth in T302 is diluted to 40 $g.l^{-1}$ dry cell weight with buffer (1.4 $g.l^{-1}$ KH_2PO_4, 6.5 $g.l^{-1}$ NaCl), then homogenised by H301 and stored in T301. At this point sodium hypochlorite is added to give 0.085%w/v active chlorine, and the cells are digested for 1 hr. Then the broth is again homogenised by H301 and stored in T302. A further four homogeniser passes are conducted, using T301 and T302 as storage. Finally on pass 6 the homogenate is transferred to T401. One hour is provided between each pass, and the 6 passes take a total of 26 hours.

As T401 fills, the 6th pass homogenate is centrifuged by C401 and the solids (150 $g.l^{-1}$) are passed to the tank T402 for storage. Supernatant is sent to a waste treatment facility. The solids stream is diluted with buffer to 70 $g.l^{-1}$ DCW and centrifuged again, passing the solids to T501. Supernatant is sent to a waste treatment facility. An hour is provided between each centrifuge pass, and a total of 26 hours is required to complete the two passes.

The double drum dryer D501 operates continuously, drawing solids from T501. After drying, the powder is fed to the continuous extruder E501 and then chipped.

3.3.2. Economic Analysis

All costs in this chapter are given in 1995US$. Where necessary, costs were converted using the Marshall and Swift Index (MSI) for equipment, the Producers index for chemicals, and the Consumer Price Index (CPI) for miscellaneous costs (See Table 3.3). The plant location is assumed to be the United States and thus has a location factor of 1.

Table 3.3: Economic indices for selected years (Various (1995)).

	Marshall and Swift Equipment Cost Index	Producers Index	Consumer Price Index
1995	1032	385.4	167.6
1990	915.1	-	-
1987	813.6	-	129.7
1986	-	336.5	-
1977	505	-	-

3.3.3. Design and Costing of Equipment

Each item of equipment was sized as described in the following sections.

Fermentation

The relevant fermentation data from Chapter 2 are shown in Table 3.4.

Table 3.4 - Fermentation data from Chapter 2.

	initial	final	increase per litre of final broth
time (h)	5.7	51.7	(46 h)
volume (ml)	1605	6905	768 $ml.l^{-1}$
glucose consumed (g)	11.0	3457	499 $g.l^{-1}$
oxygen consumed (mol)	0.0	46.3	6.71 $mol.l^{-1}$
ammonia consumed (g)	0.9	92.3	13.2 $g.l^{-1}$
PHB produced (g)	0.0	1219	176.5 $g.l^{-1}$
RCM produced (g)	2.0	345	49.7 $g.l^{-1}$

RCM (residual cell mass) is defined as dry cell weight minus PHB weight.
(95% of the observed increase in volume is due to the nutrient feeding).

This fermentation profile can be "scaled" to different final cell densities by assuming that all production and consumption rates remain unchanged on a residual-cell-mass basis. This is a reasonable assumption provided that control of PHB production is possible. The volume of

nutrient fed vs initial-medium volume can be calculated by mass balance using Equation 3.1 and Equation 3.2:

$$V_{nutrientfeed} = \frac{m_{total} - C_{initial} V_{final}}{C_{nutrientfeed} - C_{initial}} \tag{3.1}$$

$$V_{initial} = V_{final} - V_{nutrientfeed} \tag{3.2}$$

where

V	= volume per batch (kl)
C	= glucose concentration (kg.kl^{-1})
m_{total}	= per-batch mass of glucose used during fermentation (kg)

When substitution of whey is considered (assuming that the mass-basis yield of PHB and cell mass on lactose is the same as on glucose), calculation of relative volumes is similar but more involved. There are three main cases to be considered, depending on the available lactose per batch, $m_{lactose}$.

Case 1: $m_{lactose} \leq V_{initial} C_{initial,lactose}$

In this case, the bioreactor is initially charged with the available whey, then diluted to the necessary initial volume with water. Nutrient feeding is by glucose. A mass balance gives Equation 3.3:

$$V_{nutrientfeed,glucose} = \frac{m_{totalcarbonsource} - m_{lactose}}{C_{nutrientfeed,glucose}} \tag{3.3}$$

Case 2: $V_{initial} C_{initial,lactose} < m_{lactose} \leq m_{totalcarbonsource}$

There is now sufficient whey to charge to the required initial volume, with extra left over for nutrient feeding in concentrated form. When the surplus is exhausted the remaining carbon source is supplied by glucose nutrient feeding. The relative quantities are given by Equation 3.3 and Equation 3.4 .

$$V_{nutrientfeed,lactose} = \frac{m_{lactose} - C_{initial,lactose} V_{final}}{C_{nutrientfeed,lactose} - C_{initial,lactose}} \tag{3.4}$$

Case 3: $m_{lactose} > m_{totalcarbonsource}$

Under this scenario no glucose feeding is required at all. The volume of nutrient-fed lactose is

$$V_{nutrientfeed,lactose} = \frac{m_{totalcarbonsource} - C_{initial,lactose} V_{final}}{C_{nutrientfeed,lactose} - C_{initial,lactose}} \quad (3.5)$$

The Chapter 2 fermentation requires the addition of thiamine and ampicillin. The cost of thiamine is negligible, however it would not be economic to use ampicillin on a large scale. The PHB plasmid contains genetic elements that maintain plasmid stability in the absence of antibiotic selection (Lee (1994)), hence it is assumed that ampicillin would not be required for large scale production.

The basis is an annual PHB production level of 5000 tonnes. Given the PHB yield in Table 3.4 and the calculated downstream recovery of PHB (see below), this sets the volume of broth required per year. The batch cycle time is known, so applying a 1.1 integration factor to account for unscheduled downtime and occasional reduced throughput gives the number of batches per year.

The final broth volume per 52 h-batch is calculated from

$$\text{batch size} = \frac{\text{broth volume per year}}{\text{batches per year}} \quad (3.6)$$

and the fermentation data can then be used to estimate

- the volume of initial medium required per batch;
- the amount of nutrient feed required;
- the weight of ammonia gas utilized;
- the total RCM produced;
- the oxygen requirements.

The bioreactor size is calculated using Equation 3.7

$$\text{bioreactor size} = \frac{\text{52h batch size}}{\text{number of bioreactors} \times \text{working volume fraction}} \quad (3.7)$$

where the working volume fraction is 75% (Bartow (1999)). Minimum cost for this process occurs if two bioreactors are used in parallel. Care must be taken to avoid confusion between the 52 h batch size and the batch size per bioreactor.

The bioreactors are constructed from 304L stainless steel which is adequate for a commodity product like PHB. Instrumentation and associated fittings are incorporated into the Lang factor (see Table 3.7). A single seed bioreactor is used, with a working volume 5% that of each large bioreactor. The maximum cell density achieved in the seed bioreactor is 40 $g.l^{-1}$ dry cell weight.

The level of stirring required is high, at 2 $kW.m^{-3}$ (Kalk and Langlykke (1986)). This is necessary due to the high cell densities involved and the need for good oxygen mass-transfer (see the section below on compressor requirements).

Heat transfer at such high cell densities is likely to be a problem. The rate of heat transfer required can be calculated from a heat balance over the entire reactor, i.e.

$$Q_{transfer} = \sum_{\text{all compounds}} \dot{n}_i \Delta H_i \tag{3.8}$$

where

$Q_{transfer}$ = heat removal via exchanger surfaces (kW.kl(broth)$^{-1}$)

$\dot{n}_i$ = net consumption rate of the ith compound (i.e. glucose, PHB, etc) (mol.s^{-1}kl(broth)$^{-1}$)

ΔH_i = heat of combustion of the ith compound at 30 °C, approximately equal to the standard heat of combustion. (kJ.mol^{-1})

Negligible specific heat is associated with nutrient addition, ammonia addition, and the gas streams.

Nielsen and Villadsen (1994) provide a method to estimate the heat of combustion if it is not known (PHB, RCM), viz

$$\Delta \hat{H}_c^\circ = 115\kappa^* \tag{3.9}$$

where

$\Delta \hat{H}_c^\circ$ = standard heat of combustion (kJ.(mol-C)$^{-1}$)

κ^* = "degree of reduction"

For a compound with chemical formula $CH_aO_bN_c$, κ^* is calculated as $\kappa^* = 4 + a - 2b$. Table 3.5 shows the known and calculated heats of combustion for each of the reactants and products in the fermentation.

Table 3.5: Known and calculated heats of combustion for the fermentation products and substrates.

	formula	κ^*	$\Delta \hat{H}_c^\circ$ (kJ.(mol-C)$^{-1}$)	ΔH_c (kJ.mol^{-1})
Glucose	$C_6H_{12}O_6$			2803
PHB	$C_4H_6O_2$	4.5	517.5	2070
RCM	$CH_{1.9}O_{0.55}$	4.8	552	552
NH_3	NH_3			383
Formic acid	CH_2O_2			255
Acetic acid	$C_2H_4O_2$			875
Lactic acid	$C_3H_6O_3$			1367
(oxygen)	O_2			0
(CO_2)	CO_2			0
(H_2O)	H_2O			0

The experimental data are used to estimate heat production on two bases:

- production per unit volume, used for heat-exchanger-area estimates;
- total production, used to estimate total cooling load.

Figure 3.3 shows the results of these calculations.

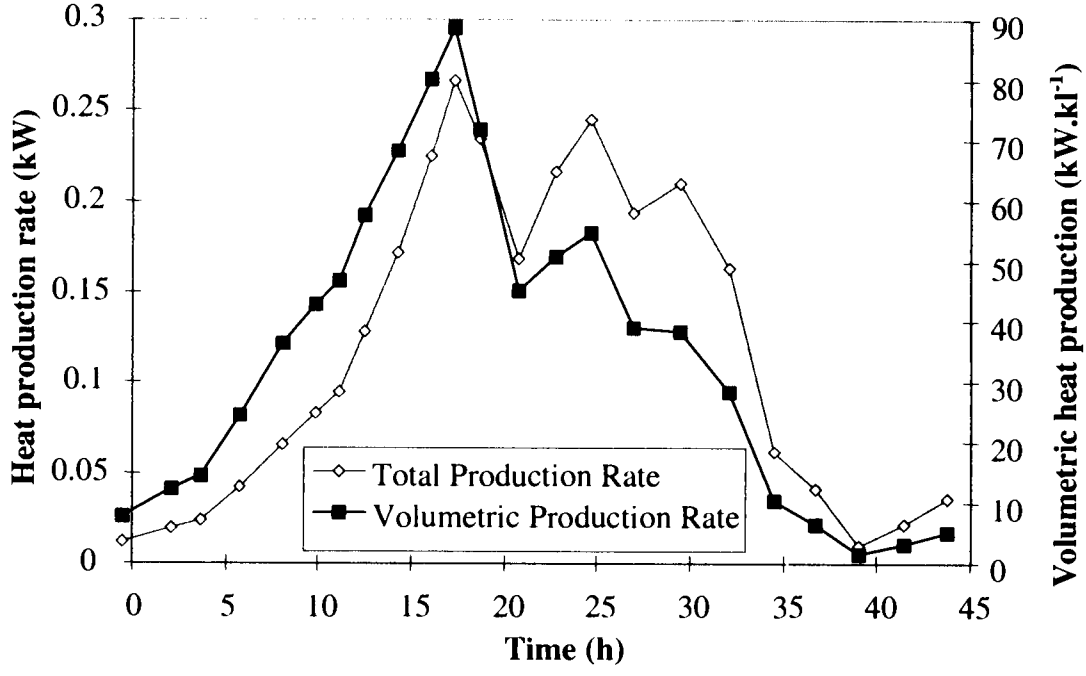

Figure 3.3: Heat production during the Chapter 2 fermentation (6.9 l final volume), on a total basis and a volumetric basis.

The maximum overall heat production rate was around 250 W for the 6.9 l fermentation, or 36 kW per kl of final broth volume. The peak volumetric heat production rate was between 70-80 $kW.kl^{-1}$, which is very high. This level of heat removal will be difficult to achieve in a large scale bioreactor.

The required heat exchanger area per kl of broth can be estimated from Equation 3.10 and Equation 3.11

$$q = UA\Delta T_{lm} \tag{3.10}$$

$$\Delta T_{lm} = \frac{\Delta T_2 - \Delta T_1}{\ln(\Delta T_2) - \ln(\Delta T_1)} \tag{3.11}$$

where

q = heat removal rate ($kW.kl^{-1}$)

U = overall heat transfer coefficient, assumed 2.4 $kW.m^{-2}K^{-1}$ (Peters and Timmerhaus (1991))

A = heat-exchanger area ($m^2.kl^{-1}$)

ΔT_{lm} = log mean temperature driving force (K)

ΔT_1 = temperature difference of entering cooling water (10 K = reactor temperature 30 °C - cooling water 20 °C)

ΔT_2 = temperature difference of exiting cooling water (assumed 5 K)

This gives a required area of 4.3 $m^2.kl^{-1}$, which is rather high. For example, to achieve this with 5 cm diameter tubes they would need to be spaced at 17 cm grid intervals. Similarly, a dimple-plate system seems possible but this is not certain. Another alternative would be to circulate the reactor contents to an external heat exchanger but this would probably cause difficulties with oxygen supply. No data in the literature could be found giving a maximum feasible heat-exchanger area for bioreactors.

Assuming that a bioreactor can be designed to meet these specifications, the capital cost of this tubing or plates is only 5-10% of the total bioreactor cost, and has been neglected.

Sterilisers

The size of S101 is calculated given the initial medium required per 52-h-batch (See fermentation design, Section 3.3.3), and assuming continuous operation. Likewise S102 is based on the required nutrient feed per 52 h-batch. Process steam is used as a heat source, requiring approximately 0.1 kg of steam per kg of liquid sterilised (Kalk and Langlykke (1986)).

Compressors and Pressure-Swing-Adsorption equipment

Sizing of compressor A201 is fairly complicated because it depends on several inter-related variables. The fermentation data from Chapter 2 can be used to obtain an oxygen demand profile. Three pertinent parameters from the profile are

- total oxygen usage, used to calculate compressor running costs;
- maximum oxygen usage rate ($mol.h^{-1}$), used to calculate maximum required flowrate;
- maximum volumetric oxygen usage rate ($mol.l^{-1}h^{-1}$), which is used when choosing stirrer power, operating pressure, and enrichment of the air supply.

The Chapter 2 oxygen demand is shown in Figure 3.4, on both a Total Usage Rate basis and a Volumetric Usage Rate basis.

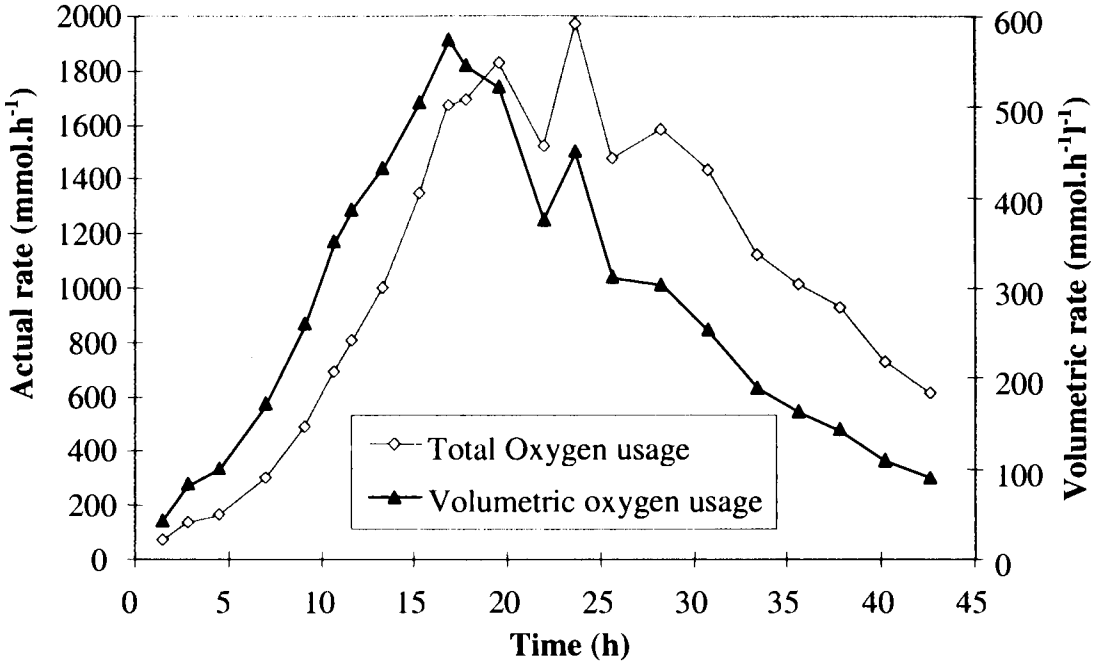

Figure 3.4: Oxygen usage rate and volumetric oxygen usage rate, for the Chapter 2 fermentation (6.9 l final volume).

At any point in the fermentation, Equation 3.12 gives the average oxygen partial pressure required to achieve the volumetric oxygen transfer rate, viz

$$N_{O2} = k_L a\left(\frac{P_{O2}}{H_{O2}} - C_{O2,broth}\right) \tag{3.12}$$

where

N_{O2} = consumption rate (=mass transfer rate) of oxygen (mmol.l(broth)$^{-1}$h^{-1})

$k_L a$ = volumetric mass transfer coefficient of oxygen (h^{-1})

P_{O2} = average partial pressure of oxygen in the gas phase (kPa)

$C_{O2,broth}$ = molar concentration of oxygen in the broth (mmol.l(broth)$^{-1}$)

H_{O2} = Henry's law constant for oxygen (kPa.l(broth).mmol^{-1})

H_{O2} can be calculated at the bioreactor temperature using Equation 3.13, yielding a value of 86 kPa.l(broth).mmol^{-1} at 30 °C (Royce and Thornhill (1991)).

$$H_{O2} = \exp\left(12.74 - \frac{133.4}{T - 206.7}\right)\Big/1000 \tag{3.13}$$

where

T = temperature (K)

The necessary inlet gas oxygen partial pressure can then be calculated from Equation 3.14:

$$P_{O2,inlet} = \frac{P_{O2}}{\left(1 - f/2\right)} \tag{3.14}$$

where

f = fraction of inlet oxygen which is utilised, assumed 20% from Chapter 2 data.

and Equation 3.15 gives the necessary inlet oxygen composition:

$$P_{O2,inlet} = P_{bioreactor} \times X_{O2,inlet} \tag{3.15}$$

where

$P_{bioreactor}$ = operating pressure (kPa)

$X_{O2,inlet}$ = oxygen mole fraction in inlet air

From Figure 3.4 above the maximum volumetric oxygen usage rate is approximately 550 mmol.l(broth)$^{-1}$h^{-1}. Typical values of $k_l a$ for large bioreactors are 1.0 -5.0 min^{-1} (Doran (1997); Atkinson and Mavituna (1987)), so assuming the best possible design we obtain a value of 5.0 min^{-1}. Under high-demand conditions the broth oxygen concentration is nearly zero. This gives an estimate for P_{O2} = 155 kPa, and hence $P_{O2,inlet}$ = 172 kPa. Assuming a maximum bioreactor design pressure of 3 bar (Atkinson and Mavituna (1987)), Equation 3.15 indicates that the inlet air must be enriched to at least 57% oxygen. Enrichment of this kind is possible using pressure-swing-adsorption (PSA) or vacuum-pressure-swing-adsorption (VPSA) systems. This involves passing air at elevated pressure (typically 5 bar) through a bed of zeolite. Nitrogen is preferentially adsorbed to the zeolite, giving an oxygen-enriched product. Once the adsorption capacity of the zeolite is reached, flow switches to a second bed in parallel whilst the first bed is regenerated by venting to atmosphere. The enriched exit air is typically 85% oxygen.

It may also be possible to reduce the necessary oxygen enrichment by increasing stirrer power or bioreactor pressure, but without experimental data it is difficult to know whether this is feasible or not.

A given inlet oxygen is obtained by blending enriched air from a PSA unit (85% oxygen) with unenriched air, as shown in Figure 3.5.

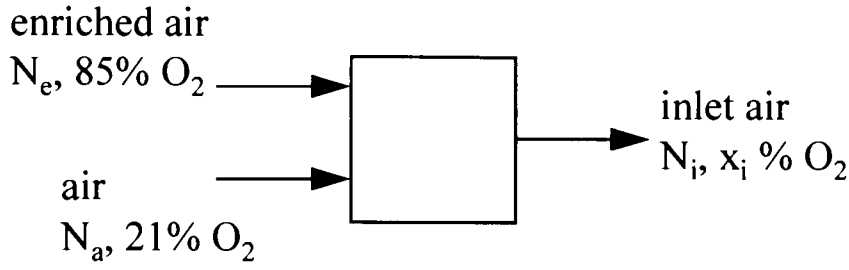

Figure 3.5: Blending of enriched air and unenriched air to obtain a bioreactor gas supply of appropriate oxygen composition. N is molar flow, x is mol fraction.

A mass balance therefore gives

$$N_e = N_i \frac{x_i - 0.21}{0.85 - 0.21} \tag{3.16}$$

and

$N_a = N_i - N_e$

where

N_a = molar flow of air (mol.s^{-1})

N_e = molar flow of enriched air with 85% oxygen content (mol.s^{-1})

N_i = molar flow of gas to bioreactor (mol.s^{-1})

x_i = molar composition of gas to bioreactor

N_i is calculated from the fermentation data using Equation 3.17

$$N_i = \frac{N_{O2}}{f} \tag{3.17}$$

In conjunction with the Chapter 2 fermentation data, these equations give the required supply profile for oxygen enriched air as shown in Figure 3.6.

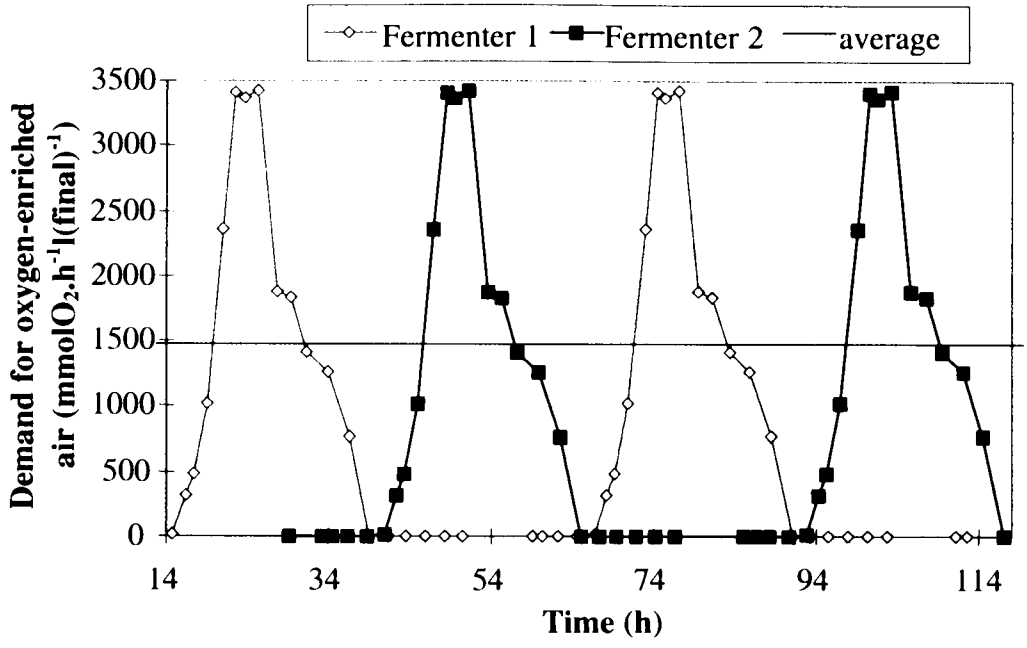

Figure 3.6: Required supply profile of oxygen-enriched air (85% oxygen) based on the Chapter 2 fermentation, assuming two bioreactors operating in parallel. The basis used is the final volume of broth in each bioreactor (3.95 l).

The PSA equipment required is sized on the basis of peak oxygen supplied ($kgO_2.h^{-1}$), as obtained from Figure 3.4. It is not feasible to average this out by storing oxygen either as compressed gas or in liquid form. The compressors for supplying unenriched air are sized on the basis of peak "brake" power, i.e. the power supplied by the driving motor. For isentropic compression the ideal power is given by Equation 3.18 (Peters and Timmerhaus (1991)):

$$W_{air} = \frac{k}{k-1} \times n_{air} \times R \times T \times \left(\left(\frac{P_2}{P_1} \right)^{\frac{(k-1)}{k}} - 1 \right) \qquad (3.18)$$

where

W_{air} = ideal power (W)

k = ratio of gas specific heat at constant pressure to gas specific heat at constant volume, 1.395 for air.

n_{air} = molar flow of gas ($mol.s^{-1}$)

R = gas constant ($8.314\ J.K^{-1}mol^{-1}$)

T = intake gas temperature (K), assumed 20 °C

P_1 = intake gas pressure (bar) = 1 bar

P_2 = delivery gas pressure (bar)

The delivery pressure is set at the bioreactor operating pressure plus 2 bar, to allow for pressure drops and liquid head. The compressor brake power is then calculated from the adiabatic power by assuming 80% efficiency (Peters and Timmerhaus (1991)). Electricity

requirements for compression of unenriched air are calculated from brake power by assuming an electric motor efficiency of 92.5% (Perry *et al.* (1984)). The electricity requirements for the PSA unit are calculated in a similar manner, assuming that the unit compresses its intake air to 5 bar, and that bed pressure drops are negligible.

Homogeniser

The costing of homogeniser H301 is straightforward, based on the processed flowrate. The ideal power consumption equals the product of pressure drop and volumetric flowrate, viz

$$W_{\text{homogeniser}} = \Delta P \times Q_{\text{homogeniser}} \tag{3.19}$$

The electricity requirement is then obtained by assuming a pump efficiency of 90% (Peters and Timmerhaus (1991)) and an electric motor efficiency of 92.5% (Perry *et al.* (1984)).

Centrifuges

The size of centrifuge C401 is governed by the necessary effective settling area, which is calculated from the volumetric flowrate by assuming a constant ratio of flowrate to area, viz Q/Σ. The recovery procedure developed by Ling (1999) used a Q/Σ of $3.5\text{x}10^{-9}$ m.s^{-1} and $4.0\text{x}10^{-9}$ m.s^{-1} for pass 1 and 2 respectively. However these are very conservative estimates for two main reasons. Firstly, the small solid-bowl centrifuge used for this work had highly non-ideal hydrodynamics, giving reduced performance (Wong (1996)). Large scale centrifuges closely approach the ideal and operate at Q/Σ values as high as $7\text{x}10^{-9}$ m.s^{-1} for relatively small protein inclusion bodies (Middelberg (1996)). Secondly, the PHA granules used in developing the process were approximately 0.85 micron mean Stokes diameter, whereas more typical values are 1.13 micron to 1.25 micron (Middelberg *et al.* (1995)). An estimate of 1.19 micron is therefore more realistic. By Stoke's law Q/Σ is proportional to the square of the particle diameter. Hence, applying these two corrections gives conservative Q/Σ values of $1.3\text{x}10^{-8}$ m.s^{-1} and $1.45\text{x}10^{-8}$ m.s^{-1} for pass 1 and 2 respectively. The sensitivity to this parameter is moderate, as established subsequently in Section 3.4.2.

The electricity requirements for the centrifuges are determined from a literature reference (Petrides *et al.* (1989)), viz

$$W_{C\cdot} = W_{C\cdot ref} \times \frac{Q_{C\cdot}}{Q_{C\cdot ref}} \tag{3.20}$$

where

$W_{C\cdot}$ = centrifuge power requirement (kW)

$Q_{C\cdot}$ = centrifuge flowrate ($m^3.h^{-1}$)

$W_{C\cdot ref}$ = reference power requirement (kW) = 27 kW

$Q_{C\cdot ref}$ = reference flowrate (m^3h^{-1}) = 1.6 m^3h^{-1}

Dryer

The double-drum dryer used for this process (D501) is costed on the basis of the required drum area. The water evaporation rate is calculated from a mass balance given the known density of PHB granules, viz

$$\dot{m}_{water} = \rho_{water}\left(Q_{dryer} - \frac{\dot{m}_{solids}}{\rho_{solids}}\right) \tag{3.21}$$

where

$\dot{m}_{water}$ = water evaporation rate ($kg.s^{-1}$)

ρ_{water} = density of water ($kg.m^{-3}$) = 1000 $kg.m^{-3}$

Q_{dryer} = flowrate to dryer ($m^3.s^{-1}$)

$\dot{m}_{solids}$ = mass flowrate of solids to dryer ($kg.s^{-1}$)

ρ_{solids} = density of solids ($kg.m^{-3}$), approximately 1180 $kg.m^{-3}$ for PHB (Horowitz and Sanders (1995))

Assuming a specific evaporation rate of $9x10^{-3}$ $kg.m^{-2}s^{-1}$ (Keey (1978)) gives the required drum area. Steam utilisation is calculated assuming a thermal efficiency of 55%, viz 1 kg of steam is required to evaporate 0.55 kg of water (Keey (1978)).

Extruder and Chipper

The cost of this unit is based on the mass processed per hour. Electricity costs are negligible.

Storage tanks and Reactor

All tanks are made from 304 stainless steel and are sized based on the mass balance volumes (see Section 3.4.1), assuming 20% ullage. (i.e. the liquid volume is 80% of the tank volume). Gentle agitation (0.1 $kW.m^{-3}$ for 26 h per 52 h-batch) is required in tanks T302, T401, T402, and T501 to prevent settling. More vigorous agitation (0.2 $kW.m^{-3}$ for 26 h per 52 h-batch) is required in the reactor tank T301. The level of NaOCl in digestion tank T301 is sufficiently low that corrosion does not pose significant problems, and all NaOCl is consumed by the end of the hour (Ling (1999)).

Whey pre-concentrator

One of the options to be explored in this chapter is replacement of the nutrient glucose feed by preconcentrated dairy whey or whey permeate. For the level of production in this study, a thermal-vapour-recompression (TVR) evaporator is the most suitable option. Such a system would require about 0.1 kg of steam per kg of water vaporised (information obtained from local supplier). The concentration achieved is limited to 200 $g.l^{-1}$, viz the solubility of lactose. There are a number of other salts present in dairy whey (see Section 3.2.2) that may precipitate out at these levels, however this should not present any design problems.

Miscellaneous

The capital and operating costs of pumps are negligible compared to the other equipment items. The cost of other small items is incorporated into the Lang Factors, shown in Table 3.7.

Capital Costs

The capital cost correlations used to estimate equipment purchase cost are shown in Table 3.6. In the case of centrifuges and dryers the correlation capacity limits were exceeded, so that (for example) a required settling area of 663 000 m^2 would require 4 centrifuges of 160 000 m^2 plus a fifth centrifuge of 23 000 m^2. This introduces discontinuities in the marginal cost and can severely affect sensitivity analyses. Hence the cost of multiple dryers and centrifuges was linearly regressed to give new cost equations without this problem.

Table 3.6: Cost correlation coefficients for major equipment items.

Item	cost in 1995US$	scaling variable X	Capacity Limits	Source
Bioreactor	$22480+1267X$	volume (kl)	0.4-380	D
Homogeniser	$10^{4.85} \times X^{0.43}$	inlet flowrate (m^3h^{-1})	?	B
Centrifuge	$10^{3.69} \times X^{0.33}$	effective area (m^2)	-160k	B
	$66430+1.606X$	effective area (m^2)	>160k	F
Unstirred tanks	$10^{3.65} \times X^{0.56}$	volume (kl)	0.4-380	A
Double Drum Dryer	$10^{4.58} \times X^{0.37}$	drum area (m^2)	4.8-46	C
	$44231+3239X$	drum area (m^2)	>46	F
Compressor	$10^{2.85} \times X^{0.94}$	brake power (kW)	75-3200	A
Pressure-Swing-Adsorption unit	$10^{4.24} \times X^{0.6}$	oxygen production ($kgO_2.h^{-1}$)	near 1250 only	E
Continuous Steriliser	$10^{4.97} \times X^{0.6}$	flowrate (m^3s^{-1})	?	B
Continuous Extruder & Pelletiser	$10^{3.46} \times X^{0.6}$	mass flowrate ($kg.h^{-1}$)	near 500 only	E
Whey evaporator	$10^{4.89} \times X^{0.6}$	water evaporation ($kg.h^{-1}$)	near 500 only	E

The sources for the correlations are: A (Peters and Timmerhaus (1991)), B (Middelberg (1996)), C (Peters and Timmerhaus (1991)), D (Atkinson and Mavituna (1987)), E (local supplier, corrected to USA), F linear regression (See text)

The total fixed capital cost and required working capital were estimated from the total equipment purchase cost, using the Lang Factors for a fluid processing plant (see Table 3.7). Based on the breakdown of Lang Factor into instrumentation cost, piping cost, etc, it was estimated that about 67% of the direct capital cost consists of depreciable equipment.

Table 3.7: Fixed capital estimation using Lang Factors (Peters and Timmerhaus (1991)).

equipment purchase cost:	100%
installation, ancillary equipment, site upgrade etc:	+246%
total direct cost:	346%
indirect costs, contractors fee, contingency:	+137%
total fixed capital investment:	483%
working capital:	+86%
startup expenses:	+43%
total capital investment:	612%

Operating Costs

These can be broken into several main categories, viz labour, maintenance, utility, waste treatment, and media plus chemicals costs.

The cost of labour is shown in Table 3.8. In addition to the base salaries, there are associated supervisory costs, labour burden (superannuation, insurance etc), and general overheads (facilities for workers). Assumed labour requirement is three shifts per day with two process workers per shift.

Table 3.8: Calculation of labour costs (Peters and Timmerhaus (1991)).

Labour	base salary	\$16.77 h^{-1}worker^{-1}
	plus supervisory labour	x115%
	plus labour burden	x125%
	plus general overheads	x160%
	(total):	x230% = \$38.57 h^{-1}worker^{-1}

Annual maintenance is estimated as (Peters and Timmerhaus (1991))

- 4.8% of the fixed capital investment for labour costs plus associated overheads;
- 3% of the fixed capital investment for materials.

The two major utilities used are steam and electricity. Appreciable cooling water is also used but the cost is not significant. Electricity cost is calculated given the power requirements of the bioreactors, compressors, PSA unit, homogenisers, centrifuges and tank stirrers, as shown in the sections above. The price of electricity is \$55 per MWh, as supplied by the Electricity Trust of South Australia and corrected to US1995 currency: this value was used because the estimates available for US-supplied electricity were highly variable and also out of date. Steam is used by the dryer, sterilisers, and whey pre-concentrator, and costs US1995\$20 per ton (Kalk and Langlykke (1986)).

Waste treatment costs are also appreciable. The cost for a given effluent is treated as the sum of a volume-based cost (US1995\$0.22 kl^{-1}), a solids-loading cost (US1995\$0.26 kg^{-1}), and a phosphate cost (US1995\$0.26 kg^{-1}) (Middelberg (1996)).

The cost of media and chemicals are detailed in Table 3.9.

Table 3.9: Cost of media and chemicals (1995US$) (Atkinson and Mavituna (1987); Kalk and Langlykke (1986); Petrides *et al.* (1995)).

	Cost
glucose syrup	\$0.539 kg^{-1}
$(NH_4)_2HPO_4$	\$1.432 kg^{-1}
$MgSO_4.7H_2O$	\$0.859 kg^{-1}
citric acid	\$2.600 kg^{-1}
KH_2PO_4	\$1.432 kg^{-1}
NaCl	\$0.115 kg^{-1}
NaOCl (12.5% active Cl)	\$0.280 l^{-1}
$(NH_4)_2SO_4$	\$0.115 kg^{-1}
other salts, trace metals	(negligible)
ammonia gas	\$0.720 kg^{-1}

General Economic Parameters

The tax rate is 40%. Straight-line depreciation with a ten year write-off period is used. Working capital is required in year 0 and is recovered at the end of the plant life. Startup expenses are incurred in year 1. Salvage value is assumed negligible. A plant life of 10 years is assumed, with a discount rate of 10%. This conservative discount rate is chosen because it reflects a 'no-risk' time value of money and thus represents the true cost of the process. To account for risk, companies sometimes use a substantially higher discount rate for their analysis, 25% or more. There are better methods for handling risk, but nevertheless the effect of discount rate is examined further in Section 3.4.2.

The net present cost to produce PHB is calculated on a year-by-year basis, where for each year:

cost = fixed capital outlay + operating expenses + startup expenses + working capital – tax credit

and

$$\text{tax credit} = \text{tax rate} \times (\text{operating expenses} + \text{startup expenses} + \text{depreciation})$$

The effective cost per kg of PHB is then obtained using the following equation:

$$\text{Cost per kg} = \frac{\sum_{i=0}^{10}\left[(\text{Cost for year i}) \times \left(\frac{1}{1+\text{discount rate}}\right)^{i}\right]}{(1-\text{tax rate}) \times (\text{total kg of PHB produced}) \times \sum_{i=0}^{10}\left(\frac{1}{1+\text{discount rate}}\right)^{i}} \qquad (3.22)$$

This is the price for which the PHB must be sold in order to break even, taking the time value of money into account.

3.4. Results and Discussion

3.4.1. Base-Case Results

The "base-case" for this chapter is as follows:

- the fermentation data are scaled back by a factor of 2.77 to avoid the need for oxygen enrichment of the air, as described in Section 3.3.3. This gives a final cell density near 80 $g.l^{-1}$;
- no whey is used;
- the fermentation duration is 46 h, giving a total batch time of 52 h.

The mass balance is shown in Figure 3.7, and the batch schedule is in Figure 3.8. A breakdown of the NPV cost is shown in Figure 3.9. Table 3.10 and Figure 3.10 show the size and cost of major equipment items. The effective production cost of PHB is 1995US$4.88 per kg over the 10 year lifetime of the plant. Estimates of the type conducted in this chapter generally have an accuracy within ±30%.

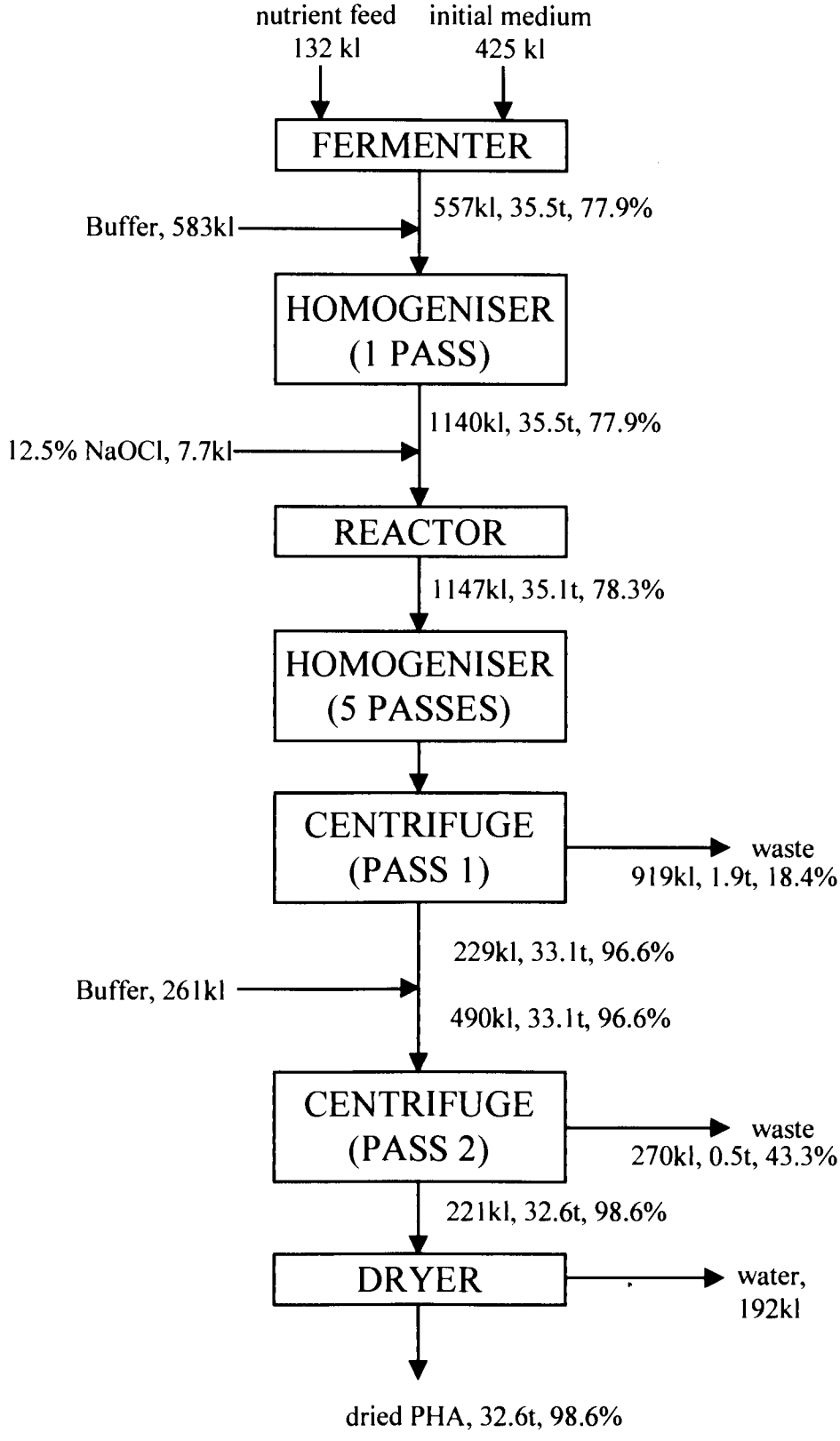

Figure 3.7: Mass balance for the base-case plant, basis is 1 full batch (52 hours). Volume in kl, mass of PHB in metric tons, PHB purity in %w/w.

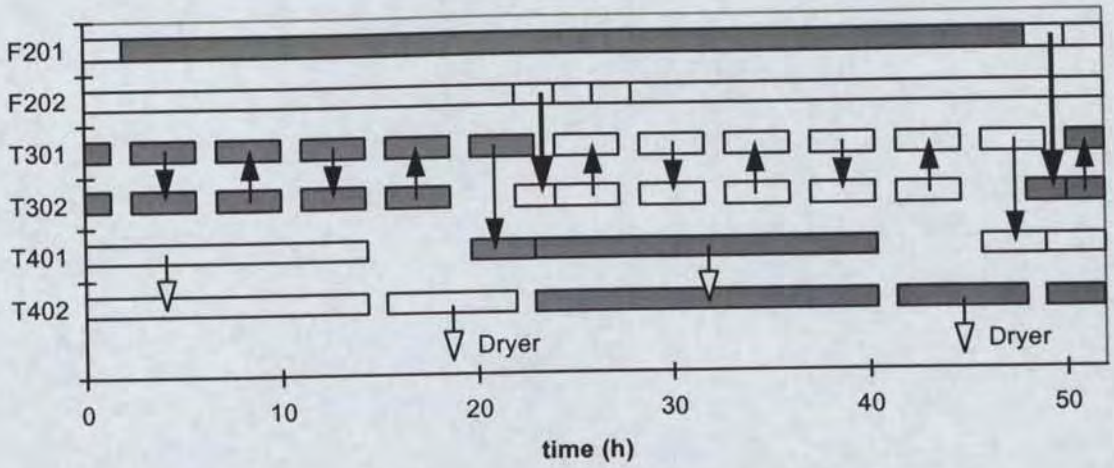

Figure 3.8: Batch schedule for equipment, times in hours. The order of events in the bioreactors is fill, ferment, drain, clean. Solid arrows are homogeniser transfers, open arrows are centrifuge transfers, thick arrows are pump transfers.

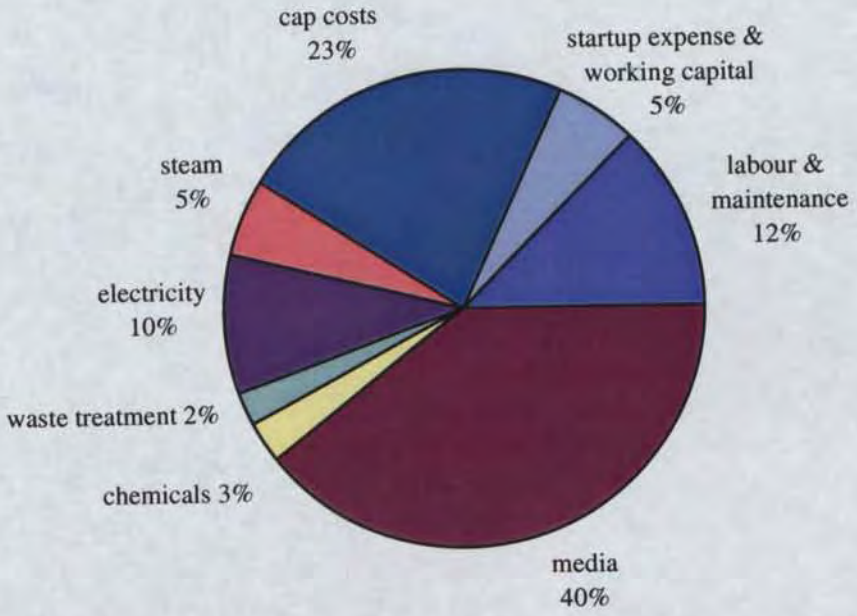

Figure 3.9: Breakdown of net present PHB cost (5000 t(PHB).yr^{-1}).

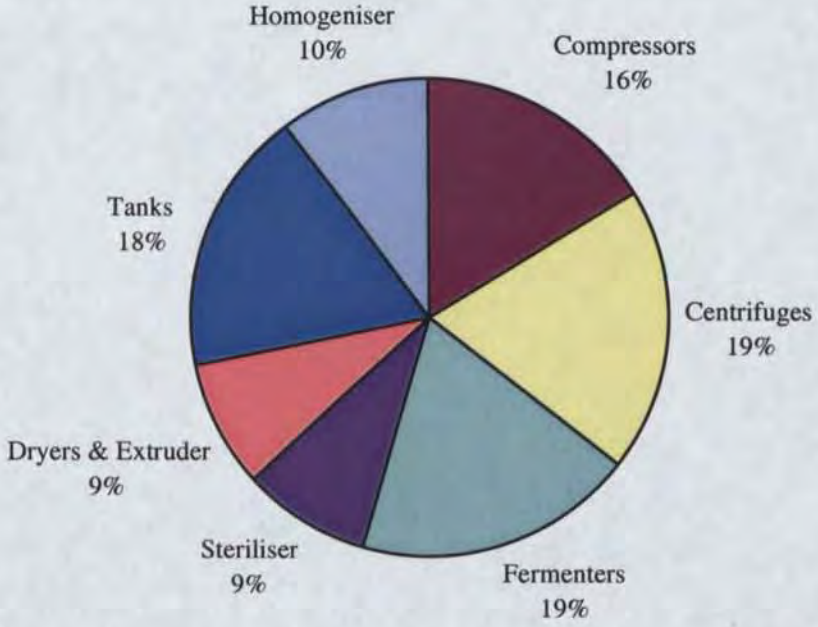

Figure 3.10: Equipment cost breakdown for the production of 5000 t(PHB).yr^{-1} from glucose.

Table 3.10: Results of economic analysis using glucose-based medium (1995US$).

	#	Total Size	Total Cost	Power Usage (MWhr/batch)	Steam usage (tons/batch)
Inoculator F203	1	21.8 kl	$50k	1	-
Bioreactors F201, F202	2	437 kl	$1,150k	51	-
Homogeniser H301	1	172 m^3h^{-1}	$654k	130	-
Centrifuges C401	5	709,000 m^2	$1,120k	28	-
Compressors S201	2	1108 kW	$1,050k	61	-
Dryers D501	3	114 m^2	$415k	-	350
Extruder & Pelletiser E501	1	627 $kg.h^{-1}$	$138k	-	-
Steriliser S101	1	9.67 m^3h^{-1}	$364k	-	43
Steriliser S102	1	3.00 m^3h^{-1}	$180k	-	14
Tank T101	1	266 kl	$103k	-	-
Tank T102	1	82 kl	$53k	-	-
Tanks T301, T302, T401	3	1430 kl	$792k	12	-
T402	1	286 kl	$107k	1	-
T501	1	221 kl	$92k	1	-
Medium Cost			$9,600k	per year	
Total Fixed Capital Investment			$30,700k		
Annual Operating Cost			$17,480k	per year (includes medium)	
Effective Production Cost			$4.88	per kilogram of PHB	

3.4.2. Sensitivity of Cost to Process Variables

Influence of final cell density

One of the major potential influences on PHA cost is the final cell density achieved. A high cell density leads to smaller bioreactor sizes, but also introduces the need for oxygen-enrichment of the inlet gas. The effects of cell density are examined by scaling back the Chapter 2 fermentation to lower densities as described in Section 3.3.3, assuming

- the production and consumption rates per gram of biomass are independent of cell concentration;
- the initial growth rate is 0.32 $g.gRCM^{-1}h^{-1}$.

This also implicitly assumes that the onset of PHB production can be properly controlled, which has not yet been demonstrated.

Figure 3.11 shows the Chapter 2 fermentation scaled back to half the final cell density. The fermentation is shortened by 2.5 h, because the initial bioreactor medium is at the same cell concentration but has greater volume. PHB yield and overall oxygen requirements are unchanged, however the peak volumetric oxygen requirement is halved and hence much less oxygen-enriched air is required. Heat removal requirements are also halved. These cost savings are counterbalanced by increased bioreactor size and stirrer power. Variation in overall cost is as shown in Figure 3.12.

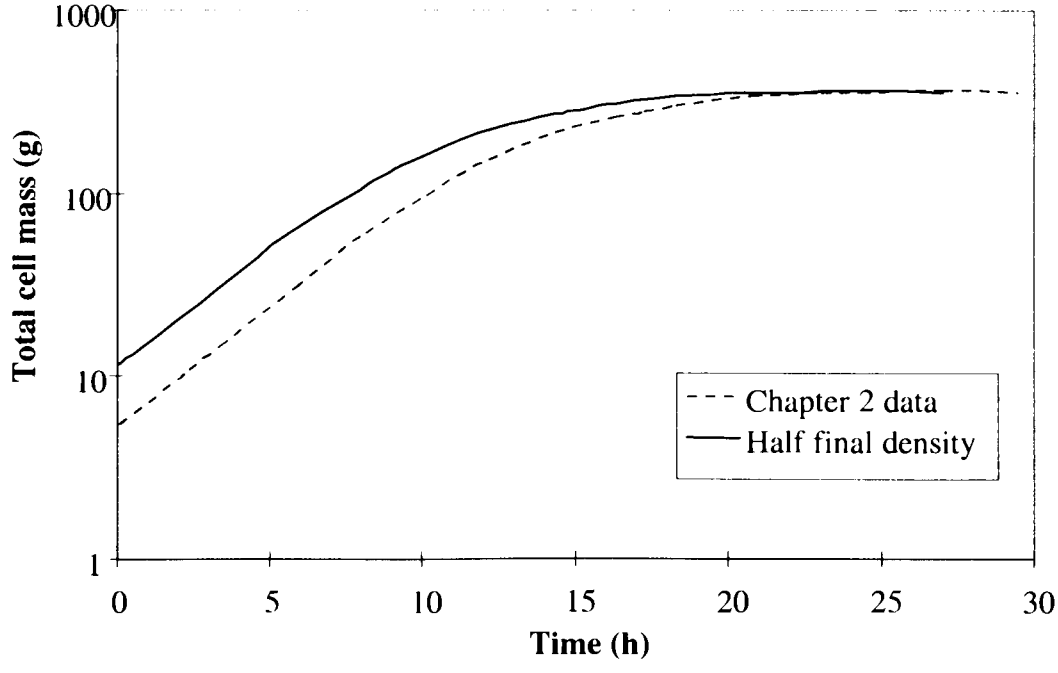

Figure 3.11: Effect on fermentation profile of scaling back the Chapter 2 fermentation data to a lower final cell density by increasing final broth volume.

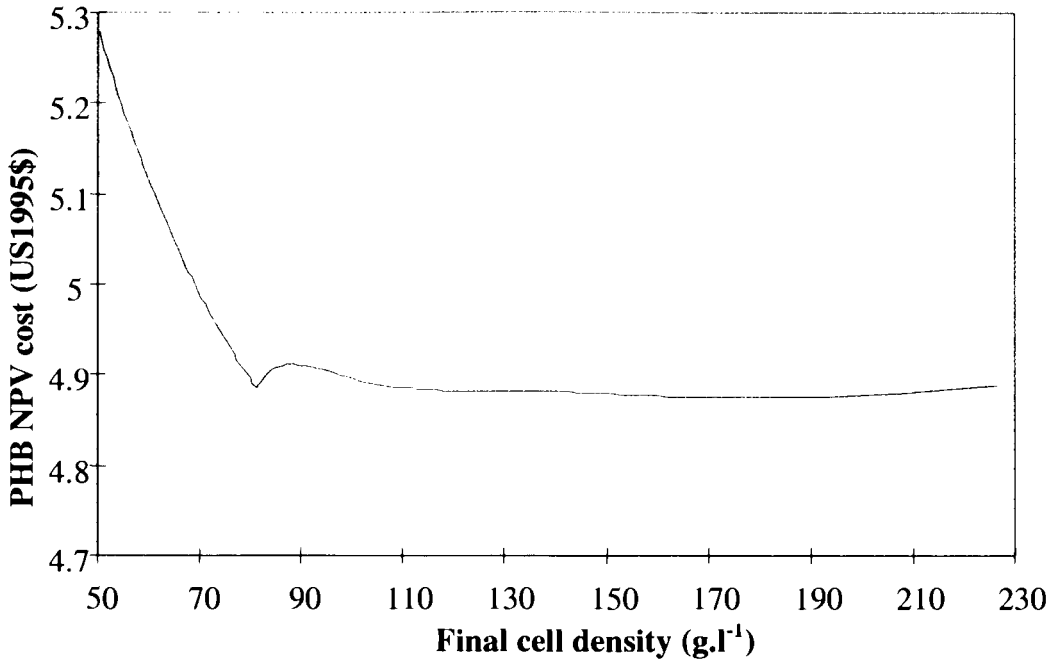

Figure 3.12: Influence of final cell density on PHB cost, at 5000 tons annual PHB production, assuming that all production and consumption rates depend only on the amount of biomass present.

Figure 3.12 shows that the PHB price is almost flat over the entire range of cell densities from 80 $g.l^{-1}$ to 225 $g.l^{-1}$. Oxygen-enriched air is required above 80 $g.l^{-1}$, cancelling out any savings from reduced bioreactor size. These data show that it is not economically attractive to increase cell density above the point where oxygen enrichment becomes necessary. Other factors would also persuade against high densities, including heat removal problems, high broth viscosity, and the explosion hazards associated with enriched oxygen feeds.

Influence of advancing or delaying termination time

The optimal time for terminating the fermentation is explored in Figure 3.13. Fermentation data were extrapolated past 46 h, since the Chapter 2 fermentation was terminated at this point. The rates from 36 - 46 h were approximately linear so this should not introduce appreciable error. The data show little effect on price over the range 46 - 52 h, hence it is apparent that 46 h is approximately the optimal fermentation duration.

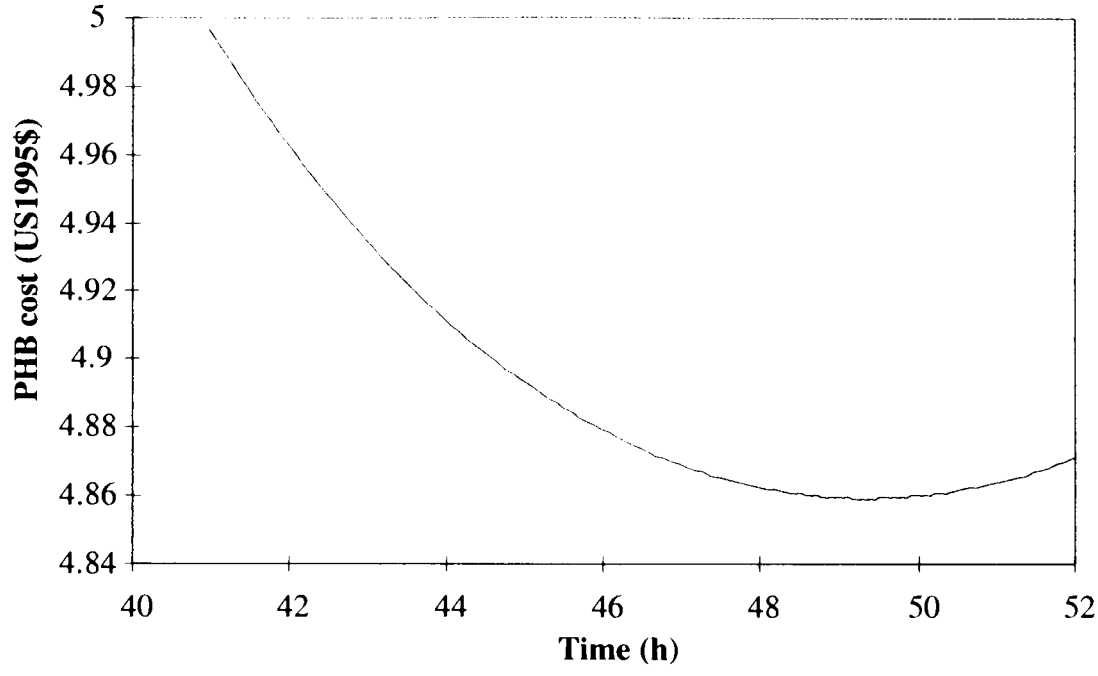

Figure 3.13: Variation in PHB production cost with duration of termination.

Influence of producing PHBV instead of PHB

As mentioned, the major product of commercial interest is PHBV rather than PHB. A very crude estimate of the PHBV cost can be made by including the purchase price of propionic acid. For P(90%HB/10%HV) the cost then becomes US1995$5.02, which is not appreciably more than for PHB. However this disregards a number of other effects that are likely to take place during PHBV production, in particular:

- reduced yield on glucose;
- reduced PHA production rate;
- reduced cell growth rate;
- difficulties in achieving proper control of polymer composition.

Adequate quantitative data on these effects are not yet available. Unfortunately, most *E. coli* strains (including XL1-Blue) do not readily assimilate propionate for use in PHBV production (see Section 1.2.5). An extensive literature search by the author led to the conclusion that endogenous production of hydroxy-valerate monomers by *E. coli* is a challenging task and probably not achievable without extensive research. After a lengthy series of experiments by the author directed at achieving acceptable levels of PHBV with recombinant *E. coli* (utilising mainly MD9101(pJM9123) (Melbourne (1995))), this avenue of research was discarded. As described in Section 1.2.5, a subsequently-published study (Choi and Lee (1999)) using a different strain-plasmid construct has demonstrated that high yield PHBV production is achievable, with a qualitatively similar fermentation profile to the Chapter 2 fermentation. It therefore seems likely that PHBV production cost will be similar to PHB, once the control of HV content has been mastered.

Influence of annual production level

Annual production level also has a moderately large impact on the PHB price, as shown in Figure 3.14. A modest doubling of plant capacity would reduce the PHB cost to US1995$4.67 kg^{-1}. Other studies (Choi and Lee (1997)) have suggested production levels of

up to 100 000 tons per year, at which level the price would be near US1995$4.30 kg^{-1}. In contrast, it is evident that smaller plants (for example to take advantage of small local supplies of cheap substrate) incur substantial cost penalties.

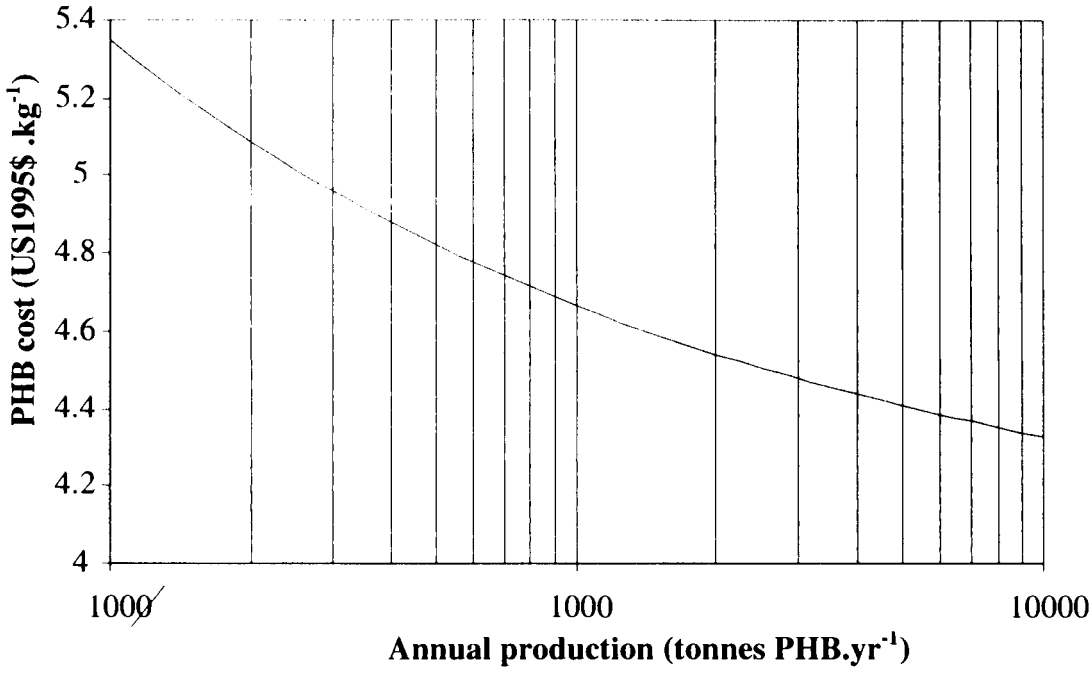

Figure 3.14: Effect of annual production level on PHB production cost.

Influence of miscellaneous variables

The sensitivity of PHB production cost to a number of variables has been examined, and summarised in Figure 3.15. The data are shown as dimensionless sensitivity, i.e. fractional change in price for a given fractional change in the variable.

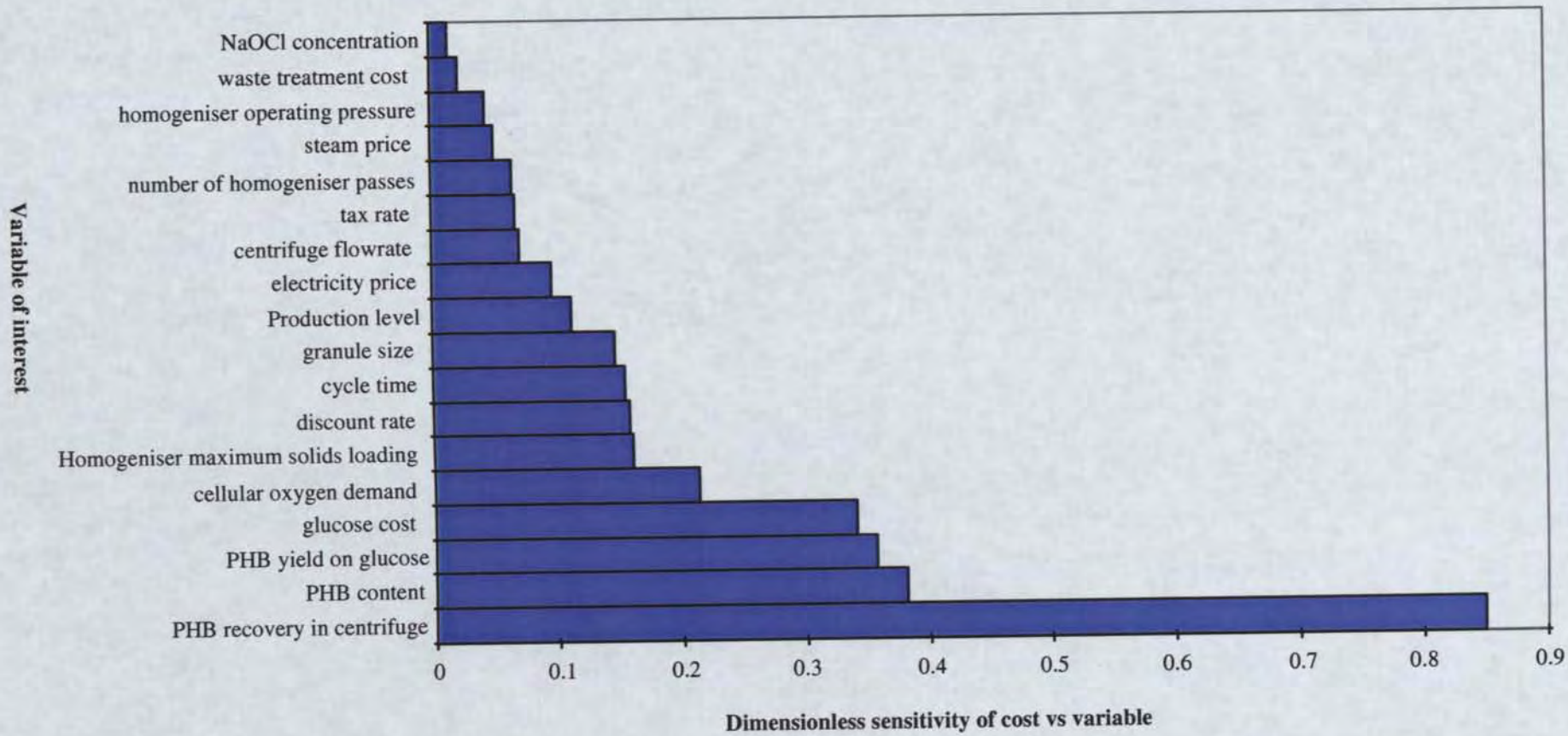

Figure 3.15: Dimensionless sensitivity $\left(\frac{\partial \ln y}{\partial \ln x}\right)$ of PHB price to various parameters at a constant annual PHB production level.

The most significant variable appears to be PHB recovery in the centrifuges. The recovery is already 95% so little improvement is possible, however even small reductions in efficiency are likely to be very detrimental. Closely related to this variable is PHB content of the cells, which also has a strong influence on price. Again, the existing level is already high (78%) so this represents more of a threat than an opportunity.

Glucose usage and cost are highly influential, reflecting the observation from Figure 3.9 that media costs dominate the net-present-value PHB cost. Small improvement in yield may be possible, however the major opportunity lies in reducing the carbon-source cost. This is discussed further below.

Cellular oxygen demand has already been discussed above, and reflects the constraint on maximum cell density rather than the cost of compressed air per se.

Homogenisers represent a significant capital and operating cost, and this is reflected by the moderate influence of homogeniser maximum solids loading. If adequate homogenisation could be achieved at higher cell densities without compromising performance (for example by reducing the broth viscosity) then this has the potential for significant savings. The number of passes is also significant.

The centrifuges are quite large, and accordingly there is a moderate effect of hydraulic capacity. Likewise the granule size is quite significant, because as described in Section 3.3.3 larger granules are easier to collect and hence smaller centrifuges can be used.

The assumed discount rate is quite significant. As mentioned in the introduction, companies sometimes assume a higher discount rate as a crude method for handling risk. If the assumed discount rate is increased to 25% then the PHB price rises to US1995\$6.14 kg^{-1}. This reflects the relatively expensive initial equipment cost which assumes increasing importance at higher discount rates.

Total cycle time is moderately significant. As outlined in Chapter 2, the fermentation can be divided roughly into an initial cell-growth phase followed by a PHB production phase. Shortening the first phase by increasing cell growth rate could therefore appreciably improve PHB price. The initial growth rate is rather slow (0.32 $g.gRCM^{-1}h^{-1}$), so it seems feasible that this could be substantially improved.

The remaining variables are of less significance, not greatly influencing the PHB price. A possible exception is the NaOCl cost. Although the sensitivity is small, the current concentration (0.85 $g.l^{-1}$ active chlorine) is low. Other studies have suggested levels as high as 13.6 $g.l^{-1}$, and under such conditions the PHB price is greatly increased.

Use of dairy whey/whey permeate

As outlined in the sensitivity analysis, reduction of carbon-source cost will have a large impact on PHB cost. A feasible option is partial replacement of glucose with whey or whey permeate. Depending on the amount of whey (permeate) available, part or all of the glucose may be replaced as follows:

a) The bioreactor is charged with whey to the required initial volume (with extra water added if necessary). Glucose nutrient feeding would then be conducted as usual.
b) If whey is available in excess of part a), the remainder can be concentrated to 200 $g.l^{-1}$ with an evaporator and used to replace part (or all) of the glucose nutrient feed.

Assuming no restriction on available whey, 100% replacement of glucose is possible, dropping the PHB cost to US1995$3.38 kg^{-1}. Unfortunately whey availability is very seasonal, as shown in Figure 3.16.

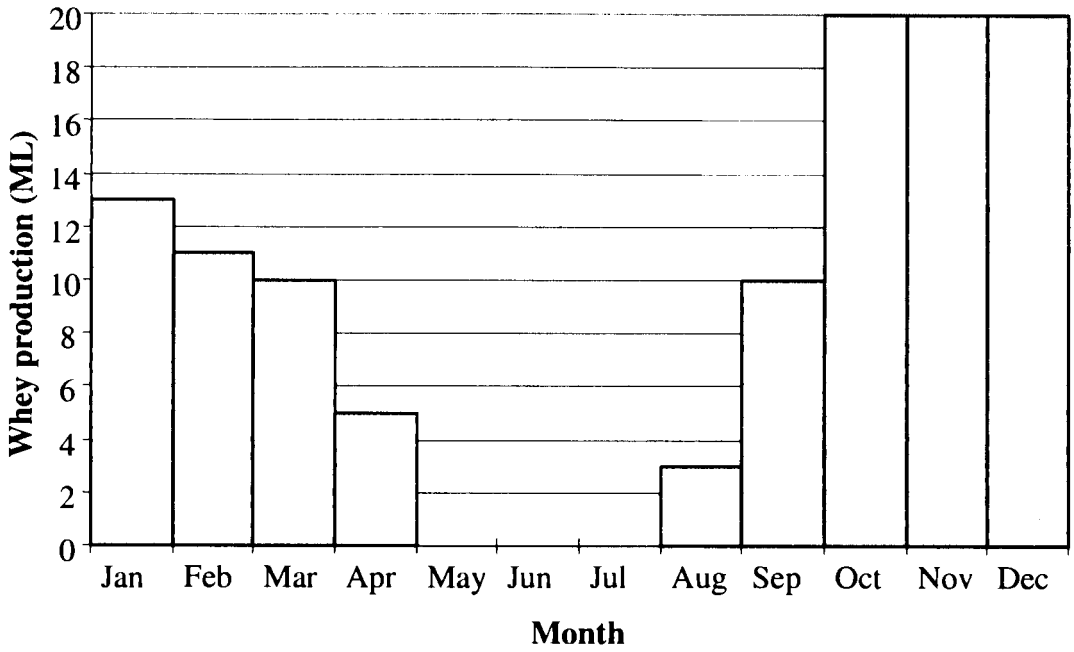

Figure 3.16: Seasonal variation in whey production for a typical large cheese factory (United Milk, Tasmania).

When these data are used, the year-averaged PHB production cost is US1995$4.67 for initial-medium-replacement, or US1995$4.54 if an evaporator is used to generate lactose nutrient feed. Glucose replacement by lactose is 12.2% and 29.03% respectively. The PHB costs are quite similar because the whey evaporator is expensive and remains idle for much of the year. It is therefore apparent that the seasonal availability of whey is a major limitation. Other substrates (for example beet molasses) may be suitable (Liu *et al.* (1998); Rusendi and Sheppard (1995)), however this has not yet been demonstrated at high cell density.

3.5. Conclusions

For the process described in this chapter, the best estimate of PHB cost is US1995$4.88 kg^{-1}. Further refinements to the process may make modest price improvements, however it seems unlikely that the cost can be reduced to less than US1995$3 kg^{-1} without fundamental modifications. At this price PHB and PHBV are not likely to be competitive with conventional polymers unless strong consumer preference or government legislation fall in their favour.

One of the major purpose of this chapter is to set the direction for further analysis, by highlighting areas where improvements will be most beneficial.

1. Production of PHB from dairy whey has significant potential to reduce the PHB price. However there are several potential problems that must be addressed, in particular its seasonal availability, the suitability of preconcentrated whey or whey permeate as a carbon source, and the consequences of high salt concentrations. As previously mentioned, Wong and Lee (1998) have demonstrated high-level PHB production (69 $g.l^{-1}$ PHB) from whey by fed-batch fermentation of *E. coli*, however some optimisation work remains. In particular the effects of high salt concentration have not been addressed, which may prove to be a serious problem at higher cell densities. Whey also contains appreciable protein, which will likely improve the fermentation performance if predigested to short peptides that *E. coli* can utilise. Further study is required to investigate this.
2. The additional costs associated with producing PHBV are difficult to estimate, especially given the potential toxicity of propionate and the likely difficulty in achieving good control of polymer composition. Nevertheless, based on the results of Choi and Lee (1999) it seems likely that PHBV production cost will not differ greatly from PHB, once the control of HV content has been mastered.
3. Oxygen requirements are a major factor affecting the PHB price, because the maximum achievable cell density is directly limited by oxygen transfer. Using oxygen-enriched air requires expensive equipment which negates the price benefits of higher cell density, and introduces additional process hazards. Reduction of the fermentation's peak volumetric oxygen requirements is therefore an important objective. The consequences of short-term oxygen limitation have also not been addressed.
4. The need for improved control of the fermentation is highly important, because the onset of PHB production must be triggered at the correct time. If synthesis starts too early the bioreactor yield will be reduced, and if too late it may be impossible to maintain adequate oxygen supply. Given the high sensitivity of cost to PHB expression level, poor repeatability of the fermentation will certainly significantly increase the cost, although in the absence of experimental data this is difficult to quantify. As described in Chapter 2, it is still not certain what causes the cells to commence PHB synthesis. This must be studied in more detail.

The results from this chapter are used to guide efforts in the remaining chapters:

- Chapter 4 develops a repeatable fermentation protocol as a 'base-case', then applies a metabolic and kinetic model to the data. These models are used to suggest ways in which PHA production could be improved, as highlighted by the sensitivities in Section 3.4.2. The models are also used to investigate potential causes for the onset of PHB production, a key requirement for improving fermentation control as outlined above.
- The economically-crucial nature of cellular oxygen requirements sets the direction for Chapter 5, which investigates the effect of oxygen limitation on PHB production. Further theoretical analysis is also conducted on the fermentation data, suggesting process improvements based on the economic sensitivities in Section 3.4.2.

- Chapter 6 addresses the method of nutrient-feeding used. Different strategies lead to tradeoffs between PHB production rate, glucose-utilisation efficiency, and cell density, all of which have significant effects on process economics as described in this chapter.

Chapter 4

4.1. Summary

The purpose of this chapter is to develop and analyse a repeatable control fermentation for the production of PHB by XL1-Blue(pSYL107). By applying a metabolic flux model and kinetic model of the PHA pathway, this chapter gives understanding of the the metabolic changes that occur during PHB production. The base case developed is also used by Chapters 5 and 6 as a control.

Two constant-glucose fed-batch fermentations of duration 25 h were carried out in a 5 l bioreactor, with measured oxygen volumetric mass-transfer coefficient (k_La) held constant at 1.1 min^{-1}. The production rates of PHB, residual cell mass, carbon dioxide, acetic acid, formic acid, lactic acid, succinic acid, pyruvic acid and ethanol were measured. The consumption rates of glucose, oxygen and ammonium ion were also measured. Specialised sampling equipment was developed and a method adapted from the literature to measure the intracellular concentrations of acetyl-CoA and 3-hydroxybutyryl-CoA. The results show that the base-case fermentation is highly repeatable and the analytical techniques are sufficiently accurate to yield useful results.

Each fermentation achieved 48% PHB with 18 $g.l(broth)^{-1}$ dry cell weight. Peak PHB production rate was 0.09 $gPHB.gRCM^{-1}h^{-1}$. PHB yield on glucose was 0.30 $mol(PHB).mol(glc)^{-1}$. There was substantial excretion of formic acid (3 $g.l^{-1}$), acetic acid (6.5 $g.l^{-1}$), lactic acid (10 $g.l^{-1}$), succinic acid (2 $g.l^{-1}$), and pyruvic acid (4 $g.l^{-1}$). Ethanol was not detected.

Four distinct phases were identified in the fermentation.

- The first phase (0 - 3.5h) consisted of exponential growth, with moderate TCA cycle flux despite the aerobic conditions. There was no excretion of acids.
- The second phase (3.5 - 6h) corresponded to the onset of oxygen limitation, which caused TCA flux to decline to zero and acetyl-CoA concentration to rise from 350 $\mu g.gRCM^{-1}$ to 600 $\mu g.gRCM^{-1}$. Pyruvate dehydrogenase flux was unaffected but pyruvate-formate-lyase flux increased from previously negligible levels, causing rapid excretion of formic acid and acetic acid. The other acids were also excreted, at a slower rate. PHB production rose sixfold, probably due to a rise in acetyl-CoA/CoA ratio as shown by kinetic analysis.
- During the third phase (6 - 10h) RCM production declined to zero and excretion of formate ceased. This was accompanied by a 75% reduction in acetic acid production and the return of acetyl-CoA concentration to 350 $\mu g.gRCM^{-1}$. Excretion of the remaining acids rose to a plateau. PHB production rate rose gradually to 0.08 $gPHB.gRCM^{-1}h^{-1}$, probably caused by an increase in enzyme activity.
- During the fourth phase (10 - 25h) the production of all metabolites gradually declined from the plateau achieved at hr 10.

The kinetics of PHB production were examined and the activity of PHA synthase was estimated at 0.6 - 0.8 $Units.mg(protein)^{-1}$, in good agreement with the literature. Likely ranges were established for 3-ketothiolase activity, 3-ketoacyl-CoA reductase activity, acetyl-CoA/CoA ratio, NADPH concentration, and NADP concentration. Metabolic control analysis performed on the PHA production pathway showed that the PHB flux is highly sensitive to

acetyl-CoA/CoA ratio (response coefficient 0.8), total acetyl-CoA + CoA concentration (response coefficient 0.7) and pH (response coefficient -1.25). It is less sensitive (response coefficient 0.25) to NADPH/NADP ratio. NADP(H) concentration (NADPH + NADP) has negligible effect. No single enzyme had a dominant flux control efficient under the experimental conditions examined (0.6, 0.25 and 0.15 for 3-ketoacyl-CoA reductase, PHA synthase and 3-ketothiolase respectively). The results showed that the rapid six-fold rise of PHB production at the onset of PHB production was probably due to the observed doubling of acetyl-CoA concentration and a doubling of acetyl-CoA/CoA ratio. The rate may have been augmented to a small degree by an increase in the NADPH/NADP ratio or a decrease in intracellular pH.

A number of areas were identified where changes to fermentation protocol or modifications to cellular genetics may significantly improve PHB production.

4.2. Introduction

4.2.1. General

The economic analysis in Chapter 3 identified several key areas of the PHA production which have a large effect on selling price. In order to investigate these effects more closely, it is necessary to analyse them in a repeatable way. The purpose of the work in this and subsequent chapters is to carefully examine the effect of environmental changes, relative to a control. Full metabolic flux analysis is used on each case, to calculate how key fluxes within the recombinant *E. coli* are affected. In order to further elucidate the underlying mechanisms, the concentrations of key intermediates in the PHA enzyme chain are also measured (viz acetyl-CoA, 3-ketobutyryl-CoA and 3-hydroxybutyryl-CoA). There are four main purposes for this chapter:

1) To establish a "base-case" fermentation for the subsequent chapters. The fermentation protocol is adapted from Chapter 2, using the recommendations in Section 2.8.2 and Section 4.2.2.
2) To verify the metabolic flux analysis model from Chapter 2 using more-rigorously-collected data.
3) To apply metabolic control analysis to the PHB pathway. Metabolic control analysis (Fell (1992)) is a mathematical modelling technique that can be used to gain insight into the control of enzymatic pathways. It has been used in several different ways to examine metabolism, for examples see Quant (1993), Hafner *et al.* (1990), and Lu and Liao (1997). In this chapter, metabolic control analysis is applied to a kinetic description of the PHB pathway. This is achieved by adapting *in-vitro* kinetic expressions for the PHA pathway to *in-vivo* fermentation conditions, and obtaining estimates of enzyme and metabolite concentrations.
4) To apply the metabolic and kinetic models to the "base-case" fermentation data, with the aims of:
   - gaining a greater understanding of the metabolic changes that occur during PHB production. In particular, identifying the factors which trigger the onset of PHB production is a high priority, as shown in Chapter 3;
   - using the models to identify metabolic manipulations which may significantly improve the process economics presented in Chapter 3.

4.2.2. Fermentation Criteria

In order to obtain meaningful results, the series of fermentations must satisfy several criteria, as follows:

1) Excellent repeatability. This requires careful control of several other parameters:
   - Cell density achieved. Very-high-cell-density fermentations (such as that described in Chapter 2) are not suitable, since random fluctuations in cell genetics and environment become highly significant.
   - Oxygen transfer rate. This requires careful attention to air flowrate, stirrer speed, and impeller positions. The impellers must be placed sufficiently below the surface of the broth so that they do not cause surface aeration at any stage. Otherwise, broth liquid level can effect a large variation in oxygen transfer rate (10-20%) when the impeller becomes partially uncovered.
   - Inoculum. The XL1-Blue(pSYL107) construct is moderately unstable due to its slow growth in minimal medium and the high metabolic burden of PHB production. In order to improve repeatability it is necessary to work from a master stock, and to minimise the number of cell doublings required to reach high density.

- Culture volume. As far as possible the volume profile should be similar in all fermentations, primarily to ensure that mixing and aeration are not affected.
- Medium composition and feed composition. This includes the amount of antifoam used, which can adversely affect oxygen transfer rate.

2) Sufficient accuracy of measurements. The cell density achieved must be sufficiently high to allow accurate measurement of metabolites. Acyl-CoA concentrations, PHB concentration, dry cell weight, and oxygen consumption are all inaccurate below a cell density of 2 $g.l^{-1}$.
3) Pseudo-steady-state operation. Although true steady-state operation is impossible in a fed-batch system, the metabolism must vary sufficiently gradually that discrete sampling can track the changes. This is related to sampling frequency and the necessary accuracy of metabolite measurements. Disturbances to the metabolism (such as foaming over, loss of pH control, or fluctuations in aeration) must be avoided unless they are specifically under study. This includes changes in the glucose concentration during batch-feeding.

4.3. Materials and Methods

4.3.1. Bacterial Strain and Plasmid

Recombinant *Escherichia coli* (*E. coli*) strain XL1-Blue (*supE44 hsdR17 recA1 endA1 gyrA96 thi relA1 lac F'(proAB+ lacIq lacZΔM15Tn10(tet^r)*) harbouring pSYL107 was used in this study (Wang and Lee (1997)). The plasmid pSYL107 contains the *R. eutropha* PHA biosynthesis genes, an *E. coli ftsZ* filamentation-suppression gene, the *parB* locus for plasmid stability, and an ampicillin resistance gene (Lee (1994)).

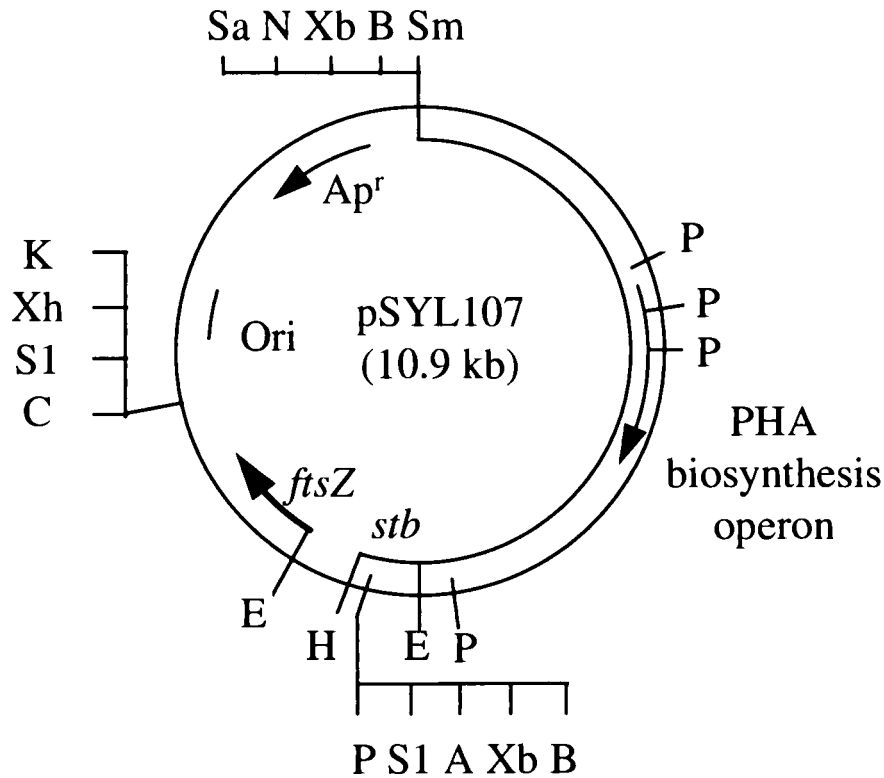

Figure 4.1: The restriction map of pSYL107 (Lee (1994)). Arrows indicate the direction of transcription. Abbreviations are: Ori, origin of replication; Ap, ampicillin; r, resistance; stb, parB locus of plasmid R1; A, AccI; B, BamHI; C, ClaI; E, EcoRI; H, HindIII; K, KpnI; N, NotI; P, PstI; Sa, SacI; S1, SalI; Sm, SmaI; Xb, XbaI; Xh, XhoI.

4.3.2. Medium and Culture Conditions

Master stock preparation

In order to improve repeatability, a master glycerol stock was prepared. 20 mL of LB medium with 100 mg.l^{-1} ampicillin was placed in a 250 ml shakeflask, then inoculated with XL1-Blue (pSYL107). The culture was incubated overnight at 30 °C at 120 rpm shaking. When optical density at 600 nm reached approximately 2.0, the culture was mixed with an equal quantity of 40%(v/v) glycerol then dispensed into twenty cryostore vials. The vials were frozen overnight in a -20 °C freezer then stored in a -50 °C freezer until use.

Medium composition

The fermentation medium was made up as follows. Solutions A to F were made up as shown in Table 4.1 and Table 4.2, then autoclaved at 121 °C for 20 minutes. In addition, a 100 $g.l^{-1}$ thiamine.HCl solution and a 100 $g.l^{-1}$ ampicillin solution were filter sterilised. All reagents were AnalaR grade or equivalent.

Table 4.1: Trace solution compositions.

Solution A		Solution B		Solution C	
$CoCl_2$	20 mg	$FeSO_4.7H_2O$	1 g	$CaCl_2$	151 mg
$Na_2B_4O_7.10H_2O$	20 mg	conc. HCl	1 ml	$CuSO_4.5H_2O$	100 mg
$(NH_4)_6Mo_7O_{24}.4H_2O$	100 mg	water	99 ml	$MnSO_4.H_2O$	38 mg
water	100 ml			$ZnSO_4.7H_2O$	220 mg
				conc. HCl	1 ml
				Solution A	10 ml
				water	89 ml

Table 4.2: Bulk solution compositions.

Solution D		Solution E		Solution F	
Na_2HPO_4	6 g	glucose (anhy)	20 g	glucose (anhy)	250 g
KH_2PO_4	3 g	water	88 ml	$MgSO_4.7H_2O$	10 g
$(NH_4)_2SO_4$	4 g			water	250 g
Na_3.citrate	2 g				
$MgSO_4.7H_2O$	0.6 g				
water	880 ml				

Table 4.3: Bulk media compositions.

Base medium		Nutrient feed	
Solution D	880 ml	Solution F	510 g
Solution B	10 ml	100 $g.l^{-1}$ thiamine	1 ml
Solution C	10 ml		
Solution E	100 ml		
100 $g.l^{-1}$ thiamine	0.1 ml		
100 $g.l^{-1}$ ampicillin	1 ml		

After cooling to room temperature, the final media and nutrient feed solution were produced as shown in Table 4.3. All media and feed solutions were accurately weighed before and after autoclaving. The composition was then adjusted to take account of water loss during autoclaving.

Fermentation

Two fed-batch fermentations were conducted. For each, 25 ml of base medium (Table 4.3) was placed in a 250 mL shakeflask then inoculated with the contents of a single master stock vial (1 ml). The flask was cultured for seven hours at 30 °C with 120 rpm shaking to an optical density of approximately 0.3. 20 mL of the culture was then inoculated into a 5 l "Microferm" bioreactor (New Brunswick Scientific Co., NJ, USA) containing 2.5 l of base

medium. Culture temperature was controlled at 30.0±0.5 °C. Stirring was at 700 rpm and air flowrate was 4.0 l(STP).min^{-1}, giving an oxygen volumetric mass-transfer coefficient (kLa) of 1.1 min^{-1} as measured by exhaust-gas analysis during the fermentation. The fermenter was pressurised to 4 kPa above atmosphere. After overnight growth, when the culture optical density (600 nm) reached approximately 0.8 this was designated as "hour zero" (hr 0). pH was measured using a combination pH probe (Mettler Toledo, Greifensee Switzerland) and controlled to 7.0 by addition of 12% (v/v) ammonia during hrs 0 to 7, or by 5 M NaOH during other periods. Dissolved oxygen was measured with an oxygen probe ($Ag/AgCl_2$ polarometric, Mettler Toledo, Greifensee Switzerland). Foaming was controlled by addition of 5% (w/w) LQ217 antifoam (Henkel, Victoria, Australia) as required. The amounts of each solution added were measured by weighing the feed bottles and transfer lines before and after the fermentation.

Batch cultivation was employed until the initial glucose charge was depleted to approximately 5 g.l^{-1} (near hr 7). Thereafter, nutrient feeding solution was added continuously to maintain glucose concentration near approximately 5 g.l^{-1}. The glucose concentration was measured hourly using a YSI2700 select biochemistry analyser (YSI Instruments, Ohio, USA), then the required feed rate and 'catchup' feed pulse were calculated by mass balance.

Analytical procedures

Cell growth was monitored by measuring the optical density at 600 nm (OD_{600}) using a spectrophotometer (Unicam 8625 UV/Vis, Cambridge, UK). Samples taken from the fermenter (usually 40 ml) were immediately chilled to 0 °C by placing in an ice bath. Samples for DCW analysis were used immediately whereas the remainder were dosed with formalin to 0.1% then frozen at -20 °C. When ready for use the samples were defrosted by placing into a 30 °C water bath for 2 minutes then vortexing and storing in an ice-slush bath.

Outlet gas was continously sampled from the exhaust line using a syringe with automatic retractor (Syringe pump model 351, Orion, Cambridge, UK) as described more fully in Appendix A. The total dead volume of fermenter headspace, disentrainment bottle and gas lines was 3 l. The composition of each gas sample was measured using the mass spectrometer detector of a Gas Chromatograph/Mass Spectrometer (Hewlett-Packard GC-MS 6890 GC, 5973 MS, Canada, USA) with an AT1000 25 m x 0.25 mm column at 60 °C (Alltech, Victoria, Australia). Column flow was 1.2 ml He.min^{-1}; 5 µl of gas was injected with split ratio 50:1 using a custom-made gas injection valve. The MS was operated in SIM mode for ions 32 (O_2), 40 (Ar), and 44 (CO_2), with a 20 ms dwell time. Standards used were ambient air, fermenter air inlet, and CO_2 standards created by vaporising a measured mass of dry ice in a sealed container of measured volume. Each sample was measured six times and the results averaged (sample std deviation was 0.2% of reading). Gas flow was measured using a domestic natural-gas totaliser (cumulative volume flowmeter) (Model 610 Emailgas, Victoria, Australia). Pressure correction for the totaliser was performed using a water manometer.

Cell concentration, defined as dry cell weight (DCW), was determined by placing an accurately weighed volume of broth (approx. 9 ml) into a predried, preweighed 12 ml polypropylene centrifuge tube along with 10 µl of formalin. After centrifugation at 20000 g for 10 min, the supernatant was decanted into a sample tube then frozen at -20 °C. The centrifuge tube was dried in an oven at 100 °C for 24 h then cooled in a dessicator and weighed.

PHB concentration was determined using a modified method from the literature (Braunegg *et al.* (1978)) as follows: Sufficient defrosted broth was added to an 8 ml glass "culture tube" (Kimax, New Jersey, USA) to give between 4-10 mg PHB (maximum 6 ml) and volume was made up to 6 ml with 0.7% w/v NaCl solution. After centrifugation at 1100 g for 10 min the supernatant was carefully removed using a blunt 11 cm needle attached to a syringe. 1 ml of reverse osmosis water was added to the tube along with 10 µl of formalin. The tube was next frozen in a -20 °C freezer whilst lying on its side, then freeze-dried to 0.1 mbar. Each tube then received 2 ml of chloroform, 2 ml of 3% (v/v) sulphuric acid in methanol, and 0.2 ml of 5.5 $g.kg^{-1}$ methyl benzoate in methanol as an internal standard. The tube was tightly sealed with a teflon-lined cap and baked at 100 °C for 4 h in a protective container, then cooled. 1 ml of MilliQ water was added and the tube vortexed for 1 min. After settling of the layers, 2 µl of the lower phase was injected into a gas chromatograph (Shimadzu GC-17A Gas Chromatograph with Class GC-10 V1.34 software, Kyoto, Japan) equipped with a Carbowax 20M (Chromosorb W-AW 60/80 mesh) packed column (6 foot by 1/8") from Alltech (Victoria, Australia). The carrier gas was nitrogen at 30 $ml.min^{-1}$. Injection temperature was 220 °C, FID detector temperature was 240 °C. The oven temperature had the following profile: 100 °C for 1 min, rising at 8 $°C.min^{-1}$ to 172 °C, then rising at 20 $°C.min^{-1}$ to 200 °C, then holding for 5 min. Standards were prepared by weighing purified PHB (Aldrich, Wisconson, USA) directly into a glass reaction tube. Residual Cell Mass (RCM) is defined as DCW ($g.l^{-1}$) minus PHB concentration ($g.l^{-1}$). PHB content (%) is defined as the ratio of PHB concentration to cell concentration. All PHB samples were measured in duplicate.

The densities of broth and of supernatant were each measured using a 10 ml glass vial designed for this purpose.

Elemental analysis of the dry-cell-weight pellet sample was determined (after grinding with a mortar and pestle) using a combustion analyser by an external company (Campbell microanalytical lab, University of Otago, Dunedin New Zealand.) Total organic carbon analysis of the supernatant was performed using combustion analysis by an external company (Hunter Laboratories, Warrabrook, NSW Australia)

The defrosted culture supernatant concentrations of formic acid, lactic acid, pyruvic acid, acetic acid and succinic acid were measured using a Shimadzu HPLC system (SPD-10A UV detector at 210 nm, LC-10AD pump unit, LC-10AS pump) Kyoto, Japan) with Class LC-10 V1.63 software. Two PRP-X300 poly(styrene-divinylbenzene) sulphonate ion-exchange columns were used in series (each 4.1 mm x 150 mm with 7 µm particle size) from Hamilton (Nevada, USA) equipped with a guard column of the same packing and operating at 40 °C (Temperature controlled oven, Timberline instruments, Boulder, Colorado USA). Appropriate standards were created from 98% formic acid solution, sodium lactate, 99.5% acetic acid solution, sodium pyruvate, and sodium succinate (All purchased from Sigma-Aldrich, USA). Glucose was measured enzymatically using the YSI2700 Select Biochemistry analyser (YSI Instruments, Ohio, USA) and double checked using HPLC (as above) with an RI detector (ERC-7510, Erma Optical Works Inc, Nevada, USA) Enzymatic test kits were also used to measure or double-check concentrations of ethanol (Boehringer Mannheim, Germany), ammonia (Boehringer Mannheim, Germany) and pyruvic acid (Sigma Diagnostics, USA). Dissolved CO_2 concentrations were calculated from rate equations (Royce (1992); Royce and Thornhill (1991)) and shown to negligible. All dilutions of samples were measured by weight. All HPLC analyses were performed in duplicate.

Acyl-CoA concentrations were measured by a method modified from several others in the literature (Mansfield *et al.* (1995); Corkey (1988); Debuysere and Olson(1983)). 1.5 ml of

0.8 molar perchloric acid was placed into an 8 ml glass "culture tube" (Kimax, New Jersey, USA) then accurately weighed and chilled to 0 °C. The tube was evacuated and approximately 1.5 ml of culture medium was rapidly (0.5 s) aspirated into it (See Appendix A). After immediate placement on ice for 5 min to extract metabolites, the tube was centrifuged for 5 min at 1100 g. The supernatant was completely withdrawn using an 11 cm blunt needle attached to a syringe and placed into another pre-chilled 8 ml glass "culture tube" containing a magnetic stirrer bead. The syringe and needle were rinsed with 500 µl of milliQ and the rinsewater added to the glass reaction tube. Whilst stirring vigorously, the pH was raised to 3.50 by dispensing chilled 5 M KOH using a variable-speed micro-peristaltic pump (Masterflex C/L model 77 120-60, USA) with peristaltic pump tubing (Cole Parmer Tygon 0.01" ID, USA). pH was measured using a micro-pH probe (Orion 9103 BN, Cambridge, UK). After neutralisation the tube was frozen in a dry ice/ethanol mixture and stored at -70 °C for a day. The sample was then freeze dried to 0.1 mbar and again stored at -70 °C. No more than a day prior to analysis, 1 ml of milliQ was added to the tube and vortexed to resuspend all deposits. The pH was adjusted to 4.00 using 5 M KOH or 0.8 M perchloric acid as necessary, then centrifuged for 10 minutes at 1100 g. The supernatant was carefully removed with an 11 cm blunt needle attached to a syringe then passed through a 0.45 µm nylon syringe filter (4 mm diameter, Alltech, Victoria, Australia) and refrozen at -70 °C. Just prior to analysis by HPLC, the sample was defrosted by holding in the hand. Analysis was by Shimadzu HPLC system (SPD-10A UV detector at 254 nm, CTO-10A temperature-controlled oven, LC-10AD pump unit, FCV-10AL flow control valve unit, GT-102 degassing unit, Kyoto, Japan) with Class LC-10 V1.4 software. The column was an Allsphere ODS-2 5U, 250 mm x 4.6 mm column from Alltech (Victoria, Australia) equipped with a guard column of the same packing and operating at 40 °C. A 96.3% (w/w) Methanol + 3.7% (w/w) chloroform organic solution was created, then the two mobile phases generated by mixing KH_2PO_4 with water and 98% formic acid, adjusting to pH 4.00 with 5 M KOH, then adding organic phase, as shown in Table 4.4. The phases were then filtered through a 0.22 µm filter (GVWP 047 00, Millipore, Massachusetts, USA) and stored in airtight bottles before use. The flowrate was 0.5 $ml.min^{-1}$ with piecewise linear gradient as follows: 0 min = 100% A, 8 min = 94.9% A, 14 min = 82.1% A, 20 min = 64.1% A, 32 min = 0% A, 42 min = 0% A, 45 min = 100% A, 55 min = 100% A and end of run. The column was rinsed with 10% water/90% methanol at the end of each day. All reagents were HPLC grade (Sigma Aldrich, USA).

Table 4.4: HPLC mobile phase compositions.

	KH_2PO_4 (w/w)	water (w/w)	formic acid ($\mu l.kg^{-1}$)	5 M KOH	organic solution (w/w)
A	1.358%	93.80%	376	Adjust pH to 4.00	4.84%
B	1.031%	59.55%	409	Adjust pH to 4.00	39.42%

4.3.3. Analysis of Data

Mass balance calculations

Gas compositions were calculated from the measured peak ratios (32/40 for oxygen, 44/40 for CO_2) using the standards previously outlined. Given the measured inlet flowrate and measured inlet composition, the consumption of oxygen and production of CO_2 could be calculated.

The data were converted to a no-sampling basis as described in Section 2.4.3. The mass of material in the bioreactor at any time was calculated by mass balance from the known addition

and removal of material (including gas flows). The final mass of material in the bioreactor was measured to correct for any unquantified additional loss of material (e.g. evaporated water). This correction was less than 5%.

Concentrations measured on a supernatant basis were converted to total-broth basis using the equation

$$C_{total-broth-basis} = C_{supernatant-basis} . \hat{m}_{supernatant} \quad (4.1)$$

where

$C_{total-broth-basis}$ = concentration of analyte (g.kg(broth)$^{-1}$)

$C_{supernatant-basis}$ = concentration of analyte (g.kg(supernatant)$^{-1}$)

$\hat{m}_{supernatant}$ = mass of supernatant per mass of broth (kg.kg(broth)$^{-1}$)

$\hat{m}_{supernatant}$ was calculated as the non-dry-cell-weight portion of the broth. This approximation was proven adequate by a dilution experiment with glucose.

The mass-production rates were converted to molar production rates and then processed using flux analysis methods as described in Section 2.4.1. The covariance matrix for each sample was estimated using Monte-Carlo simulation, based on measured errors in concentrations, volumes (etc). (R.I.S.K. software, Palisade Corporation of Newfield, using custom-written Excel software for covariance calculation). Most correlation coefficients were low (between -0.2 and 0.2) however there was high positive correlation between acid rates (0.3 - 0.5), and high negative correlation between RCM and PHB rates (-0.3 to -0.8).

Flux analysis

The flux network used to analyse the fermentations in this (and subsequent) chapters has been described in Section 2.3. There are several improvements for this set of data over those collected in Chapter 2:

- oxygen consumption has been measured and the measurement accuracy of CO_2 production has been improved;
- pyruvate production has been measured;
- succinate excretion has been measured.

This gives the flux network as shown in Figure 4.2.

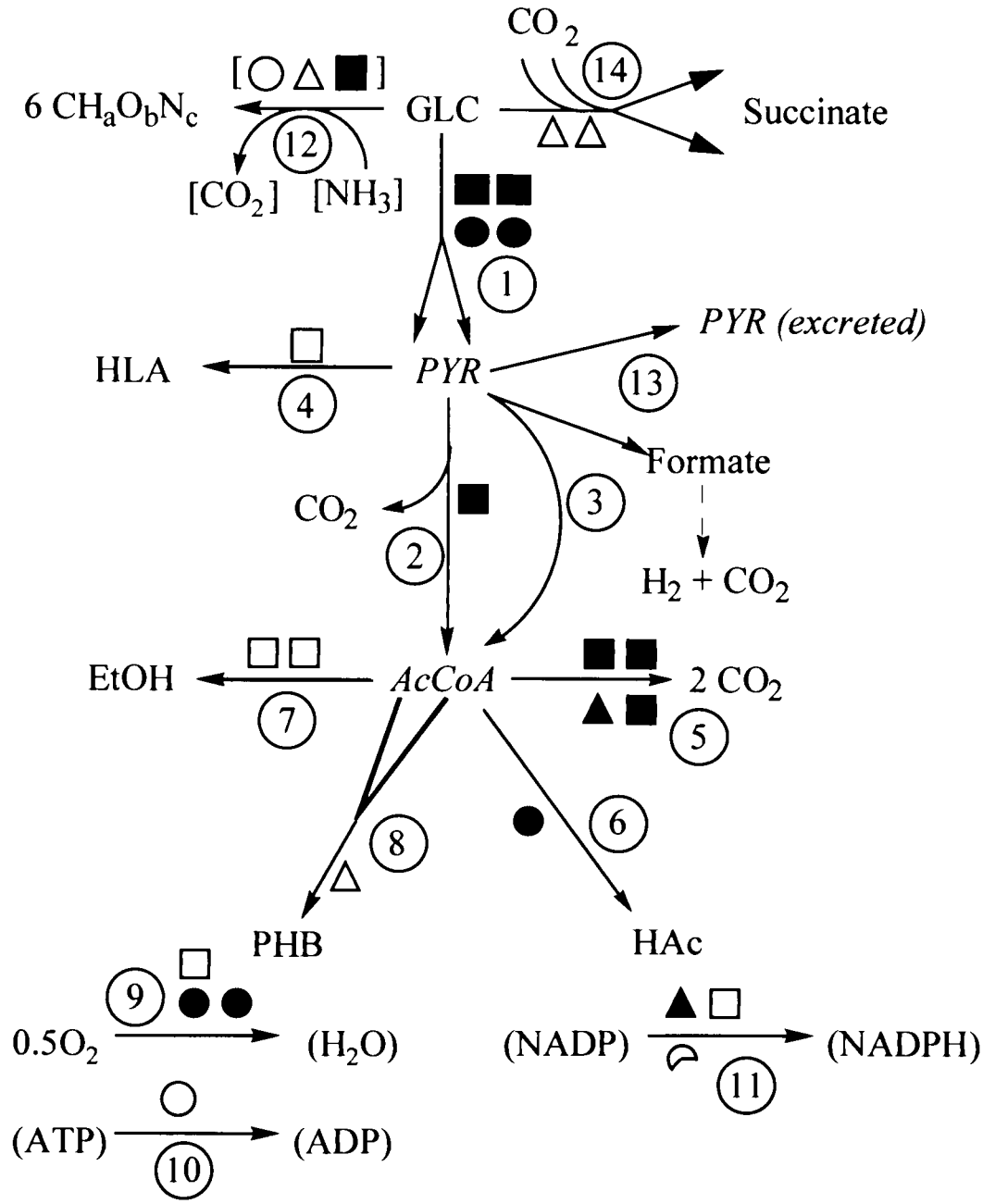

Figure 4.2: Pictorial representation of the flux network for Chapter 4, with flux labels shown in open circles. Cofactor requirements are indicated by ○ = ATP, □ = NADH, △ = NADPH. Open shapes indicate consumption (of ATP, NADH, or NADPH), filled shapes indicate production. ᔓ indicates consumption of 2/3 ATP, [] indicate variable cofactor requirements.

4.4. Results

4.4.1. Repeatability of the Fermentation

The control fermentation was performed twice: once with full data collection and once with reduced data collection. Figure 4.3 and Figure 4.4 demonstrate the excellent repeatability observed. The PHB profiles match exactly, and the residual cell mass (RCM) profiles match to within 5% apart from the first and second sample. This discrepancy is probably due to measurement error at low levels of dry cell weight. Figure 4.5 compares the total glucose utilisation of each fermentation: once again the agreement is excellent.

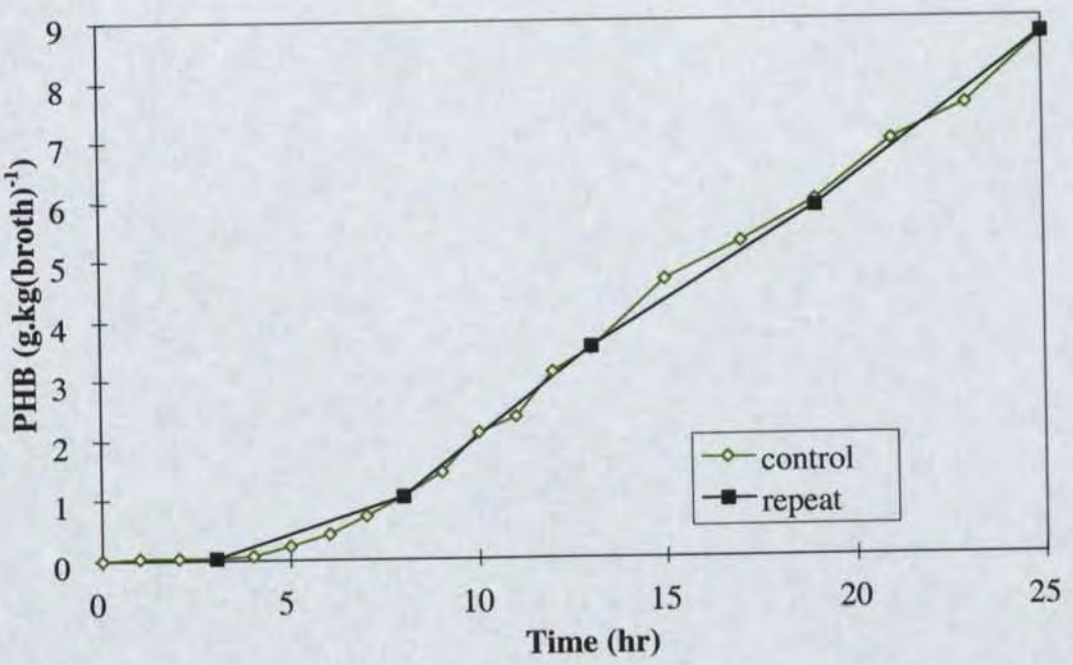

Figure 4.3: Comparison of PHB profiles for control fermentation and repeat of control.

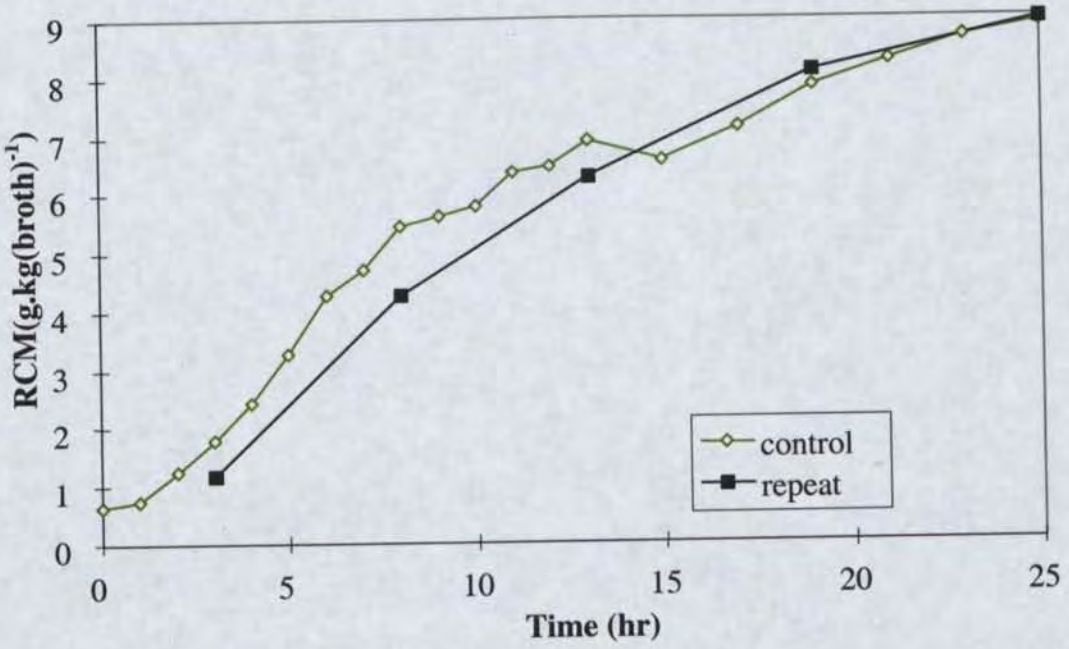

Figure 4.4: Comparison of residual cell mass (RCM) profile for control fermentation and repeat of control.

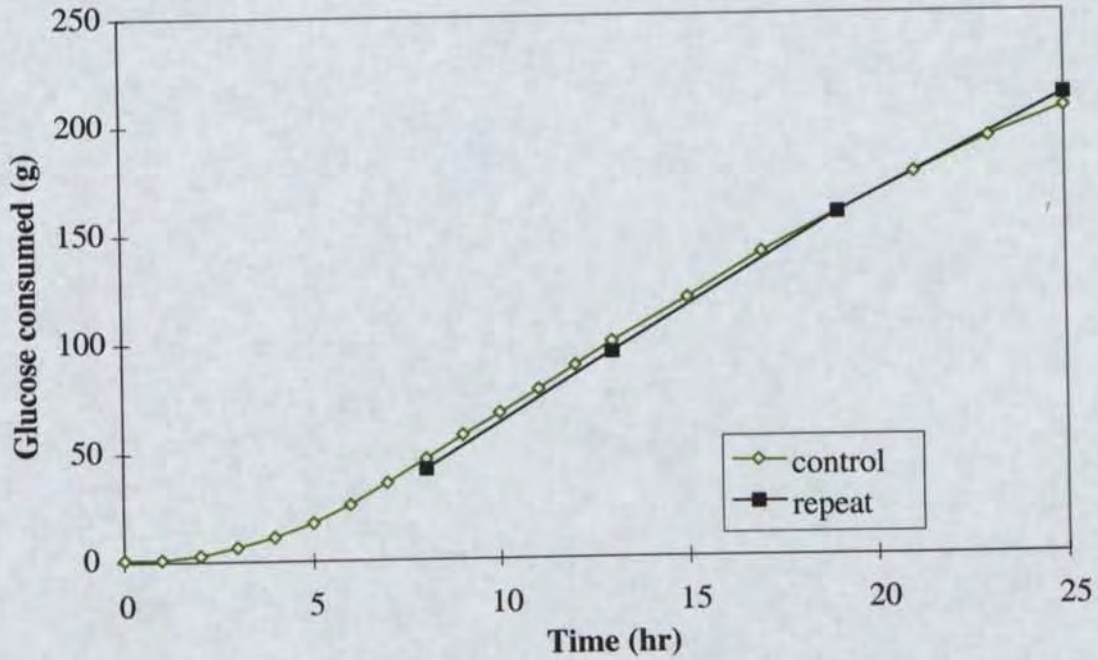

Figure 4.5: Comparison of glucose utilisation profile for control fermentation and repeat of control.

These experiments show that the control fermentation is repeatable and satisfies the criteria specified in the introduction.

4.4.2. General Fermentation Results

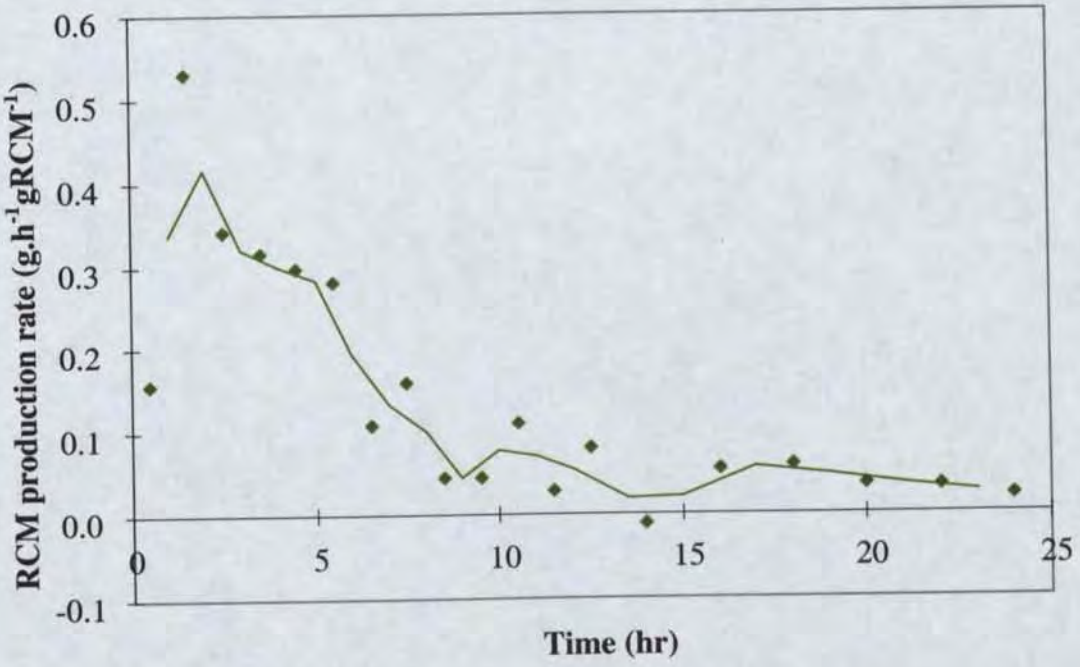

Figure 4.6: Specific growth rate (of residual cell mass) for control fermentation (CON).

Figure 4.4 and Figure 4.6 and show that cell growth is exponential until hr 5. During this period the growth rate is approximately 0.35 h^{-1}, corresponding to a doubling time of 2.1 h. This is similar to the value obtained in Chapter 2 (0.3 h^{-1}), and is quite slow for *E. coli*. After hr 5, the growth rate rapidly declines to approximately 0.05 h^{-1}, and thereafter slowly decreases to 0.03 h^{-1}. The rapid drop in growth rate is almost certainly caused by oxygen limitation, which occurs at hr 3.5 (See Figure 4.7).

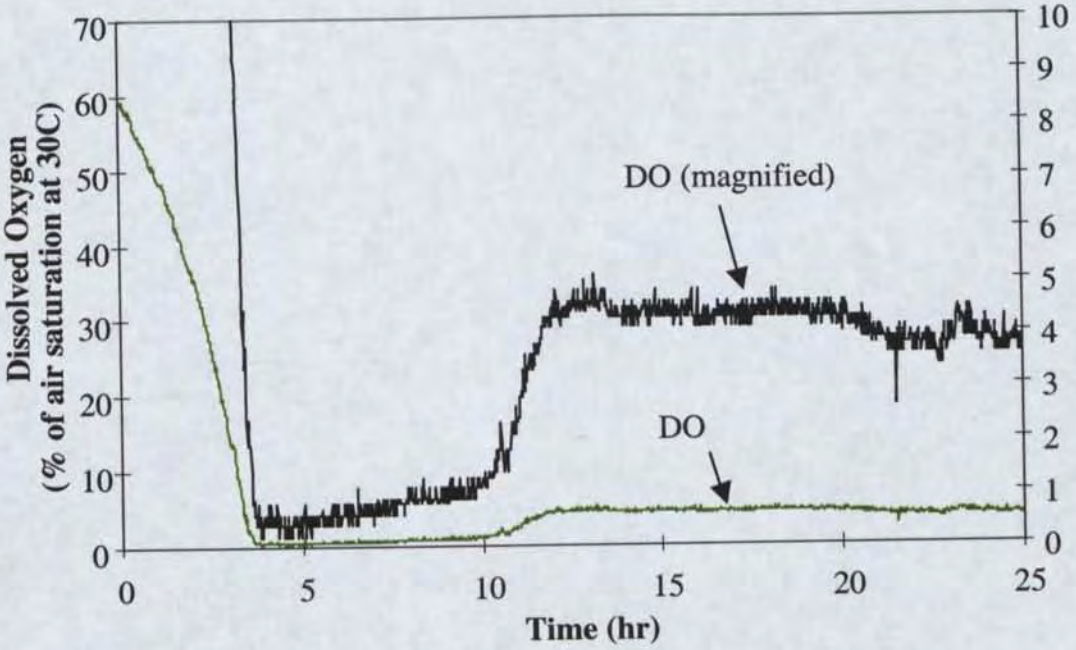

Figure 4.7: Dissolved oxygen concentration (DO) profile.

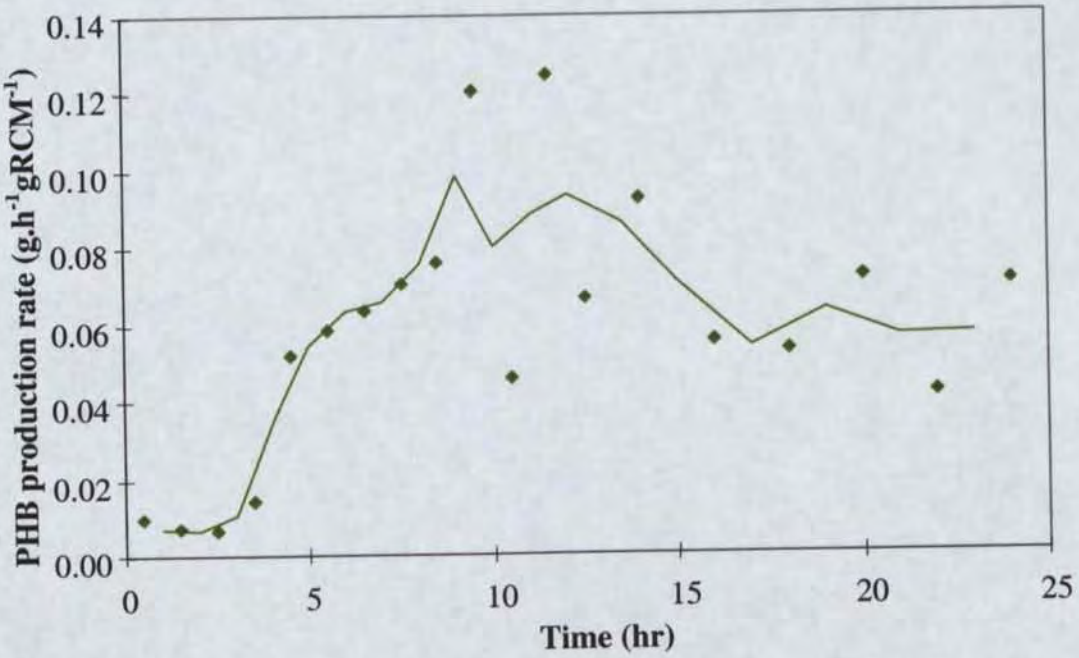

Figure 4.8: PHB specific production rate.

The PHB production profile (Figure 4.8) is quite noisy because PHB measurement has a standard error of 5%, which is large compared to the change from sample to sample. The profile shows several interesting features. Firstly, PHB synthesis occurs at a basal rate of 0.008 gPHB.gRCM^{-1}h^{-1} during the initial aerobic phase. Dividing this rate by the RCM synthesis rate (0.35 gPHB.gRCM^{-1}h^{-1}) gives the observed initial PHB content, approximately 2.3% of dry cell weight. The PHA enzymes are known to be constitutively expressed in *E. coli*, so this steady-state basal rate is not surprising. Within the first hour or two of oxygen limitation, the PHB synthesis rate rapidly rises to 0.05 gPHB.gRCM^{-1}h^{-1}, a six-fold increase. It seems likely that a change in metabolite concentrations is responsible for the increased PHB production. Other explanations, such as an increase in plasmid copy number due to reduced growth rate, seem less likely given the rapid increase (less than one generation time). Section 4.8 discusses in more detail the metabolic changes caused by oxygen limitation. The data show that oxygen limitation is almost certainly the cause of the typical biphasic growth profile exhibited by PHB-producing *E. coli* at low-to-moderate cell densities, i.e. a cell-accumulation phase followed by a PHB accumulation phase. It should be noted that at higher cell densities oxygen limitation may not be the cause, as described in Chapter 5.

From hr 4.5 to hr 10 there is a linear increase in synthesis rate from 0.05 gPHB.gRCM^{-1}h^{-1} to 0.09 gPHB.gRCM^{-1}h^{-1}. This linear increase is also observed in the subsequent fermentations, described in Chapters 5 and 6. The possible causes of this are discussed in Section 4.7.2. After hr 10, the PHB synthesis rate plateaus at 0.09 gPHB.gRCM^{-1}h^{-1}, where it remains until hr 13 or so. Thereafter it gradually declines to 0.06 gPHB.gRCM^{-1}h^{-1} by termination (hr 25). In comparison, the Chapter 2 high-cell-density fermentation (HCDF) shows a peak rate near 0.14 gPHB.gRCM^{-1}h^{-1} which was sustained for more than 12 hours before declining to 0.05 gPHB.gRCM^{-1}h^{-1} over the next 24 hours. The reason for the higher rate and longer duration is not apparent but may be related to oxygen limitation as shown in Chapter 5.

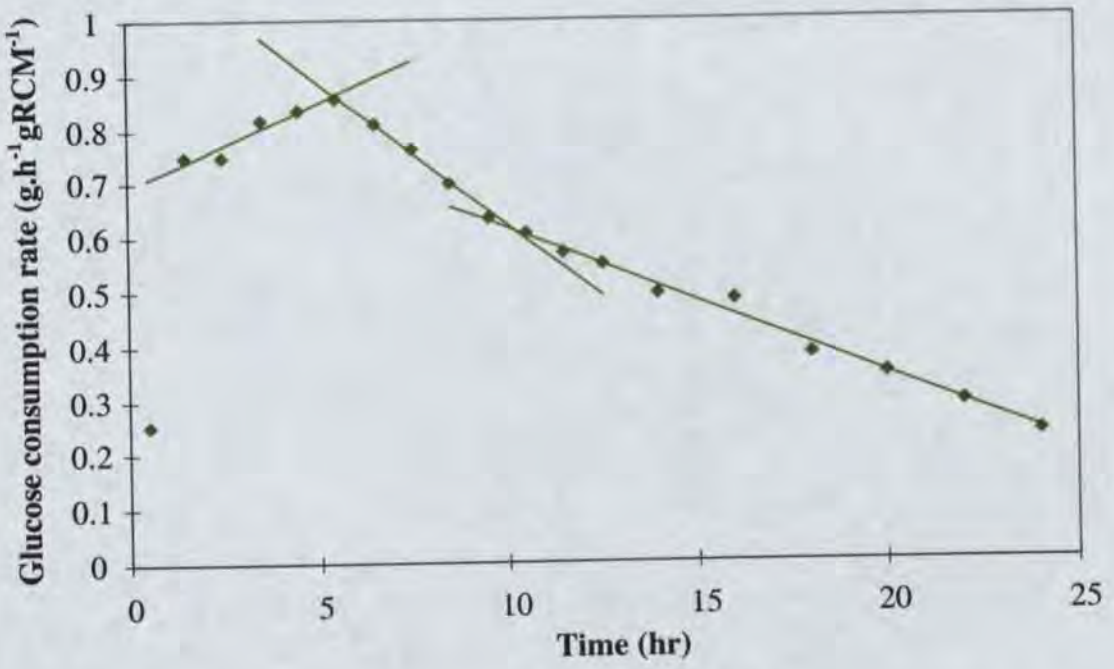

Figure 4.9: Glucose specific consumption rate.

The glucose consumption profile (Figure 4.9) shows that glucose consumption is initially 0.75 gGlc.gRCM^{-1}h^{-1}, rising slowly to 0.86 gGlc.gRCM^{-1}h^{-1} by hr 5, thereafter steadily declining to 0.6 gGlc.gRCM^{-1}h^{-1} by hr 9-10. At this point, there is an obvious change in slope, such that glucose demand now declines linearly to 0.2 gGlc.gRCM^{-1}h^{-1} by hr 25. If this decline were to continue linearly, glucose utilisation would cease entirely at hr 33. The cell yield on glucose over the first four hours (prior to appreciable PHB synthesis) is 86 gRCM.molGlc^{-1} (0.48 gRCM.gGlc^{-1}). This is slightly higher than the HCDF (81 gRCM.molGlc^{-1}) and is also at the upper limit of the literature values (70-85 gRCM.molGlc^{-1}) for glucose-limited chemostat cultures of *E. coli* (Neijssel *et al.* (1996)). This probably reflects experimental error in dry cell weight measurement at low cell densities.

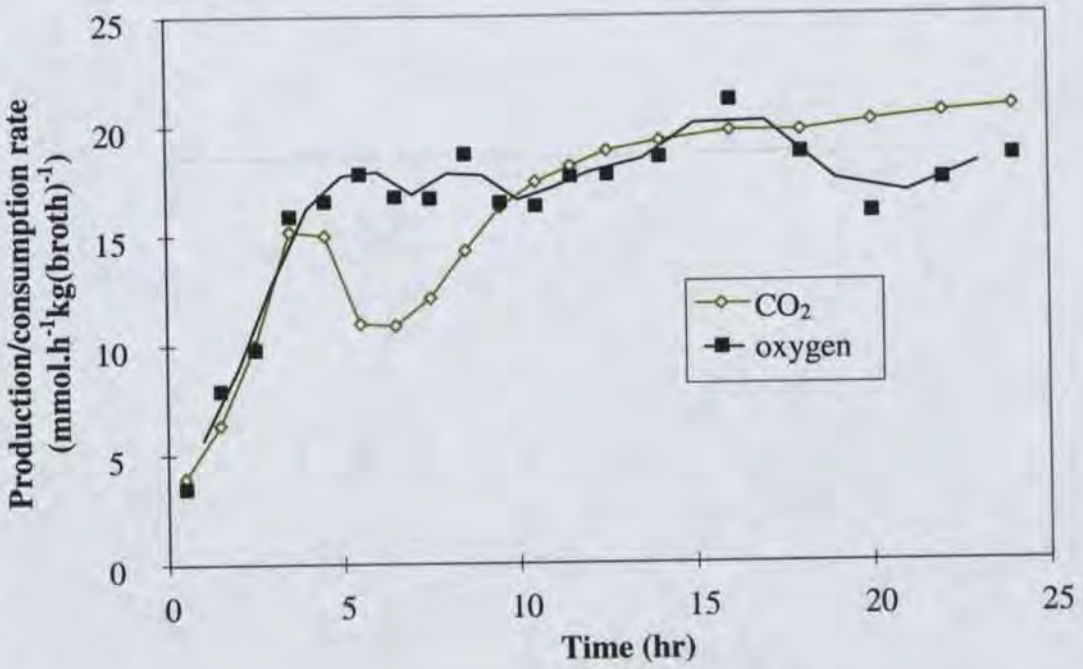

Figure 4.10: CO_2 production rate and oxygen consumption rate.

Figure 4.10 shows the CO_2 production and oxygen consumption curves. As expected, oxygen consumption climbs steadily until it reaches a plateau (18 mmol.kg(broth)$^{-1}$h^{-1}). At this point oxygen becomes limiting and thereafter the rate stays constant, indicating that the volumetric mass-transfer coefficient (k_La) is constant (1.1 min^{-1}). The noisiness in the oxygen data is due to the method of measurement: because inlet composition is 21% oxygen and exhaust composition is approximately 20%, measurement errors are magnified by a factor of 20. In contrast, carbon dioxide exhibits much lower errors. During the initial non-oxygen-limited period, cellular oxygen usage is constant at 8 mmol.gRCM^{-1}h^{-1}. This compares well with the high-cell-density fermentation in Chapter 3, and also to the literature value of 10 mmol.gDCW^{-1}h^{-1} for *E. coli* in aerobic glucose-limited chemostats (Neijssel *et al.* (1996)). It compares less well with the literature estimate of 20 mmol.gRCM^{-1}h^{-1}, obtained for *E. coli* B/r (wild type) on a variety of growth substrates (Ingraham *et al.* (1983)).

Initially the carbon dioxide profile matches the oxygen profile closely, indicating a respiratory quotient (RQ) of approximately unity, as expected for aerobic growth. Once oxygen limitation occurs however, the CO_2 rapidly drops to 11 mmol.kg(broth)$^{-1}$h^{-1} (RQ = 0.611). After hr 6, the CO_2 rate rises rapidly to 18 mmol.kg(broth)$^{-1}$h^{-1} by hr 10-11, raising the RQ

above 1. Thereafter the CO_2 rate gradually rises to 21 mmol.kg(broth)$^{-1}h^{-1}$ by hr 24. When examined on a per-gRCM basis, Figure 4.11 shows similar trends in CO_2 rate. The rate is initially quite constant (6.5 mmol.gRCM$^{-1}h^{-1}$), with a gentle linear increase similar to the glucose consumption profile. At the point of oxygen limitation, CO_2 production abruptly decreases by 65% to 2.4 mmol.gRCM$^{-1}h^{-1}$, rising very gradually to a plateau of 2.85 mmol.gRCM$^{-1}h^{-1}$ at hr 10. Production remains steady till hr 15, whereafter it gradually declines to 2.4 mmol.gRCM$^{-1}h^{-1}$ by hr 23. As discussed in Section 4.5, the rapid drop in CO_2 is caused by shutdown of the TCA cycle.

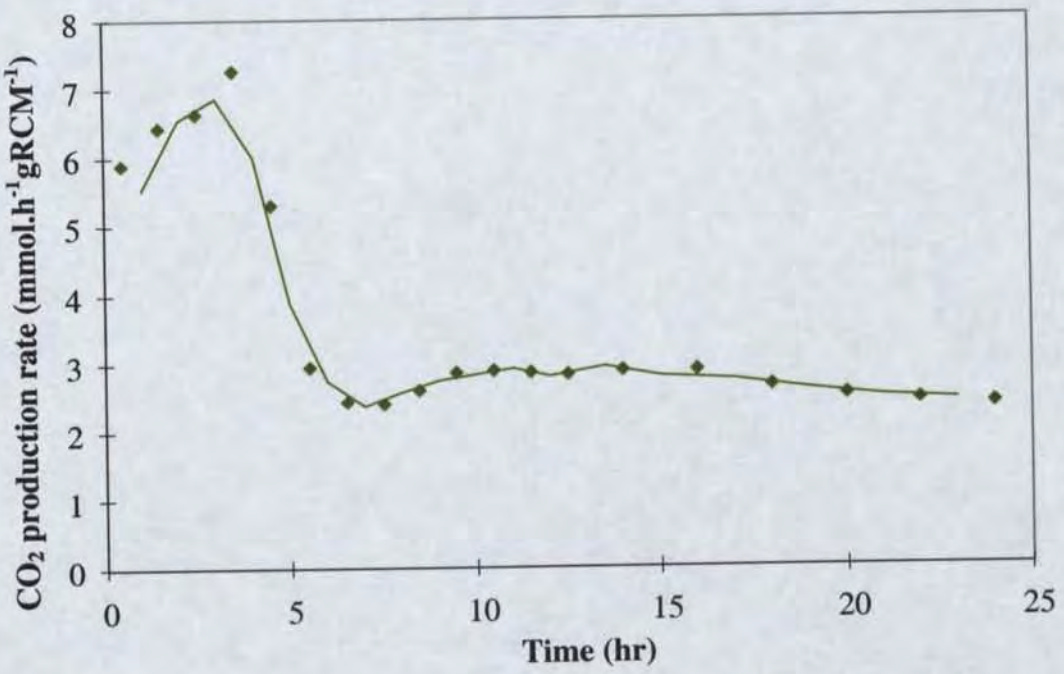

Figure 4.11: CO_2 production rate on an RCM basis.

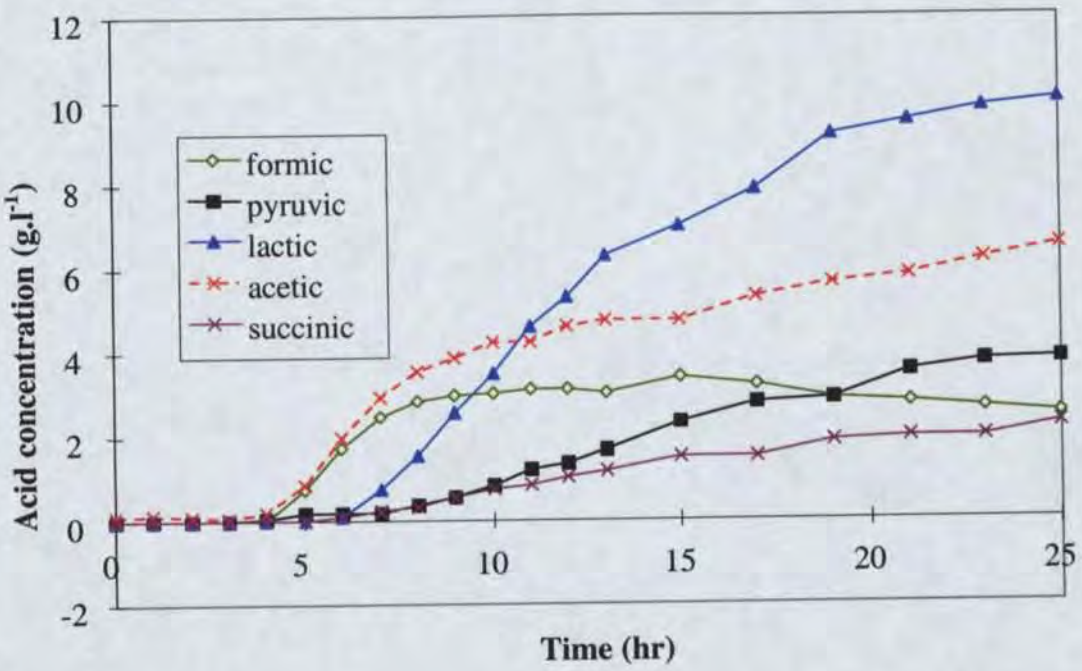

Figure 4.12: Acid excretion profile.

Figure 4.12 clearly shows that there is rapid excretion of fermentative byproducts. Based on the HCDF, the presence of lactic, acetic and formic acid were expected. With the exception of formate, the levels are higher than the previous fermentation, despite the lower cell density. It seems likely that the different method of glucose feeding is responsible, since lactate and acetate can be re-used during pH-stat feeding. As in the HCDF, ethanol production is almost completely absent (less than 0.1 $g.l^{-1}$).

Succinate was not previously detected, however it is a normal fermentation byproduct and is not unexpected. The excretion of pyruvate is completely unexpected since unlike the other acids it has high energetic utility to the cell and is not a normal fermentation byproduct. Aerobic carbon-sufficient chemostats have been observed to excrete "overflow" products such as acetate and pyruvate (the "Crabtree" effect) due to metabolic imbalances (Neijssel *et al.* (1996)). However this is not observed under semi-aerobic or anaerobic conditions. (Acetate excretion as an overflow product is distinct from its role in fermentative metabolism). The XL1-Blue strain may therefore have a mutation in some aspect of its central metabolism. It is also possible that this anomalous production of pyruvate is related to enhanced PHB synthesis, since XL1-Blue has been selected from many other strains for its high PHB yield.

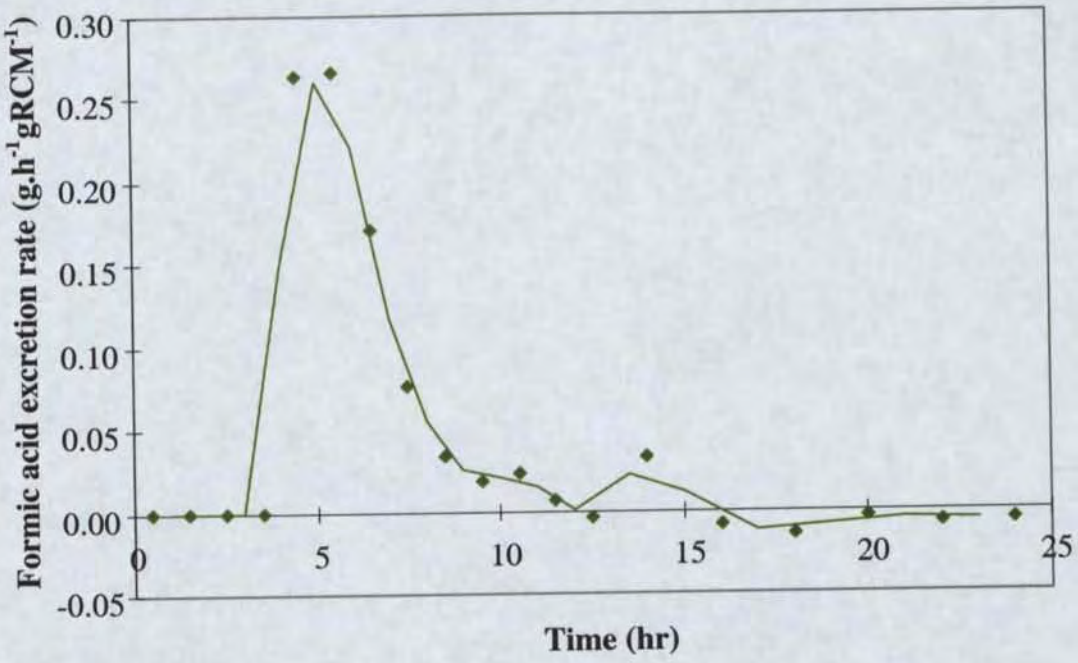

Figure 4.13: Formic acid exretion rate.

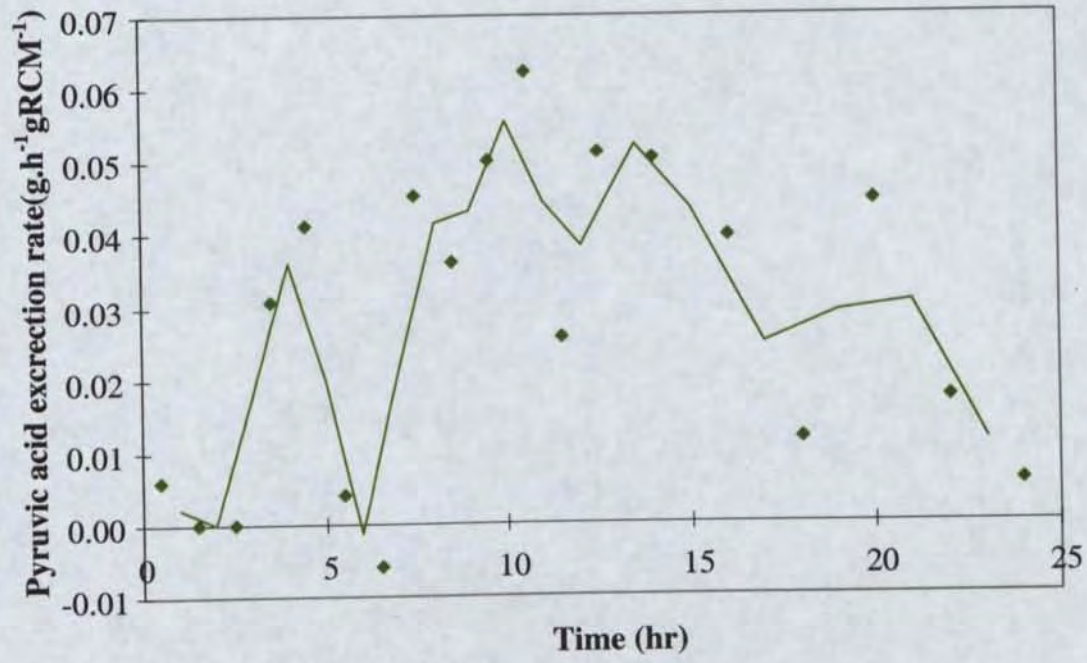

Figure 4.14: Pyruvic acid excretion rate.

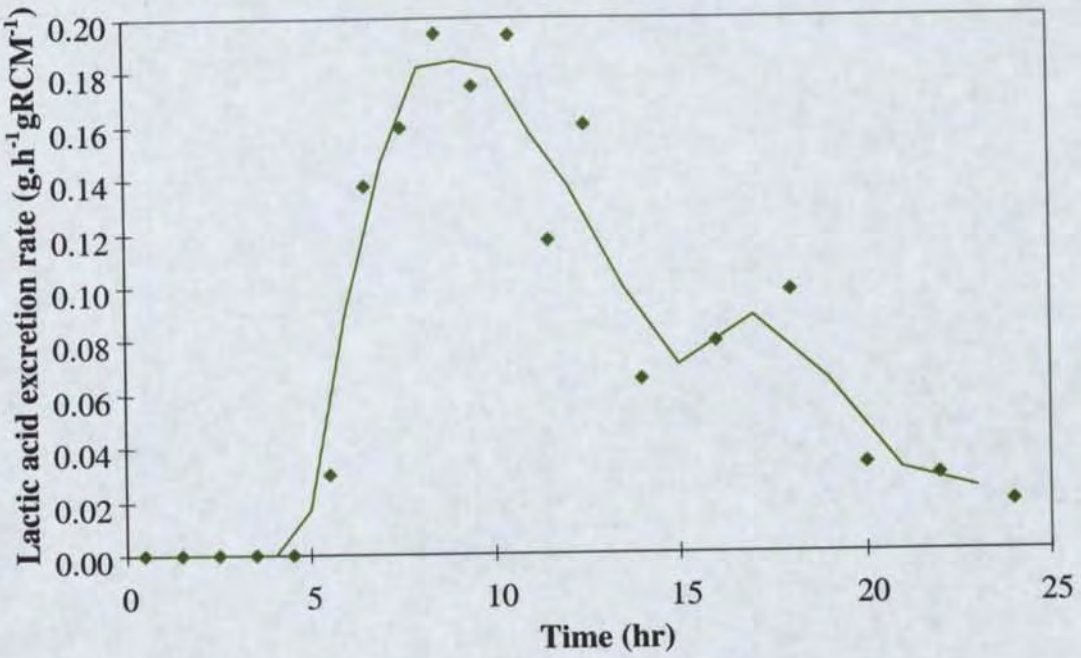

Figure 4.15: Lactic acid excretion rate.

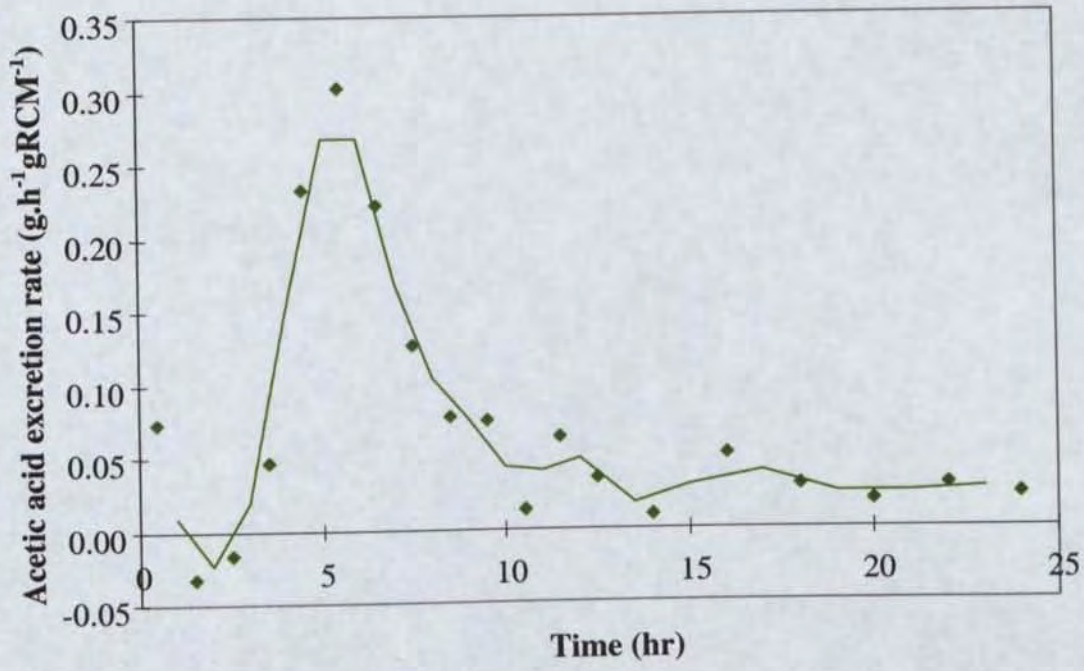

Figure 4.16: Acetic acid excretion rate.

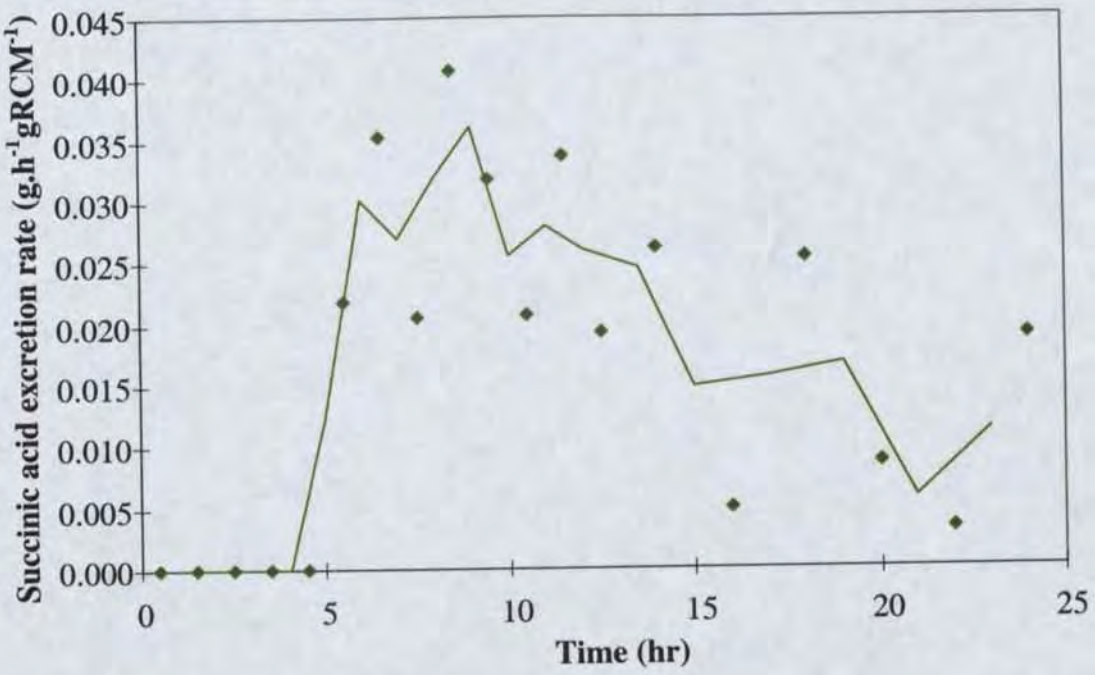

Figure 4.17: Succinic acid excretion rate.

The acid excretion rates (Figures 4.13 to 4.17) clearly show that acid excretion did not commence until oxygen limitation at hr 3.5 - 4. Within experimental error, excretion of all acids commenced simultaneously, although lactic and succinic acid production appear to be delayed by an hour. Both acetic and formic acids show a strong maximum (0.25 $g.gRCM^{-1}h^{-1}$) in excretion rate which is sustained for no more than 2-3 h. Thereafter their rates rapidly decline to 10% of this maximum by hr 10. Acetic acid excretion continues slowly but formic acid essentially ceases. In comparison, succinic, lactic and pyruvic acids show a qualitatively different profile: they rise rapidly to a maximum at hr 5 - 7, and thereafter decline far more gradually than acetic and formic acid. The reasons for these observations are discussed subsequently in Section 4.8.

The profile of ammonium ion concentration is shown in Figure 4.18, indicating that it stayed within acceptable limits for the whole fermentation.

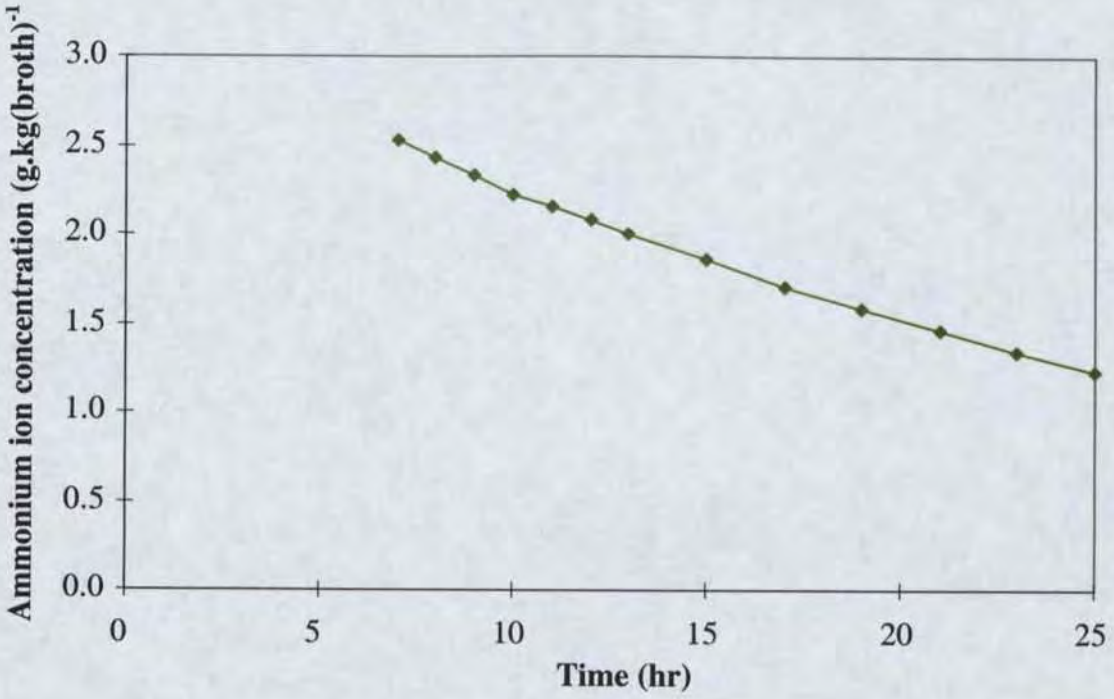

Figure 4.18: Ammonium ion concentration during the fermentation.

4.4.3. Acyl-CoA Metabolite Measurements

Method development

The method was adapted from the literature (Mansfield *et al.* (1995); Corkey (1988); Debuysere and Olson(1983)), and after several modifications now yields typical chromatograms as shown in Figure 4.19

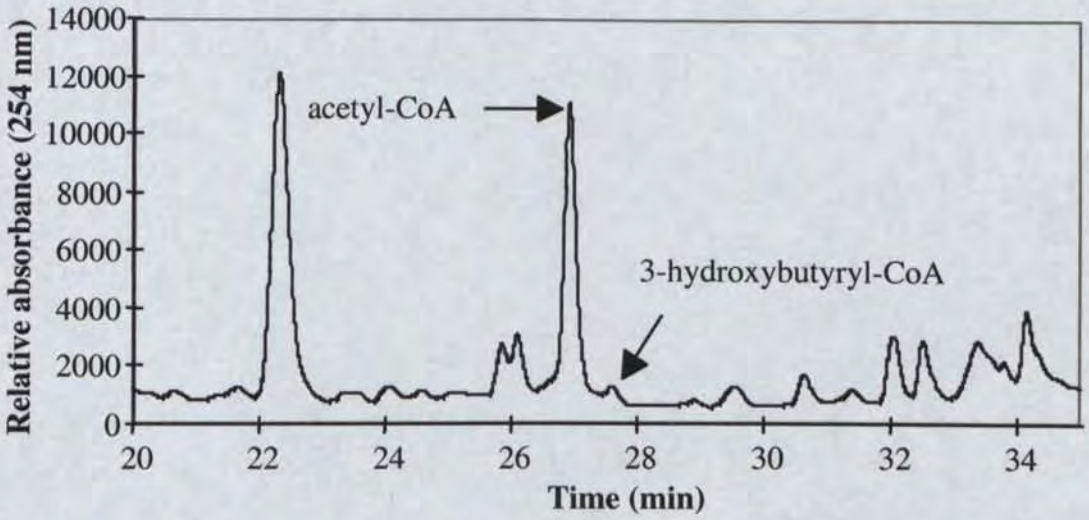

Figure 4.19: Typical acyl-CoA chromatogram.

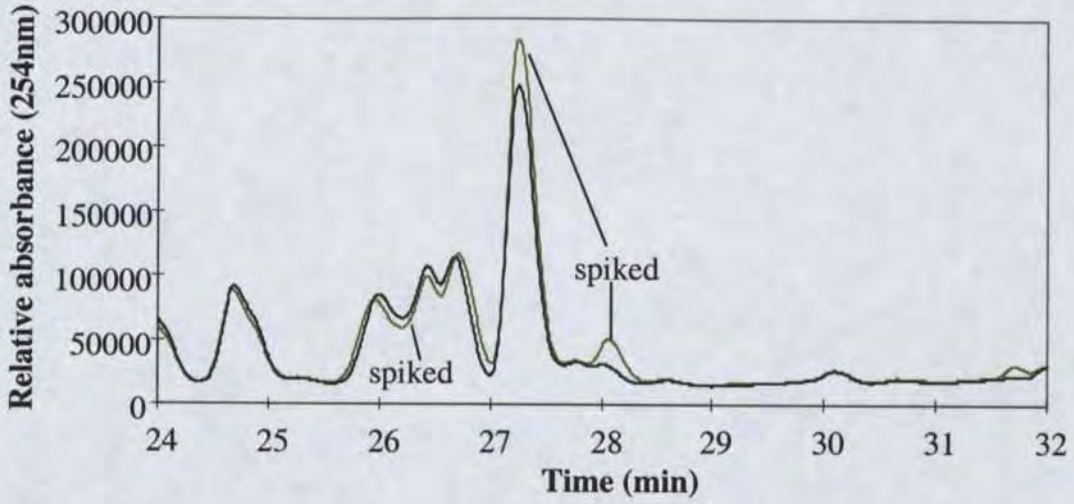

Figure 4.20: Another typical acyl-CoA chromatogram spiked with acetyl-CoA and 3-hydroxybutyryl-CoA.

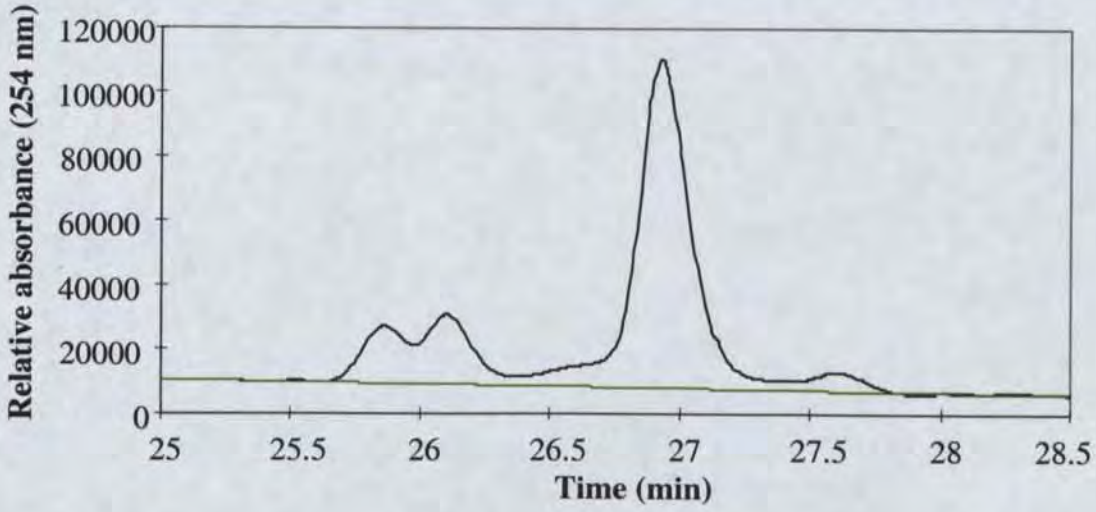

Figure 4.21: Baseline-fitting strategy on a typical acyl-CoA chromatogram.

The major difficulty that occurs when quantifying peaks is placement of an appropriate baseline. This has most impact on the 3-hydroxybutyryl-CoA peak, because it is small. In contrast the acetyl-CoA peak is less affected. Curve-fitting software (Peakfit V4.00, Jandel Scientific, San Rafael California) was used to calculate peak areas. The baseline was marked in as demonstrated in Figure 4.21, then an EMG curve was fitted to each peak using least-squares.

The degradation of acyl-CoAs was quantified by spiking base fermentation medium with known amounts of acetyl-CoA, acetoacetyl-CoA and 3-hydroxybutyryl-CoA, then taking this sample through the same sampling and analysis procedure as for normal broth samples. The results are shown in Table 4.5.

Table 4.5: Degradation of acyl-CoA during sampling & analysis.

Analyte	Proportion recovered	Std Deviation
acetyl-CoA	93.6%	1.0%
acetoacetyl-CoA	93.8%	2.3%
3-hydroxybutyryl-CoA	90.6%	0.5%

Mean recovery and sample standard deviation and was estimated from four replicates.

Repeats of actual fermentation samples showed approximately 5% standard deviation for acetyl-CoA and 10-15% standard deviation for 3-hydroxybutyryl-CoA. Depending on the exact baseline position chosen, the calculated peak areas could also vary by up to +/-10% for acetyl-CoA and +/-50% for 3-hydroxybutyryl-CoA. However this systematic error does not affect sample-to-sample variation (i.e. the profile shape).

Fermentation results

Figure 4.22 shows the concentrations of acetyl-CoA and 3HB-CoA, on a RCM basis. It shows an initial acetyl-CoA level of 350 μg.gRCM^{-1}. This rises to 600 μg.gRCM^{-1} during the onset of oxygen limitation, then declines slowly back to 350 μg.gRCM^{-1} by hr 9. Thereafter it exhibits a gradual decline to 300 μg.gRCM^{-1} by hr 24. As previously described, the TCA cycle flux diminished when oxygen limitation commenced, reducing demand for acetyl-CoA. This is the likely cause of the increased acetyl-CoA concentration during hrs 3.5 - 6, a period of metabolic adjustment. Likewise the level of constancy during the later phase is not surprising given that acetyl-CoA is a central metabolite and is strongly regulated. However a very interesting observation is that the level of acetyl-CoA is the same during both aerobic growth and oxygen-limited growth, after the transitional peak. This is surprising given the gross differences in metabolism. The causes of this are not apparent.

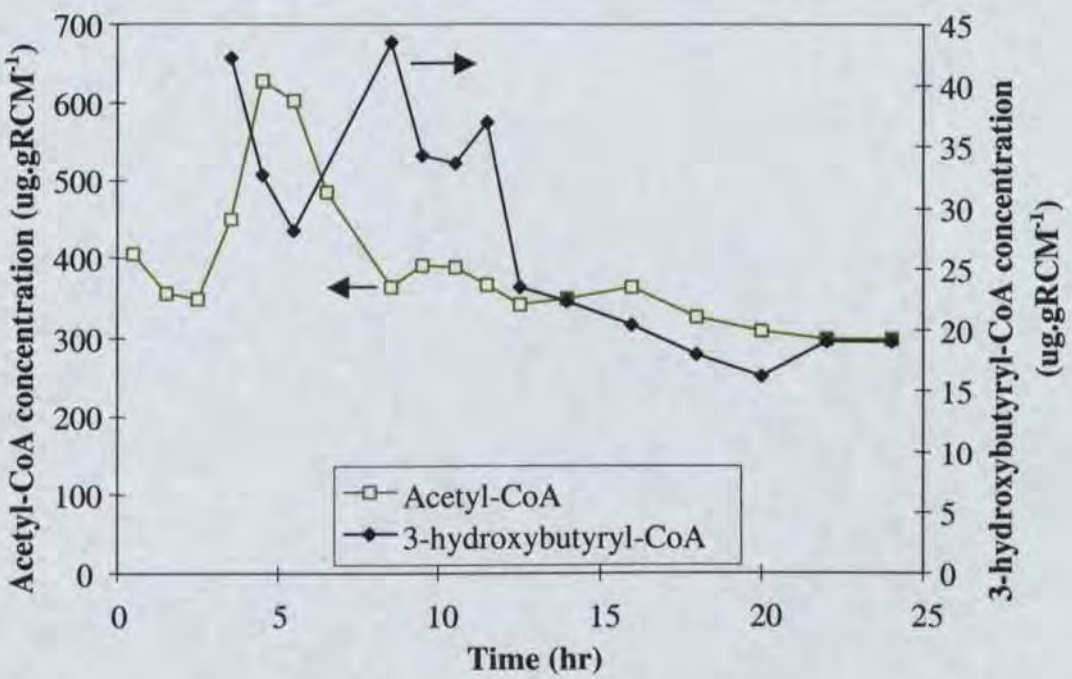

Figure 4.22: Concentration of acetyl-CoA and 3-hydroxybutyryl-CoA on an RCM basis.

3-hydroxybutyryl-CoA concentrations were much lower than acetyl-CoA and hence more difficult to quantify. Meaningful estimates are not available before hr 3. Unfortunately, this means that data are not available for the period prior to oxygen limitation. The initial concentration lies between 30 and 40 $\mu g.gRCM^{-1}$, and remains fairly constant until hr 10. At this point it appears to drop to 25 $\mu g.gRCM^{-1}$, and then slowly declines to 20 $\mu g.gRCM^{-1}$ by the end of the fermentation. It should be borne in mind that the concentrations may exhibit some systematic error due to baseline problems in the chromatograms.

The values obtained compare well with the literature, as shown in Table 4.6.

Table 4.6: Literature values for acyl-CoA concentrations.

Study	Details	acetyl-CoA ($\mu g.gRCM^{-1}$)	3HB-CoA ($\mu g.gRCM^{-1}$)
This study		300-600 +/-20%	15-40 +/- 50%
A	*R. eutropha*	1100	24
B	wild type *E. coli*	520	--
C	*E. coli* K12	660	--

A cell volume of 2 $ml.gRCM^{-1}$ was assumed for the data from (Jackowski (1996)). Sources of data: A (Mansfield *et al.* (1995)), B (Jackowski (1996)), C (Chohnan *et al.* (1998)).

The steady-state turnover time of the pools of metabolites can be estimated using the following equation

$$t_t = \frac{[acyl - CoA]}{flux} \tag{4.2}$$

where

t_t = turnover time (s)

$[acyl - CoA]$ = concentration of metabolite ($\mu mol.gRCM^{-1}$)

$flux$ = flux through pool ($\mu mol.gRCM^{-1}.s^{-1}$)

For acetyl-CoA a representative flux is 2.5 $mmol.gRCM^{-1}h^{-1}$ (flux 2 plus flux 3) and the pool size is 0.5 $\mu mol.gRCM^{-1}$ (400 $\mu g.gRCM^{-1}$), giving a turnover time of 0.7 s. For 3HB-CoA the flux is 0.75 $mmol.gRCM.h^{-1}$ and the pool size is 0.025$\mu mol.gRCM^{-1}$ (20 $\mu g.gRCM^{-1}$), giving a turnover time of 0.12 s. These turnovers are very rapid and place stringent demands on the sampling method. If the pha enzymes are not rapidly inactivated the metabolite pools could change appreciably. However the acyl-CoA concentrations gave good repeatability and were independent of sampling volume, hence the sampling procedure used was probably adequate.

4.5. Flux Analysis and Discussion

The carbon balance for each sample ranged between 75-95% closure and was generally around 90%. The overall mass balance is quite good (93% closure). A total organic carbon analysis of the culture failed to detect any missing carbon, hence there was probably a calibration error in the glucose feed. This slight systematic error will have only minor effects on the quantitative flux distributions.

The final distribution of metabolic byproducts (at hr 25) is given in Table 4.7. Only 20% of the glucose carbon moles are converted to PHB, compared with:

- 49% for the high-cell-density fermentation (HCDF) in Chapter 2; and
- 66% theoretical maximum (Yamane (1993));

Organic acids account for most of the wastage, viz a total of 40% on a mol-C basis.

Table 4.7: Overall mass balance on control fermentation.

	mol per 100 mol glucose	mol-C per 100 mol-C glucose
carbon dioxide	109	18
RCM (mol-C-equivalents)	89	15
PHB	30	20
acetic acid	32	11
formic acid	16	3
lactic acid	33	16
pyruvic acid	13	6
succinic acid	6	4
	Overall closure:	93%

The redox balance also closed well, apart from during the first few hours when oxygen consumption was difficult to measure accurately. On an individual sample basis the error statistic did not indicate any systematic errors. However the overall error statistic did suggest a small systematic error (98% probability). As previously mentioned, this is probably caused by a calibration error in the glucose feed.

Figure 4.23 shows that there is only a gradual decline in the rate of PHB production on a per-residual-cell-mass basis. Since the overall glucose flux is declining, this results in increased diversion of flux to PHB production, as shown by the glucose basis. For some reason, PHB production is persisting at a high rate relative to the remaining metabolic activity. This is discussed further in Section 4.8.

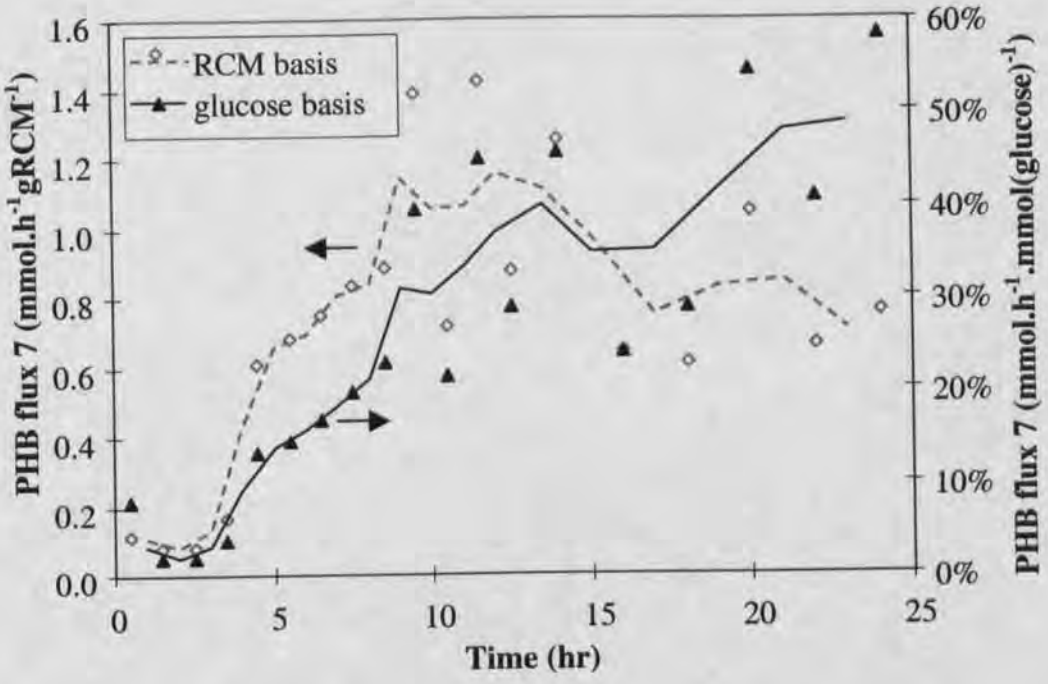

Figure 4.23: PHB production on an RCM basis and a glucose-flux basis.

On a residual cell mass basis, the ATP dissipation flux shows a initial rate of approximately 20 mmol.gRCM^{-1}h^{-1}, which begins to decline steadily from hr 5 onwards, eventually reaching 10 mmol.gRCM^{-1}h^{-1} at hr 24. On a glucose basis however, the initial ATP yield from glucose is near 4 mol/mol, and remains essentially constant until hr 10. Thereafter it rises to its final value of 7 mol/mol by hr 24. This shows that despite the cell diverting increasing amounts of its flux toward energy production, the amount of ATP available continues to decrease. It is difficult to draw any conclusions from the ATP profile because there is considerable uncertainty in the efficiency of ATP generation from NADH (See Section 2.3).

When compared with the HCDF, the control fermentation's (CON) ATP profile is qualitatively similar, however the numerical values are somewhat lower (25-30 mmol.gRCM^{-1}h^{-1} for HCDF vs 15-20 mmol.gRCM^{-1}h^{-1} for CON)

Although several studies have shown that the TCA cycle is generally not active during aerobic growth of *E. coli* on glucose (Cronan and LaPorte (1996)), the flux analysis very clearly demonstrates that XL1-Blue(pSYL107) makes extensive use of the TCA cycle during aerobic exponential growth on glucose. TCA cycle flux (flux 5) shows a high initial rate (55% mol/mol of glucose), which abruptly declines to 3% once oxygen limitation commences. This is expected, since production of acetic acid, formic and pyruvic acid are accompanied by the generation of large amounts of NADH, replacing the energy-production role of the TCA cycle. The flux remains low until hr 12, whereafter it rises to 8-10%. This trend is discussed subsequently in Section 4.8.

Figure 4.24 shows the acid fluxes on a glucose-supply basis. It is immediately apparent that when acetic acid production commences, the increased flux to acetyl-CoA is supplied entirely by pyruvate-formate lyase (flux 3). It is not until hr 9-10 when formic acid flux drops to zero that pyruvate dehydrogenase (flux 2) makes an appreciable contribution. It is also interesting

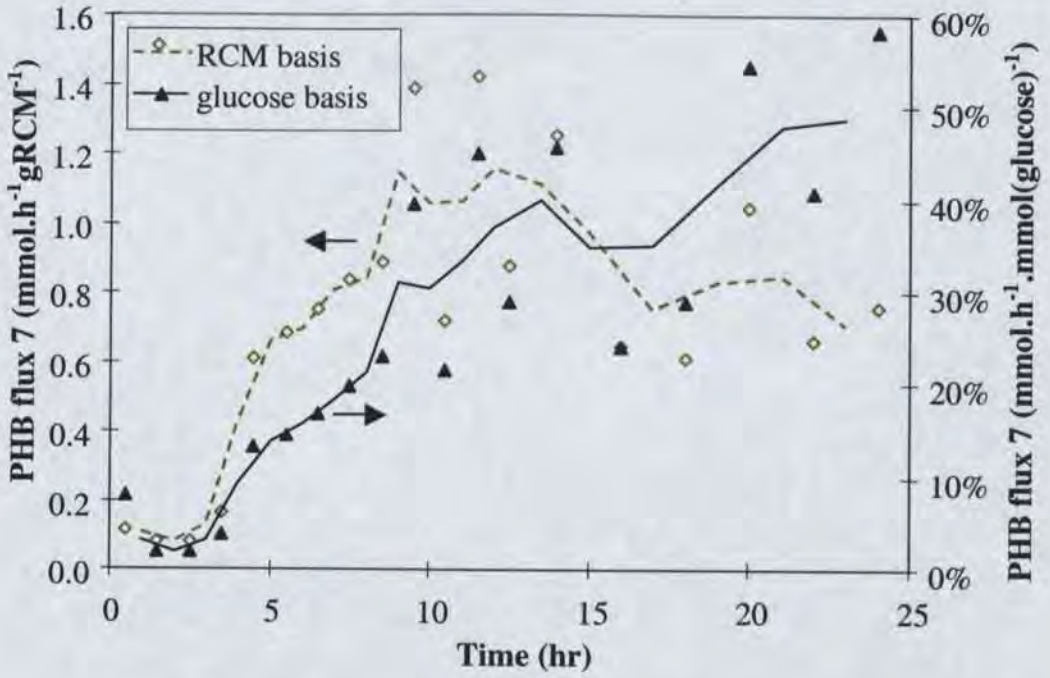

Figure 4.23: PHB production on an RCM basis and a glucose-flux basis.

On a residual cell mass basis, the ATP dissipation flux shows a initial rate of approximately 20 mmol.gRCM^{-1}h^{-1}, which begins to decline steadily from hr 5 onwards, eventually reaching 10 mmol.gRCM^{-1}h^{-1} at hr 24. On a glucose basis however, the initial ATP yield from glucose is near 4 mol/mol, and remains essentially constant until hr 10. Thereafter it rises to its final value of 7 mol/mol by hr 24. This shows that despite the cell diverting increasing amounts of its flux toward energy production, the amount of ATP available continues to decrease. It is difficult to draw any conclusions from the ATP profile because there is considerable uncertainty in the efficiency of ATP generation from NADH (See Section 2.3).

When compared with the HCDF, the control fermentation's (CON) ATP profile is qualitatively similar, however the numerical values are somewhat lower (25-30 mmol.gRCM^{-1}h^{-1} for HCDF vs 15-20 mmol.gRCM^{-1}h^{-1} for CON)

Although several studies have shown that the TCA cycle is generally not active during aerobic growth of *E. coli* on glucose (Cronan and LaPorte (1996)), the flux analysis very clearly demonstrates that XL1-Blue(pSYL107) makes extensive use of the TCA cycle during aerobic exponential growth on glucose. TCA cycle flux (flux 5) shows a high initial rate (55% mol/mol of glucose), which abruptly declines to 3% once oxygen limitation commences. This is expected, since production of acetic acid, formic and pyruvic acid are accompanied by the generation of large amounts of NADH, replacing the energy-production role of the TCA cycle. The flux remains low until hr 12, whereafter it rises to 8-10%. This trend is discussed subsequently in Section 4.8.

Figure 4.24 shows the acid fluxes on a glucose-supply basis. It is immediately apparent that when acetic acid production commences, the increased flux to acetyl-CoA is supplied entirely by pyruvate-formate lyase (flux 3). It is not until hr 9-10 when formic acid flux drops to zero that pyruvate dehydrogenase (flux 2) makes an appreciable contribution. It is also interesting

to note that from hr 10 onwards, acetic acid production remains constant at 25% of glucose supply flux. Likewise, pyruvate and succinate fluxes remain constant at 18% and 3% respectively. In contrast, lactate flux steadily declines after its peak (60%) at hr 10.

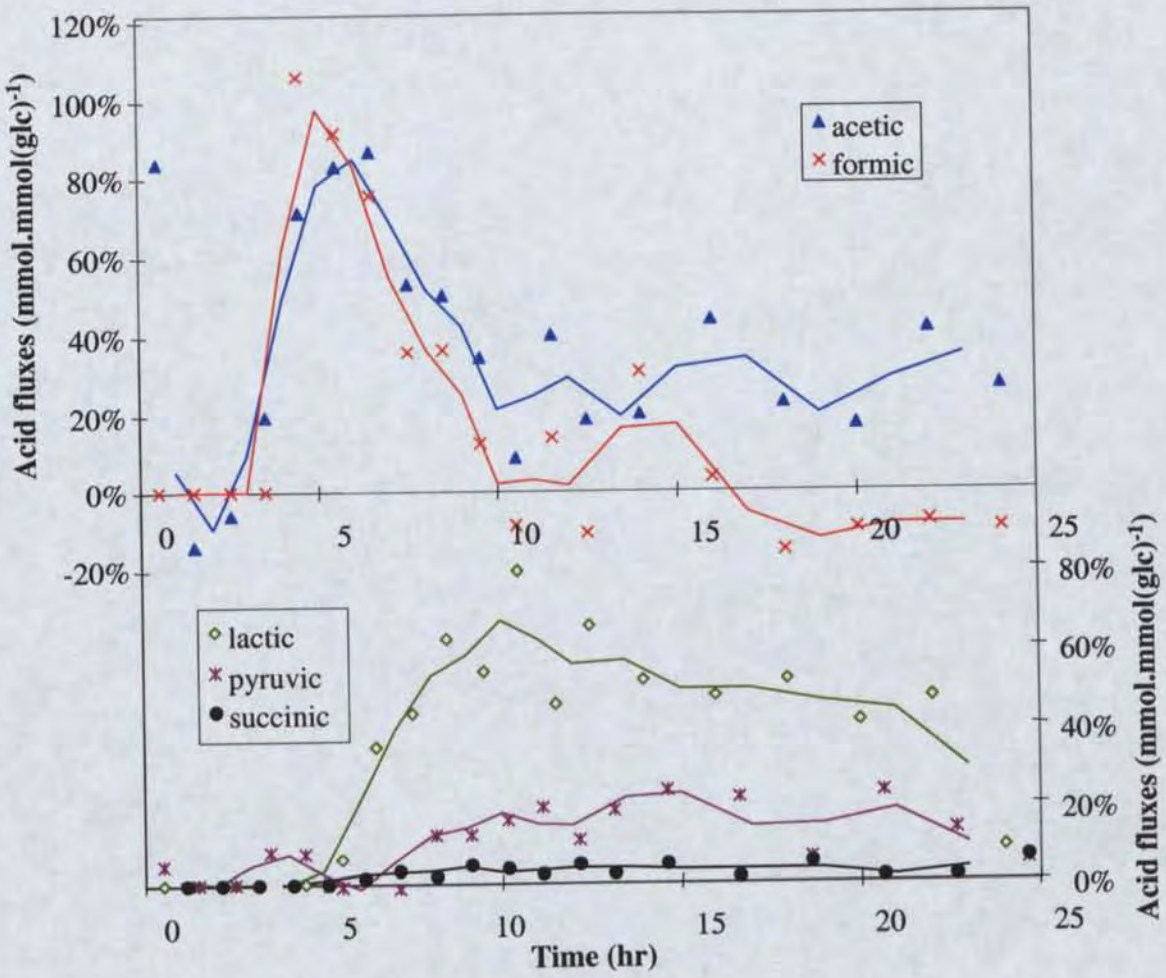

Figure 4.24: Acid fluxes on a glucose-supply basis.

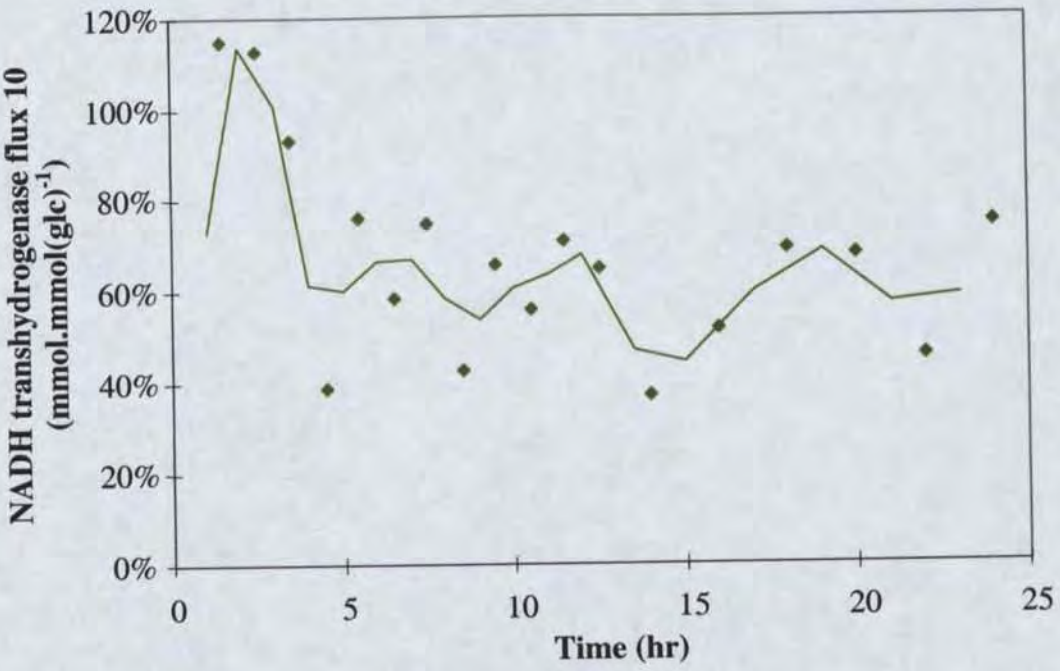

Figure 4.25: Lumped NADPH generation flux.

Figure 4.25 shows the lumped NADPH generation flux (flux 11). This is the sum of generation by the energy-linked NAD(P)H transhydrogenase and the pentose-phosphate bypass. Initially it is constant at 110 mmol NADPH per 100 mmol glucose (4.4 mmol NADPH.gRCM^{-1}h^{-1}). Once oxygen limitation occurs, it rapidly drops to 60 mmol NADPH per 100 mmol glucose, and thereafter remains constant. This is a very interesting result because it shows that the metabolism is capable of generating more NADPH than is utilised during PHB production. Hence if PHB production can be increased through other alterations to fermentation protocol or cellular genetics, there should be sufficient NADPH generation capacity to satisfy the increased demand.

4.6. Formulation of PHB Kinetic Model

4.6.1. Introduction

As described in Section 4.2.1, metabolic control analysis can be used to provide useful information about the important variables affecting PHB production. However two prerequisites for this analysis are

- a kinetic description of the PHB pathway, and
- estimates of the concentrations of pathway enzymes and metabolites.

Section 4.6 describes how these requirements can be satisfied. Section 4.7 then uses metabolic control analysis to analyse the model.

4.6.2. Kinetic description of the PHB pathway

The kinetics of PHB accumulation have been studied extensively in *R. eutropha* and rate expressions for the three PHA enzymes are available (Leaf and Srienc (1998)).

3-ketothiolase kinetics

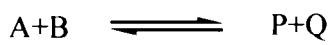

where

A	= acetyl-CoA
B	= acetyl-CoA (second substrate)
P	= CoA
Q	= acetoacetyl-CoA

This reaction is reversible with equilibrium greatly favouring the left. It follows a ping-pong Bi-Bi mechanism and hence an appropriate form of the rate equation is

$$\frac{r}{r_{max}} = \frac{AB - {PQ}/{K_{eq}}}{K_b A + K_a B + AB + {K_q V_1 P}/{V_2 K_{eq}} + {K_p V_1 Q}/{V_2 K_{eq}} + {V_1 PQ}/{V_2 K_{eq}} + {K_q V_1 AP}/{V_2 K_{ia} K_{eq}} + {K_a BQ}/{K_{iq}}} \quad (4.3)$$

where

r	= forward reaction rate (μM(substrate).min^{-1})
r_{max}	= maximum forward reaction rate (μM(substrate).min^{-1})
A	= first substrate (acetyl-CoA) concentration (μM)
B	= second substrate (also acetyl-CoA) concentration (μM)
P	= first product (CoA) concentration (μM)
Q	= second product (acetoacetyl-CoA) concentration (μM)
${V_1}/{V_2}$	= ratio of maximum forward reaction rate to maximum reverse reaction rate
K_{eq}	= equilibrium constant
$K_a, K_b, K_p, K_q, K_{ia}, K_{ib}, K_{ip}, K_{iq}$	= various kinetic constants (μM)

3-ketoacyl-CoA reductase kinetics

A+B ⇌ P+Q

where

A	= acetoacetyl-CoA
B	= NADPH
P	= 3-hydroxybutyryl-CoA
Q	= NADP

This enzyme has been less thoroughly studied but probably follows a rapid equilibrium random Bi-Bi mechanism and hence has a rate equation of the form

$$\frac{r}{r_{max}} = \frac{AB - {PQ}/{K_{eq}}}{K_{ia} K_b + K_b A + K_a B + AB + {K_q V_1 P}/{V_2 K_{eq}} + {K_p V_1 Q}/{V_2 K_{eq}} + {V_1 PQ}/{V_2 K_{eq}}} \quad (4.4)$$

In this case

A	= first substrate (acetoacetyl-CoA) concentration (μM)
B	= second substrate (NADPH) concentration (μM)
P	= first product (3-hydroxybutyryl-CoA) concentration (μM)
Q	= second product (NADP) concentration (μM)

Because the reaction involves hydrogen ions, the equilibrium constant varies with pH:

$$K'_{eq} = \frac{[3-hydroxybutyryl-CoA][NADP]}{[acetoacetyl-CoA][NADPH][H^+]}$$

hence a pseudo-equilibrium-constant can be defined at the pH of interest:

$$K_{eq} = K'_{eq}.10^{-pH} \tag{4.5}$$

$$K_{eq} = K'_{eq}.[H^+]$$

$$K_{eq} = \frac{[3-hydroxybutyryl-CoA][NADP]}{[acetoacetyl-CoA][NADPH]}$$

PHA synthase kinetics

$$A + B_n \longrightarrow B_{n+1}$$

where

A	= 3-hydroxybutyryl-CoA
B_n	= PHA chain comprised of n monomers
B_{n+1}	= PHA chain comprised of n+1 monomers

This enzyme is considered diffusion-limited and hence has the form

$$\frac{r}{r_{max}} = \frac{[3-hydroxybutyryl-CoA]}{K_m + [3-hydroxybutyryl-CoA]} \tag{4.6}$$

Table 4.8 lists literature values of the equation parameters:

Table 4.8: Kinetic constants for thiolase, reductase and synthase (Leaf and Srienc (1998)).

thiolase				reductase		synthase	
K_{eq}	$4x10^{-5}$	K_q	64.6 μM	$K_{eq}(7.2)$	500	K_m	720 μM
V_1/V_2	$2.5x10^{-4}$	K_{ia}	5.96 μM	K_a, K_{ia}	5 μM		
K_a	$3.78x10^{-3}$ μM	K_{ib}	841 μM	$K_b K_{ib}$	19 μM		
K_b	840 μM	K_{ip}	12.4 μM	K_p, K_{ip}	16.5 μM		
K_p	31.4 μM	K_{iq}	$1.62x10^{-2}$ μM	K_q, K_{iq}	31 μM		

Under the conditions of this experiment, the rate equations can be simplified to the following:

3-ketothiolase:

$$\frac{r}{r_{max}} = \frac{A^2 - 25000.AA.C}{840.A + A^2 + 67.7A.C} \tag{4.7}$$

where

A = acetyl-CoA concentration (μM)
AA = acetoacetyl-CoA concentration (μM)
C = CoA concentration (μM)

3-ketoacyl-CoA reductase:

$$\frac{r}{r_{max}} = \frac{AA.PH - {}^{1}/_{K_{eq}}.P.HB}{95 + 19.AA + 5.PH + AA.PH + {}^{2879}/_{K_{eq}}.HB + {}^{1532}/_{K_{eq}}.P + {}^{93}/_{K_{eq}}.HB.P} \tag{4.8}$$

where

AA = acetoacetyl-CoA concentration (μM)
PH = NADPH concentration (μM)
HB = 3-hydroxybutyryl-CoA concentration (μM)
P = NADP concentration (μM)
K_{eq} = modified equilibrium constant, (500 at pH 7.2), calculated using Equation 4.9.

$$K_{eq} = 7.924\times10^{9}.[H^{+}] = 7.924\times10^{9}.10^{-pH} \tag{4.9}$$

PHA synthase:

$$\frac{r}{r_{max}} = \frac{HB}{720 + HB} \tag{4.10}$$

where

HB = 3-hydroxybutyryl-CoA concentration (μM)

General Caution

The results of the following section must be viewed with caution, because they rely on a number of assumptions that are difficult to verify. In particular

- The chemical environment *in vitro* may be very different to the cytoplasmic environment with respect to redox potential, ion concentrations, and cofactor concentrations.
- The *in-vitro* kinetics were measured at low enzyme concentrations, which may not reflect the *in-vivo* kinetics. The cytoplasm of *E. coli* is a viscous mixture where diffusion and crowding effects can greatly influence enzyme activities.
- The activity coefficients of metabolites are probably far from unity, due again to the high cytoplasmic concentrations of ions and macromolecules.
- The true cytoplasmic volume may be significantly in error. Ideally, this volume should be measured at various points through the fermentation, using for example the taurine method described in the work of Cayley *et al.* (1991).

Nevertheless the kinetics provide useful qualitative insights into the observed fermentation behaviour.

4.6.3. Intracellular Concentrations of Enzymes and Metabolites

The second requirement for metabolic control analysis is estimates of the variables in the kinetic equations, viz concentrations of enzymes and metabolites. These estimates are described below.

Acetyl-CoA and 3-hydroxybutyryl-CoA

Acetyl-CoA and 3HB-CoA have been measured on a gRCM basis, and must be converted to an intracellular concentration for kinetic analyses. This poses a number of problems, because the cytoplasm is a viscous mixture where much of the available water is bound to macromolecules as water of hydration. Indeed the concept of concentration becomes somewhat ill defined and ideally an activity is required instead. The situation is complicated further because PHB granules in the cell occupy a significant fraction of the cytoplasmic volume. Nevertheless a number of reasonable assumptions can be made that permit the derivation of an expression for cytoplasmic volume as a function of PHB accumulation (See Appendix B).

$$\hat{V}_{\text{true}} = \hat{V}_{\text{nominal}} + \frac{X}{\rho_{PHB}.(1-X)}\left(\frac{s_0}{r_0} - 1\right) \tag{4.11}$$

where

$\hat{V}_{\text{true}}$ = true intracellular volume (ml.gRCM^{-1})

$\hat{V}_{\text{nominal}}$ = literature intracellular volume (ml.gRCM^{-1}), a function of medium osmolarity

X_{PHB} = mass fraction PHB in cell

ρ_{PHB} = density of PHB granules (g.ml^{-1}) = 1.18 (Horowitz and Sanders (1995))

$\frac{s_0}{r_0}$ = non-wall-associated residual cell mass, 75% (see Appendix B)

Interestingly this gives a maximum theoretical PHB content of between 81%-89% depending on medium osmolarity, which agrees rather well with the maximum experimental values of around 85% (Lee *et al.* (1994d)). At such high levels of PHB however the assumptions become unrealistic: cells with such high levels of PHB are severely distorted by the granules and take on the appearance of a sausage stuffed with golf balls.

Having estimated the true intracellular volume, it is now possible to convert both acyl-CoA concentration and PHB synthesis rate to a volumetric basis, viz

$$[x] = \frac{\hat{x}}{\hat{V}_{true}} \tag{4.12}$$

where

$[x]$ = acyl-CoA concentration or PHB rate, intracellular-volume basis (μM or μM.h^{-1} respectively)

$\hat{x}$ = acyl-CoA concentration or PHB rate, RCM basis (μmol.gRCM^{-1} or μmol.gRCM^{-1}h^{-1} respectively)

The resultant acetyl-coA and 3HB-CoA profiles are shown in Figure 4.26.

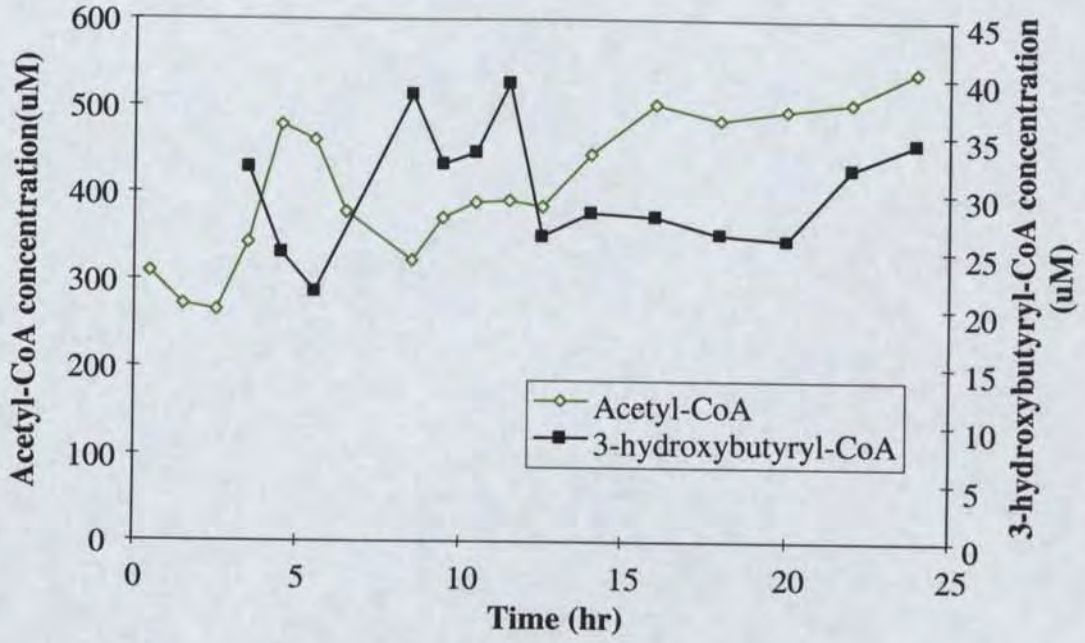

Figure 4.26: 3-hydroxybutyryl-CoA concentration and acetyl-CoA concentration on an intracellular volume basis.

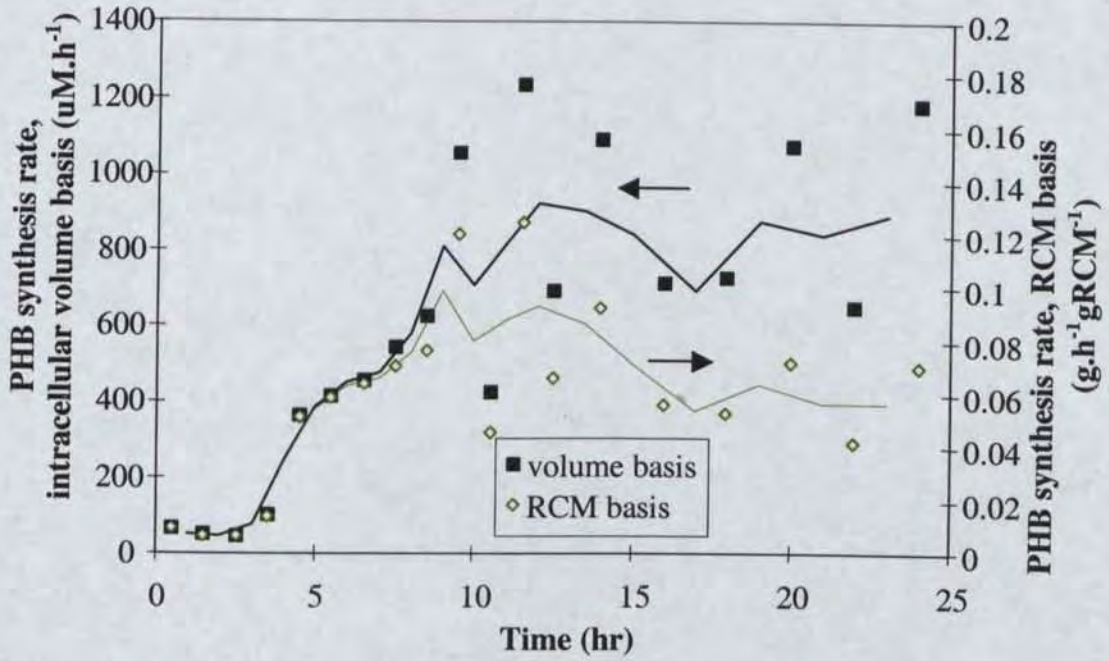

Figure 4.27: PHB synthesis rate on both an RCM basis and an intracellular volume basis.

Figure 4.27 shows the PHB synthesis rate on both an RCM basis and a volumetric basis, highlighting the effect of decreased intracellular volume. Although synthesis rate declines on an RCM basis, it remains steady on a concentration basis within experimental error (±30% in Figure 4.27). This suggests that the apparent decline in PHB productivity (per gRCM) may be simply due to reduced intracellular volume, resulting from PHB accumulation and increased osmolarity of the medium. Likewise, 3HB-CoA concentration appears much more constant on a volumetric basis (Figure 4.26) than on the RCM basis (Figure 4.22).

PHA Synthase Activity

For this experiment, the PHB production rate (r) and the concentration of 3-hydroxybutyryl-CoA (HB) are known, allowing calculation of the maximum reaction velocity r_{max} (and hence enzyme activity) using Equation 4.10. The results are shown in Figure 4.28. The activity ($mM.hr^{-1}$ basis) shows a gradual rise till hr 10, and thereafter remains approximately constant. This suggests that the observed decline in PHB synthesis rate per gRCM after hr 10 is caused by reduction in cytoplasmic volume, rather than a decline in the levels of PHA enzymes. The gradual rise over the period hr 5 to hr 10 probably reflects an increasing level of PHA enzymes in the cells. This seems feasible because the copy number of plasmids tends to increase when cell growth is slowed (Brendel and Perelson (1993); Engberg and Nordstrom (1975)), causing the expression of recombinant genes to increase relative to chromosomal genes.

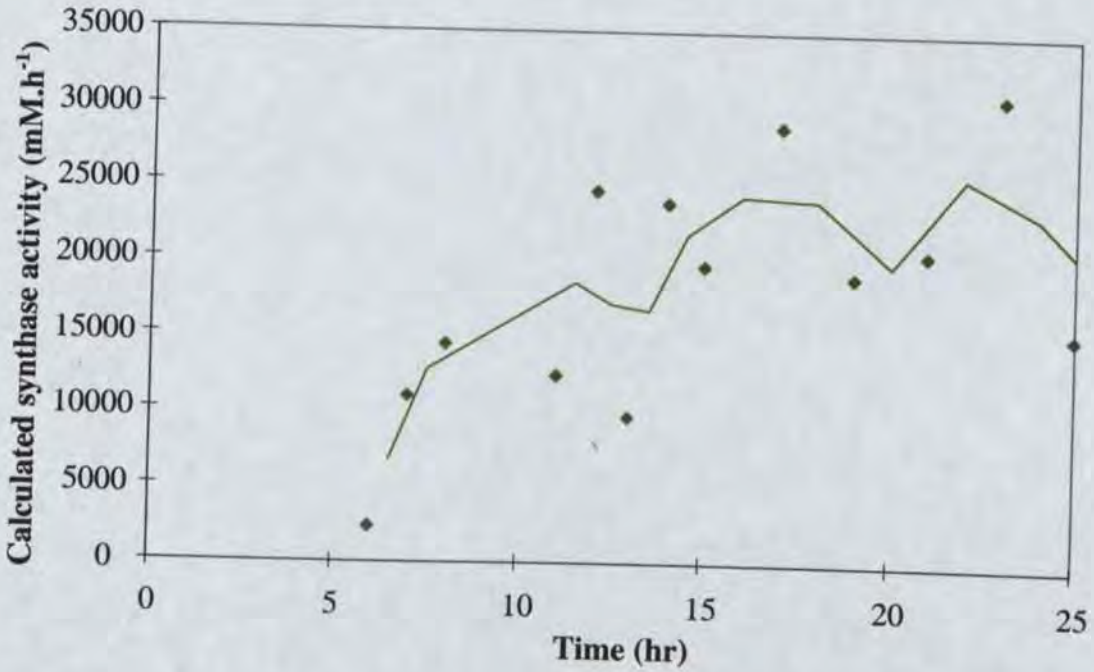

Figure 4.28: Profile of PHA synthase activity.

Table 4.9: PHA synthase activities.

Source	Description	Activity ($U.mg(protein)^{-1}$)	Fermentation PHB synthesis rate ($g.gRCM^{-1}h^{-1}$)	Fraction of maximum possible rate (%)
This study	estimated from batch data	0.6 - 0.8 (at 30 °C)	0.08	4.0%
SJS	inducible PHA genes, complex medium	1-2 (at 25 °C)	0.12	2.9%
JK	inducible PHA genes, complex medium	0.015 - 0.030 (at 25 °C)	0.06	94%
JSP	R. eutropha	1-4 (at 25 °C)	0.08	1.1%
DAM	R. eutropha, chemostat	1.08 (30 °C, estimated using kinetics)	0.089	(2.9%)
PS	R. eutropha	0.18 (at 30 °C)	N/A	N/A

Where necessary it is assumed that *E. coli* and *R. eutropha* contain 0.55 mg protein per mg of residual cell mass (Neidhardt and Umbarger (1996)). For estimated activity in *R. eutropha*, intracellular volume was assumed to be 1.4 $mL.g^{-1}$ (Leaf and Srienc (1998)). N/A indicates no data available. One Unit is defined as the consumption of 1 µmol of substrate per minute. Sources of data; SJS (Sim *et al.* (1997)), JK (Kidwell *et al.* (1995)), JSP (Park *et al.* (1995)), DAM (Mansfield *et al.* (1995)), PS (Schubert *et al.* (1988)).

The calculated enzyme activity can be converted to a Units per mg-protein basis and compared with various literature values, as in Table 4.9.

The comparison shows that the estimated specific activity is quite similar to most other values obtained with recombinant *E. coli* and with *R. eutropha*. Interestingly the PHB synthesis rate in the work of Kidwell *et al.* (1995) is quite similar to the other studies where synthase activity was up to 100 times greater. This seems highly unlikely, since it would require an intracellular 3-hydroxybutyryl-CoA concentration of 11.3 mM. Hence their measured synthase activity is probably incorrect.

Estimation of Remaining Variables

The remaining variables in the kinetic equations were not measured, viz CoA concentration, acetoacetyl-CoA concentration, NADPH concentration, NADP concentration, intracellular pH, and the activity of 3-ketothiolase and 3-ketoacyl-CoA reductase. However there are estimates of their values in the literature, as described below.

Acyl-CoA concentrations:

Table 4.10 shows various literature values of CoA and acetyl-CoA.

Table 4.10: Literature measurements intracellular acetyl-CoA and CoA concentrations.

Study	Notes	Total CoA	CoA	acetyl-CoA	acetyl-CoA/CoA ratio
(this)	*E. coli*	N/A	N/A	250-500 μM	N/A
SJ1	*E. coli*	530 μM	73 μM	423 μM	5.8
SC	*E. coli* K12	452 μM	81 μM	307 μM	3.8
SJ2	*E. coli*	406 μM	56 μM	324 μM	5.8
TAL	*R. eutropha*	N/A	100 μM	1000 μM	10

N/A indicates data not available. Total -CoA = CoA + acetyl-CoA + succinyl-CoA + malonyl-CoA. SJ1 = (Jackowski and Rock (1986)), SC = (Chohnan *et al.* (1998)), SJ2 = (Jackowski (1996)), TAL = (Leaf and Srienc (1998))

A potential problem that arises when viewing this table is that:

- the ratio of acetyl-CoA to CoA is well above unity even in wild type *E. coli* under aerobic conditions;
- acetyl-CoA comprises the majority (typically 75%) of the total -CoA pool.

Yet Figure 4.26 shows a doubling of acetyl-CoA concentration at hr 5, which would not be possible if it comprised 75% of the total -CoA pool. There are several likely explanations for this observation:

- extra CoA is being synthesised during this period, increasing the overall -CoA pool size;
- there is a larger pool of other -CoA metabolites (e.g. succinyl-CoA) than the literature indicates;
- the acetyl-CoA/CoA ratio is initially closer to unity than in the literature.

For the purposes of this analysis it is assumed that the CoA concentration can vary independently of acetyl-CoA to give the same acetyl-CoA/CoA ratios observed in other studies.

The only available estimate of acetoacetyl-CoA concentration comes from Mansfield *et al.* (1995), viz 0.05 $\mu mol.gRCM^{-1}$. They also state that CoA concentration = 0.13 $\mu mol.gRCM^{-1}$ and acetyl-CoA = 1.38 $\mu mol.gRCM^{-1}$. Unfortunately these values are not consistent because (assuming correct CoA and acetyl-CoA measurements) the 3-ketothiolase rate equation places the maximum possible acetoacetyl-CoA concentration at only 0.00059 $\mu mol.gRCM^{-1}$. Hence the acetoacetyl-CoA concentration is almost certainly incorrect, leaving no reliable estimate for it.

NADPH and NADP

Unfortunately there are few literature estimates for these values, the available estimates are listed in Table 4.11.

Table 4.11: Literature measurements of intracellular concentrations of NADPH and NADP.

Source	Description	NADPH + NADP (μM)	NADPH/NADP
TP	*E. coli*	200	3
JN	many bacteria	-	0.6 - 1
TAL	*R. eutropha*	400	3

Sources of data: TP (Penfound and Foster (1996)), JN (Nielsen and Villadsen (1994)), TAL (Leaf and Srienc (1998))

Intracellular pH

Slonczewski and Foster (1996) and Kroll and Booth (1983) state that *E. coli* maintain their cytoplasmic pH at 7.4 - 7.8 over a wide range of extracellular pH (5.0 to 9.0). Diez-Gonzalez and Russell (1997) confirm pH 7.6 for aerobically growing *E. coli*, but give values of pH 6.8-7.0 for anaerobically growing *E. coli*.

Enzymatic activity

The available literature data (shown in Table 4.12) vary over a wide range, especially 3-ketothiolase activity.

Table 4.12: Literature measurements of 3-ketothiolase and 3-ketoacyl-CoA reductase.

Source	Description	3-ketothiolase activity (U.mg(protein)$^{-1}$)	3-ketoacyl-CoA reductase activity (U.mg(protein)$^{-1}$)
SJS	inducible PHA genes, complex medium	0.1 (25 °C)	1 - 1.5 (25 °C)
JK	inducible PHA genes, complex medium	4 - 12 (25 °C)	2 - 4 (25 °C)
JSP	R. eutropha	0.3 - 0.5 (25 °C)	0.13 - 0.18 (25 °C)
PS	R. eutropha	0.43 (30 °C)	0.77 (30 °C)

Where necessary it is assumed that *E. coli* and *R. eutropha* contain 0.55 mg protein per mg of residual cell mass (Neidhardt and Umbarger (1996)). N/A indicates no data available. One Unit (U) is defined as consumption of 1 μmol of substrate per minute. Sources of data: SJS (Sim *et al.* (1997)), JK (Kidwell *et al.* (1995)), JSP (Park *et al.* (1995)), PS (Schubert *et al.* (1988)).

Probability Distributions

The value of each variable listed above is not known with certainty. Hence each one must be assigned a probability function for its possible values, based on the literature estimates. These are summarised in Table 4.13:

Table 4.13: Assumed variable probability distributions for simulation of PHB enzyme kinetics.

Variable	Distribution Used	Minimum	Most probable	Maximum
Acetyl-CoA Concentration (μM)	triangular	300	450	600
Acetyl-CoA/CoA ratio	log triangular	1	3.9	15
3-ketothiolase activity (U.mg (Protein)$^{-1}$)	log triangular	0.1	0.9	8
NADPH + NADPH pool (μM)	triangular	200	300	400
NADPH/NADP ratio	log triangular	0.5	3	10
pH	triangular	7.4	7.6	7.8
3-ketoacyl-CoA reductase activity (U.mg (Protein)$^{-1}$)	triangular	1	2.5	4
3-hydroxybutyryl-CoA concentration (μM)	triangular	20	27.5	35
PHB production rate (g.gRCM^{-1}h^{-1})	(constant)	--	0.08	--

If values for all variables were available, the system would be over-specified by three degrees of freedom, corresponding to the three kinetic rate-equations. One degree of freedom was utilised by estimating the activity of PHA synthase using Equation 4.10. The two remaining degrees of freedom are used to

1. obtain an estimate for acetoacetyl-CoA concentration;
2. perform a redundancy check on the variables, giving "revised" estimates.

Because the rate equations (3-ketothiolase and 3-ketoacyl-CoA reductase) are coupled by the unknown acetoacetyl-CoA concentration, steps 1 and 2 above must be performed simultaneously. The method of solution is to solve each rate equation (Equation 4.7 and Equation 4.8) independently for acetoacetyl-CoA concentration, thus yielding two different probability functions. The probability distribution of each variable in Equation 4.7 and Equation 4.8 must therefore be revised, based on the knowledge that the acetoacetyl-CoA concentration must match for both rate equations. In other words, an expression is required for the conditional probability function of each variable given that the steady-state mass-balance constraint is satisfied, viz the distribution of acetoacetyl-CoA is common to both equations. Appendix C shows the derivation of the appropriate equations.

For the estimated distribution of acetoacetyl-CoA concentration:

$$P(A_i|Satisfied) = \frac{P(A_i)P(B_i)}{\sum_{k=1}^{n}(P(B_k)P(A_k))} \tag{4.13}$$

In these equations,

$P(A_i)$ is the relative frequency of the i^{th} bin of the original acetoacetyl-CoA histogram obtained using the 3-ketothiolase rate equation.

$P(B_i)$ is the relative frequency of the i^{th} bin of the original acetoacetyl-CoA histogram obtained using the 3-ketoacyl-CoA reductase rate equation.

$P(A_i|Satisfied)$ is the relative frequency of the i^{th} bin of the revised acetoacetyl-CoA histogram

For variables affecting the 3-ketothiolase rate equation (for example acetyl-CoA concentration):

$$P(X_i|Satisfied) = \frac{\sum_{k=1}^{n}(P(B_k)P(A_k, X_i))}{\sum_{k=1}^{n}(P(B_k)P(A_k))} \tag{4.14}$$

where

$P(X_i|Satisfied)$ is the relative frequency of the i^{th} bin of the variable's revised histogram.

$P(A, X)$ is the joint relative frequency distribution for the variable and the original acetoacetyl-CoA concentration, as determined from the rate equation for 3-ketothiolase.

For variables affecting the 3-ketoacyl-CoA reductase rate equation (for example NADPH concentration):

$$P(X_i|Satisfied) = \frac{\sum_{k=1}^{n}(P(A_k)P(B_k, X_i))}{\sum_{k=1}^{n}(P(A_k)P(B_k))} \tag{4.15}$$

where

$P(B, X)$ is the joint relative frequency distribution for the variable and acetoacetyl-CoA concentration, as determined from the rate equation for 3-ketoacyl-CoA reductase.

A Monte Carlo simulation technique was used to generate the output probability functions. The initial variable probability distributions used are shown in Table 4.13.

Figure 4.29 shows the acetoacetyl-CoA probability distributions obtained. The degree of overlap is quite small, indicating that the initial assumptions are somewhat mutually

contradictory. When Equation 4.13 is applied to the data, Figure 4.30 is obtained. The most-likely-value for acetoacetyl-CoA concentration is in the vicinity of 0.12 μM (0.11 μg.gRCM^{-1}) which is a factor of 300 less than the 3-hydroxybutyryl-CoA concentration. This explains why no acetoacetyl-CoA was detected using HPLC.

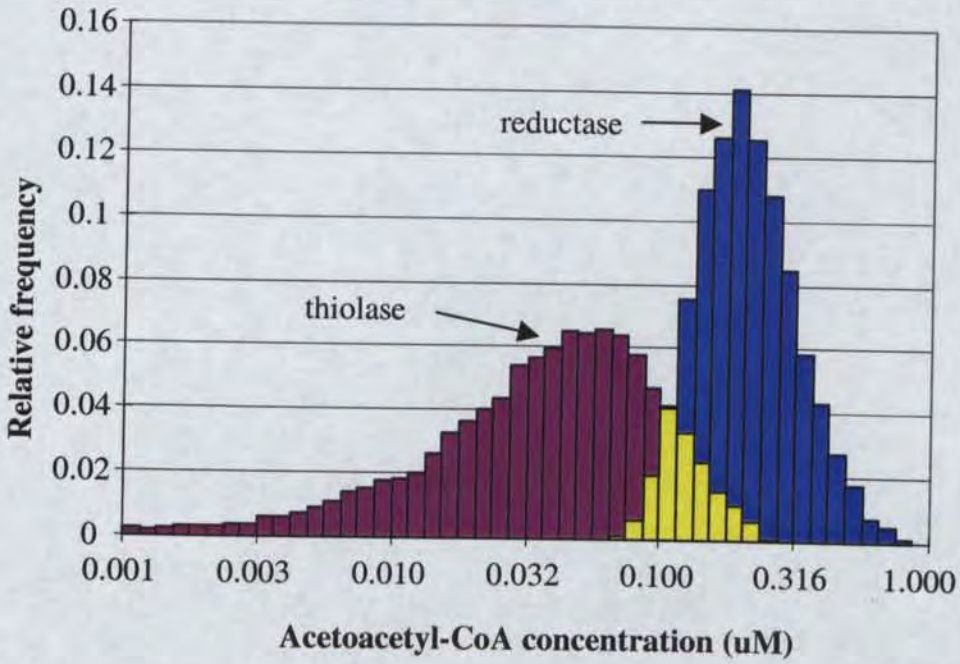

Figure 4.29: Distribution of acetoacetyl-CoA concentration obtained from 3-ketothiolase and 3-ketoacyl-CoA reductase independently.

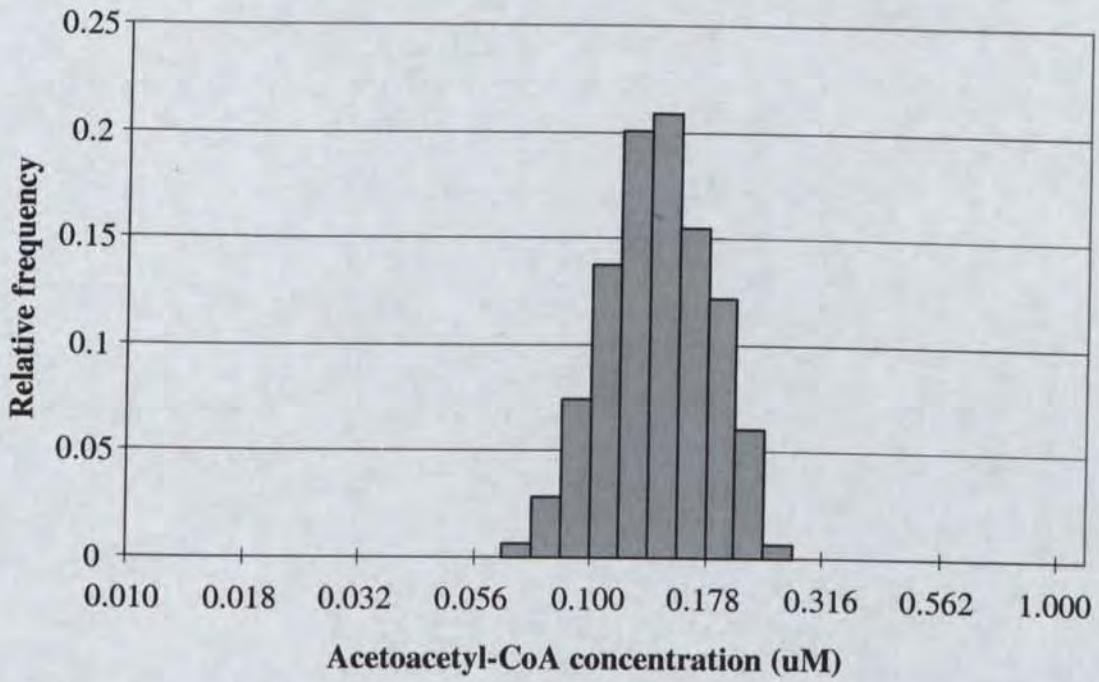

Figure 4.30: Conditional distribution of acetoacetyl-CoA.

Applying Equations 4.14 and 4.15 yields the revised distributions of each variable. The acetyl-CoA/CoA ratio changes appreciably, indicating that for this experiment the correct ratio during PHB synthesis is probably at least 8:1. This is somewhat higher than all the literature values for *E. coli*, as shown in Table 4.10. The probable 3-ketothiolase activity (Figure 4.32) also shifts significantly, casting doubt on the literature value of 0.1 U.mg(Protein)$^{-1}$ in Table 4.12. The most likely values are between 1-4 U.mg(Protein)$^{-1}$.

Figure 4.35 shows an appreciable change in the NADPH/NADP ratio, once again tending to values somewhat higher than originally expected. The most likely ratio is in the range 3:1 to 5:1.

In contrast to these three variables, most of the other variables were not appreciably affected by the constraints. Figure 4.33 shows a slight shift to higher 3-ketoacyl-CoA reductase activities (most likely value = 2 - 3 U.mg(Protein)$^{-1}$). Acetyl-CoA concentration was also mostly unaffected (Figure 4.34). The distributions of the remaining variables (pH, 3-hydroxybutyryl-CoA concentration and NADPH+NADP concentration) were not visibly affected. The revised estimates of all variables are summarised in Table 4.14.

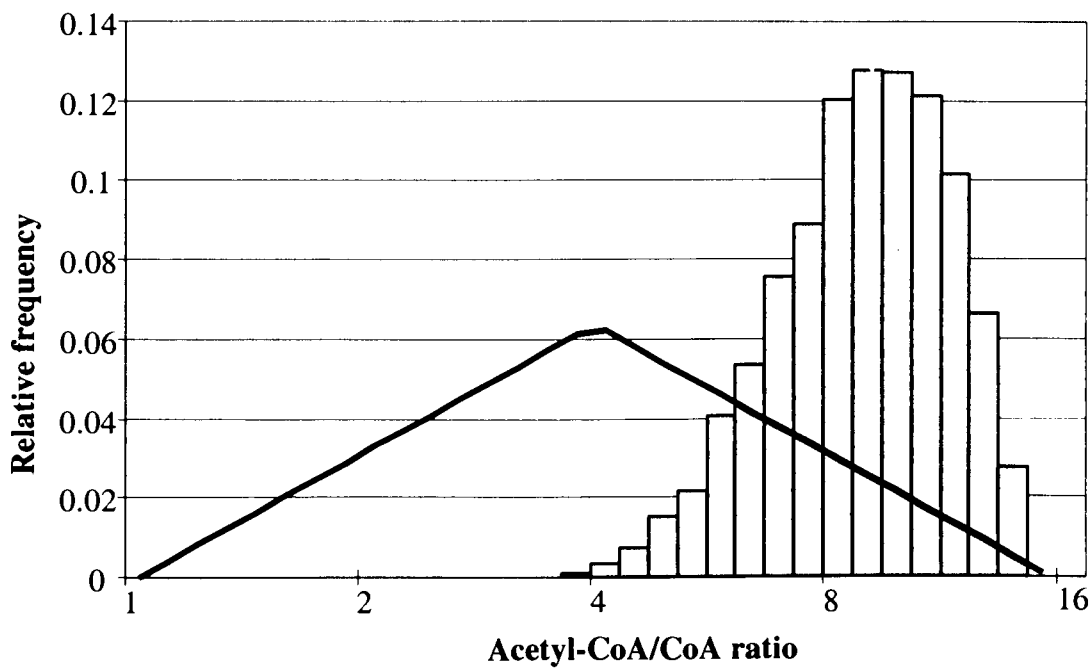

Figure 4.31: Revised probability distribution for acetyl-CoA/CoA ratio. The original distribution is shown as a solid line.

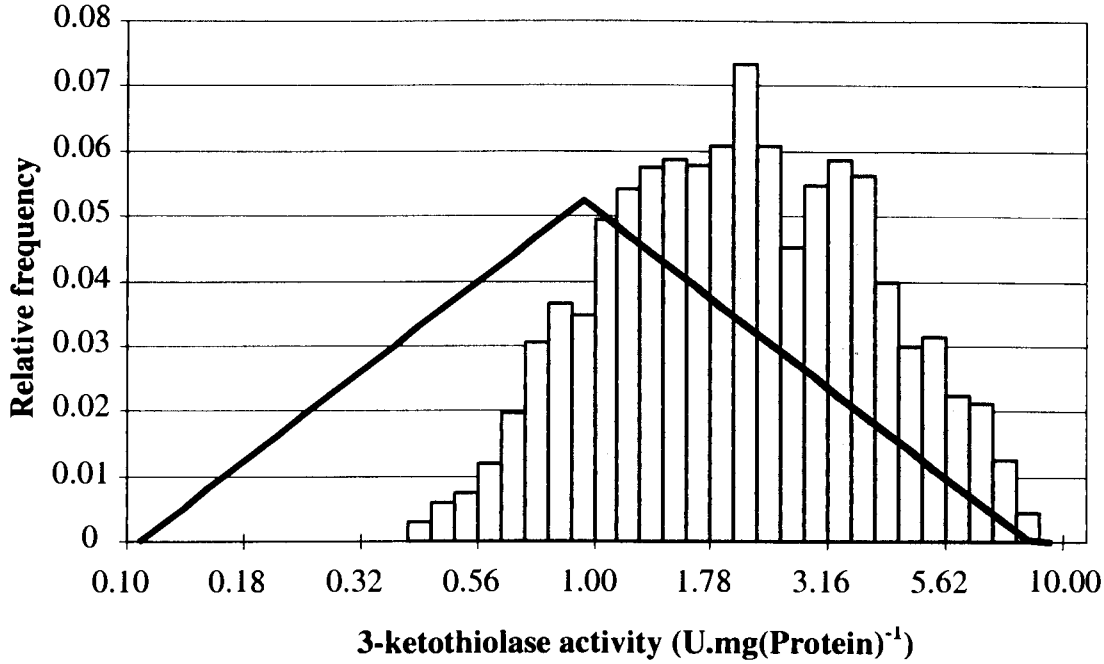

Figure 4.32: Revised probability distribution for 3-ketothiolase activity. The original distribution is shown as a solid line.

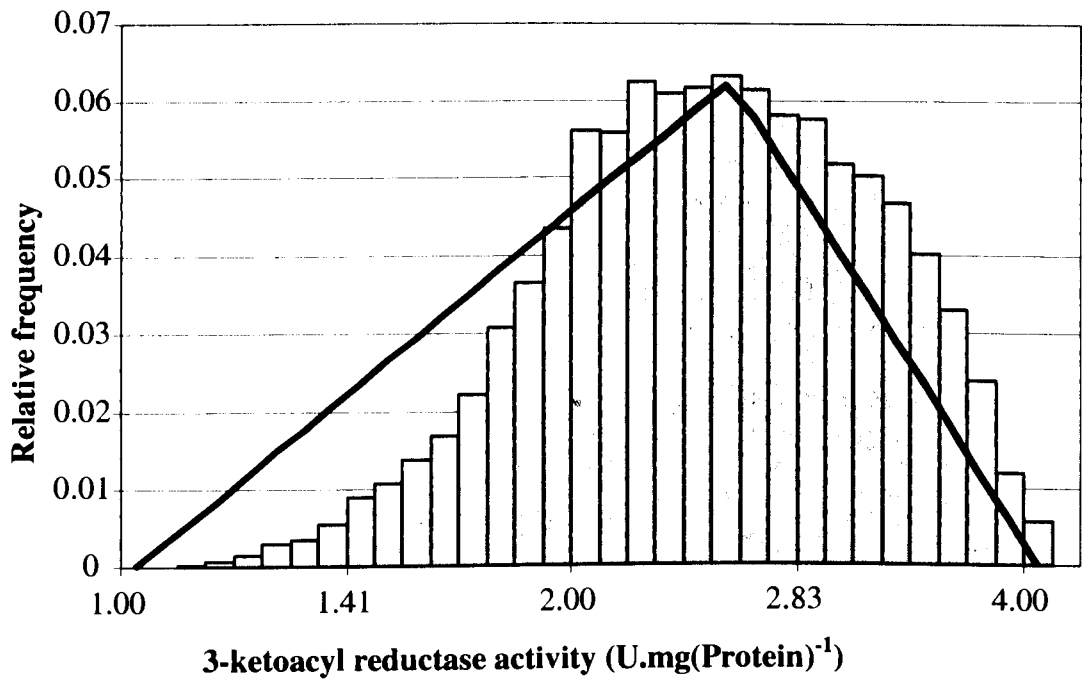

Figure 4.33: Revised probability distribution for 3-ketoacyl-CoA reductase activity. The original distribution is shown as a solid line.

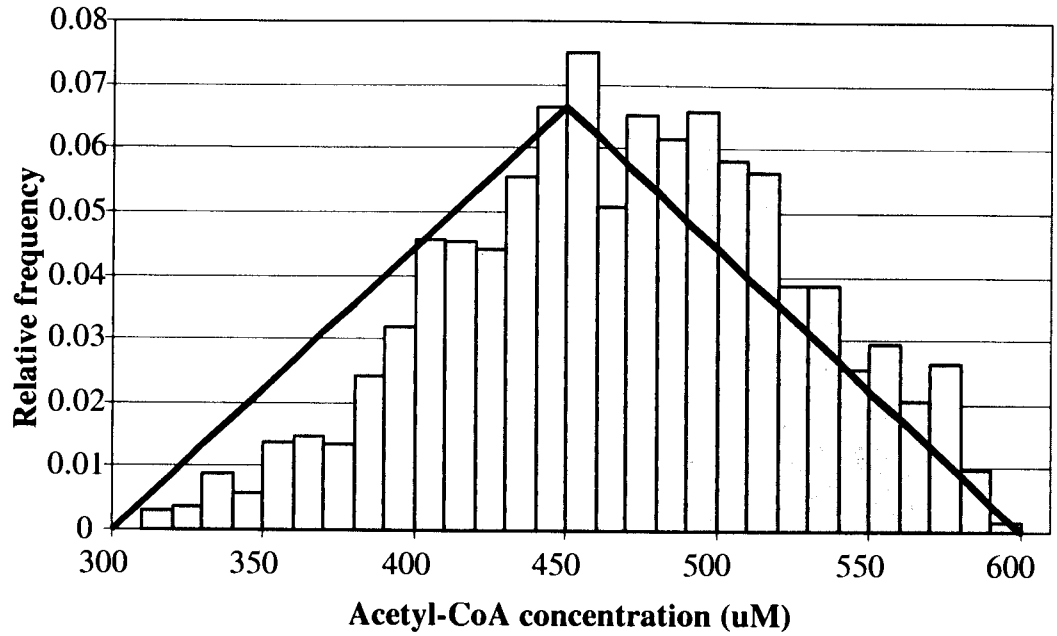

Figure 4.34: Revised probability distribution for acetyl-CoA concentration. The original distribution is shown as a solid line.

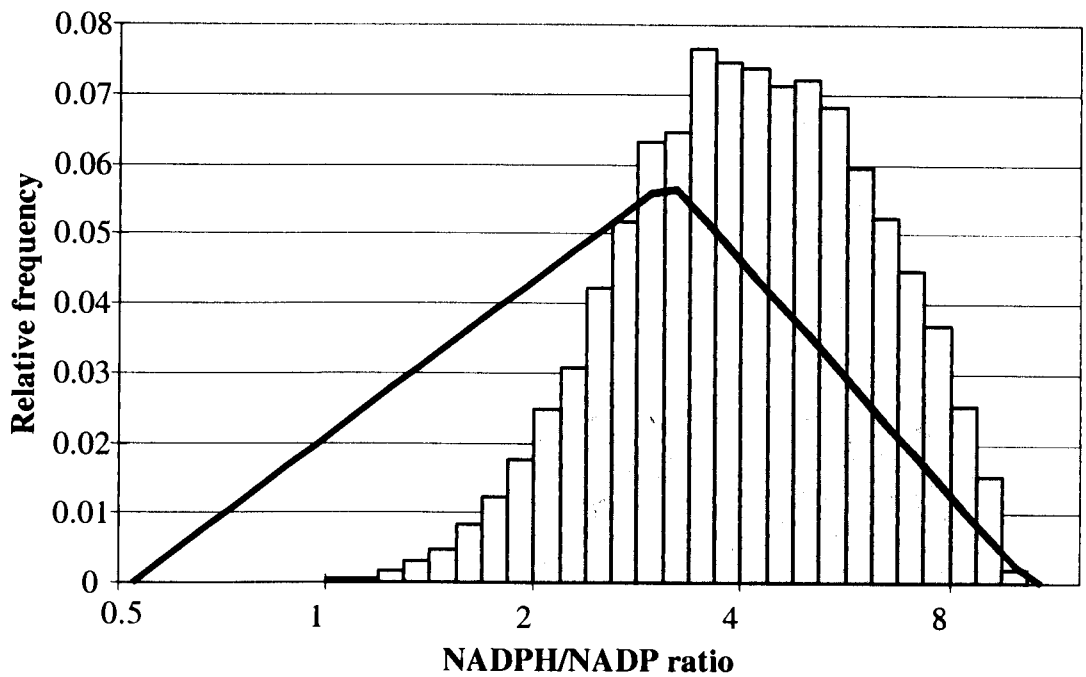

Figure 4.35: Revised probability distribution for NADPH/NADP ratio. The original distribution is shown as a solid line.

Table 4.14: Revised estimates of variables.

Variable	Most likely range	Variable	Most likely range
Acetyl-CoA Concentration (μM)	400 - 500	NADPH + NADPH pool (μM)	250-350
Acetyl-CoA/CoA ratio	8:1 - 10:1	NADPH/NADP ratio	3:1 - 5:1
3-ketothiolase activity (U.mg (Protein)$^{-1}$)	1-4	pH	7.5 - 7.7
3-hydroxybutyryl-CoA concentration (μM)	24 - 31	3-ketoacyl-CoA reductase activity (U.mg (Protein)$^{-1}$)	2-3

Although not discussed further, it should be noted that the constraints have introduced considerable correlation between the variables. This is retained for the modelling below.

4.7. Metabolic Control Analysis

As described in Section 4.2.1, metabolic control analysis is a useful mathematical modelling technique for gaining insight into the control of enzymatic pathways. Section 4.6 has formulated the necessary kinetic model and provided estimates for the values of its variables, hence allowing Section 4.7 to examine the major metabolic factors affecting PHB synthesis.

4.7.1. System Response Coefficients

Metabolic control analysis is based on using "response coefficients" to compare the magnitude of system response to differential changes in different input variables, viz

$$R_X^Y = \frac{X}{Y}\frac{\partial Y}{\partial X} \tag{4.16}$$

where

X	= input variable (e.g. acetyl-CoA/CoA ratio)
Y	= system response (e.g. PHB production rate)
R_X^Y	= response coefficient of Y to X

When Y is the flux through the pathway and X is the activity of an enzyme in the pathway, R_X^Y is termed a "flux control coefficient". For a linear pathway, the flux control coefficients are all positive and must sum to unity. Qualitatively speaking, enzymes with a high flux control coefficient exert more influence on flux than those with a low coefficient. When Y is an the pathway flux and X is another effector (for example a metabolite concentration), the value of R_X^Y can easily fall outside the range of 0 to 1, and once again large values indicate higher influence on pathway flux. This form of metabolic control analysis is strictly valid for small perturbations only, because the coefficients shift as the metabolic state changes. Nevertheless it can be useful to estimate the relative importance of model parameters.

The flux control coefficients can be calculated from the kinetic expressions for 3-ketothiolase, 3-ketoacyl-CoA reductase and PHB-synthase, given the revised variable estimates. They are presented in Figure 4.36, Figure 4.37, and Figure 4.38. It appears that no single enzyme greatly limits the PHB flux. 3-ketoacyl-CoA reductase has the highest probable coefficient (0.6), followed by PHA synthase (0.25) and 3-ketothiolase (0.1- 0.15). Tentatively this suggests that increasing (for example) synthase activity at the expense of 3-ketoacyl-CoA reductase activity will decrease the PHB flux. Supporting evidence is given in Sim *et al.* (1997), where the level of synthase was increased substantially, probably at the expense of thiolase and reductase given limited cell protein synthesis ability. The polymer molecular weight decreased but polymer synthesis rate did not appreciably improve.

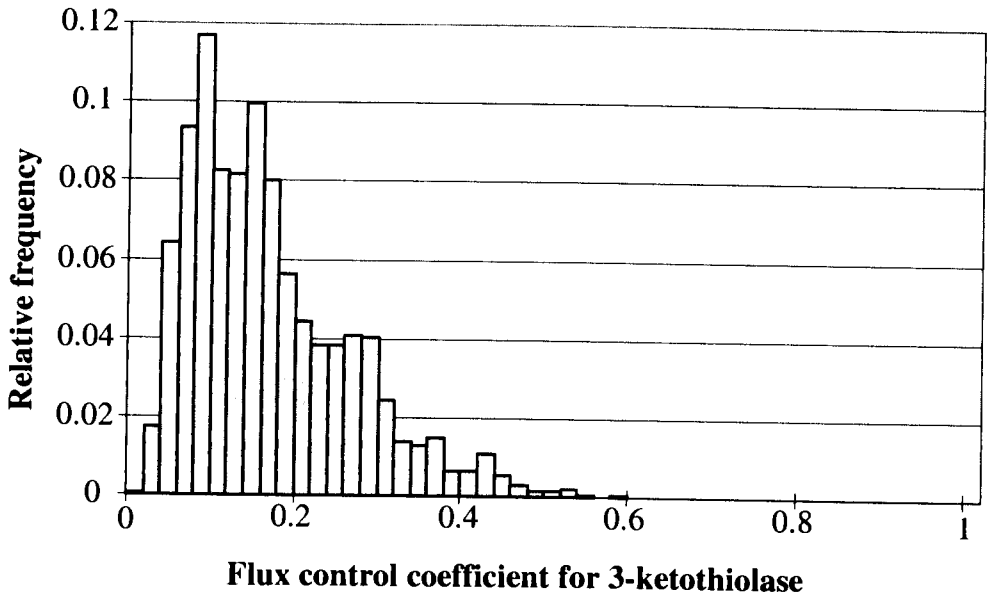

Figure 4.36: Flux control coefficient for 3-ketothiolase.

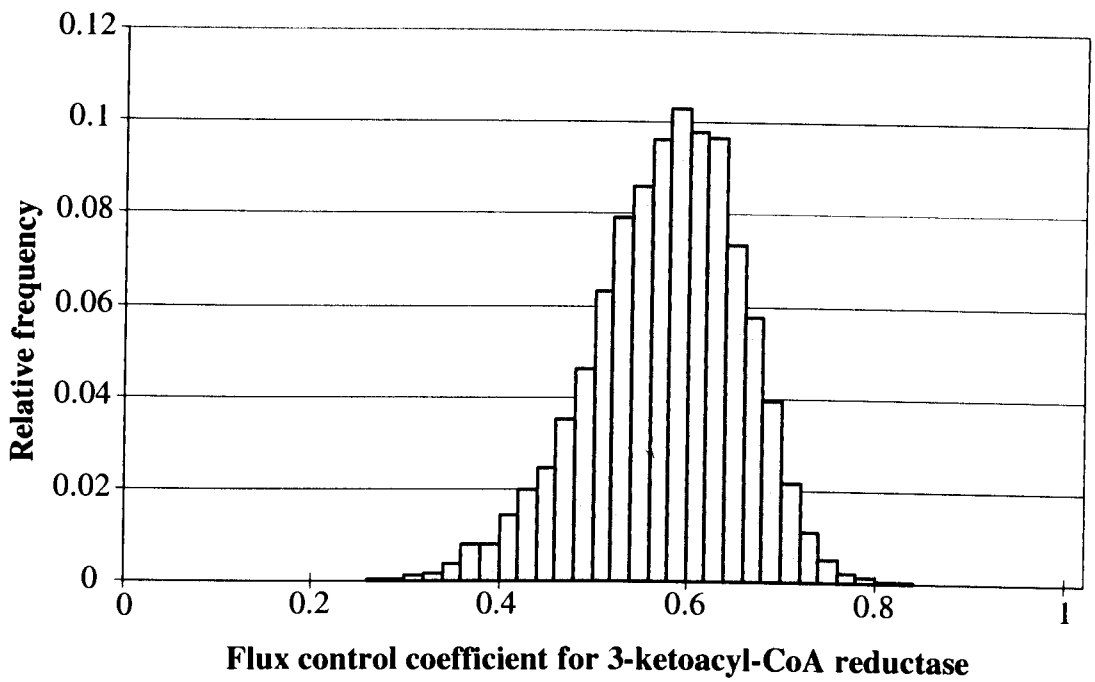

Figure 4.37: Flux control coefficient for 3-ketoacyl-CoA reductase.

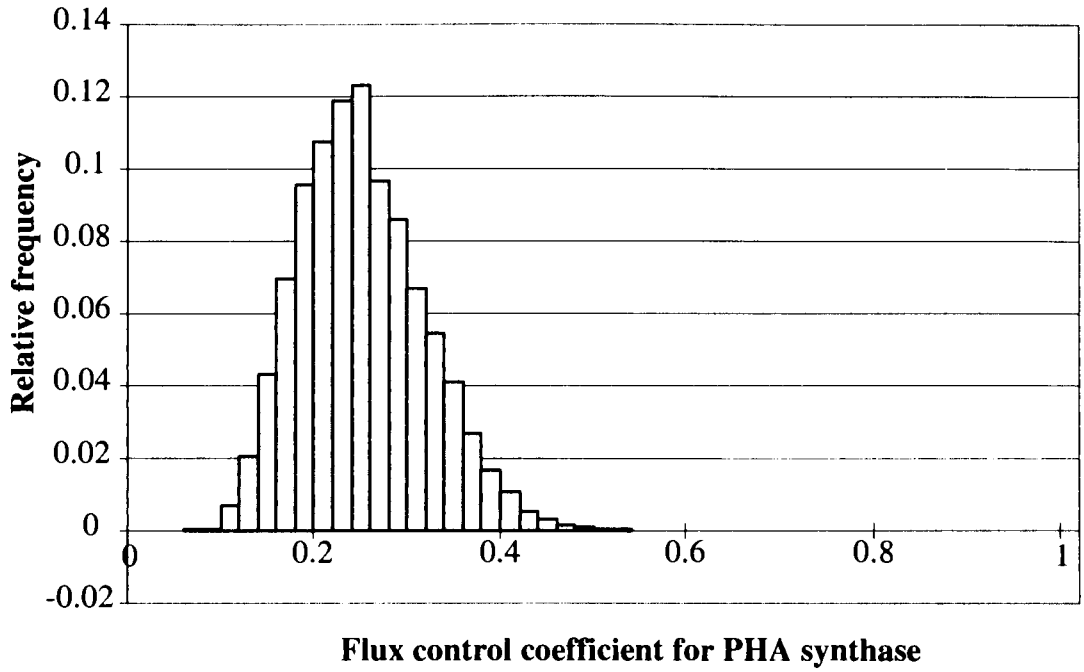

Figure 4.38: Flux control coefficient for PHA synthase.

In a similar fashion, the concentration response coefficients are calculated from the kinetics and are shown below. The acetyl-CoA/CoA ratio (at constant acetyl-CoA concentration) has a high response coefficient, near 0.8. Increasing this ratio therefore has the potential to substantially improve PHB synthesis. Likewise, the response coefficient for acetyl-CoA is also high (0.7). This may seem unusual given that the ratio of acetyl-CoA to CoA is held constant. It arises from the fact that both substrates of 3-ketothiolase are the same (i.e. acetyl-CoA), giving a squared acetyl-CoA term in the rate equation (Equation 4.7). Interestingly this implies that increasing overall CoA-thioester levels may improve PHB production even if the ratio of acetyl-CoA to CoA remains unchanged.

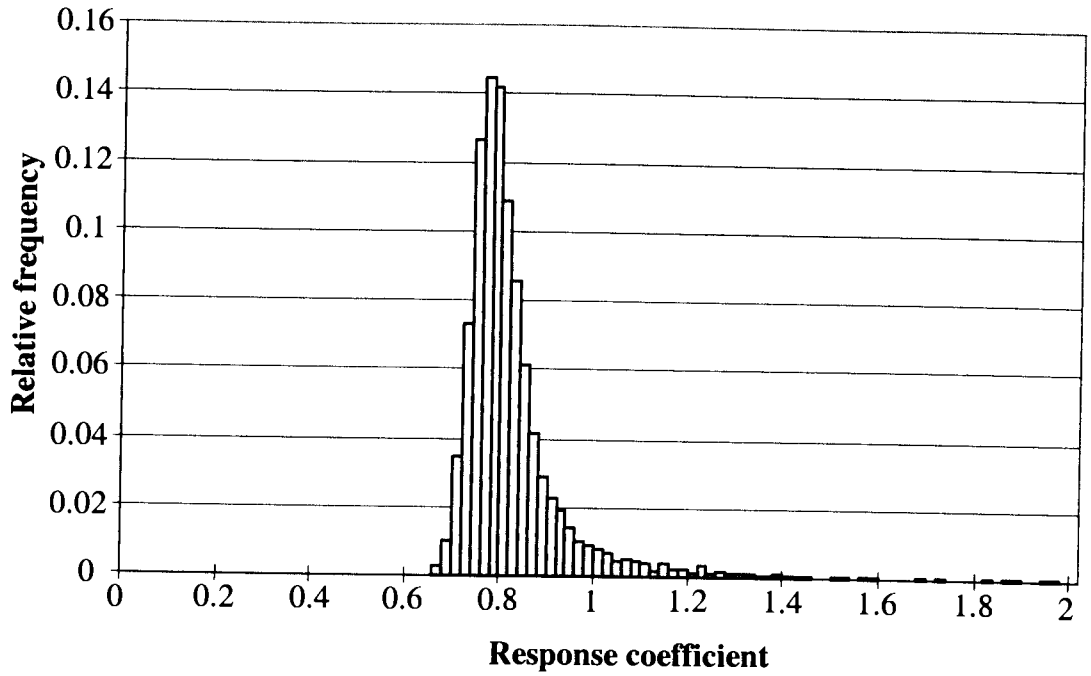

Figure 4.39: Response coefficient for acetyl-CoA/CoA ratio, at constant acetyl-CoA concentration.

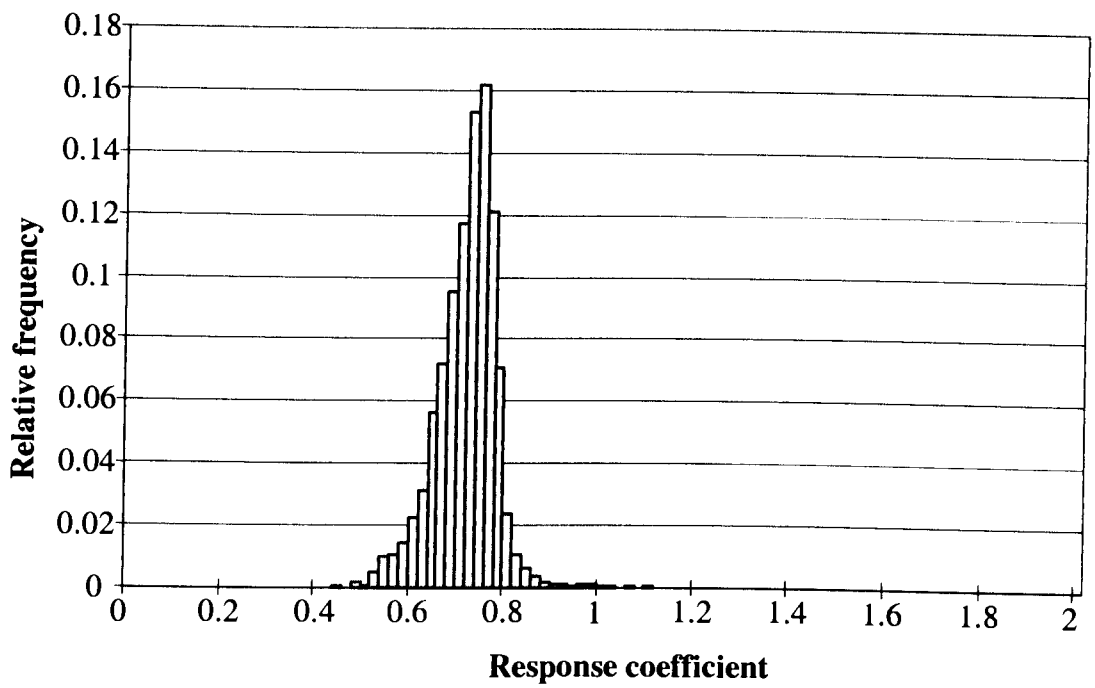

Figure 4.40: Response coefficient for acetyl-CoA concentration, at constant acetyl-CoA/CoA ratio.

Figure 4.41 shows the response coefficient for the NADPH/NADP ratio (at constant NADPH + NADP). This is quite low (0.2 - 0.3) compared with the acetyl-CoA/CoA ratio response coefficient on a constant poolsize basis (0.9). The underlying reason for this can be deduced from the rate equations (Equation 4.7 and Equation 4.8). They are shown below rewritten in a ratio form, viz

$$\frac{V}{V_{max}} = \frac{A.{}^{A}/_{C} - 25000.AA}{840.{}^{A}/_{C} + A.{}^{A}/_{C} + 67.7A} \tag{4.17}$$

and

$$\frac{V}{V_{max}} = \frac{AA.{}^{PH}/_{P} - {}^{1}/_{K'_{eq}}.HB}{{}^{95}/_{P} + 19\,{}^{AA}/_{P} + 5\,{}^{PH}/_{P} + AA.{}^{PH}/_{P} + {}^{2879}/_{K'_{eq}}.{}^{HB}/_{P} + {}^{1532}/_{K'_{eq}} + {}^{93}/_{K'_{eq}}.HB} \tag{4.18}$$

Under the conditions of this experiment, the denominator of the thiolase rate equation (Equation 4.17) is dominated by the 67.7A term. Hence an increase in the ${}^{A}/_{C}$ ratio (at constant A) brings about a nearly proportional rise in $\frac{V}{V_{max}}$. Additionally the thiolase is operating quite close to equilibrium (the first term in the numerator is only 1.5 - 2 times the second term) hence the effect of ${}^{A}/_{C}$ is magnified further. In contrast 3-ketoacyl-CoA reductase suffers from substantial inhibition by NADPH: the denominator (Equation 4.18) is dominated by the $5\,{}^{PH}/_{P}$ term, and therefore a rise in the ${}^{PH}/_{P}$ ratio has a smaller effect on reaction rate. Additionally the reductase is far from equilibrium (the first numerator term is ten times the second) and hence unlike 3-ketothiolase there is no amplification of incremental changes in the ratio.

Figure 4.42 shows that the response coefficient for total NADPH + NADP concentration is quite small (0.06 - 0.09), as expected from Equation 4.18. The only terms in this equation affected by a rise in P or PH (at constant ${}^{PH}/_{P}$ ratio) are quite small in magnitude compared to the other terms, and hence have little effect on rate.

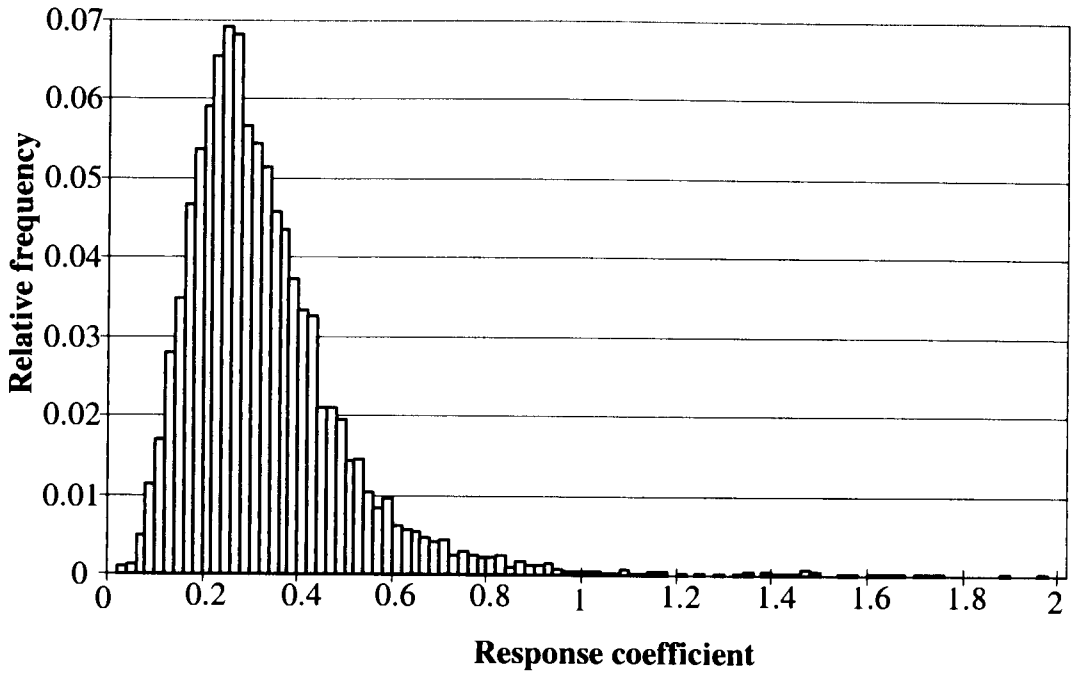

Figure 4.41: Response coefficient for NADPH/NADP ratio at constant NADPH+NADP concentration.

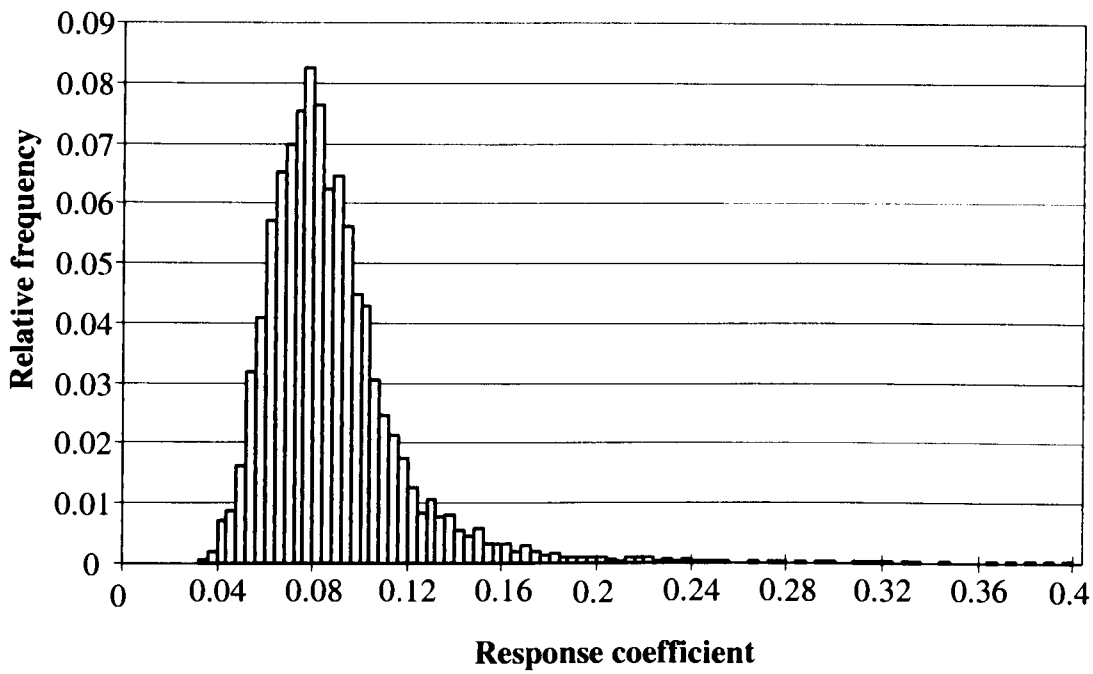

Figure 4.42: Response coefficient for total NADPH + NADP concentration at constant NADPH/NADP ratio.

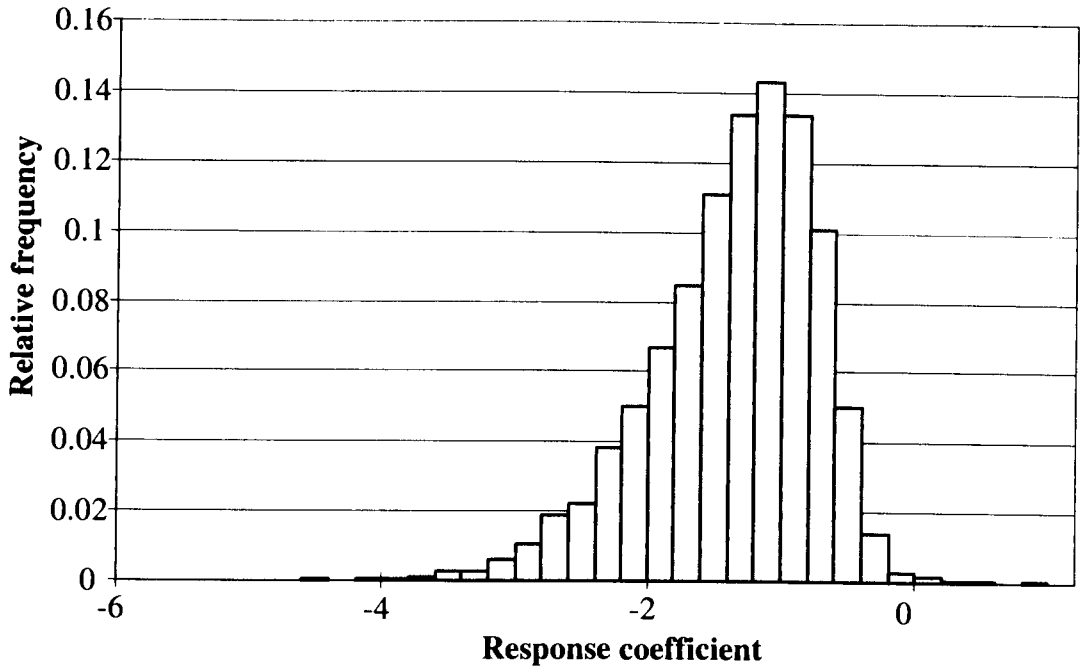

Figure 4.43: Response coefficient for pH.

The response coefficient of pH is rather high (-1 to -1.5) as shown by Figure 4.43. Although this may seem surprising, it reflects the logarithmic nature of the pH scale. As such it should be remembered that the possible variations in pH are much less than for the other variables.

4.7.2. Analysis of the Rapid Rise in PHB Production at hr 3.5

In addition to the information above, the kinetic modelling can assist in discovering what underlying changes might have caused the rapid increase in PHB synthesis rate at hr 3.5. Given the parameters established for the rapid production phase (Table 4.14), we can calculate the required change in a variable to achieve the observed rise in PHB rate. In particular the change in PHB production rate appears to occur in two stages: The first stage is a rapid sixfold increase at hr 3.5 from 0.008 gPHB.gRCM^{-1}h^{-1} to 0.050 gPHB.gRCM^{-1}h^{-1}. Following this there is a slow rise to about 0.080 gPHB.gRCM^{-1}h^{-1} by hr 10.

The high response coefficients of acetyl-CoA and the acetyl-CoA/CoA ratio suggest that they may be responsible for the rapid initial rise. A reasonable estimate for the initial acetyl-CoA ratio is given in Table 4.10, viz between 3.5 to 6, which corresponds to a doubling of this ratio. When coupled with the observed doubling in acetyl-CoA concentration at hr 3.5 to 5, the expected increase in PHB production rate is shown in Figure 4.44. A fivefold most-likely increase is observed, which agrees quite well with the observed sixfold increase. The enzyme activities were adjusted in this calculation to give the observed initial rate of 0.008 gPHB.gRCM^{-1}h^{-1}.

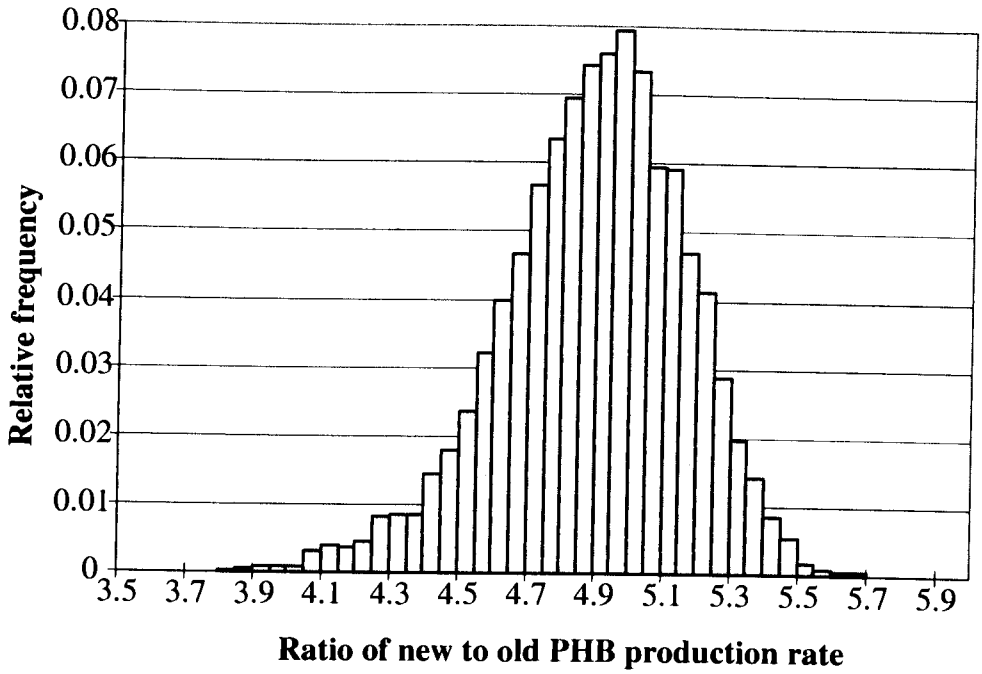

Figure 4.44: Ratio of new PHB production to initial PHB production after a doubling of acetyl-CoA concentration and of acetyl-CoA/CoA ratio.

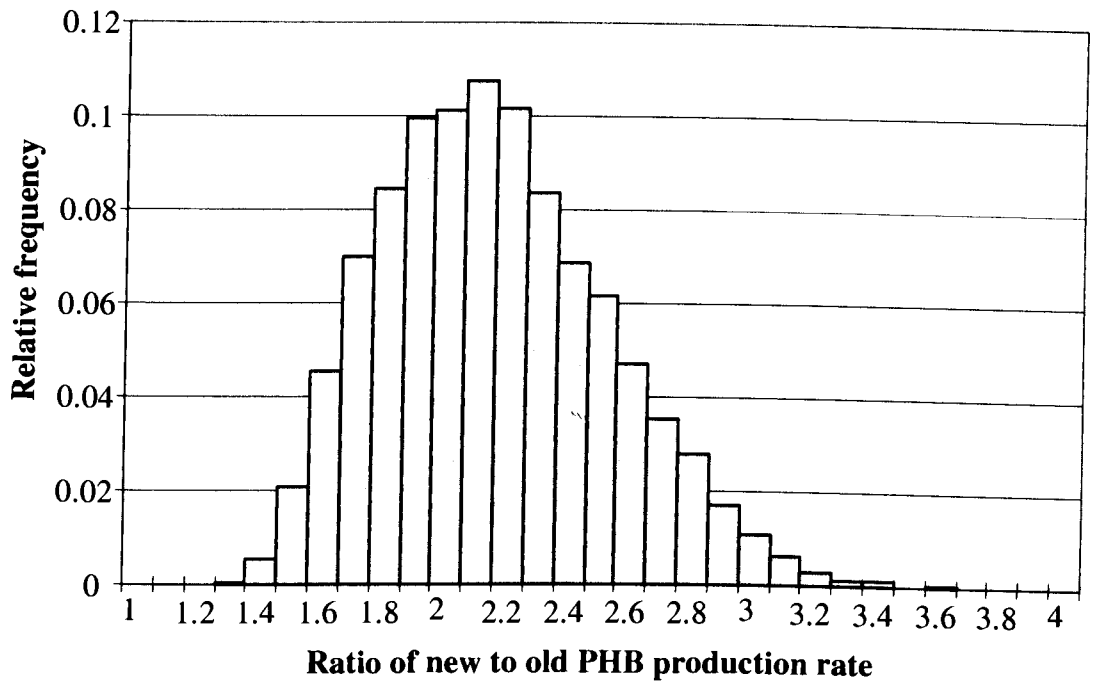

Figure 4.45: Ratio of new PHB production to initial PHB production after a sixfold increase in NADPH/NADP ratio.

When this analysis is repeated for the other most likely candidate, viz NADPH/NADP ratio (Figure 4.45), the result is quite different. Even a sixfold increase in NADPH/NADP ratio gives a mere 1.8- to 2.2- fold increase in PHB production rate.

The high response coefficient of pH suggests that a pH decrease upon oxygen exhaustion may significantly influence PHB rate, given that *E. coli* has an intracellular pH of near 7.6 under aerobic conditions but 6.9 under anaerobic conditions. The effect of a 0.4 pH drop is a mere 10-20% increase in rate as shown in Figure 4.46. Hence this explanation can be disregarded.

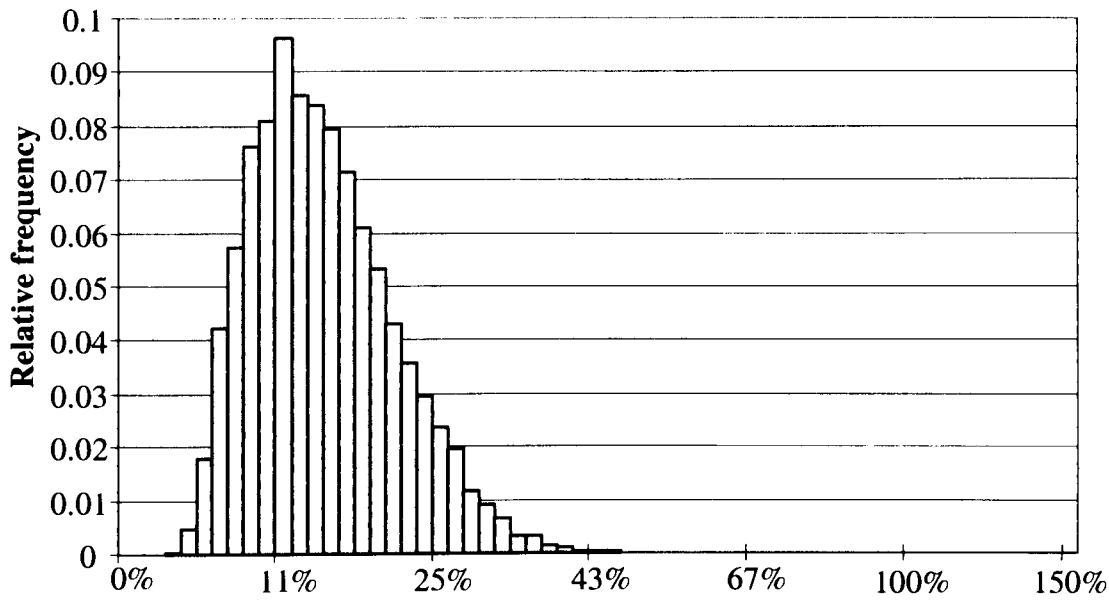

Figure 4.46: Increase in PHB production rate upon decreasing pH by 0.4 units.

In summary it appears that the initial rapid sixfold rise in PHB production (at hr 3.5) could easily have been caused by a doubling of the acetyl-CoA/CoA ratio and the observed doubling of acetyl-CoA concentration. This may have been augmented to some small degree by a rise in NADPH/NADP ratio, or a decline in pH. From this point on, the continued slow rise in PHB production was probably caused by a rise in enzyme activities, as described in Section 4.7.2. This is supported by the calculated PHA synthase activity (Figure 4.28), which exhibits a gradual rise in activity over the period up until hr 10.

4.8. Further Discussion

The fermentation can be split into four distinct phases, which do not necessarily correspond to those in Section 2.7.

Phase 1 - exponential growth , hr 0-3.5.

During this time all rates are approximately constant, as expected for unrestricted growth.

Phase 2, onset of oxygen limitation, hr 3.5 - 6.

Oxygen limitation commences at hr 3.5. A number of events occur at this point. Firstly, PHB production increases 6-fold almost immediately. TCA cycle flux ceases entirely, causing CO_2 production to drop by 60%. Since the oxygen supply is being held constant, the oxidative phosphorylation rate rapidly declines to 0.95 mol O_2 per mol glucose supplied. Production of acetic acid, formic acid and pyruvic acid commence immediately, but lactic acid and succinic acid do not. Residual cell mass production and glucose consumption do not change appreciably. PDH flux (flux 2) declines rapidly from 60% of glucose flux to only 30%. The concentration of acetyl-CoA rapidly doubles to a peak value, then rapidly declines back to its former value.

The likely causes of these observations can be readily explained. Once oxygen limitation commences at the start of Phase 2, oxidative phosphorylation cannot consume all the NADH being produced by the TCA cycle, hence the NADH/NAD ratio begins to rise. This allosterically inhibits citrate synthase and α-ketoglutarate dehydrogenase, causing the TCA cycle flux to decrease. (See Figure 4.47) Pyruvate-formate-lyase (in flux 3) is activated by the rise in NADH, and in conjunction with the declining TCA cycle flux, causes the acetyl-CoA concentration to rise. Both NADH and acetyl-CoA inhibit the pyruvate dehydrogenase complex, causing intracellular pyruvate to accumulate. The rise in NADH and pyruvate lead to production of lactic acid, however this is insufficient to prevent pyruvic acid excretion to the medium. The accumulation of pyruvate also further enhances formic acid production. The increased acetyl-CoA and pyruvate levels cause excretion of acetic acid, at a rate which matches the PFL flux. As shown in Section 4.7.2, the rapid increase in PHB production is probably caused by the increased acetyl-CoA concentration in conjunction with a decline in CoA concentration. A rise in NADPH/NADP may also assist to a lesser degree, potentially coupled through from NADH/NAD by the transhydrogenase. In wild-type *E. coli*, pyruvate kinase (part of flux 1) is also inhibited by NADH, which would prevent the intracellular accumulation of pyruvate. The observation that this does not occur with XL1-Blue(pSYL107) suggests that it may contain a mutation which prevents NADH inhibition of pyruvate kinase.

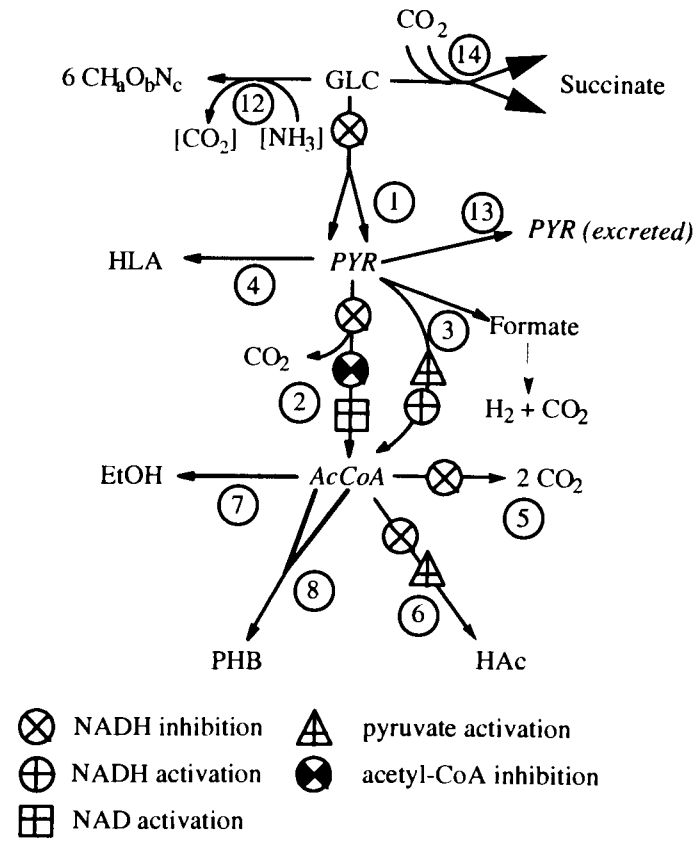

Figure 4.47: Allosteric control of central metabolism (adapted from Lehninger *et al.* (1993)).

It appears that when the dissolved oxygen level reaches 0%, residual cell mass production is rapidly inhibited within the first hour, dropping by 50% from hr 3.5 to hr 4.5. Yet Figure 4.48 shows that ATP production per gRCM actually increases over the same period, due to an increased contribution from substrate-level phosphorylation. Figure 4.49 shows this more clearly in terms of available ATP per gRCM synthesised. Hence it seems unlikely that insufficient ATP production is the cause of the initial RCM flux decline. A more likely explanation is that the low oxygen tension induces widespread changes in enzyme levels. *E. coli* possesses at least two global regulation systems dependent on oxygen tension, viz Arc (aerobic respiration control) and Fnr (fumarate nitrate reduction) (Lynch and Lin (1996)). A second possibility is a large decline in the efficiency of ATP production from NADH, due to changing levels of NDH I vs NDH II and cytochrome bd vs cytochrome o as outlined in Section 2.3 (Gennis and Stewart (1996)). This seems unlikely given the magnitude of the changes in Figure 4.48.

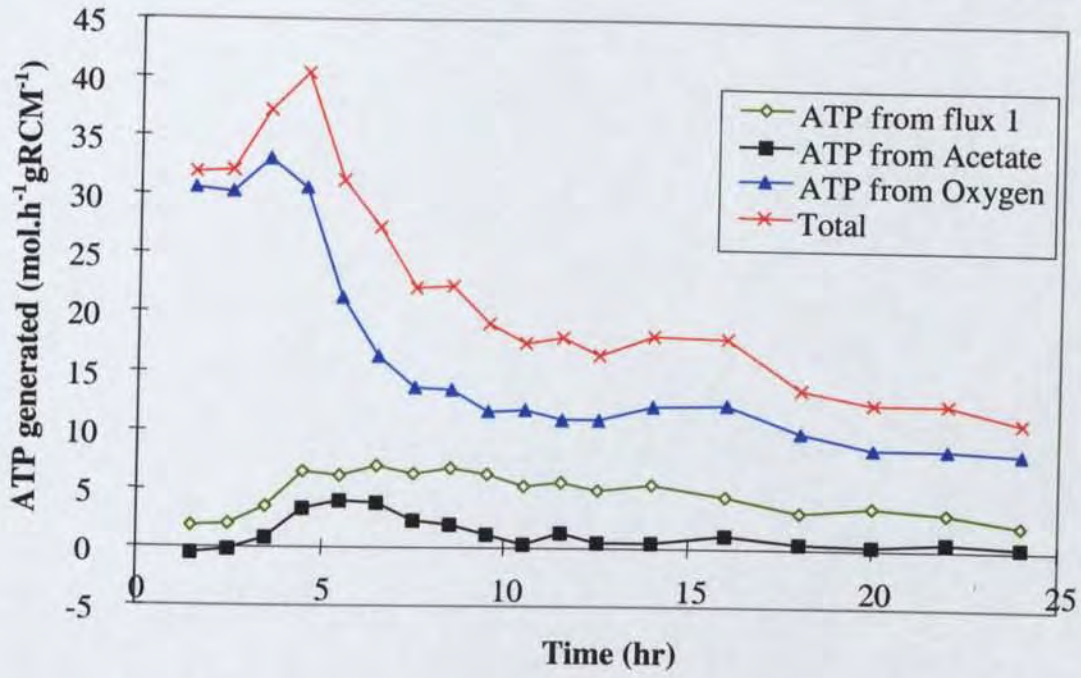

Figure 4.48: Breakdown of ATP production rate.

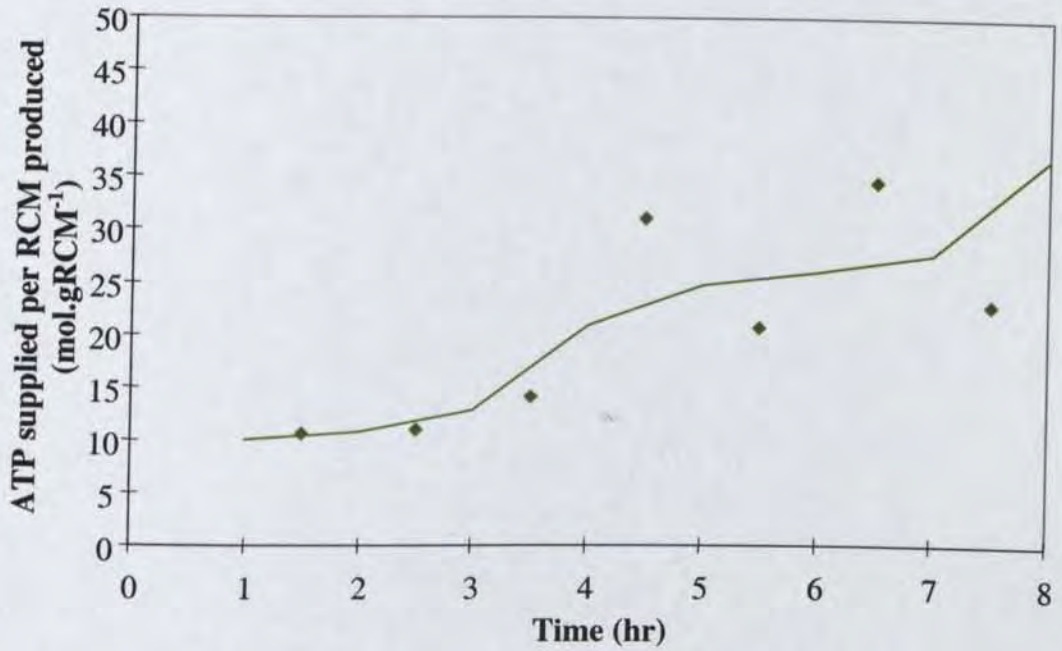

Figure 4.49: ATP produced per gram of RCM synthesised.

Phase 3, gradual metabolic shift phase, hr 6 - 10.

By the end of phase 2, TCA cycle flux drops to zero. The previously mentioned Arc global regulator is probably largely responsible for this, in conjunction with a high NADH/NAD ratio. Formic acid and acetic acid excretion are at a maximum. As phase 3 progresses, the

activity of pyruvate-formate-lyase (in flux 3) begins to decrease. The reason for this is not clear, but is probably either

- cumulative oxygen damage, since the active enzyme form is oxygen-labile; or
- a decline in the level of NADH, which fits with the observation that PFL flux begins to decline soon after TCA cycle flux ceases (and hence TCA cycle NADH generation ceases). This also agrees well with the measured NADH and NAD profiles given by Wimpenny and Firth (1972): upon changing from aerobic to anaerobic conditions, the NADH concentration rapidly tripled, then declined back to its original level over the next hour. Likewise the NAD concentration dropped by 75%, then slowly rose back to half of its aerobic value. Given that the onset of oxygen limitation is more gradual in this experiment, it seems possible that similar changes are occurring during phases 2 and 3.

By the end of phase 3 formic acid production has rapidly decreased from 90% of glucose flux to 0%. Likewise acetic acid flux decreases from 80% of glucose flux to 25%. In contrast, lactic acid, pyruvic acid and succinic acid production climb to a plateau. PHB production rises linearly from 15% of glucose flux (0.06) to 30% of glucose flux (0.09). Glucose consumption declines rapidly from 0.85 to 0.6 $gGlc.gRCM^{-1}h^{-1}$, which may be related to the constant supply of oxygen on a glucose basis (0.95 mol O_2 per mol glucose supplied).

During phase three, the growth rate steadily decreases to 0.05 $g.gRCM^{-1}h^{-1}$. As mentioned in Section 4.6.3 this allows the copy number of pSYL107 to increase, and hence express higher levels of PHB enzymes. This effectively "hijacks" the cellular machinery for synthesis and maintenance of DNA, RNA and proteins. In turn this reduces the synthesis of cellular machinery itself, with the net result that residual cell mass synthesis declines to a low basal level. As shown in Section 4.6.3, the activity of the PHA enzymes also increases over this period, probably for the same reason, giving rise to the observed increase in PHB production rate.

Phase 4, slow decline, hr 10- 25

After the peak of metabolic activity at hr 10, another metabolic shift occurrs. This is demonstrated by several observations:

- the dissolved-oxygen concentration suddenly rises from 1% to 4.5% (Figure 4.7);
- the rate of decline in glucose flux abruptly lessens (from -0.053 $(g(glc).gRCM^{-1}h^{-1})h^{-1}$ to -0.027 $(g(glc).gRCM^{-1}h^{-1})h^{-1}$) (Figure 4.9);
- The production rates of acetic, pyruvic and succinic acid stabilise, whereas the lactic acid rate begin a slow decline (Figure 4.24).

Once residual cell mass production decreases to its basal level, the total activity of all cellular enzymes begins to abate, causing a gradual decline in all fluxes. PHB production uses an ever-increasing proportion of glucose flux (Figure 4.23) from RCM and lactic acid, but nevertheless declines on an RCM basis. As suggested in Section 4.6, this may simply be due to reduced intracellular volume available for synthesis.

One anomalous observation is the sudden rise in dissolved oxygen at the start of phase 4. It occurs very promptly after cessation of formic acid flux, suggesting a link with NADH levels, but this is probably coincidence. The rise indicates a slightly reduced consumption of oxygen, despite the fact that supply remains limiting. This is probably due to a change in the enzymes of the respiratory chain. For example, *E. coli* possesses both cytochrome bd ubiquinol oxidase and cytochrome o ubiquinol oxidase. They each catalyse the same reaction (viz the final step in the respiratory chain) however the oxygen affinity of cytochrome bd is orders of magnitude higher than cytochrome o. Under conditions of low oxygen tension, the levels of cytochrome bd are increased at the expense of cytochrome o. Thus, the observed rise in

dissolved oxygen may reflect a switch from cytochrome bd back to cytochrome o as the oxygen tension rises above a regulatory threshold.

4.9. Conclusions

4.9.1. Potential for Improved PHB Production

The observations on the control fermentation suggest a number of manipulations which may lead to improved PHB production.

- Reduction of acid production. A large fraction of the glucose consumed (40%) was wasted by conversion to organic acids. Furthermore, accumulation of acids is known to inhibit the growth of *E. coli* and to reduce expression of recombinant proteins (Aristidou *et al.* (1995); Goel *et al.* (1995b)). Potentially, the excretion could be reduced in several ways, viz
  - avoiding oxygen deprivation;
  - using batch feeding techniques (e.g. pH-stat feeding) that restrict glucose supply and reutilise excreted acids;
  - genetic engineering to reduce glucose uptake and hence avoid accumulation of intracellular pyruvate (Goel *et al.* (1995a));
  - removal of acid-production genes (for example pyruvate-formate-lyase). However such an approach may lead to increased excretion of intermediates such as pyruvate and possible toxicity effects.
- For some reason the specific PHB production rate did not reach the peak levels achieved in the high-cell-density fermentation, and also declined more rapidly after its plateau. The fact that production rate was climbing until the metabolic shift at hr 10 suggests that delaying the onset of that shift could permit higher rates to be achieved. Unfortunately the reason for the shift is not clear, but appears related to RCM production. More experiments are required to elucidate the reason for the decline (for further discussion see Chapter 5). Given the slow degradation rate of proteins (10 hr halflife according to Nielsen and Villadsen (1994)) it may be possible to raise PHA enzyme concentrations to high levels during an initial phase, for example by feeding with complex nutrients for a short period. Thus the PHB synthesis rate would remain elevated above the level it would otherwise have achieved. The high-cell-density fermentation (Chapter 2) also suggests that extending the RCM production phase after PHB synthesis has commenced can yield higher PHB synthesis rates.
- The slow decline during the last phase of PHB production suggests that the cells may be too metabolically inactive for sufficient cell maintenance. Transiently increasing the growth rate (for example by addition of a small amount of complex nutrient) may therefore permit the cells to replenish their metabolism and arrest its decline. This would require further experimentation to verify.
- The metabolic control analysis indicates a large influence of acetyl-CoA/CoA ratio on PHB production rate. If the supply of acetyl-CoA could be increased this may have substantial benefits. Likewise, mutants with abnormally high levels of total -CoA have the potential to substantially increase the PHB flux, because the concentration of acetyl-CoA has a large influence even at constant acetyl-CoA/CoA ratios. Shi *et al.* (1999) examined an pta^-/ack^- strain containing PHB genes which lacked the ability to excrete acetate and therefore would probably have elevated internal acetyl-CoA concentrations. PHB production was not improved by the mutation, although interpretation is difficult because of the lack of a good control.
- Although not as marked as acetyl-CoA, an increase in the ratio of NADPH/NADP will likely improve PHB flux significantly. This could potentially be achieved by metabolical engineering to force more flux through the PPP pathway, or through nicotinamide transhydrogenase. Observations on the NADPH generation flux show that NADPH demand during PHB synthesis was less than during RCM synthesis, so such manipulation

should be readily achievable. Further analysis would be required to verify this. Shi *et al.* (1999) utilised a pgi$^-$ mutant which increases flux through NADPH-generation pathways, however cell growth was greatly impaired and PHB synthesis was not improved. Unlike acetyl-CoA, merely increasing the poolsize of NADPH+NADP would probably not have substantial benefits.

- As shown by the metabolic control analysis, choosing a mutant which operates at lower intracellular pH may significantly improve the PHB production rate. Such mutants exist, whose intracellular pH can vary over a wide range (Diez-Gonzalez and Russell (1997)).
- The kinetic analysis shows that a possible cause of the decline in PHB production is reduction of intracellular volume over time. One factor causing this is the accumulation of PHB granules, but more significant is the osmolarity of the culture medium. As this increases, the cell's cytoplasmic space shrinks and hence reduces the available space for PHB synthesis. The major contributor to osmolarity rise in this fermentation was addition of sodium hydroxide for pH control, and hence avoiding acid excretion or using an alternative pH control method would reduce the detrimental osmolarity effect. This effect poses a potential problem when using concentrated dairy whey, which contains high levels of salts in addition to lactose.
- It seems likely that PHB production could be initiated by causing the acetyl-CoA/CoA ratio to rise without the need for oxygen exhaustion, potentially permitting higher and more sustained PHB production. This might be achieved by inhibiting the activity of the TCA cycle or by enhancing pyruvate dehydrogenase activity. Another possibility is activation of pyruvate-formate-lysase activity, in conjunction with formate-hydrogen-lyase to avoid formate accumulation.

4.9.2. Summary and Directions for Remaining Chapters

This chapter has successfully achieved several outcomes needed by Chapters 5 and 6:

- a repeatable "base-case" fermentation was developed from the Chapter 2 fermentation. This fermentation can hence be used as a control for investigating the effects of oxygen limitation (Chapter 5) or nutrient feeding (Chapter 6);
- the metabolic flux model described in Chapter 2 was refined and verified using rigorously collected fermentation data.

In addition, a kinetic model of PHA production was adapted and applied to the data. In conjunction with the metabolic flux analysis it yielded insights into the metabolic behaviour of XL1-Blue(pSYL107) during PHB production. In particular:

- it suggests that oxygen limitation may be responsible for the onset of PHB production, and gives a likely explanation in terms of metabolic regulation. This is investigated further in Chapter 5, with the aim of gaining additional metabolic understanding;
- estimates of intracellular cofactor concentrations and enzyme concentrations were obtained;
- it established the sensitivity of PHB production rate to changes in cofactor concentrations and enzyme concentrations.

In conjunction with the economic analysis in Chapter 3, this chapter also identifies several areas where significant improvements to the PHB production process are possible.

Chapter 5

5.1. Summary

The aim of this chapter is to investigate the effects of oxygen supply on PHB production by the recombinant *E. coli* XL1-Blue(pSYL107). Of particular interest is answering the questions:

- Is oxygen limitation responsible for triggering PHB synthesis? If not, what is?
- Can oxygen supply be reduced during the PHB synthesis phase without impairing PHB production? Is there a minimum rate of supply required?
- What are the likely effects of scaleup to large-scale bioreactors, which will exhibit poor-mass-transfer characteristics?

Two constant-glucose fed-batch fermentations of duration 25 h were carried out in a 5 l bioreactor. The first ("high-oxygen") fermentation was carried out identically to the control fermentation in Chapter 4, except that the oxygen volumetric mass-transfer coefficient (k_La) was held constant at 3.5 min^{-1} instead of 1.1 min^{-1}. The second ("low oxygen") fermentation was carried out identically with the control up to hr 10, and at this point the stirrer speed was abruptly reduced, attenuating k_La to 0.79 min^{-1}. For each fermentation the production rates of PHB, residual cell mass, carbon dioxide, acetic acid, formic acid, lactic acid, succinic acid, pyruvic acid and ethanol were measured. The consumption rates of glucose, oxygen and ammonium ion were also measured, along with the intracellular concentrations of acetyl-CoA and 3-hydroxybutyryl-CoA.

The "high-oxygen" fermentation achieved 60% PHB with 48 g.l(broth)$^{-1}$ dry cell weight. Peak PHB production rate was 0.11 gPHB.gRCM^{-1}h^{-1}. PHB yield on glucose was 0.41 mol(PHB).mol(Glc)$^{-1}$. Peak excretion levels were: formic acid(1.1 g.l^{-1}), acetic acid(7.6 g.l^{-1}), lactic acid(31 g.l^{-1}), succinic acid(1.1 g.l^{-1}), pyruvic acid(3.1 g.l^{-1}), and ethanol(0.8 g.l^{-1}).

In contrast the "low-oxygen" fermentation achieved only 44% PHB with 14 g.l(broth)$^{-1}$ dry cell weight. Peak PHB production rate was 0.07 - 0.09 gPHB.gRCM^{-1}h^{-1}. PHB yield on glucose was 0.23 mol(PHB).mol(Glc)$^{-1}$. Peak acid excretion levels were: formic acid(4.5 g.l^{-1}), acetic acid(6.8 g.l^{-1}), lactic acid(16 g.l^{-1}), succinic acid(3.2 g.l^{-1}), and pyruvic acid(3.7 g.l^{-1}). Ethanol was not detected.

The acid excretion patterns could be divided into three groups:

- pyruvic and acetic acid, which followed the same medium concentration profile for each fermentation independent of the actual cell density, and were unaffected by oxygen supply once below a critical level;
- lactic acid, which showed the same excretion on a residual-cell-mass basis and was dependent on oxygen supply (RCM basis);
- formic acid and succinic acid, whose excretion rates were not related to oxygen supply in a straightforward manner. The data suggest that improving the well-mixedness of the fermenter markedly reduces the excretion of formic and succinic acids.

To a first approximation, the oxygen supply level (volumetric basis) determined the cell-mass achieved. On a residual-cell-mass basis the "high-oxygen" fermentation was nearly identical to the control fermentation (Chapter 4). During the "low-oxygen" fermentation, the sudden

cut in oxygen supply caused a corresponding sudden decrease in PHB production and increase in lactic acid production. Other fluxes (especially glucose uptake) were not greatly affected. At high cell densities the onset of PHB accumulation is not obviously linked to oxygen limitation, but may be due to transient limitation (i.e. 'anaerobic zones' formed by poor mixing).

Linear optimisation studies were used to obtain an estimate for the minimum rate of oxygen supply required to avoid acid production. It was also shown that the cells appear to be quite well optimised for maximum ATP production given a limited oxygen and glucose supply. It is stoichiometrically possible to double the PHB yield on glucose in several ways, including reducing the rate of glucose uptake.

Scaleup to large bioreactor sizes may present difficulties due to poor mixing, which appears to enhance formic and succinic acid production, and impair PHB production. At production rates similar to those of the high-cell-density fermentation in Chapter 3, an oxygen partial pressure in the gas feed of at least 240 kPa is required to avoid acid excretion (assumed oxygen-mass-transfer-coefficient = 1.0 min^{-1}).

5.2. Introduction

5.2.1. General

The Chapter 3 economic analysis clearly demonstrated that aeration cost is a major contributor to PHA selling price. Two reasons for this were identified:

1. The capital and operating costs of the compressors is significant.
2. Above a certain level of oxygen demand it becomes necessary to use oxygen-enriched air. This is not economical, hence the cell density is limited to a sub-optimal level.

A reduction in the fermentation aeration requirements may therefore allow substantial cost savings. This may be achieved in two main ways:

1. Improving the oxygen transfer rate. In the control fermentation for example, the inlet oxygen concentration was 21% and the exhaust was 20%. Hence 100 litres of gas was pumped through the bioreactor for every litre of oxygen actually used. Ideally, the flowrate of gas through the bioreactor would be just sufficient to maintain dissolved oxygen at the minimum concentration necessary, giving maximum driving force for oxygen transfer. It is therefore of interest to discover what this minimum concentration might be.
2. Reducing oxygen demand, without impairing PHB production rate or molar yield on glucose. Potentially, the usefulness of oxygen to the cell during PHB production may be either ATP production or redox balancing (or both). In each case there are possible improvements that can be made. It is therefore of interest to discover which of the two is more important. Improving the tolerance of the bacteria to oxygen deprivation may also be possible.

Two different fermentations are conducted in this chapter.

1. A 'high-oxygenation' fermentation (HOF), where the oxygen supply is held constant at a higher level than for the Chapter 4 control fermentation (CON). The main objective of this is to investigate more fully whether oxygen supply is the trigger for PHB production, as postulated in Chapter 4. A secondary objective is to determine the scalability of the data to higher cell-densities/oxygen-supply-levels. It is expected that the HOF will follow essentially the same profiles as the CON, on a per-gram-biomass basis.
2. A 'low-oxygenation' fermentation (LOF), where the oxygen supply is initially held constant at the same level as the CON, but then abruptly reduced when PHB production is underway. This will demonstrate whether oxygen supply can be reduced during the PHB accumulation phase without impairing PHB production rate and yield.

The fermentations follow the same protocol as the "base-case" fermentation developed in Chapter 4, apart from oxygenation levels. The changes due to altered oxygen supply can then be directly contrasted against the Chapter 4 CON.

The HOF and LOF also provide further verification of the metabolic and kinetic models developed in Chapter 4. The understanding of metabolic changes gained in Chapter 4 is extended, in particular:

- confirming that oxygen deprivation triggers the onset of PHB production;
- quantifying the short-term and long-term effects of oxygen deprivation on PHB production;
- suggesting more aspects of the fermentation where improvements in PHB production are feasible, and possible ways of implementing them;
- making comparisons with the 'high-cell-density' fermentation (HCDF) in Chapter 2 to yield further insights into factors influencing PHB production and the role of oxygenation.

5.2.2. Literature Studies on Oxygen Deprivation

Several authors have studied the effects of oxygen deprivation on *E. coli*. In particular:

- Varma *et al.* (1993a) predicted the effects of reduced oxygen consumption, by linearly optimising the metabolic network to achieve maximal ATP production. At fixed growth rate, the predicted excretion is shown in Figure 5.1. Excretion of lactic acid, succinic acid, and pyruvic acid are not predicted by this model.

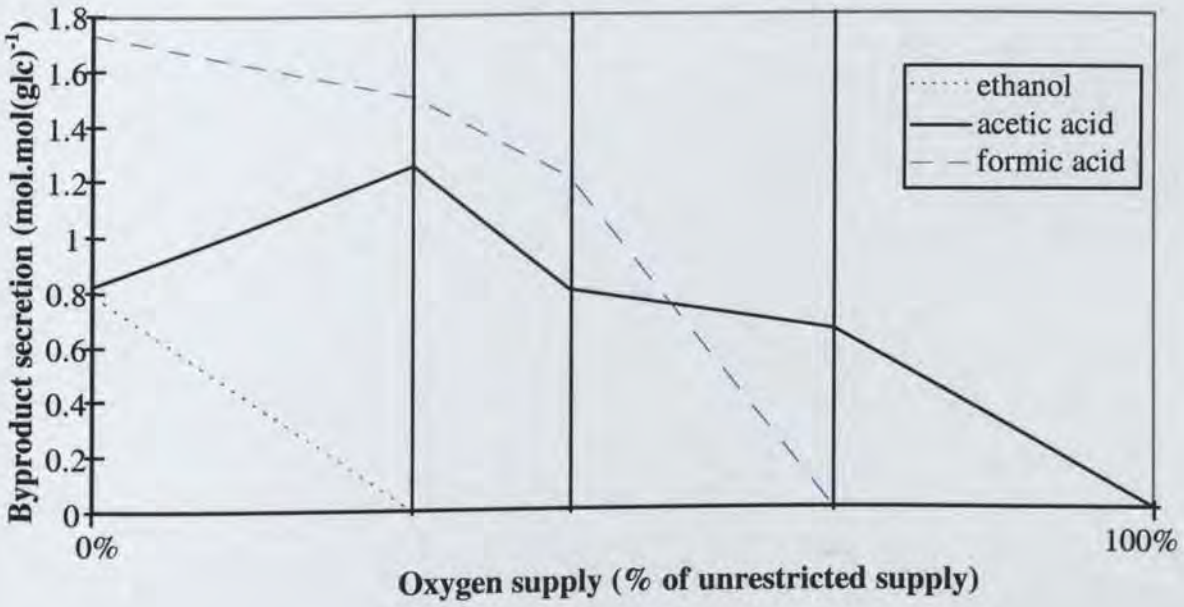

Figure 5.1: Optimal by-product secretion and growth for a range of oxygenation rates. Adapted from Varma *et al.* (1993a).

- Ko *et al.* (1993) examined the effect of oxygenation on acetate excretion, and the data show that the rate of acetate excretion is essentially independent of oxygen supply once oxygen limitation has commenced.
- Wang and Lee (1997) conducted experiments with XL1-Blue(pSYL107) and found that PHB synthesis was generally divided into two phases, viz
  - Phase I - "growth phase", low level of PHB content
  - Phase II - "PHB accumulation phase", cell synthesis ceases and rapid PHB synthesis occurs.
  - The trigger for the switch from one phase to another could not be identified.
  - The same study showed that oxygen limitation and complex nutrient supplementation had large effects on the fermentation profile. These studies are summarised in Table 5.1.

Table 5.1: Results of a study (Wang and Lee (1997)) into the effects of oxygen limitation on PHB production by XL1-Blue(sYL107) in bioreactors using a defined minimal medium.

	DCW ($g.l^{-1}$)	PHB ($g.l^{-1}$)	PHB %	bioreactor productivity ($gPHB.l^{-1}h^{-1}$)	Maximum PHB synthesis rate ($gPHB.gRCM^{-1}h^{-1}$)	PHB yield on glucose ($gPHB.g(glc)^{-1}$)
A	206	150	73%	3.4	0.11	27%
B	11	3.0	28%	-	-	-
C	204	157	77%	3.2	0.12	-
D	154	101	66%	2.8	-	28%
E	101	81	80%	2.1	0.15 - 0.20	37%

A = oxygen concentration maintained above 7% of saturation. B = oxygen limited to 1-3% during Phase I. C = oxygen limited to 1-3% during Phase II. D = oxygen limited to 0% during Phase II. E = typical fermentation with complex or semi-defined media, oxygen concentration maintained above 7% of saturation.

These results indicate that moderate oxygen limitation may be slightly beneficial to PHB yield, if applied during Phase II (Case C vs A). Limitation during Phase I impairs PHB production (B vs C), whereas exhaustion of oxygen also impairs productivity (D vs A & C).

Compared with earlier studies on complex and semi-defined media (Case E) the PHB yield on glucose was somewhat lower (Case A). Additionally the peak PHB synthesis rates were less. However the PHB productivity and final concentration were better for the defined medium. This occurred because the cells switched from Phase I to Phase II at 60 $gDCW.l^{-1}$ for the defined medium, compared with only 30 $gDCW.l^{-1}$ for the complex & semi-defined media. Hence the final cell density and PHB concentration were higher.

5.3. Materials and Methods

Two fermentations were performed for the work in this chapter. All methods were identical with those described in Chapter 4 with the following exceptions:

1. In the first experiment the oxygen volumetric mass-transfer coefficient (k_La) was held at 3.5 min^{-1} (vs 1.1 min^{-1} for the control) by adding an extra impeller and using a stirrer speed of 900 rpm.
2. The second fermentation was carried out identically with the control up to hr 10. At this point the stirrer speed was abruptly reduced to 600 rpm (k_La = 0.79 min^{-1}).

5.4. Results

5.4.1. General Fermentation Results

The profiles of RCM, PHB, and dissolved oxygen are shown in Figure 5.2, Figure 5.3, and Figure 5.4.

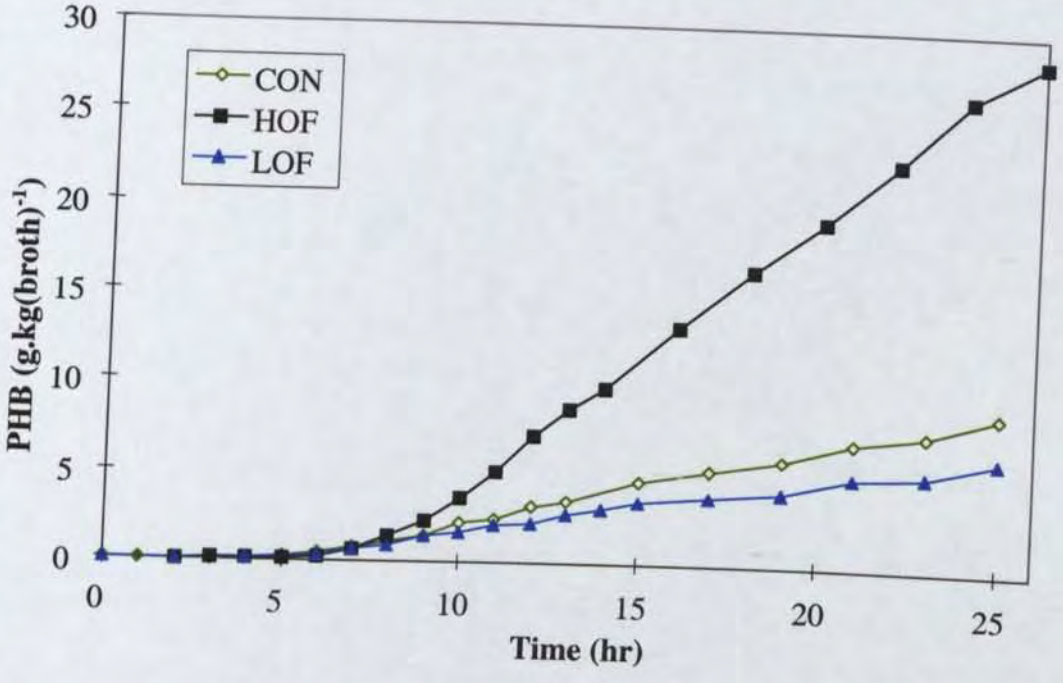

Figure 5.2: Comparison of PHB profiles for high- (HOF) and low- (LOF) oxygen supply relative to the control (CON).

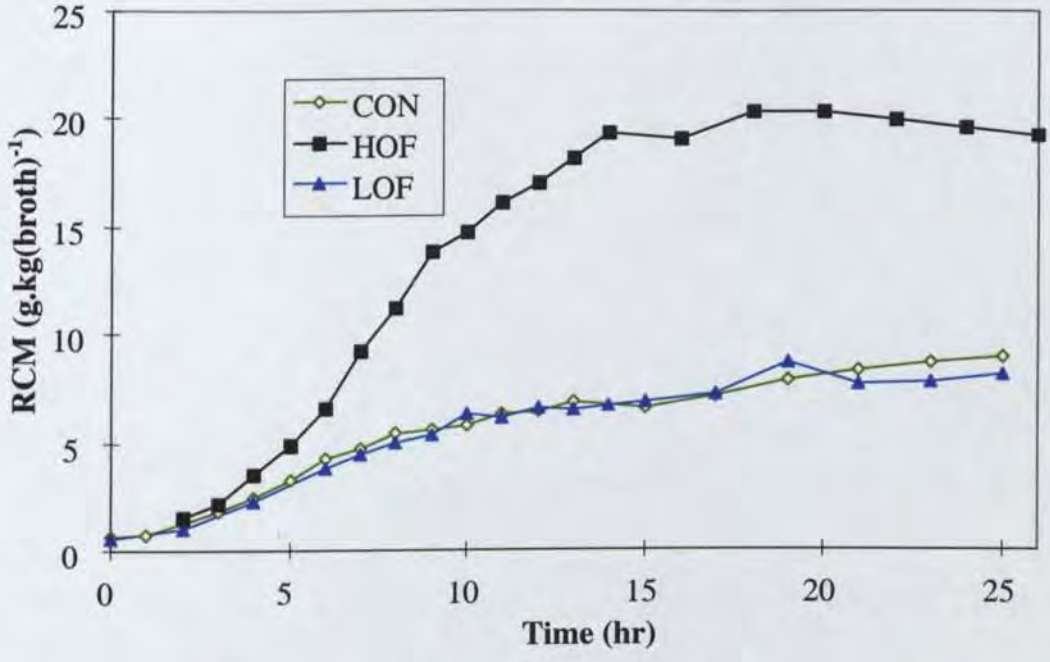

Figure 5.3: Comparison of RCM profiles for high- (HOF) and low- (LOF) oxygen supply relative to the control (CON).

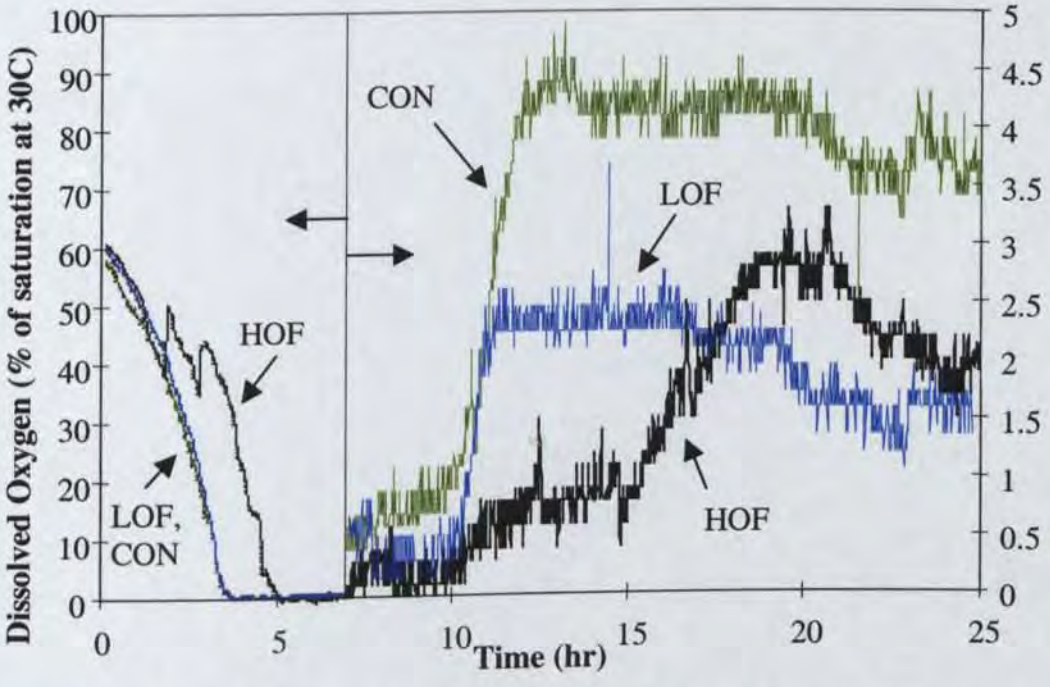

Figure 5.4: Dissolved oxygen profiles of high- (HOF) and low- (LOF) oxygen supply relative to the control (CON).

It is immediately apparent that the high-oxygen fermentation (HOF) has greatly improved levels of PHB and cell mass relative to the control (CON). In contrast, the low-oxygen fermentation (LOF) shows similar levels of residual cell mass but much lower levels of PHB. All three fermentations exhibit the same rise in dissolved oxygen concentration (to 1-4%) at hr 10-15. If this effect also occurs at high cell density, it becomes difficult to infer the exact

oxygen supply from the oxygen-limitation fermentation in Section 5.2.2 (Wang and Lee (1997)). (Table 5.1 Case C) A wide range of oxygen supply rates could have given the observed 1-3% dissolved oxygen level, and it is no longer certain that oxygen was supplied at a critical level. Hence the close match of case C and case A may simply be due to similar oxygen supply rates.

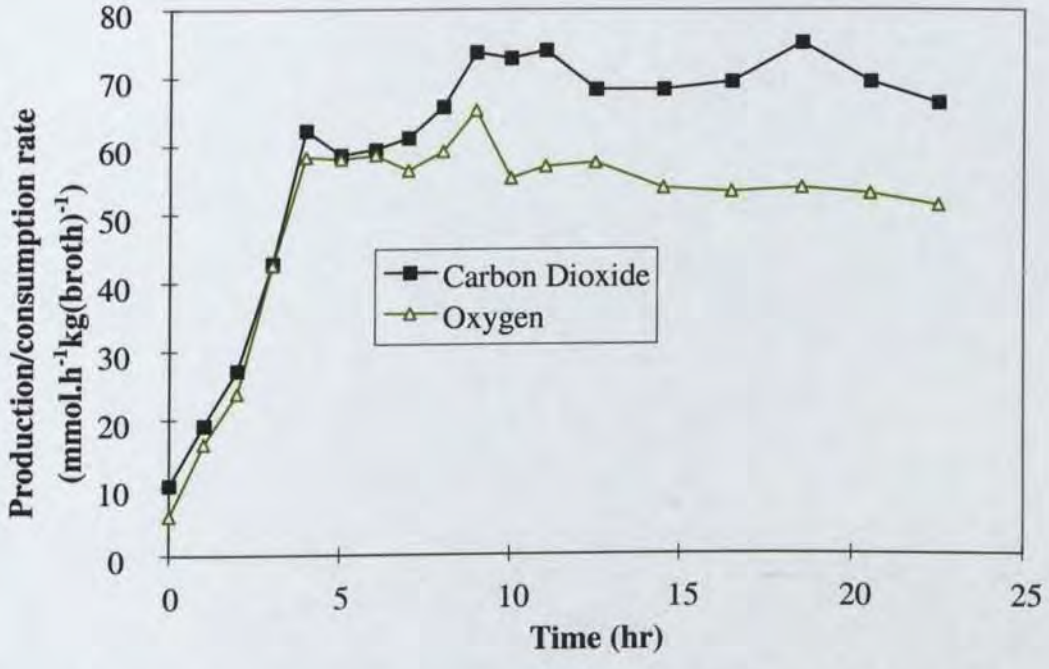

Figure 5.5: CO_2 production rate and oxygen consumption rate for the high-oxygen fermentation.

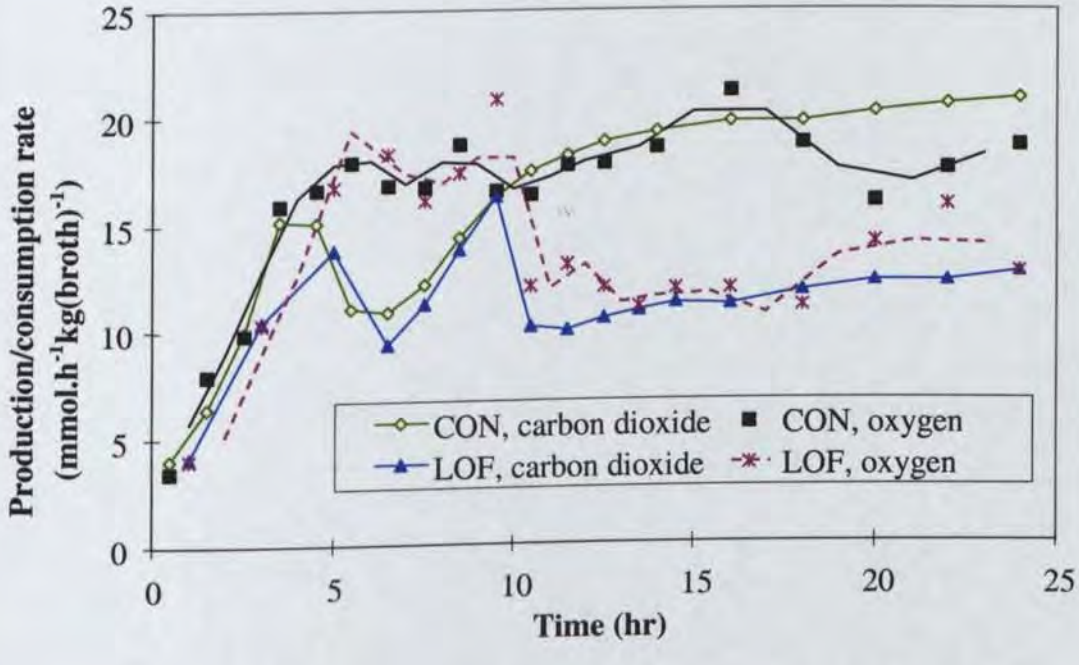

Figure 5.6: CO_2 production rate and oxygen consumption rate for the low-oxygen (LOF) vs control (CON) fermentations.

An intriguing observation to be made from Figure 5.5 and Figure 5.6 is that the HOF does not exhibit a dip in CO_2 production rate upon oxygen limitation, unlike the CON and LOF profiles. Instead there is a plateau for four hours, before rising to a new plateau in a similar fashion to the other two fermentations. The reason for this is not yet clear but is investigated further in Section 5.5. As expected the LOF shows an almost identical profile to the CON up till hr 10. At this point both oxygen and CO_2 rates rapidly drop to a new plateau.

The figures below show production profiles on an RCM basis. The time scale for the HOF has been adjusted to give the same origin relative to the onset of oxygen limitation, i.e. in all fermentations the onset of oxygen limitation is at approximately hr 3.5.

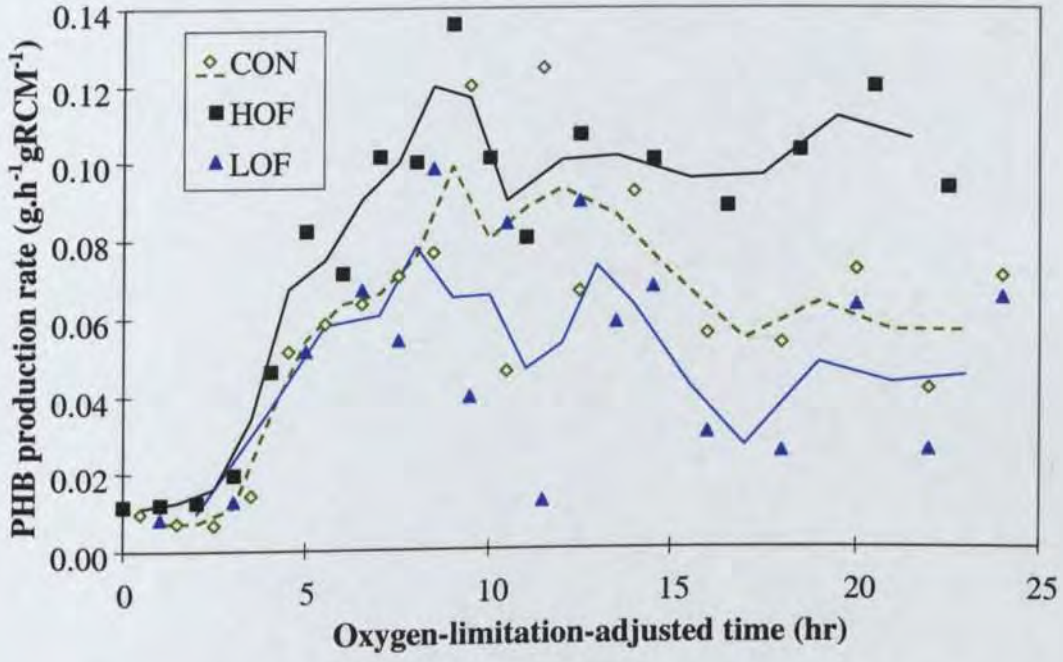

Figure 5.7: PHB production rate for the control (CON), low-oxygen (LOF) and high-oxygen (HOF) fermentations.

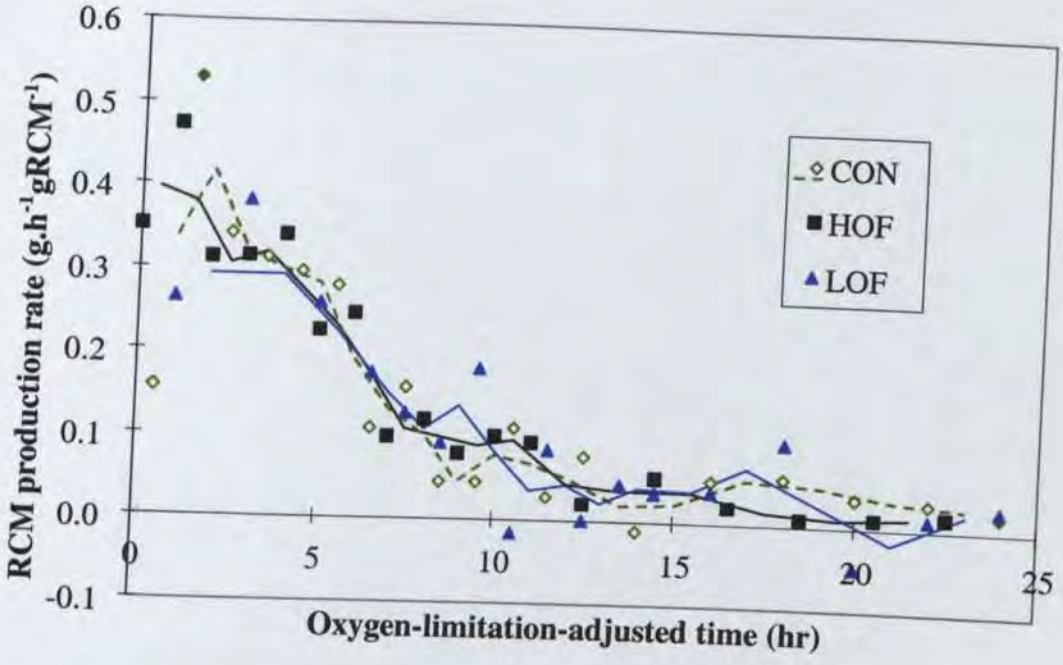

Figure 5.8: RCM production rate for the control (CON), low-oxygen (LOF) and high-oxygen (HOF) fermentations.

A striking feature of Figure 5.8 is that the RCM production profiles are all approximately the same. It appears that from hr 16 onwards the HOF is slightly lower than the CON but this may simply be experimental error. At any given time the HOF cell density was approximately three times that of the CON, indicating that RCM production on an RCM basis was essentially independent of cell concentration.

In contrast, PHB production shows large differences between the fermentations. The HOF rate rises perhaps more quickly than the CON, achieves a higher level (0.10 gPHB.gRCM^{-1}h^{-1} vs 0.08 gPHB.gRCM^{-1}h^{-1}) and unlike the CON does not appear to decline over the remainder of the fermentation. The HOF level is quite similar to the high-cell density fermentations described in Table 5.1 (0.11-0.12 gPHB.gRCM^{-1}h^{-1}) The LOF follows approximately the same PHB profile as the CON up to hr 10, although it appears to diverge at hr 9. This is most likely experimental error. After hr 10 the PHB production rate is reduced by approximately 20%.

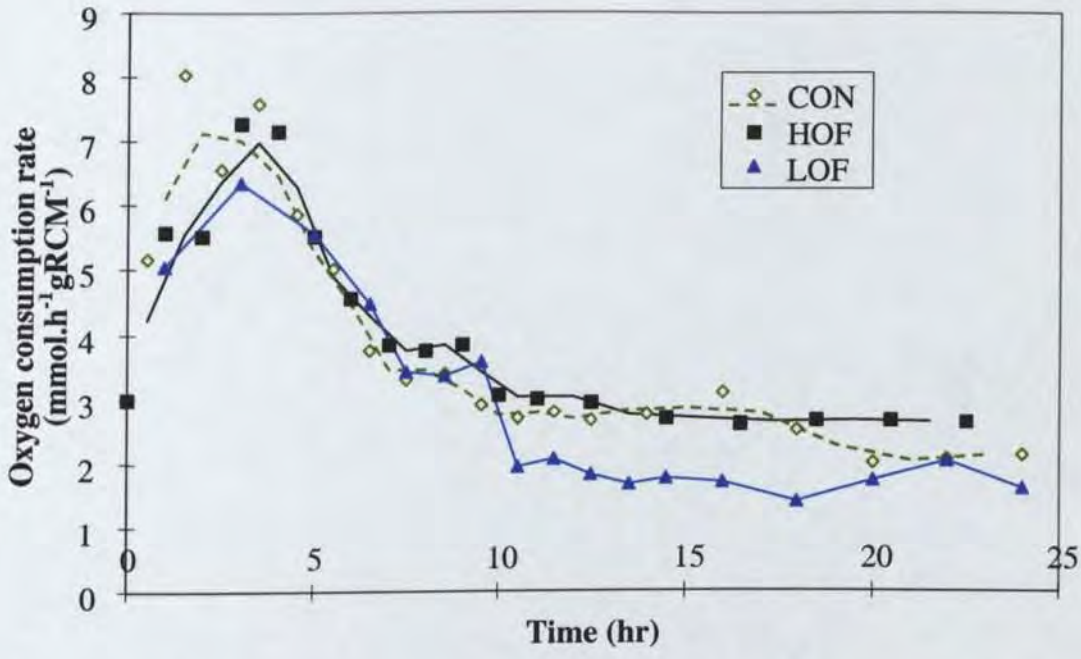

Figure 5.9: Oxygen consumption rate on an RCM basis, for control (CON), low-oxygen (LOF) and high-oxygen (HOF) fermentations.

As Figure 5.9 shows, all three oxygen consumption profiles match closely, apart from LOF which abruptly decreases at hr 10. The LOF oxygen consumption appears to remain constant after hr 10 whereas the CON consumption gradually declines. Although not shown, the profiles of glucose consumption are essentially identical (within +/-5%) for all three fermentations, indicating that glucose uptake is unaffected by reduced oxygen supply.

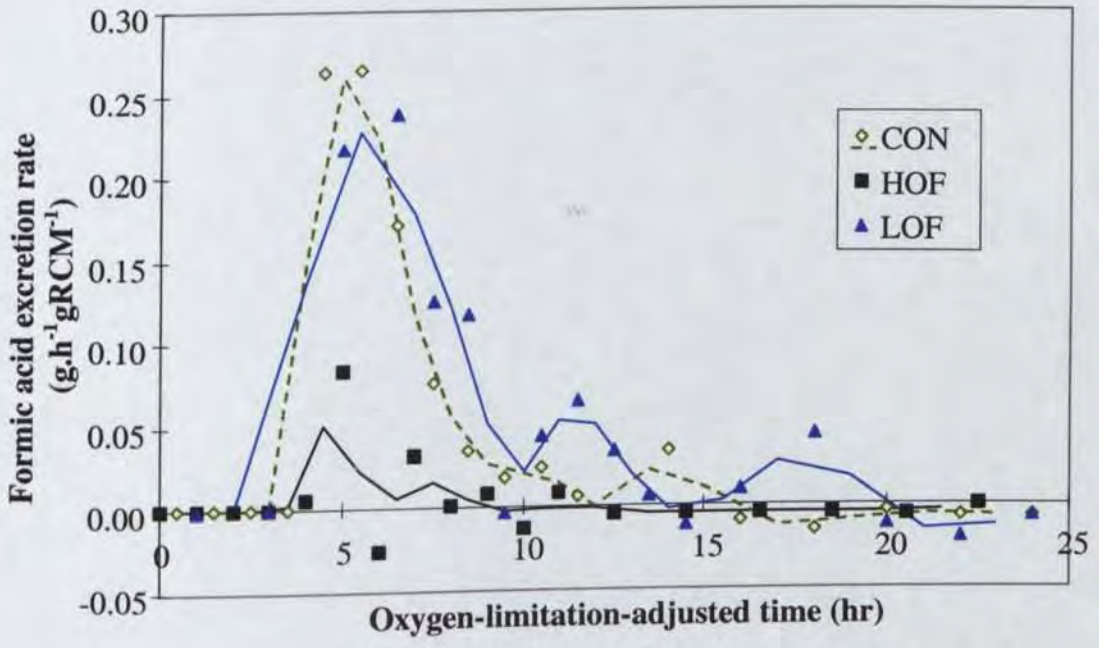

Figure 5.10: Formic acid production rate (smoothed) for the control (CON), low-oxygen (LOF) and high-oxygen (HOF) fermentations.

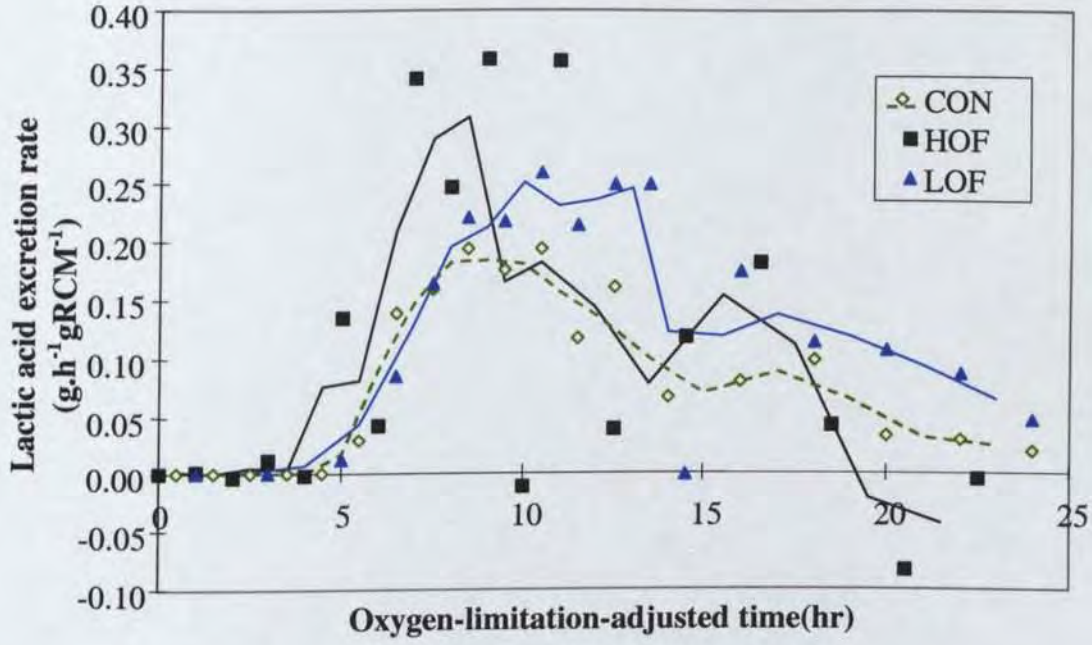

Figure 5.11: Lactic acid production rate (smoothed) for the control (CON), low-oxygen (LOF) and high-oxygen (HOF) fermentations.

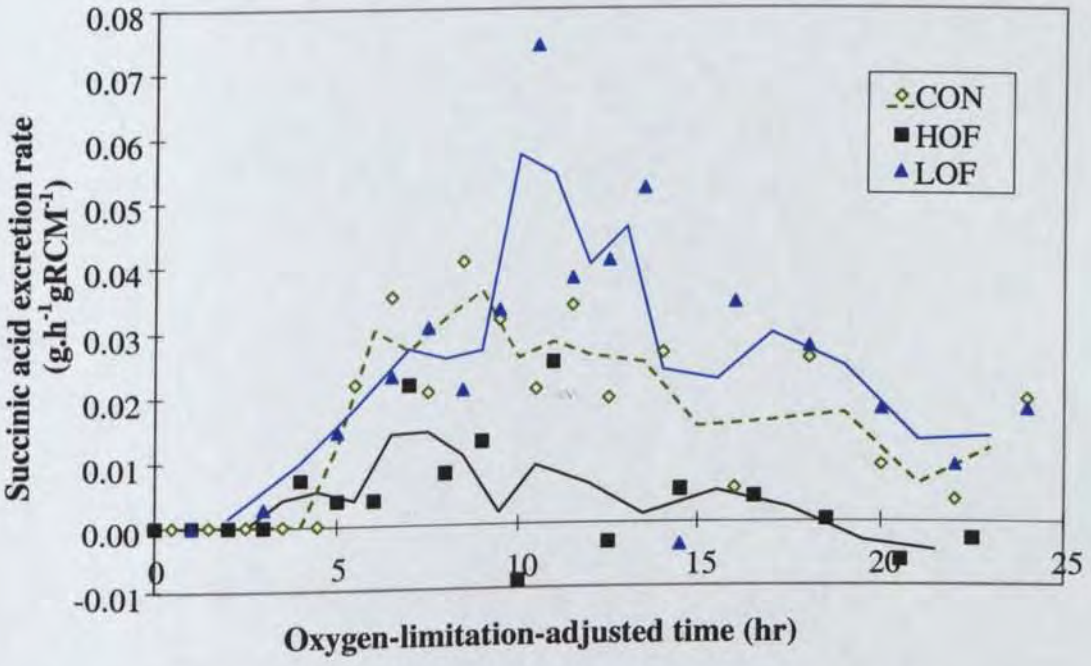

Figure 5.12: Succinic acid production rate (smoothed) for the control (CON), low-oxygen (LOF) and high-oxygen (HOF) fermentations.

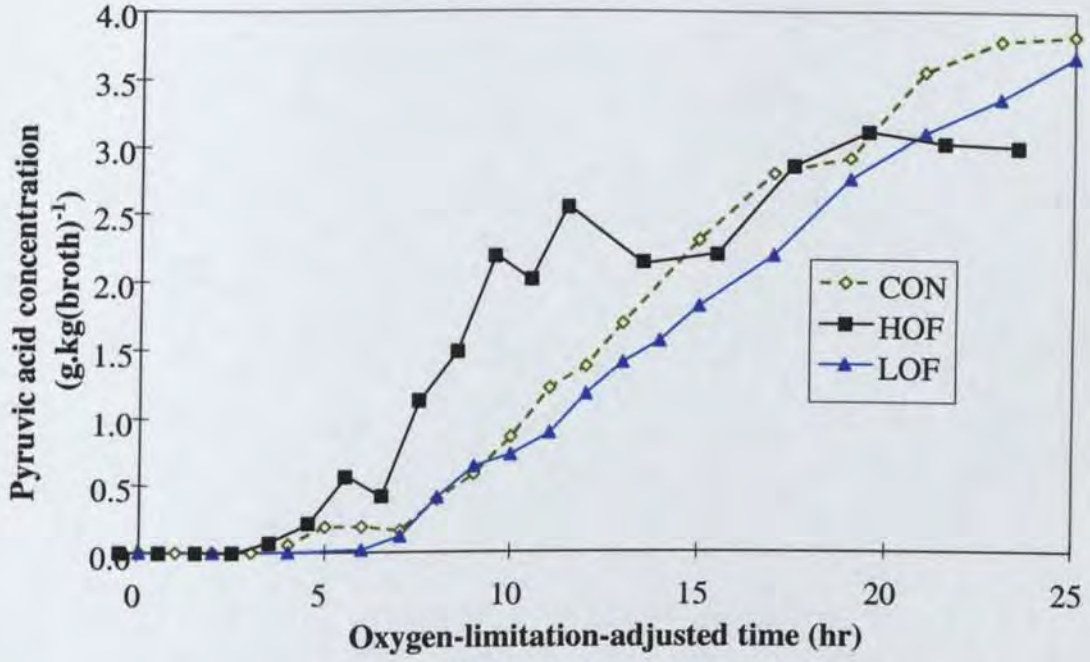

Figure 5.13: Pyruvic acid broth concentration for the control (CON), low-oxygen (LOF) and high-oxygen (HOF) fermentations.

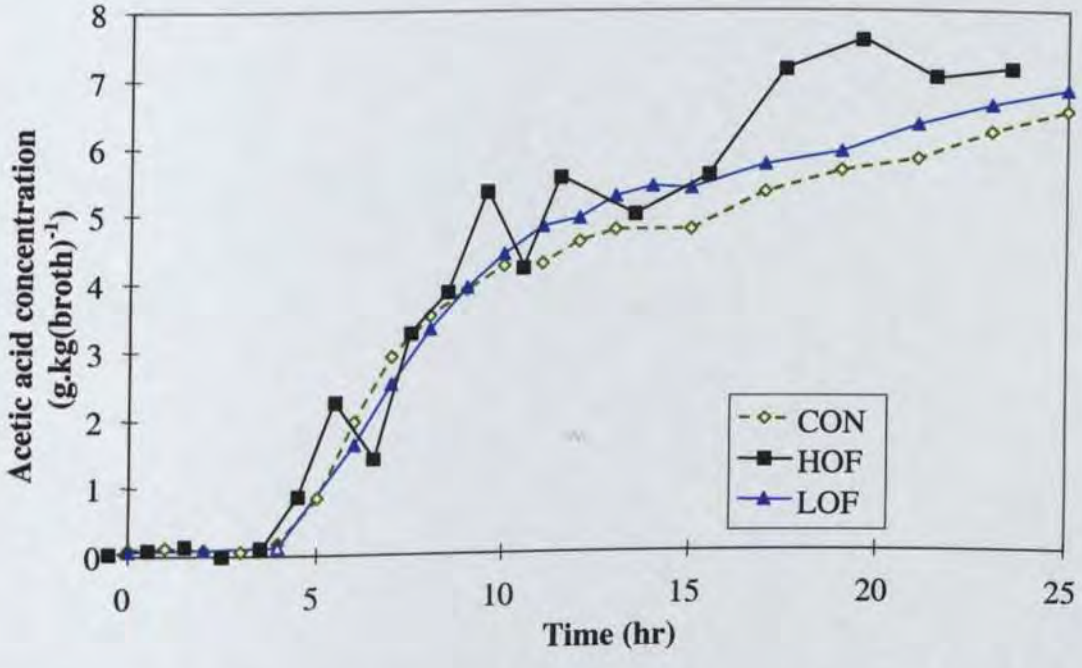

Figure 5.14: Acetic acid broth concentration for the control (CON), low-oxygen (LOF) and high-oxygen (HOF) fermentations.

The acid excretion rates (formic acid, pyruvic acid, lactic acid, acetic acid, succinic acid) show interesting differences between the fermentations. In all cases the LOF and the CON fermentation match well before hr 10. However after the abrupt reduction in oxygen supply at hr 10 the LOF shows some deviations. Firstly, the formic acid production rate is elevated for 2 h, thereafter returning to zero. The lactic acid rate also immediately increases by 30% and

thereafter remains greater than the CON. Likewise succinic acid rate is elevated by 30-50% and follows a similar relative profile. In contrast, both pyruvic acid and acetic acid follow approximately the same profile for both CON and LOF, as shown on a broth-concentration basis.

The HOF lactic acid excretion rate matches the CON quite closely, apart from hrs 5-9 when it is somewhat higher. In contrast the HOF shows only 30% of the CON succinic acid rate and 20% of the formic acid rate. On a concentration basis the formic acid concentration reaches only 30% of the CON concentration, and during hrs 15 to 25 the excreted formic acid is completely reutilised. HOF acetic acid production appears to match the CON very closely throughout most of the fermentation. Agreement in pyruvic acid production is less striking but nevertheless similar levels are achieved.

The acid metabolites can thus be grouped into 3 categories based on their observed behaviour:

- Pyruvic acid and acetic acid, whose excretion appears controlled mostly by the extracellular concentration, since the broth concentration profiles match closely with the CON. Their excretion does not appear influenced by changes in oxygen supply (apart from the initial onset of oxygen limitation).
- Lactic acid, which is linked to changes in oxygen supply (on a $gRCM^{-1}$ basis) and appears independent of broth concentration and cell density.
- Formic acid and succinic acid, whose excretion rate appears independent of broth concentration and inversely linked to the level of oxygenation. Unlike lactic acid however, their excretion does not appear solely linked to oxygen availability on a $gRCM^{-1}$ basis. This raises the question of what other factors are affecting the production rate. The two most likely explanations are:
  - there may be other metabolic differences, for example the elevated level of PHB production in the HOF may be affecting metabolism in a way that reduces formic acid and succinic acid excretion;
  - the microenvironment of the cell may differ in some way between the HOF and the CON fermentation. For example the reduced mixing level of the CON and LOF may have allowed the formation of anaerobic zones, enhancing formic acid and succinic acid production. This is supported by literature work (Xu *et al.* (1999)) which showed that creating locally oxygen-deficient zones enhances formic acid production by *E. coli*. The peak production rate quoted (0.21 $g.gRCM^{-1}h^{-1}$) agrees very closely with the peak initial rates shown in Figure 5.10. No succinate excretion was observed in this study. However the pathway to succinate is enhanced by CO_2, and hence localised zones with low oxygen and high CO_2 concentration could account for the difference in succinate production.

Unlike the CON and LOF, low levels of ethanol excretion were detected in the HOF, as shown in Figure 5.15. Excretion commenced at approximately the same time as lactic acid, at the point where dissolved oxygen content was a minimum, indicating that ethanol production only occurred under nearly anaerobic conditions.

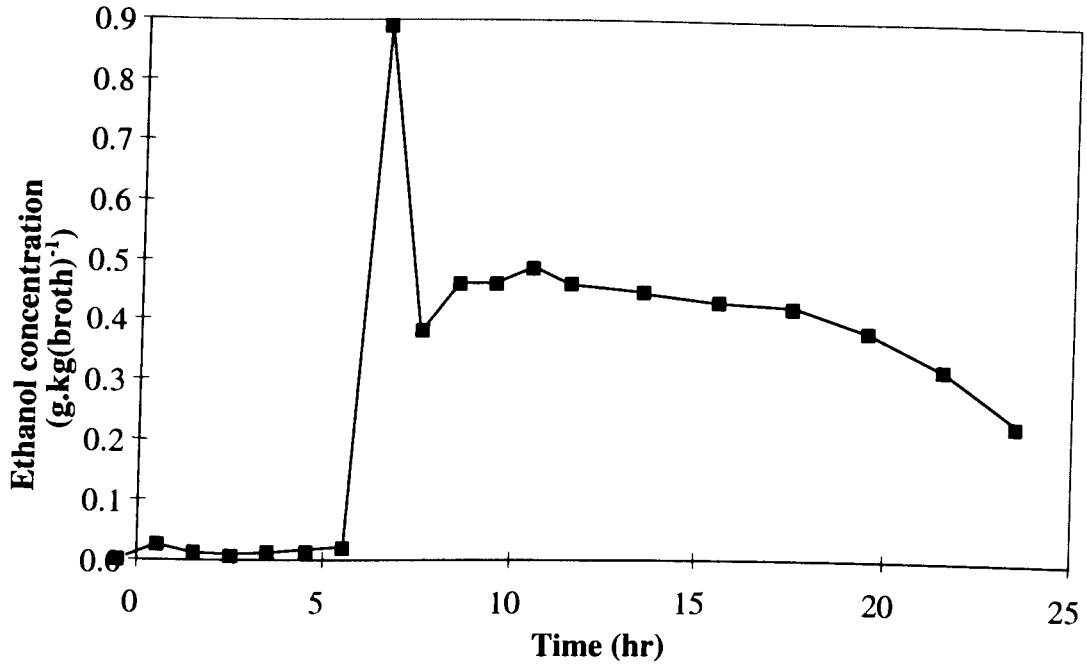

Figure 5.15: Ethanol excretion profile for the high-oxygen fermentation.

5.4.2. Acyl-CoA Profiles

The acyl-CoA profiles are shown in Figure 5.16. The LOF samples prior to hr 7 were lost, however the remaining samples up to hr 10 agree closely with the CON. At the point of oxygen-supply restriction there is a marked drop in acetyl-CoA concentration from 380 to 310 μg.gRCM^{-1}. Thereafter the acetyl-CoA level follows much the same profile as the CON, within experimental error. The HOF shows approximately the same shape as the CON, viz a rise at the onset of oxygen limitation and then a decline. However the initial values appear somewhat lower than the CON and the peak is not as pronounced. Also, the level gradually increases from hr 8 onwards, in contrast to the CON where a steady decline is observed. The reasons for these differences are not apparent, but may be related to improved mixing and/or the reduced excretion of formic acid. Section 5.7 describes these differences in more detail.

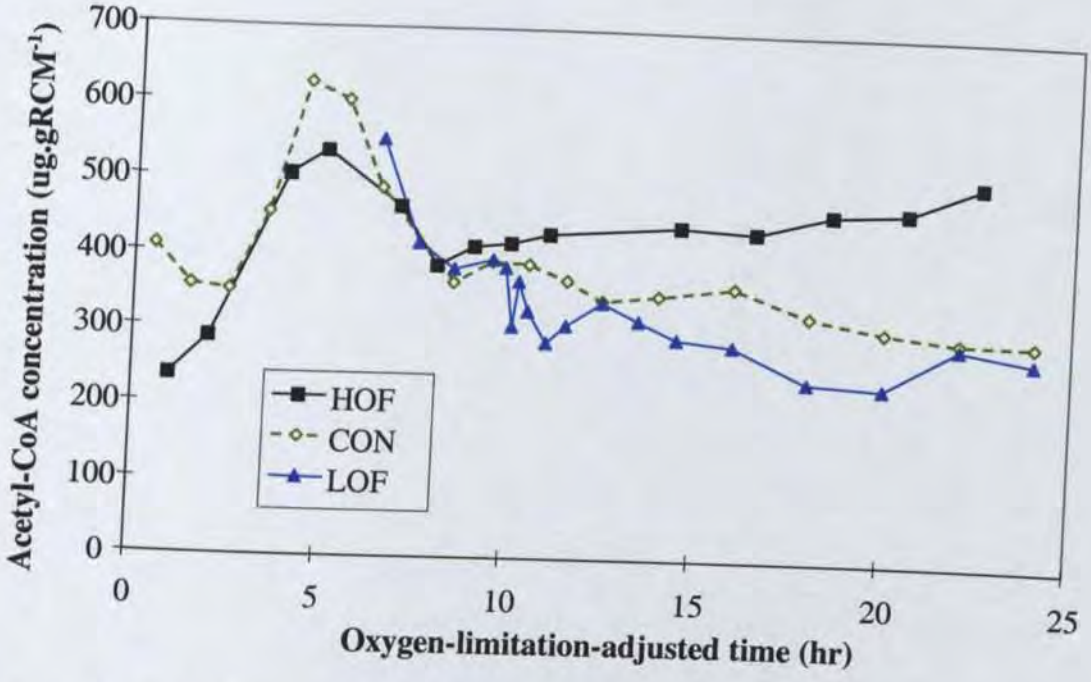

Figure 5.16: Cellular acetyl-CoA content for the control (CON), low-oxygen (LOF) and high-oxygen (HOF) fermentations.

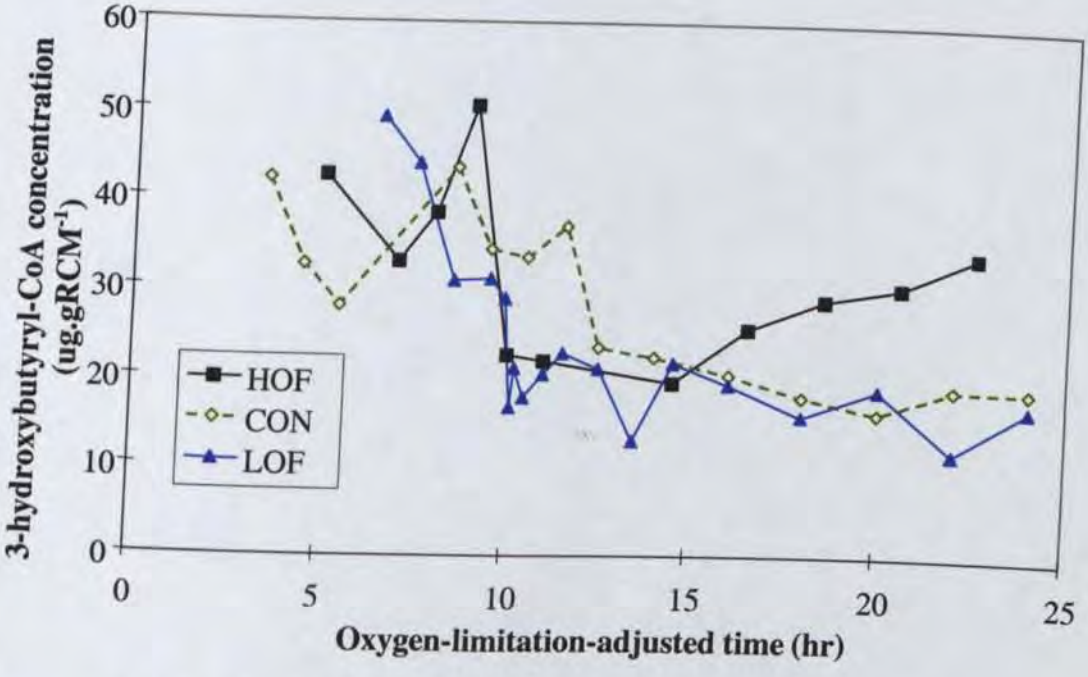

Figure 5.17: Cellular 3-hydroxybutyryl-CoA content for the control (CON), low-oxygen (LOF) and high-oxygen (HOF) fermentations.

As previously mentioned in Section 4.4.3, quantification of 3-hydroxybutyryl-CoA was difficult. The results are shown in Figure 5.17 and suffer from a high level of noise. The LOF shows a large drop immediately after the reduction in oxygen supply at hr 10, which is reflected in the reduced PHB production level. However from hr 13 onwards the LOF and CON have approximately the same 3-hydroxybutyryl-CoA content, despite the 20% lower

PHB production rate of LOF. Therefore the activity of PHA synthase (on a $gRCM^{-1}$ basis) must differ between the LOF and the CON. This is explored further below. The HOF 3-hydroxybutyrl-CoA content is similar to the CON up till hr 15, although the profile is rather noisy. However from hr 15 onwards, the HOF 3-hydroxybutyryl-CoA content gradually rises in a similar manner to acetyl-CoA content (Figure 5.16). The significance of this is not known.

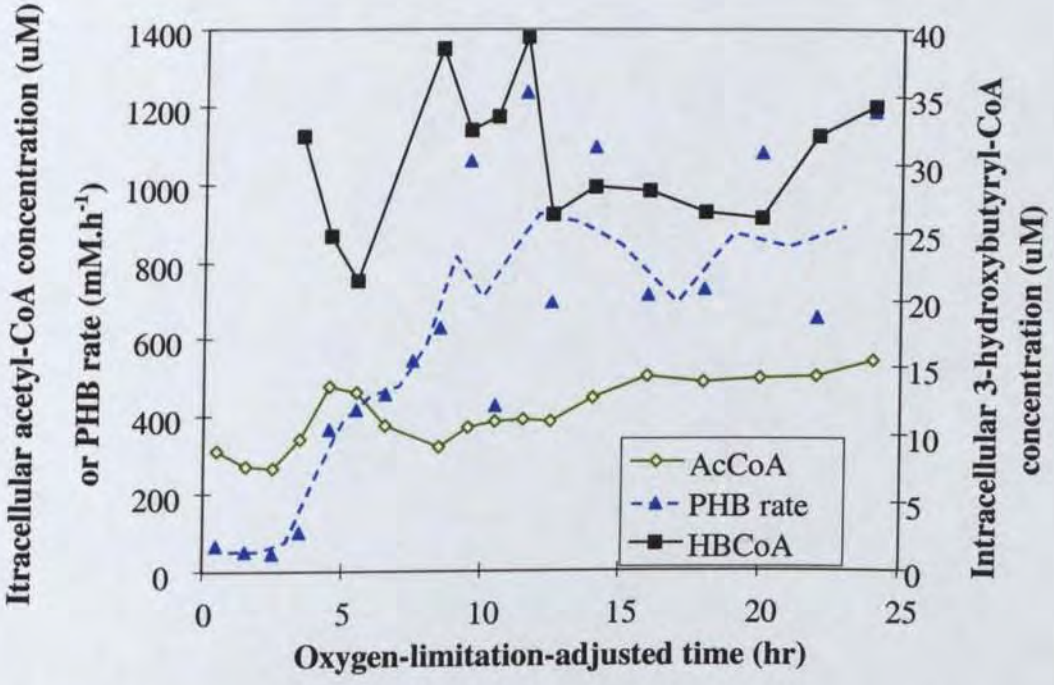

Figure 5.18: Intracellular acetyl-CoA concentration, 3-hydroxybutyryl-CoA concentration and PHB synthesis rate (smoothed) for the control fermentation.

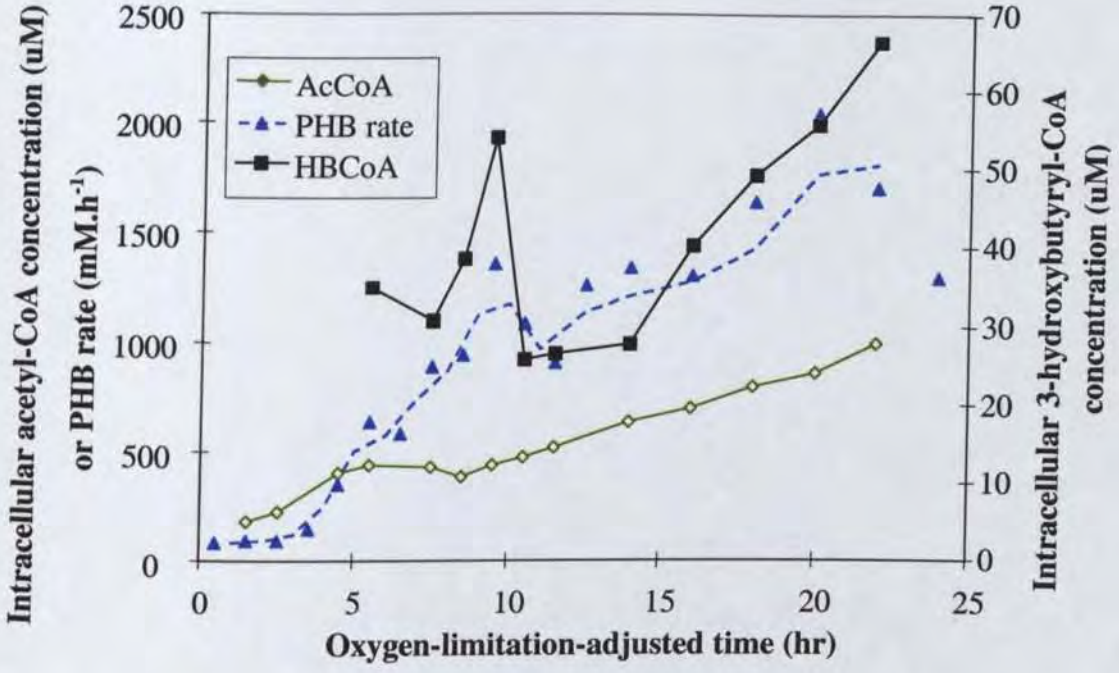

Figure 5.19: Intracellular acetyl-CoA concentration, 3-hydroxybutyryl-CoA concentration and PHB synthesis rate (smoothed) for the high-oxygen fermentation.

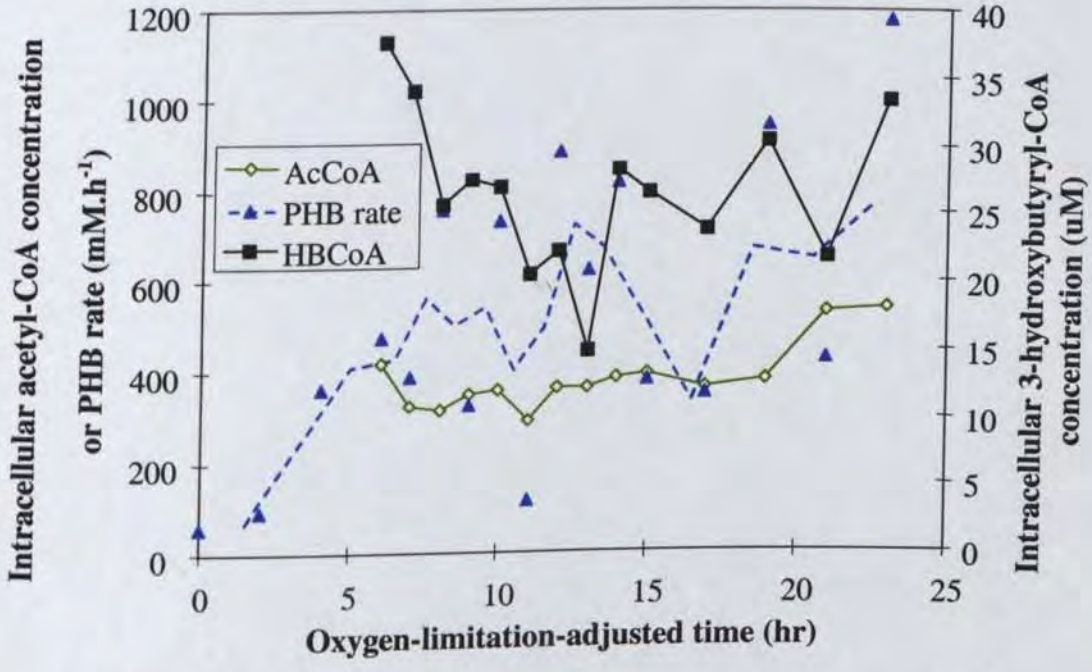

Figure 5.20: Intracellular acetyl-CoA concentration, 3-hydroxybutyryl-CoA concentration and PHB synthesis rate (smoothed) for the low-oxygen fermentation.

Figure 5.18,
Figure 5.19, and Figure 5.20 show the profiles of acyl-CoA intracellular concentrations for each fermentation. The features observed in the CON fermentation (Section 4.6.1) are not as evident for the LOF and HOF. The HOF in particular shows a large rise in intracellular levels, which seems unlikely. The most likely explanation is that one (or more) of the assumptions made when calculating the intracellular volume are no longer adequate. In the case of the HOF it may be due to cell lysis as described in Section 5.5. The results of
Figure 5.19 must therefore be viewed with caution.

The calculated PHA synthase activity curves (intracellular volume basis) are shown in Figure 5.21. The activity of each is quite similar prior to hr 8. The HOF activity appears to rise slightly higher than the CON, and similar to the CON the activity stays approximately steady in the later stages. The LOF also compares well with the CON, and there is no apparent effect of the oxygen reduction at hr 10. In the later stages the activity may be reduced below the CON, but this is not certain because the curves are rather noisy.

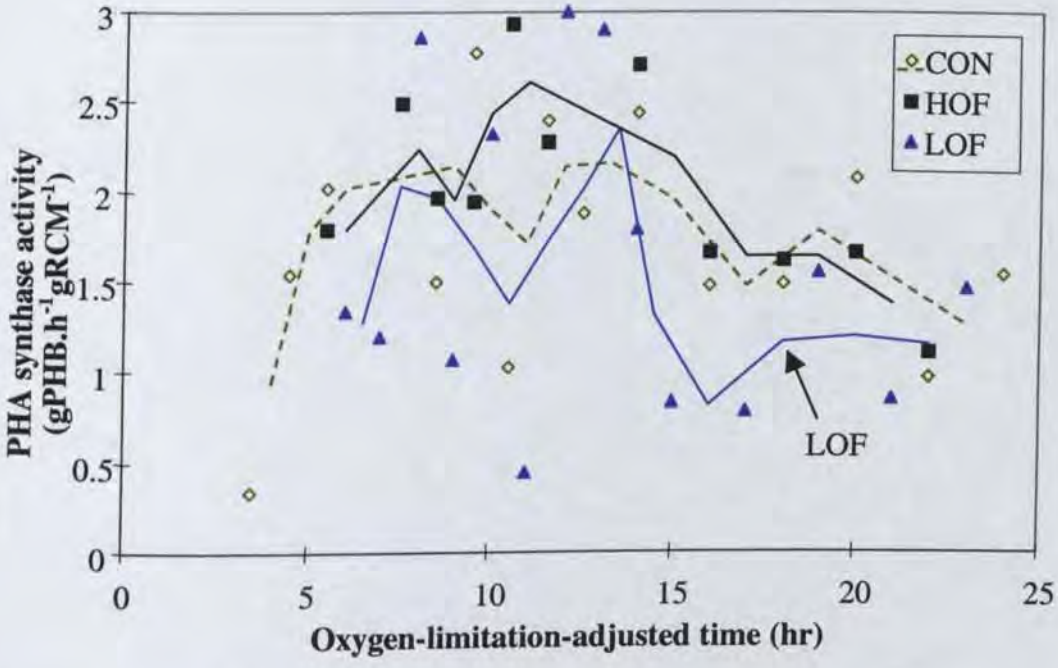

Figure 5.21: Calculated PHA synthase activity (smoothed, intracellular volume basis) for the control, low-oxygen and high-oxygen fermentations.

5.5. Flux Analysis And Discussion

5.5.1. Flux Analysis

The carbon balance for each fermentation is shown in Table 5.2. Overall balance is excellent for the LOF but rather poor for the HOF. No missing carbon was identified by total-organic-carbon analysis of the broth and supernatant. However adjusting the supernatant to pH 2 with sulphuric acid gave considerable precipitate (up to 5% of the dry cell weight), indicating the likely presence of protein. The HOF result is thus probably due to release of cell contents at higher cell densities, undetected by dry-cell-weight measurement or total-organic-carbon analysis. (The accuracy of the total-organic-carbon analysis was suspect for precipitate-containing solutions.) A striking observation from the table is that the yield of RCM is essentially constant. This is very interesting given the range of variation in the other yields, implying that cell production is strongly controlled and that variation in oxygen supply merely redistributes fluxes in order to maintain RCM production at the same level. This is discussed further in Section 5.7.

Table 5.2: Overall carbon balance for the control, low-oxygen and high-oxygen fermentations.

	mol per 100 mol glucose			mol-C per 100 mol-C glucose		
	LOF	CON	HOF	LOF	CON	HOF
carbon dioxide	78	109	139	13	18	23
RCM (mol-C-equivalents)	81	89	81	13	15	14
PHB	23	30	41	15	20	27
acetic acid	35	32	15	12	11	5
formic acid	26	16	0.0	4	3	0
lactic acid	56	33	35	28	16	18
pyruvic acid	13	13	4.2	7	6	2
succinic acid	8.5	6	0.7	6	4	0.5
ethanol	0	0	0.6	0	0	0.2
Overall closure:				98%	93%	89%

The yield of PHB is much improved for the HOF (41% mol(PHB).mol(glc)$^{-1}$ = 0.20 g(PHB).g(glc)$^{-1}$) but is still well below the Chapter 2 high-cell-density-fermentation level (75% mol(PHB).mol(glc)$^{-1}$ = 0.36 g(PHB).g(glc)$^{-1}$). Carbon wastage to acid production was reduced from 40% to 25%, although CO_2 production increased from 18% to 23%. In contrast the LOF wasted nearly 57% to acids. An interesting observation is that the ratio of CO_2 yield to PHB yield is quite similar for all three fermentations, viz 3.39, 3.39 and 3.63 for LOF, HOF and the CON respectively. The significance of this (if any) is not clear.

The redox balance for the LOF was excellent (generally around 97% in the later stages of the fermentation) however the HOF did not balance well (typically 90%).

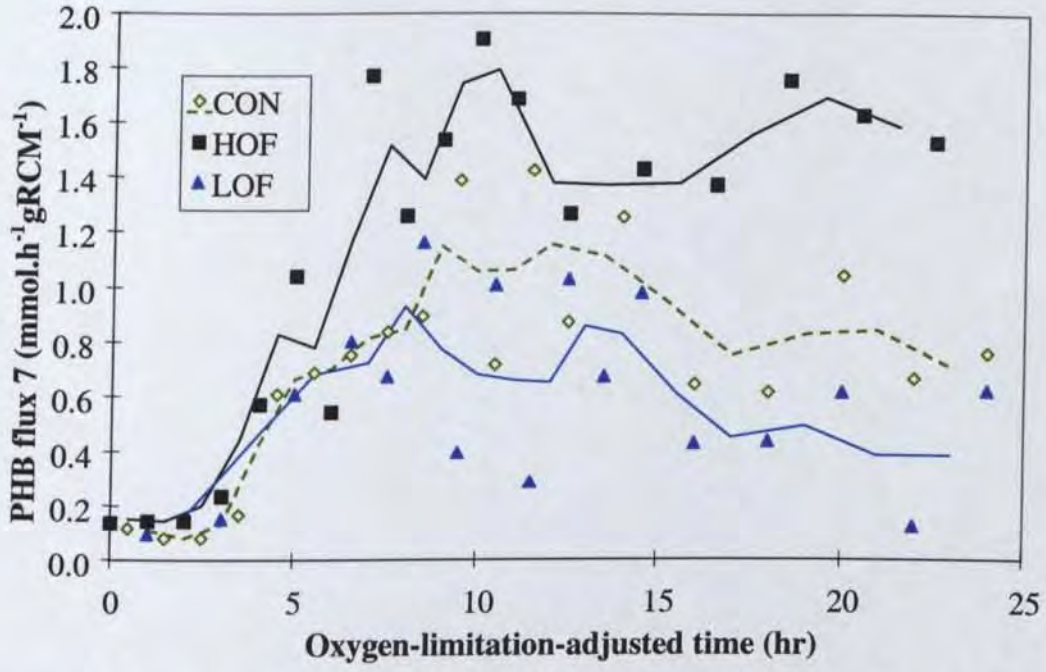

Figure 5.22: PHB production rate (smoothed) on an RCM basis for the control (CON), low-oxygen (LOF) and high-oxygen (HOF) fermentations.

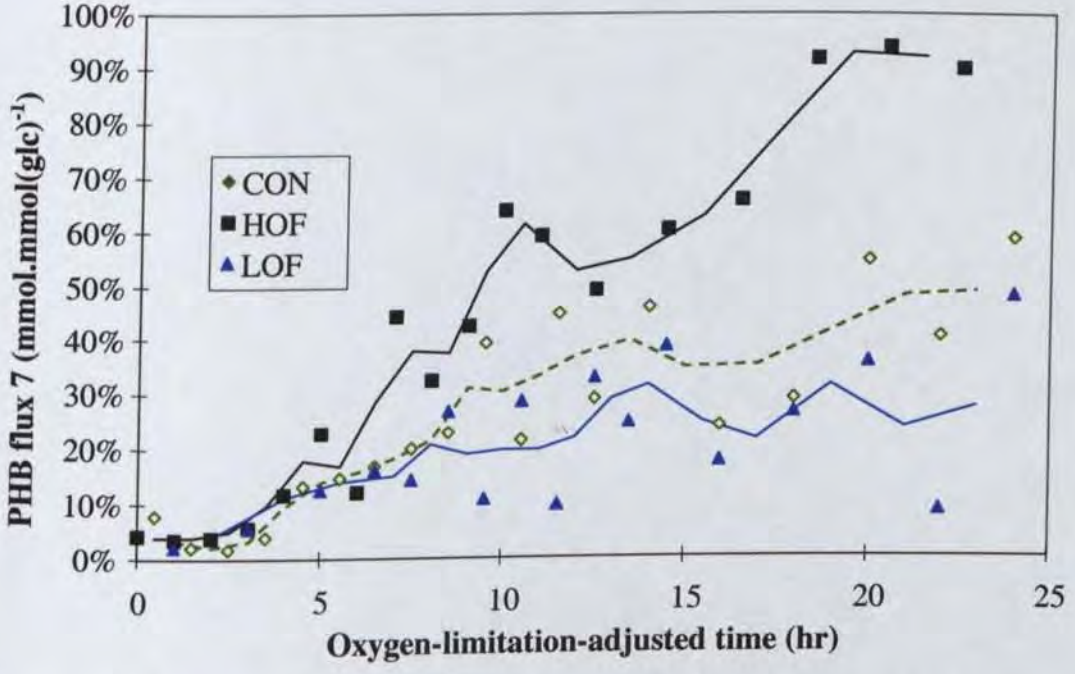

Figure 5.23: PHB production rate (smoothed) on a glucose basis for the control (CON), low-oxygen (LOF) and high-oxygen (HOF) fermentations.

Figure 5.22 shows that the HOF maintains a steady PHB production rate but both the CON and LOF suffer gradual decline.

The ATP production profiles (Figure 5.24) compare well, demonstrating that ATP dissipation is very similar for all three fermentations before hr 10. From hr 10 onwards, the LOF shows

somewhat reduced dissipation, which indicates that the reduction in oxygen availability resulted in lowered ATP supply.

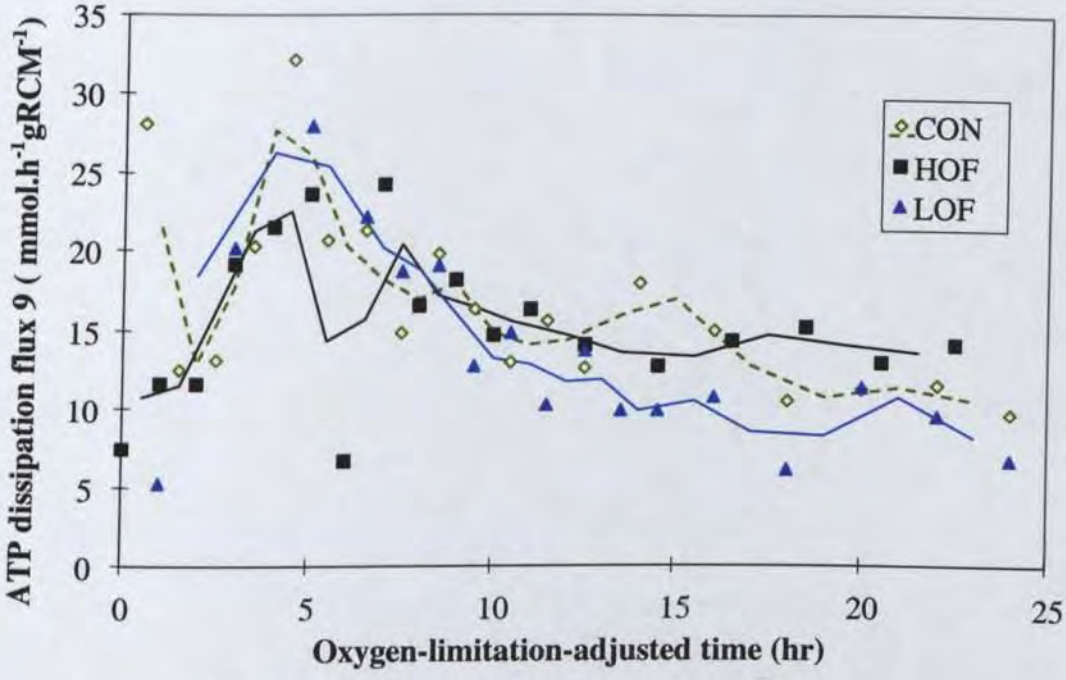

Figure 5.24: ATP production (smoothed) on an RCM basis for the control (CON), low-oxygen (LOF) and high-oxygen (HOF) fermentations.

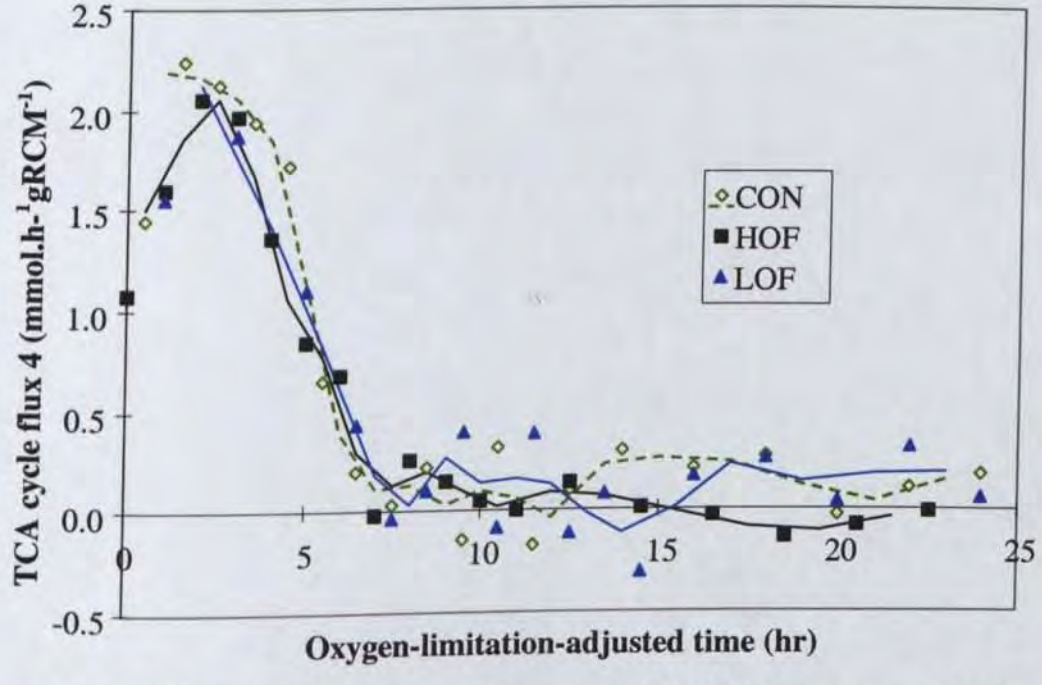

Figure 5.25: TCA cycle flux (smoothed) for control (CON), low-oxygen (LOF) and high-oxygen (HOF) fermentations.

Figure 5.25 shows the TCA cycle fluxes. It appears that in all three fermentations the TCA cycle flux rises to a peak over the first 3 h. This is anomalous because the cells are exhibiting

exponential growth and dissolved oxygen is well above limiting values. Systematic error is a possibility. A second observation is that all three fermentations show nearly identical profiles up to hr 12, and in particular the LOF oxygen limitation at hr 10 has no discernible effect. This confirms the Chapter 4 observation that the TCA cycle shuts down completely once oxygen limitation commences.

From hrs 12-15 onwards, both the LOF and CON appear to regain a low level of TCA cycle activity. In contrast the HOF TCA flux remains at zero, within experimental error.

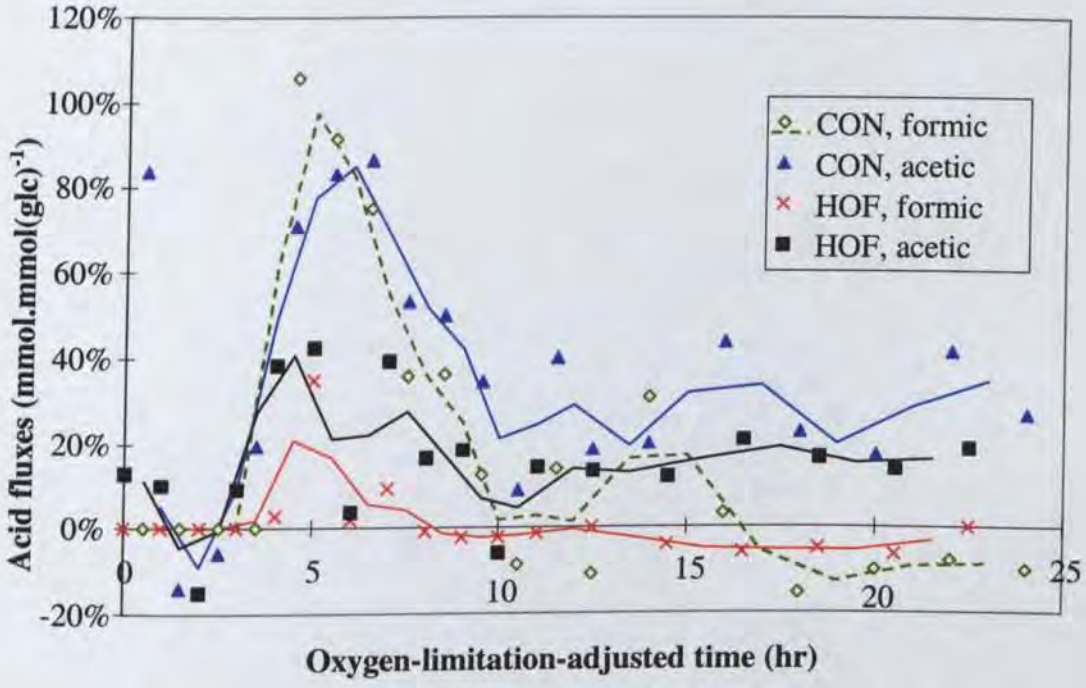

Figure 5.26: Fluxes (smoothed) to formic acid and acetic acid for the control (CON) and high-oxygen (HOF) fermentations.

Figure 5.26 shows that the HOF excretion of formic acid and acetic acid is somewhat different to the CON (the LOF profiles match the CON closely so they are not shown). The profiles have the same shape, however when acetic acid production commences formic acid production does not increase sufficiently to satisfy the extra flux to acetyl-CoA. This is also shown by the pyruvate-dehydrogenase flux (flux 2), which rises steadily from 50% of glucose flux at hr 0 to 200% at hr 23. In contrast the CON fermentation flux showed a dip from 50% to 30% over hrs 3 to 5. This leads to an absence of a dip in CO_2 production for the HOF (see Figure 5.7 and Figure 5.6) because the decline in TCA CO_2 is compensated for by the increased CO_2 from pyruvate dehydrogenase.

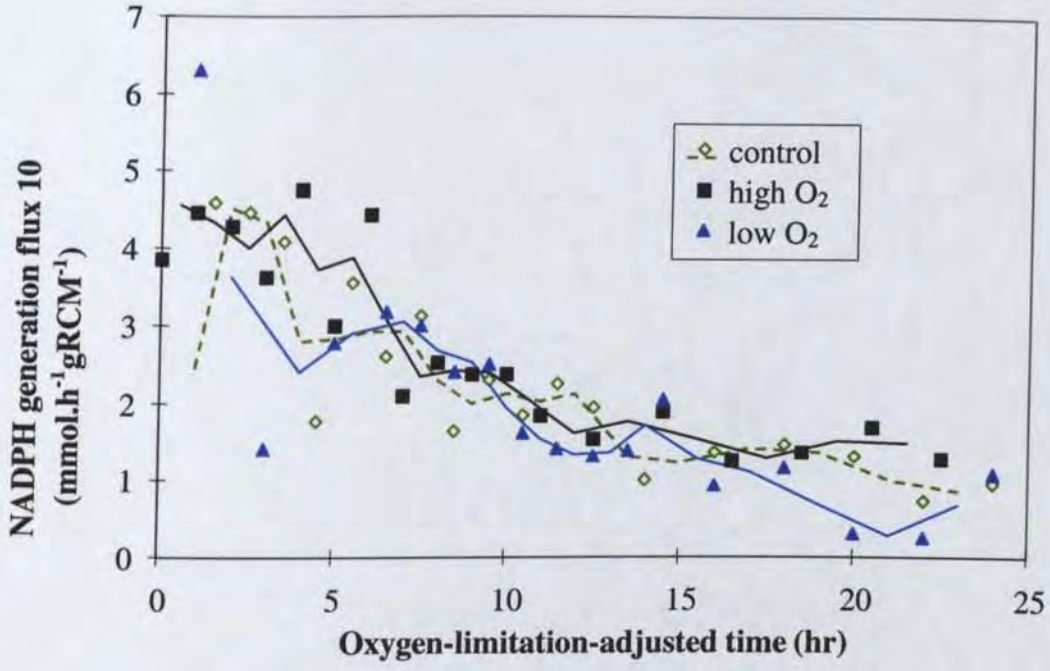

Figure 5.27: Lumped NADPH generation flux (smoothed) for control, low-oxygen and high-oxygen fermentations.

The NADPH generation fluxes match very well for all three fermentations (see Figure 5.27). The HOF lacks the brief dip exhibited by the CON and LOF at hrs 3-5, however for the most part the profiles are identical. The LOF does appear to have a lower NADPH generation from hr 18 onwards. These observations are significant because they imply a constant NADPH demand/supply regardless of the level of oxygenation or PHB production. For the first 6-8 hrs most of this is used for RCM production, and thereafter it is used almost entirely for PHB production. The constancy of supply suggests that NADPH may be a major limiting factor in PHB production, at odds with the conclusions of Chapter 4.

5.6. Comparison with the High-Cell-Density Fermentation.

Several difficulties arise when comparing the low-cell-density fermentations with the Chapter 2 high-cell-density fermentation (HCDF). In particular:

- the medium composition is somewhat different;
- the method of glucose feeding is different;
- the onset of oxygen limitation is more gradual;
- volume-dilution effects become highly significant;

Nevertheless the comparisons yield useful information. Figure 5.28 and Figure 5.29 show the specific synthesis rate of PHB and RCM for the CON, HOF, and HCDF. The timescale for the HCDF has been adjusted so that the onset of PHB synthesis is aligned for all three fermentations.

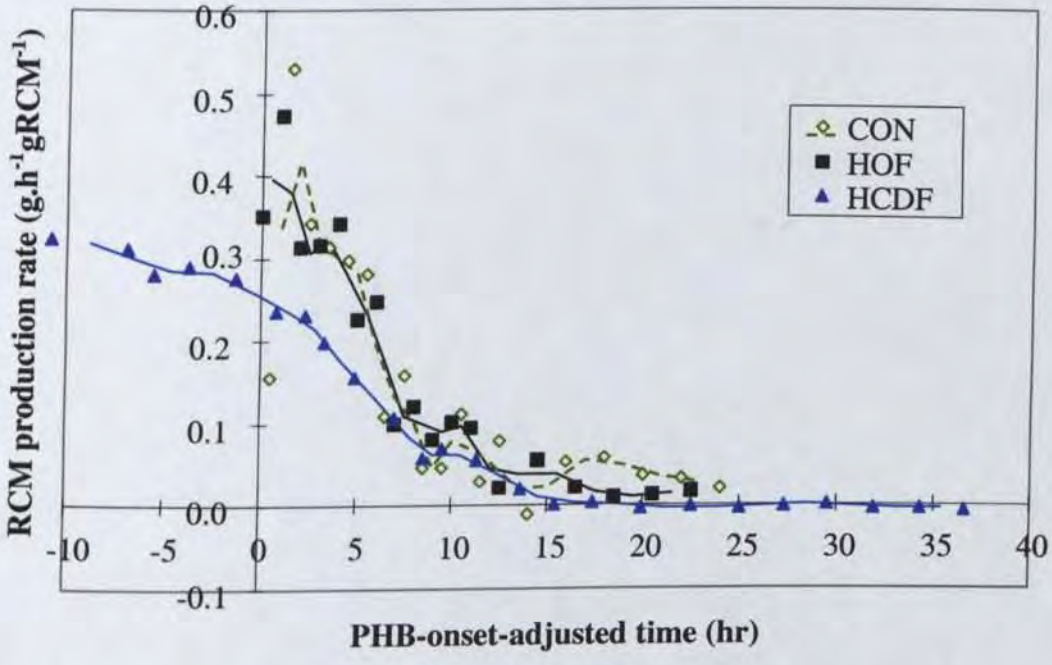

Figure 5.28: RCM production rate (smoothed, on a gRCM basis) for the control, high-oxygen, and high-cell-density fermentations.

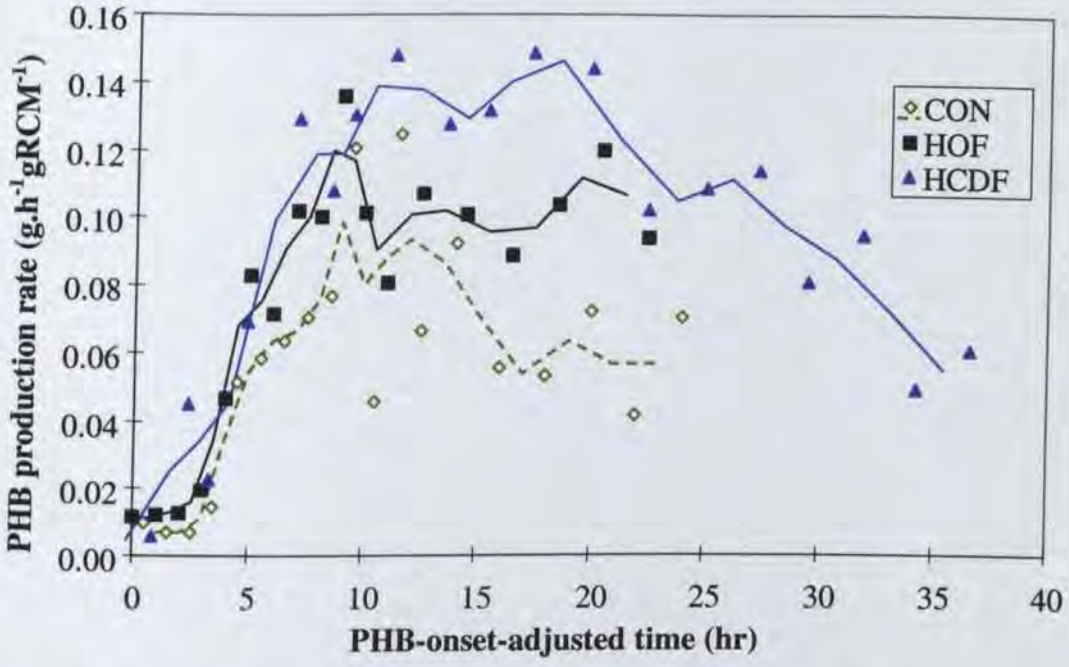

Figure 5.29: PHB production rate (smoothed, on a gRCM basis) for the control, high-oxygen, and high-cell-density fermentations.

Several interesting observations can be made. Firstly the shape of the HCDF RCM profile is rather different than for the HOF and CON. The initial rate is similar (0.3 $g.gRCM^{-1}h^{-1}$) however the decline is far more gradual. In all three cases, the RCM rate is approximately equal at hr 10. Each curve also exhibits a change in slope at hr 9-10, coinciding with a plateau in PHB production rate. The HCDF PHB production rate rises at approximately the same speed as the other fermentations, however it continues to rise for longer and hence reaches a plateau 40% higher than the HOF. Both the HOF and HCDF show a stable PHB production rate for at least 10 h, however the HOF does not continue for long enough to determine whether its PHB rate follows the HCDF trend.

It is not apparent what caused the decline in RCM production and onset of PHB production in the HCDF. Figure 5.30 shows that HCDF RCM production is slowly declining over hr -10 to hr 3. This slow decline may be due to the very high cell density achieved (65 $g.l^{-1}$ at hr 3), or alternatively a slow onset of oxygen limitation as described below. At hr 3 a distinct metabolic change is observed: PHB production commences in earnest and the RCM production rate begins to decline more rapidly. In the low-cell-density fermentations this was clearly caused by oxygen limitation, however for the HCDF (and also the high-cell-density fermentations described in Table 5.1) there was ample oxygen available. Nutrient feeding commenced at hr -5 and is hence not a likely cause. There are several possible explanations that remain:

- Another nutrient became limiting. The levels of phosphate, sulphate and ammonium were adequate however some of the trace minerals (for example iron) may have been depleted.
- Oxygen limitation was occurring but was not detected by the oxygen probe. The 90% response time of the probe is in the order of a minute, hence rapid transients are not detected. Also, the location measured may not reflect the true average concentration in the fermenter. At high cell densities it is likely that the level of mixing was insufficient to prevent formation of anaerobic zones. Evidence for this includes:

- formic acid excretion occurs at hr -5 (Figure 5.31) despite the apparently high levels of dissolved oxygen;
- the HCDF oxygen consumption rate was not measured but a redox balance allows an estimate. The profile shows a steady level of 8-9 mmol.gRCM^{-1}h^{-1} until hr -5, then a decline to 6 mmol.gRCM^{-1}h^{-1} by hr 3.

These observations are consistent with the gradual onset of oxygen limitation from hr -5 to 0, which may have triggered a cascade of events similar to those described in Section 5.7, for example an increased intracellular NADH level or the induction of global regulation systems dependent on oxygen tension. Gradual oxygen limitation of this kind may also help explain the observed slow decline in RCM production.

- The rate of RCM production may have declined to a critical level (0.24 g.gRCM^{-1}h^{-1}), below which positive feedback ensured a switch from RCM production to PHB production. (As described in Section 5.7, this might potentially occur as a result of a rise in plasmid copy number at low growth rates.).

Further experiments are required to discover the correct explanation.

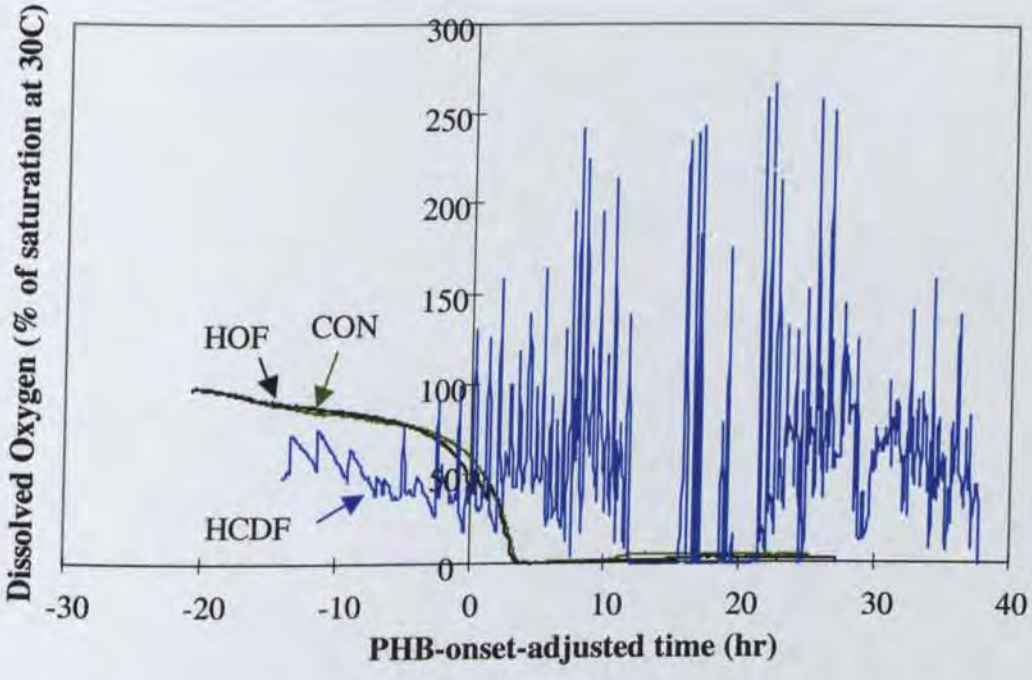

Figure 5.30: Dissolved-oxygen profiles for the control (CON), high-oxygen (HOF) and high-cell-density (HCDF) fermentations.

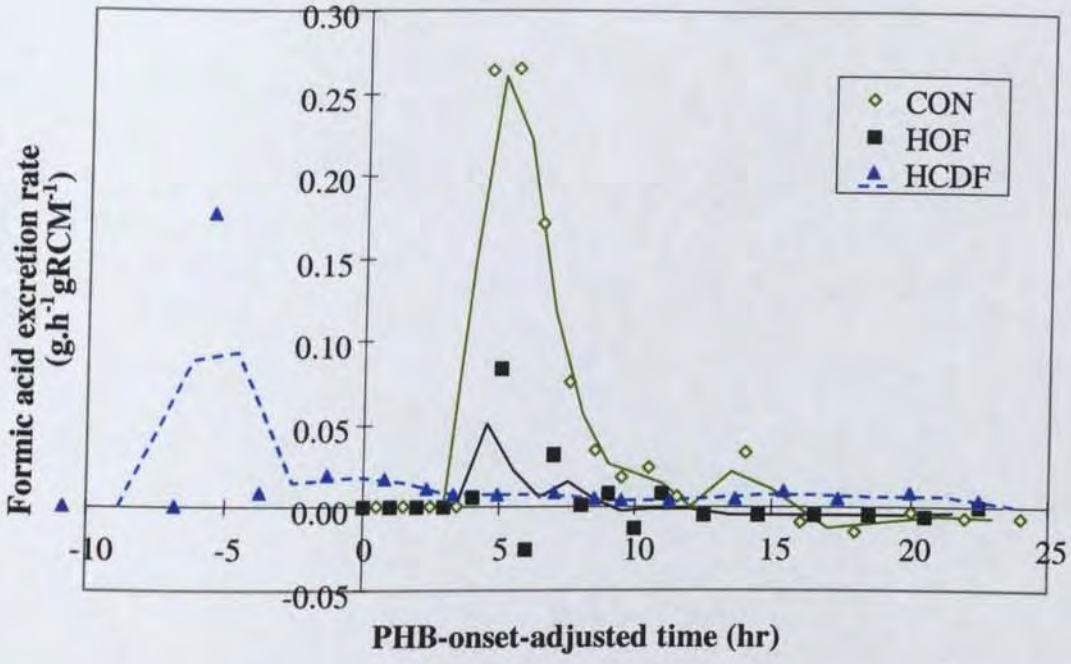

Figure 5.31: Formic acid production for the control, high-oxygen and high-cell-density fermentations.

The TCA flux (Figure 5.32) shows a completely different profile for the HCDF vs the low cell densities. In particular the initial flux is nearly double, which is almost certainly incorrect. It seems likely that a systematic error in the HCDF is responsible, probably the CO_2 production rate, since

1. the TCA cycle flux is highly sensitive to the measured CO_2 production rate;
2. as described in Chapter 2 there were several difficulties with the CO_2 rate measurements.

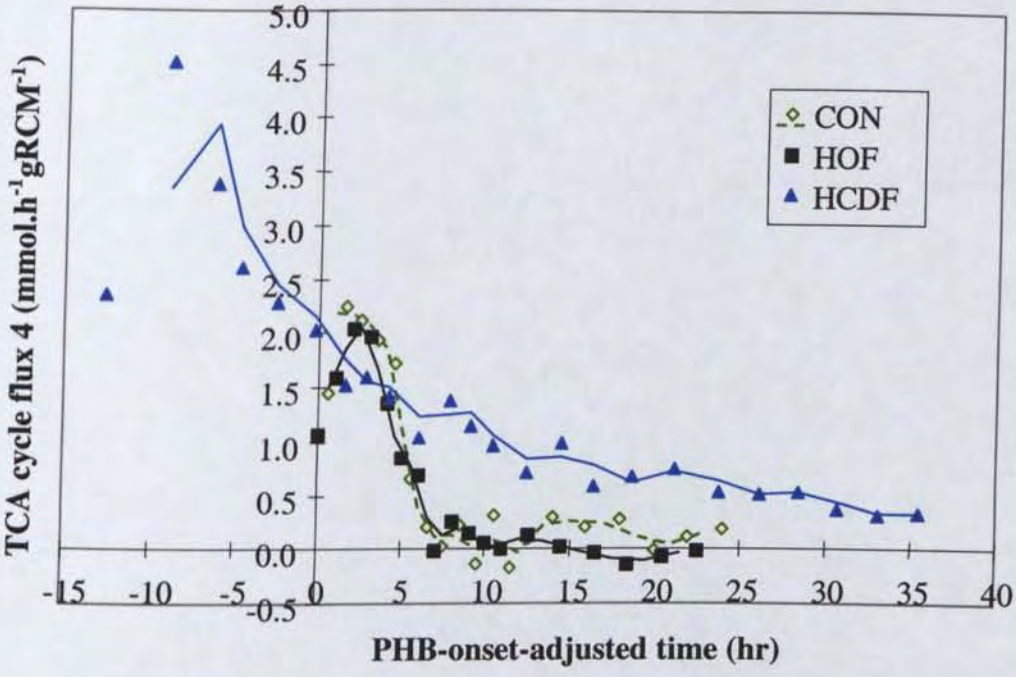

Figure 5.32: TCA cycle flux for the control, high-oxygen and high-cell-density fermentations.

5.7. Further Discussion.

5.7.1. Fermentation Time-course

The sequence of events in the LOF and HOF bears strong resemblance to that of the CON, as described in Chapter 4. Each fermentation shows four distinct stages.

Phase 1 - exponential growth , hr 0-3.5.

In each case the growth is unrestricted until the onset of oxygen limitation.

Phase 2, onset of oxygen limitation, hr 3.5 - 6.

The onset of oxygen limitation initiates a cascade of events that is similar for each fermentation. A rapid (six-fold) rise in PHB production is observed, TCA cycle flux drops to zero, and excretion of formic, pyruvic and acetic acids commences immediately. Lactic and succinic acid excretion commences after an hour, along with a surge of ethanol for the HOF.

The likely explanation for these events is unchanged from Chapter 4. A rise in NADH/NAD shuts down the TCA cycle which causes the acetyl-CoA/CoA ratio to rise. This in turn causes the abrupt increase in PHB production rate, which is the same for all three fermentations. Pyruvate-formate-lyase flux (3) is activated by the rise in NADH, however the HOF shows much less formic acid production than the others. The most likely explanation for this is that the HOF mixing is better, preventing the formation of local anaerobic zones and hence reducing formic acid & succinic acid excretion. There is a rise in intracellular pyruvate despite the increased flux to acetyl-CoA, possibly caused by diversion of RCM flux to glycolysis. This increased pyruvate level causes excretion of pyruvate. The elevated levels of pyruvate and NADH/NAD enhance lactic acid production.

Phase 3, gradual metabolic shift phase, hr 6 - 10.

In each case the same basic events occur, viz:

- cessation of TCA cycle flux and formic acid flux;
- return of acetic acid flux to a low level, due to enhanced PHB synthesis and declining formic acid synthesis;
- lactic-, pyruvic-, and succinic- acid production reach their maxima (gRCM basis);
- RCM production reaches a low basal level;
- achievement of maximum PHB flux (gRCM basis), due to increasing PHA synthase activity.

However there are some differences, in particular the HOF plateau PHB production rate is somewhat higher than the others. The cause of this is not clear, but may be related to reduced acid excretion and improved mixing.

Phase 4, slow decline, hr 10- 25

The LOF diverges from the CON during this phase, due to the reduction in oxygen supply at hr 10. An immediate drop in PHB production is evident, accompanied by a step increase in lactic acid production. The increase is expected because the reduced oxygen availability leads to increased NADH levels, in turn enhancing lactate dehydrogenase (flux 4) and inhibiting pyruvate dehydrogenase (flux 2). This reduces the acetyl-CoA/CoA level, and causes a drop in PHB production. However the data are too noisy to be certain of this explanation.

The intracellular concentration of pyruvate probably declines slightly, if at all, since the observed pyruvate excretion flux does not change markedly. Succinic acid production undergoes a step increase, but the reason for this is not certain because control of the succinic acid pathway is not well understood. Formic acid production recommences for a short time, however another unknown factor soon returns the flux to zero. Acetic acid production is almost completely unaffected, which does not correspond with the suggested increase in NADH level. The data in Section 5.4.1 suggest that acetic acid production is a function solely of the medium concentration. This is difficult to explain in terms of the metabolism kinetics, and further experiments would be necessary to verify it.

Apart from the LOF changes caused by the reduction in oxygen supply, the profiles of each fermentation are quite similar during phase 4. The acetic, pyruvic and succinic acid fluxes stabilise (on a glucose basis) and the lactic acid flux steadily declines. The overall glucose flux declines, evidence of a general metabolic slowdown. All fermentations show the same abrupt rise in dissolved oxygen near hr 10, probably due to a change in the enzymes of the respiratory chain, as described in Section 2.3.

Overall features

Three of the most striking observations when comparing the fermentations are:

- glucose consumption on a gRCM basis is the same for all three fermentations until hr 15. This indicates that oxygen limitation does not have an immediate effect on the uptake of glucose. From hr 15 onwards the LOF shows reduced glucose consumption, indicating that a longer term effect of oxygen deprivation (for example reduced enzyme levels) also occurs;
- RCM production on a gRCM basis is essentially identical for all three fermentations until hr 15. Thereafter the HOF appears lower than the CON, which may reflect cell lysis;
- NADPH generation flux on a gRCM basis is closely matched between all three fermentations.

These observations suggest that the cell metabolism is strongly regulated and is essentially independent of PHB production.

The fermentations performed have tested two aspects of oxygen usage:

1. the effect of using a different oxygen supply throughout the entire fermentation (HOF);
2. the effect of changing the oxygen supply midway through the fermentation (LOF).

The HOF demonstrates that to a first approximation, increasing the oxygen supply will proportionally increase the concentration of residual cell mass and PHB, i.e. the production rates are almost independent of the cell density. However other factors are significant, as shown by the reduced level of formic acid excretion. It is likely that the well-mixedness of the fermentation is also important, and improves PHB production. This has dire implications for production in large-scale fermenters where achieving good mixing is often difficult. In addition it appears that acetic- and pyruvic- acid production is linked to extracellular concentration, which gives higher PHB yields (glucose basis) for the HOF since the per-gRCM excretion of these acids is lower. The HOF also achieved a higher PHB synthesis rate during phase 3. This may also be linked to the rapid excretion of formic acid by the LOF and CON during phase 2 and 3.

The LOF shows that, contrary to what may have been expected, reducing oxygen supply markedly inhibits PHB production. This occurs because the cell attempts to maximise ATP production while using increased lactic acid excretion to eliminate the excess NADH,

diverting flux away from the acetyl-CoA pool and hence impairing PHB synthesis. There may be a rise in NADPH/NADP due to coupling by the transhydrogenase, but as Section 4.7 shows its effect is likely to be small and cannot compensate for the reduced acetyl-CoA/CoA ratio. The HOF indicates that if a fourth fermentation had been conducted with a constant oxygen supply equal to the final LOF level (i.e. k_La 0.79 min^{-1}), the profiles on a gRCM basis would have approximately matched the CON profile. Hence the LOF cellular metabolism is effectively elevated relative to this "fourth fermentation", and mimics the effect of increasing PHB production at fixed oxygen supply. The drop in LOF oxygen supply was 29% whereas the PHB production rate declined only 20%, suggesting that increasing the level of cellular enzymes (e.g. by addition of complex nutrients) without increasing oxygen supply may achieve an increase in PHB production rate. However the lactic acid production rate is also likely to increase dramatically, reducing PHB yield on glucose.

5.7.2. Stoichiometric Optimisation of the Network

In a similar fashion to the work of Varma *et al.* (1993a), the metabolic network can be analysed by linear optimisation to gain an understanding of what metabolic rearrangements are possible.

Minimum possible oxygen supply

A simple redox balance in the absence of RCM production shows that to avoid excretion of acids (in the absence of formate-hydrogen-lyase activity) the oxygen supply must be at least

$$X \geq 1.5P \tag{5.1}$$

where

X = oxygen consumption rate (mmol.gRCM^{-1}h^{-1})
P = PHB production rate (mmol.gRCM^{-1}h^{-1})

There are only two ways in which oxygen supply can be reduced below this level:

1. permitting excretion of succinic acid (and thereby causing a large drop in ATP production); or
2. permitting simultaneous excretion of formic acid and ethanol.

Both of these occur at the expense of PHB yield. For the high-cell-density fermentations the plateau PHB production rate is near 0.12 gPHB.gRCM^{-1}h^{-1} (1.4 mmol(PHB).gRCM^{-1}h^{-1}), hence the stoichiometric-minimum oxygen rate required to avoid acid excretion is 2.1 mmol.gRCM^{-1}h^{-1}. Given an RCM level near 80 g.l(broth)$^{-1}$ at this point, 170 mmol(O_2).l(broth)$^{-1}$h^{-1} (equivalent to 20 l(air).l(broth)$^{-1}$h^{-1} of STP air) is required. Obviously, to achieve satisfactory mass transfer the actual rate would be several times higher than this, in the order of 1 l(STP air).l(broth)$^{-1}$min^{-1}. This is somewhat less that the supply rate used in the Chapter 2 high-cell-density fermentation, viz 2.5 l(STP air).l(broth)$^{-1}$min^{-1} (approximately).

The minimum necessary oxygen partial pressure in the inlet gas can also be calculated, as follows:

$$N_{O2} = k_L a.\left(\frac{P_{O2,inlet}}{H_{O2}} - C_{O2,broth}\right) \tag{5.2}$$

where

N_{O2} = mass transfer rate of oxygen (mmol.l(broth)$^{-1}$h^{-1})

$k_L a$ = volumetric mass transfer coefficient of oxygen (h^{-1})

$P_{O2,inlet}$ = partial pressure of oxygen in the gas phase (kPa)

$C_{O2,broth}$ = molar concentration of oxygen in the broth (mmol.l(broth)$^{-1}$)

H_{O2} = Henry's law constant for oxygen (kPa.l(broth).mmol^{-1})

H_{O2} can be calculated at the bioreactor temperature using Equation 5.3, yielding a value of 86 kPa.l(broth).mmol^{-1} at 30 °C (Royce and Thornhill (1991)).

$$H_{O2} = \exp\left(12.74 - \frac{133.4}{T - 206.7}\right) \Big/ 1000 \tag{5.3}$$

where

T = temperature (K)

If we assume a value for $k_L a$ of 1.0 -5.0 min^{-1} (typical for large fermenters, according to Doran (1997); Atkinson and Mavituna (1987)) and further assume that broth oxygen concentration is nearly zero, Equation 5.2 yields

$P_{O2,inlet} \geq 48$ - 240 kPa

This minimum-value-under-ideal-conditions is extremely high and it is difficult to see how it may be achieved in practice without very good mixing, oxygen-enriched air, and/or pressurised operation.

ATP production stoichiometry

The ATP produced under the conditions of Equation 5.1 is

$$ATP = 2P + 4X \tag{5.4}$$

and if this is insufficient then the most efficient way to gain extra ATP (at fixed oxygen supply) is via simultaneous production of acetic acid, ethanol and formic acid in a 1:1:2 molar ratio. The extra ATP gained in this way is rather small. If we assume a minimum oxygen supply (Equation 5.1) then the total ATP at constant PHB production level is

$$ATP = 8P + 3G \tag{5.5}$$

where

G = extra glucose imported and converted to acetic acid, ethanol and formic acid (mmol.gRCM^{-1}h^{-1})

which gives a dimensionless sensitivity of 2.67, i.e. for every 1% increase in ATP production the PHB yield on glucose is reduced by 2.67%.

Maximising ATP yield

The first question to be investigated is whether ATP yield can be increased without compromising PHB production. Or conversely, whether the cells are already regulating themselves in such a way as to generate the maximum possible ATP.

Taking a typical sample from the HOF (hr 12.5) we observe the fluxes shown in column **1** of Table 5.3. If we hold constant the RCM production, glucose uptake rate, oxygen consumption and PHB production, linear optimisation for maximum ATP produces the flux distribution shown in column **2**. The existing flux to lactic acid is re-routed to formic and acetic acid, producing a 13% gain in ATP production. This flux pattern is similar to what was observed for the HOF during the first hour of oxygen limitation (Figure 5.10, hr 5). However the experimental data show that extended formic acid production appears to be prevented by kinetic or regulatory factors. Hence, if we add the constraint that formic acid production is zero and re-optimise the network, we obtain the column **3** flux distribution. Interestingly the distribution is quite similar to the base-case distribution, with only a 2.5% possible increase in ATP production. This small gain is achieved by avoiding pyruvate excretion, and also by reducing TCA flux to zero. Hence it appears that the cell is already regulated for nearly maximum ATP production at hr 12.5, given that formic acid production is not possible. Repeating the analysis with several other datapoints yields qualitatively similar results.

Table 5.3: High-oxygen-fermentation sample at hr 12.5 optimised for maximum ATP production.

rates ($mmol.gRCM^{-1}h^{-1}$)	**1** base case	**2** Unrestricted	**3** No formic acid
RCM production	0.18 (fixed)		
oxygen usage	2.76 (fixed)		
glucose uptake	2.58 (fixed)		
PHB production	1.27 (fixed)		
formic acid production	0.00	2.95	-
acetic acid production	0.35	2.25	0.78
pyruvic acid production	0.06	-	-
lactic acid production	1.69	-	(1.47)*
succinic acid production	0.01	-	-
ethanol production	0.01	-	(1.47)*
ATP dissipation	14.14	15.98	14.5
PHB yield on glucose (mol/mol)	49% (fixed)		

* Under these conditions lactic acid production and ethanol production are equivalent, the total excretion of lactic acid plus ethanol is 1.47 $mmol.gRCM^{-1}h^{-1}$.

Maximising PHB yield

Another question of interest is whether PHB yield on glucose can be improved, and what must be sacrificed in terms of ATP production to do so. As before, the HOF hr 12.5 sample is used

as the base case. If we fix RCM, oxygen, and glucose then Column **2** in Table 5.4 shows that the PHB yield can theoretically be increased from 49% to 93%, by diverting flux through pyruvate-formate-lyase instead of pyruvate dehydrogenase. The cost is an 8% reduction in ATP production. Also, excretion of formic acid would occur, unless formate-hydrogen-lyase could be employed to convert it to hydrogen and CO_2. If the system is additionally constrained to avoid formic acid excretion, the resultant flux distribution is shown as column **3**. The gain in yield is reduced, and succinic acid production is employed to eliminate surplus redox.

An alternative way to improve PHB yield is to hold PHB production fixed but reduce the uptake of glucose. This has the advantage that it may be more feasible than trying to increase (e.g.) PHB enzyme concentration. Column **4** shows that an efficiency of 80% is achievable in this manner, however ATP production is reduced by 16%. In the case of column **4**, there is actually excess oxygen and the TCA cycle is used to generate extra NADH.

The final question is to ask what can be achieved if we alter both glucose uptake and PHB production. If formic acid production is permitted, Column **5** shows that ideally large changes in glucose uptake, PHB production and production of formic acid are desirable. This seems infeasible. However the 'no formic acid' alternative is far more reasonable. 91% yield can be achieved by increasing PHB production and also *reducing* glucose uptake by 24%. The price is a 14% reduction in ATP production.

These two sets of results show that glucose uptake is too rapid for best PHB yields, given a rate of PHB production constrained by kinetics. The excessive glucose uptake produces excess NADH which is eliminated via lactic acid. This flux distribution probably arises to maximise ATP production, given that formic acid production is impossible for kinetic or regulatory reasons. It is not clear whether this ATP is required for maintenance or whether it is simply being spilled in futile cycles. In addition the ATP gains achieved in this way are rather small, since about 75% of the ATP is produced by oxidative phosphorylation. These results give rise to two suggestions, viz:

1. improving the efficiency of ATP production from NADH (e.g. using different cytochromes) may allow large increases in PHB yields at a given level of oxygenation, by avoiding acid excretion;
2. blocking the excretion of acids in some manner may substantially improve the PHB yield without greatly reducing ATP production.

Another interesting result from these two studies is the absence of pyruvate excretion from any optimal solution. Therefore the cell only excretes pyruvate for kinetic-imbalance reasons, and this represents a metabolic inefficiency.

Table 5.4: High-oxygen fermentation sample at hr 12.5 optimised for maximum PHB yield on glucose.

rates ($mmol.gRCM^{-1}h^{-1}$)	1 base case	2 vary PHB F	3 vary PHB noF	4 vary glc F & noF	5 vary both F	6 vary both noF
RCM production	0.18 (fixed)					
oxygen usage	2.76 (fixed)					
glucose uptake	2.58	(fixed)	(fixed)	1.58	5.54	1.97
PHB production	1.27	2.39	2.03	(fixed)	5.36	1.79
formic acid production	0.00	1.82	-	-	10.7	-
acetic acid production	0.35	-	-	-	-	-
pyruvic acid production	0.06	-	-	-	-	-
lactic acid production	1.69	-	-	-	-	-
succinic acid production	0.01	-	0.36	-	-	-
ethanol production	0.01	-	-	-	-	-
TCA cycle flux	0.14	-	-	0.26	-	-
ATP dissipation	14.14	12.98	12.00	11.91	16.93	12.17
PHB yield on glucose (mol/mol)	49%	93%	79%	80%	97%	91%

F indicates formic acid excretion allowed, noF indicates formic acid excretion is not allowed.

Effect of an abrupt reduction in oxygen supply

A final linear optimisation study is used to examine the effect of a cut in oxygen supply, as applied to the experimental data. Table 5.5 shows data from the LOF just before the 28% reduction in oxygen supply at hr 10. Column **2** shows that ATP production is already near its maximum. Column **3** shows that the 28% reduction in O_2 supply lowered the maximum possible ATP production by 19%, even after eliminating all PHB production. Likewise the maximum possible PHB yield is also reduced (at constant RCM, glucose and formic acid) from 69% to 59%, with a massive drop in ATP production. This drop in ATP is caused primarily by the need to oxidise NADH, which diverts glucose to succinate and impairs ATP generation from substrate-level phosphorylation. These observations match the experimentally observed effects, viz reduced PHB yield and increased acid excretion.

Table 5.5: Low-oxygen-fermentation sample at hr 10 optimised before (1, 2, 4) and after (3, 5) a 28% reduction in oxygen supply.

rates (mmol.gRCM^{-1}h^{-1})	1 base	2 max ATP	3 max ATP, O_2 cut	4 max yield	5 max PHB yield, O_2 cut
RCM production	0.81	(fixed)	(fixed)	(fixed)	(fixed)
oxygen usage	3.54	(fixed)	2.54 (fixed)	(fixed)	2.54 (fixed)
glucose uptake	4.06	(fixed)	(fixed)	(fixed)	(fixed)
PHB production	0.77	(fixed)	0.00	2.79	2.39
formic acid production	1.10	(fixed)	(fixed)	(fixed)	(fixed)
acetic acid production	1.70	2.55	2.71	-	-
pyruvic acid production	0.34	-	-	-	-
lactic acid production	2.44	(2.42)**	(3.80)*	-	-
succinic acid production	0.11	-	-	0.47	0.87
ethanol production	0.00	(2.42)**	(3.80)*	-	-
TCA cycle flux	0.27	-	-	-	-
ATP dissipation	16.12	17.15	13.86	11.71	6.66
PHB yield on glucose (mol/mol)	19%	19%	0%	69%	59%

* Under column 3 conditions lactic acid production and ethanol production are equivalent, the total excretion of lactic acid plus ethanol is 3.80 mmol.gRCM^{-1}h^{-1}.

** Under column 2 conditions lactic acid production and ethanol production are equivalent, the total excretion of lactic acid plus ethanol is 2.42 mmol.gRCM^{-1}h^{-1}.

5.8. Conclusions

5.8.1. Potential for Improved PHB Production

- The data suggest that accumulation of formic acid is undesirable and may prevent PHB production from achieving high levels during phase 2 and 3. It seems likely that the level of PHB enzymatic activity achieved during this period is critical for a high production rate during the remainder of the fermentation. It is difficult to tell whether formic acid is a symptom (e.g. of anaerobic zones causing severe oxygen deprivation) or a cause (formic acid concentrations inhibiting growth). This could be studied further by eliminating pyruvate-formate-lyase activity, or by dosing the medium with formic acid.
- If local anaerobic zones are being formed at lower agitation rates, there may be several ways to overcome the problem. A previous study (Tsai *et al.* (1996)) has shown that expression of a haemoglobin enzyme from *Vitreoscilla* improves the growth of *E. coli* under microaerobic conditions. The reasons given were enhanced ATP production efficiency and better 'buffering' of oxygen level. Either of these mechanisms would likely improve PHB production. A more speculative suggestion is based on the observation that the low solubility of oxygen in water causes the sensitivity to mixing. In contrast the solubility of other electron acceptors (e.g. nitrate) is orders of magnitude higher. Hence, an alternative electron acceptor added to the medium may potentially be utilised by the cells during short periods of oxygen deprivation.
- The low-cell-density fermentation data confirm that oxygen deprivation will initiate PHB synthesis, and that thereafter much of the rise in PHB production rate is due to increased enzyme activity during phase 3. This suggests that extending phase 3 by controlling the oxygen level may improve production rate without impairing PHB yield. For example, if the maximum achievable k_La is 3.7 min^{-1}, the oxygen supply could commence at 1.0 min^{-1}. Once PHB production had commenced due to the onset of oxygen limitation, the supply of oxygen could be gradually increased whilst maintaining oxygen limitation, in order to prolong PHB enzyme synthesis for as long as possible. Once the maximum k_La of 3.7 min^{-1} was achieved, the PHB synthesis rate may therefore be elevated whilst still achieving high PHB yield on glucose.
- Much of the detrimental effect of limiting oxygen supply is caused by the need to eliminate excess NADH produced by glycolysis. Pyruvate-dehydrogenase (flux 2) contributes half of this NADH, hence a reaction that bypasses PDH without producing NADH could alleviate the problem. Such a reaction is pyruvate-formate-lyase in conjunction with formate-hydrogen-lyase, which effectively uses the reducing power of NADH to generate acetyl-CoA and hydrogen from pyruvate. There is some evidence that FHL may be active in the HOF, since the medium concentration of formic acid steadily declines after hr 10. FHL is generally expressed only under anaerobic conditions and only when formic acid has accumulated to high levels. If FHL activity could be induced earlier, the amount of excess NADH (and hence lactic acid) production would be reduced by up to 100% of glucose uptake flux, depending on the oxygen supply level. An alternative to FHL may be the aerobic formate dehydrogenase, previously mentioned in Section 2.3.
- The production of excess NADH is not so much a problem of insufficient oxygen as of excess glucose uptake. *E. coli* appear to be evolved for maximum substrate uptake rates rather than for efficient substrate usage. It may therefore be possible to avoid acid excretion entirely by modulating the glucose uptake enzymes (Goel *et al.* (1995a); Goel *et al.* (1995b)). The success of this strategy would depend on the degree to which the cells are ATP-limited. Encouraging results were obtained by Shi *et al.* (1999), who used α-methyl-glucoside as a competitive inhibitor of glucose uptake during PHB synthesis. They demonstrated that acid excretion was greatly reduced without impairing PHB production,

although CO_2 generation was increased. To some extent, a similar effect can be achieved by reutilising excreted acids, e.g. pH-stat glucose feeding. However this method cannot be as efficient in the sense of ATP production, may lead to excessive medium salt concentrations, and also subjects the cells to cyclic variations which may cause other inefficiencies.

- The data in Table 5.1 show an elevated PHB synthesis rate for complex media vs minimal media (0.15 to 0.20 $gPHB.gRCM^{-1}h^{-1}$ vs 0.11-0.12 $gPHB.gRCM^{-1}h^{-1}$). This supports the Chapter 4 suggestion that PHB production may be improved by addition of a small amount of complex nutrient. The data also show that complex media lead to an earlier onset of PHB accumulation, which is detrimental to total yield. However this could be overcome by waiting until PHB accumulation has commenced before using complex nutrients.

5.8.2. Summary and Directions for Remaining Chapters

This chapter builds on the metabolic understanding of PHB production obtained in Chapters 2 and 4:

- Oxygen limitation is confirmed as the environmental trigger for PHB production in XL1-Blue(pSYL107).
- The long-term and short-term effects of oxygen deprivation have been elucidated by comparison with the Chapter 4 control fermentation and the Chapter 2 high-cell-density fermentation. In particular the effects on acid excretion and PHB production rate have been quantified.
- Linear optimisation studies were used to show the importance of oxygen as a redox sink, and to quantify the maximum theoretical performance of *E. coli* for PHB production.

In the economic context provided by Chapter 3, several possible improvements to the PHB production process have been identified.

Chapter 6 leads naturally on from the work in this chapter, in conjunction with the Chapter 3 economic analysis. It investigates the effect of altered nutrient-feeding strategy, which has the potential to reduce glucose uptake rate and hence increase efficiency as shown in Section 5.7.2.

Chapter 6

6.1. Summary

The aim of this chapter is to investigate the effects of a pH-stat feeding method on PHB production by the recombinant *E. coli* XL1-Blue(pSYL107).

A fed-batch fermentation of duration 25 h was carried out in a 5 l bioreactor using glucose-based minimal medium. The method was identical to the control fermentation in Chapter 4, except that from hr 10 onwards the nutrient feeding method was changed from constant-glucose-concentration to pH-stat. The production rates of PHB, residual cell mass, carbon dioxide, acetic acid, formic acid, lactic acid, succinic acid, pyruvic acid and ethanol were measured. The consumption rates of glucose, oxygen and ammonium ion were also measured, along with the intracellular concentrations of acetyl-CoA and 3-hydroxybutyryl-CoA. Rapid sampling of acyl-CoA levels and off-gas concentrations was conducted during two periods of glucose exhaustion.

The pH-stat fermentation closely matched the Chapter 4 control. Cellular PHB content was 52% at 18.5 $g.l(broth)^{-1}$ dry cell weight. Peak PHB production rate was 0.09 $gPHB.gRCM^{-1}h^{-1}$, with a PHB yield on glucose of 0.35 $mol(PHB).mol(glc)^{-1}$. Peak excretion levels were formic acid (2.7 $g.l^{-1}$), acetic acid (7.1 $g.l^{-1}$), lactic acid (10.5 $g.l^{-1}$), succinic acid (1.5 $g.l^{-1}$), and pyruvic acid (2.2 $g.l^{-1}$). Ethanol was not detected.

During periods of glucose exhaustion, pyruvic acid was assimilated from the medium. Other acids were not assimilated. The overall effects of repeated glucose exhaustion and growth on pyruvic acid are small: reduced net pyruvic acid excretion (40%), reduced glucose consumption (10-15%), and increased CO_2 production (5-8%). PHB yield on glucose was improved by 16%. PHB production rate was not affected. There may have been a small increase in acetic acid production and a small decrease in lactic acid production.

Transient analysis revealed that during growth on pyruvic acid for short periods the oxygen usage, carbon dioxide production, and acetyl-CoA levels were unaffected. However 3-hydroxybutyryl-CoA concentration and hence PHB production rate were depressed by 20-40%.

6.2. Introduction

6.2.1. General

The Chapter 3 economic analysis highlighted the economic importance of tradeoffs between PHB production rate, glucose-utilisation efficiency, and cell density. Nutrient-feeding strategy has significant effects on each of these, and is therefore investigated in this chapter. In a similar manner to Chapter 5, the short-term and long-term effects on PHB production are studied by following the same experimental protocol as developed in Chapter 4. This allows the effects of the altered nutrient-feeding strategy to be isolated by direct comparison with the control.

By applying the metabolic flux model from Chapter 4, the pH-stat fermentation (PSF) will also provide greater understanding of the metabolism, in particular the causes of acid excretion.

6.2.2. Fed-batch Methods:

A common fermentation-design problem is nutrient feeding. In general, fed-batch operation must be used to achieve cell densities above a few grams per litre, and it has been applied to the production of many different products (Yee and Blanch (1992); Lee (1996b)). The main benefits from fed-batch operation are:

- avoiding nutrient inhibition (glucose levels greater than 50 $g.l^{-1}$ are inhibitory for *E. coli*);
- reducing the rate of oxygen consumption (growth rate control by substrate limitation) and hence avoiding acid production due to oxygen limitation;
- avoiding the production of inhibitory end products during rapid aerobic growth, in particular acetic acid.

Extremely high cell densities are achievable, up to 160-200 g(dry cell weight).l^{-1}. At these levels, viscosity, mixing patterns and heat transfer are all significant problems, however oxygen transfer is usually the limiting factor. Build-up of salt concentration can also cause difficulties. It is usually preferable, for example, to use NH_4OH for pH control rather than NaOH.

Several types of nutrient feeding methods are commonly used:

1. Predetermined feeding profile:
   - Linear addition. The amount of biomass will theoretically be proportional to the amount of glucose fed, if the feedrate is sufficiently low.
   - Exponential addition. Ideally, this will result in a constant specific growth rate, if the feedrate does not exceed the metabolic capacity of the cells.
2. Feedback control for constant concentration:
   - direct measurement by a glucose analyser;
   - dry cell weight estimation in conjunction with a known yield of biomass on glucose. Estimates of dry cell weight can be obtained from:
     - culture fluorescence, which is a function of the total amount of NAD(P) present in the broth;
     - optical density.
   - measurement of acetic acid concentration: an increase in acetate concentration indicates that the glucose level is too high and the feed rate should be reduced. This method has a somewhat slower response time than the others, but can still be effective;

- measurement of CO_2 evolution rate: CO_2 production is assumed proportional to carbon source consumption.

3. Repeated cycling (glucose exhaustion):
   - DO-stat (dissolved oxygen): this method is based on the sudden rise in DO that occurs when glucose concentration drops to zero. DO-stat gives rapid response times when using minimal media, but only a small response in complex media. Cell densities of up to 125 gDCW.l^{-1} have been achieved using DO-stat with *E. coli*;
   - pH stat: the underlying principle is that when glucose becomes exhausted the pH of the medium changes. This can be due to rapid NH_4^+ excretion or uptake of acids (especially acetic acid) (Yee and Blanch (1992)). Depending on the medium and organism used this pH change may be positive or negative. pH-stat gives a slower response than DO-stat in defined media, but provides a clearer response in complex media.
4. 'Optimal Control':
   The so-called 'Optimal Control' strategy seeks to optimise the fermentation performance by calculating the deviation from optimal conditions and applying corrective action based on a model of the culture, for example by altering the glucose feedrate or ammonium ion feedrate. (Dhir *et al.* (2000)). The major drawbacks of this method are the need for a good phenomenological model, and the risk of instability if the control algorithm is not properly tuned. The need for realtime data can also be problematic.

The growth medium significantly affects the effectiveness of indirect techniques: complex media make control more difficult because they generally contain multiple carbon sources. The best results for PHB production in *E. coli* have been with pH-stat fed batch culturing (Lee *et al.* (1995b)).

6.3. Materials and Methods

A single fermentation was performed, following an identical protocol to the control fermentation in Chapter 4, with the following differences:

- From hr 10 onwards, continuous nutrient feeding was halted and the glucose concentration was permitted to decline to zero. At this point the resultant pH rise (from pH 6.95 to pH 7.05) triggered feeding of a pulse of nutrient solution. This method of nutrient feeding was repeated for the remainder of the fermentation. The amount of nutrient added was calculated to give an average of 1.5 triggerings per hour, viz about 1.8 g(glc).l(broth)$^{-1}$.
- At two selected glucose exhaustion points (first near hr 13.5, second near hr 20), frequent sampling was conducted on acyl-CoA concentration and gas production. Samples were taken according to the schedule shown in Table 6.1. The gas samples were taken directly from the fermenter gas-exhaust port and the CO_2 evolution rate was corrected for dynamic mass-transfer effects as shown in Appendix A.

Table 6.1: Frequent-sampling schedule for acyl-CoA concentration and fermenter headspace gas concentration.

	acyl-CoA sample time (min)	gas sample time (min)
Pre-exhaustion	approx -4	approx -3.5
Point of glucose exhaustion	+0	+0.5
	+3	+3.5
	+6	+6.5
Triggered nutrient manually at minute 8		
	+9	+9.5
	+12	+12.5

6.4. Results

6.4.1. General Fermentation Results

Figure 6.1 compares the PHB and RCM profiles for the control (CON) and pH-stat (PSF) fermentations. RCM concentration is essentially identical for both. PHB concentration matches closely until hr 20, and thereafter it appears that the PSF PHB production rate may be slightly higher (10%).

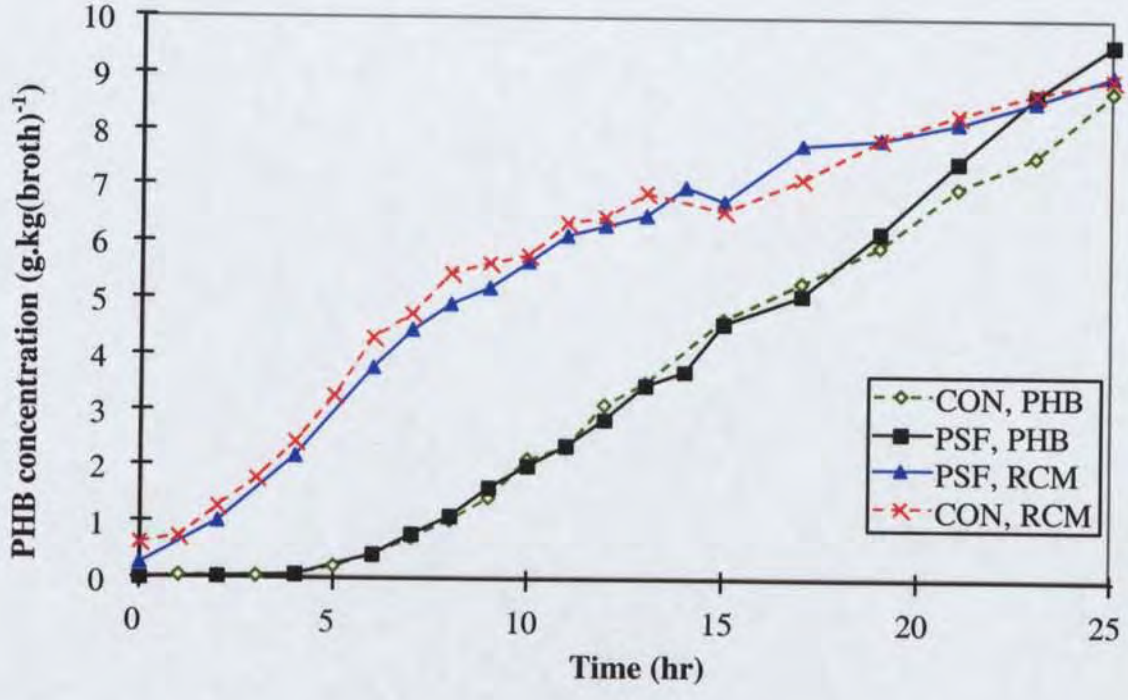

Figure 6.1: Profiles of PHB and residual-cell-mass concentration for the control (CON) and pH-stat fermentations (PSF).

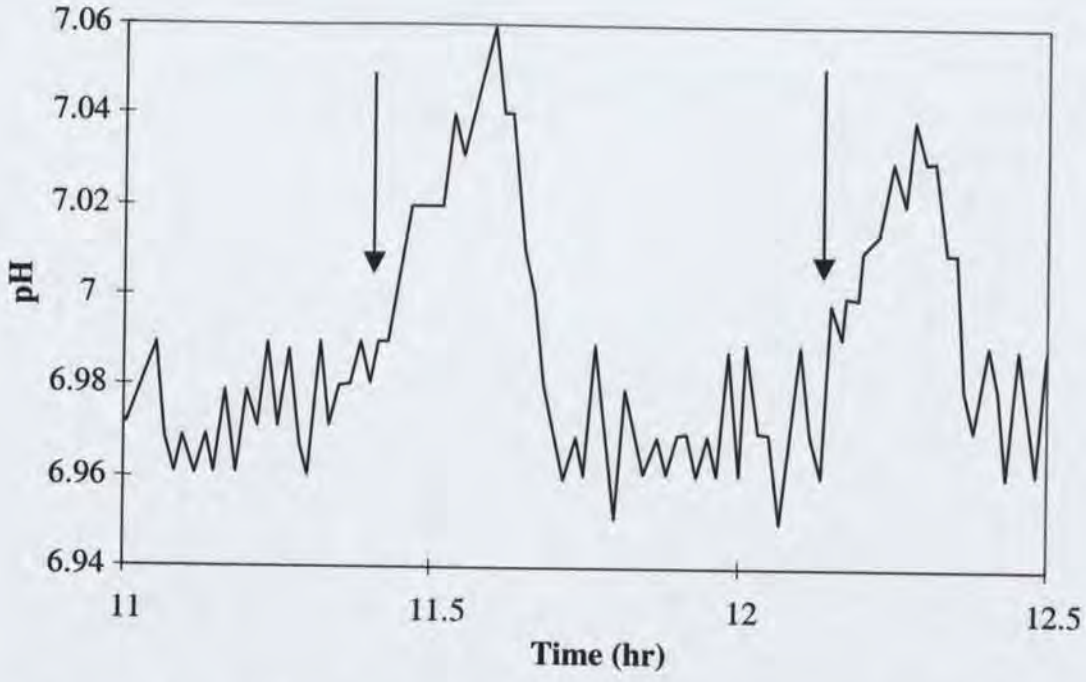

Figure 6.2: Short segment of the pH profile of the pH-stat fermentation, showing two glucose-exhaustion events.

A segment of the pH profile is shown as Figure 6.2. The first glucose exhaustion occurred at approximately hr 11.4, whereupon the pH slowly rose to the nutrient trigger-point (7.05). Immediately after the nutrient pulse the pH declined rapidly to the lower control limit. Two unexpected observations from the data are:

- the pH rise was very slow, approximately 0.006 units per minute;
- the PSF DO profile (not shown) is identical to that of CON, with no effect of glucose exhaustion. As described in Section 6.2.1, glucose exhaustion in minimal medium usually causes a rise in dissolved oxygen due to reduced NADH production.

The cause of these observations is apparent from the acid production profiles. Although noisy, all profiles are very similar for the CON and PSF, with the exception of pyruvic acid (Figure 6.3). Pyruvic acid production rate matched well prior to hr 11.5, viz the first glucose exhaustion. Thereafter the PSF average production rate is substantially below that of CON. Hence it seems likely that when glucose became exhausted, pyruvate was immediately reutilised by the cell with little change in production of other acids. The pH rise due to uptake of pyruvate was thus counterbalanced by the continued excretion of other acids, giving only a slow rate of pH increase. Likewise oxygen consumption remained high. During the first few glucose-exhaustions there is evidence that lactic acid excretion was reduced and acetic acid excretion was enhanced (Figure 6.4 and Figure 6.5), but from hr 15 onwards this is no longer the case.

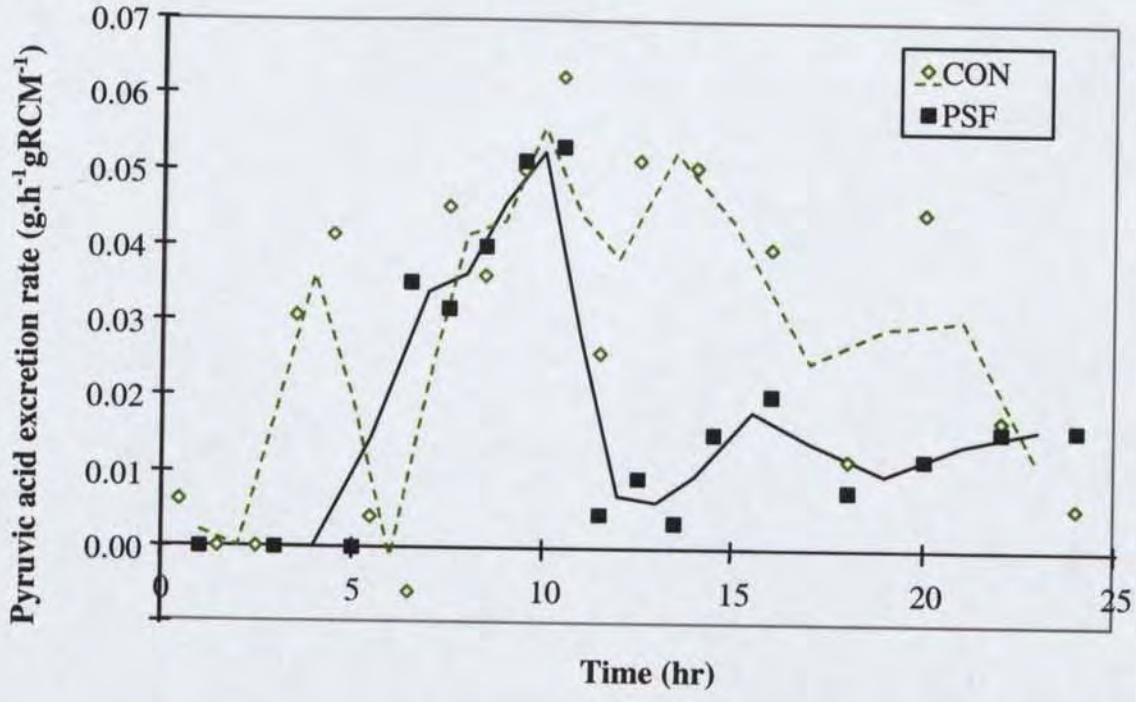

Figure 6.3: Specific production rate (smoothed) of pyruvic acid for the control (CON) and pH-stat (PSF) fermentations.

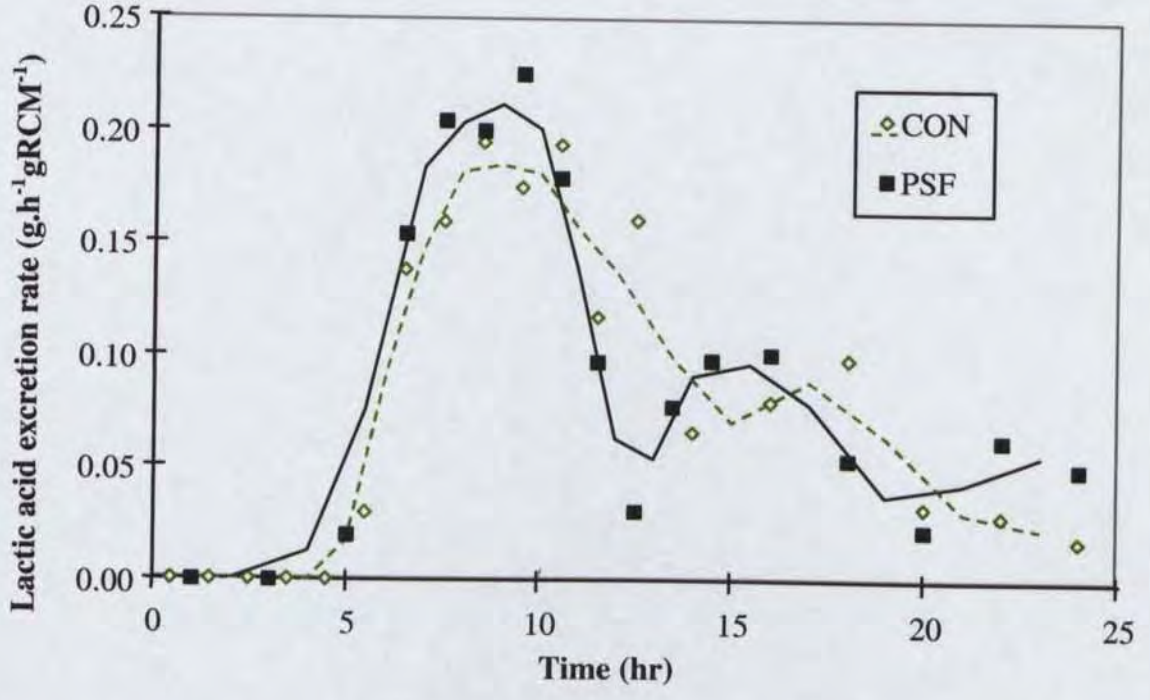

Figure 6.4: Specific production rate (smoothed) of lactic acid for the control (CON) and pH-stat (PSF) fermentations.

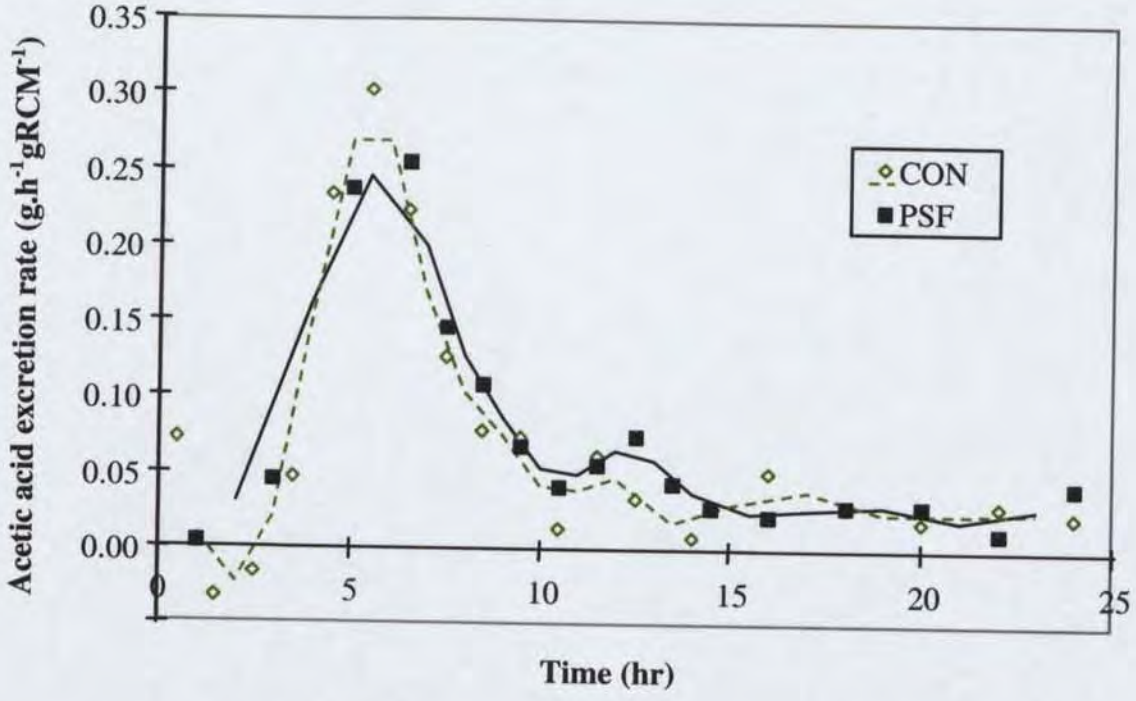

Figure 6.5: Specific production rate (smoothed) of acetic acid for the control (CON) and pH-stat (PSF) fermentations.

The specific consumption rate of O_2 was essentially identical for the CON and PSF. Likewise the CO_2 profile was identical, apart from hr 11 onwards when the PSF CO_2 production appears elevated over CON by 5-8%. As expected glucose consumption was reduced from hr 11 onwards, by about 10-15% (Figure 6.6). The PSF glucose rate also appears to decline less slowly than for the CON, so that by hr 23 the rates match despite the different feeding methods. The reason for this is not clear.

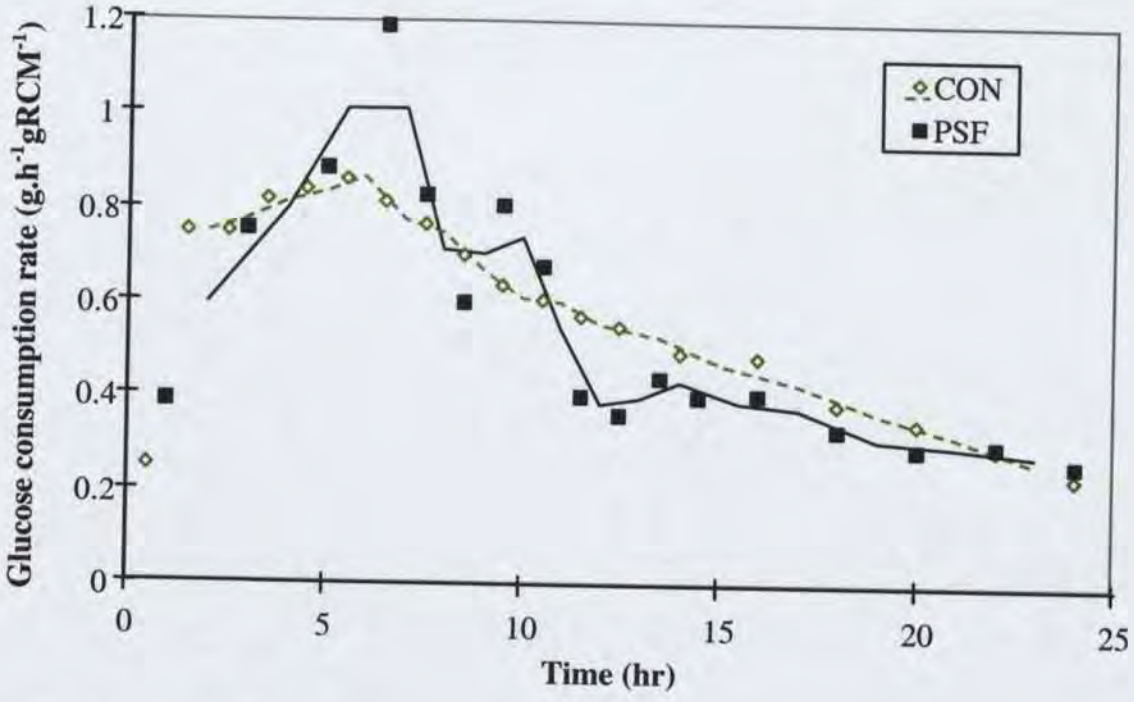

Figure 6.6: Specific glucose consumption rate (smoothed) for control (CON) and pH-stat (PSF) fermentations.

6.4.2. Transient Off-gas Measurements

Figure 6.7 shows that the onset of glucose limitation did not appear to have any significant effect on the carbon dioxide production rate. However in both cases there was a brief 10% increase in CO_2 production rate immediately after nutrient was added to the bioreactor. Although the duration of this enhanced rate is not directly observed, it must be short because the overall average rate for the hourly sample was about the same as the rate during glucose exhaustion. The increased rate probably reflects a brief period when both glucose and pyruvic acid were being utilised, before a metabolic switch back to pyruvic acid excretion. The data therefore indicate that during growth on pyruvic acid for short periods, the pyruvate dehydrogenase (flux 2) is unaffected, since from hr 10 onwards it is responsible for generating most of the CO_2.

It was expected that substituting pyruvic acid for glucose would lead to less NADH production and hence reduced oxygen consumption, but two observations do not support this:

- the oxygen consumption profiles (not shown) appear unaffected by glucose limitation, although the noise level is about 10% so it is difficult to be certain;
- the dissolved oxygen concentration is completely unaffected.

The reason for the disparity is not apparent.

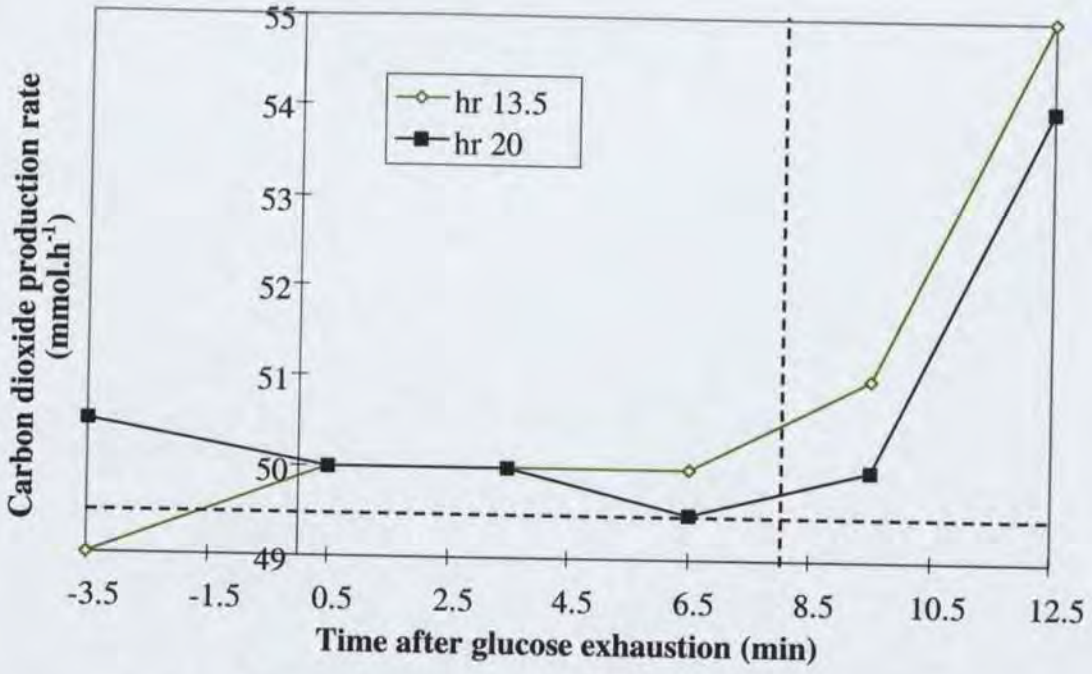

Figure 6.7: Transient CO_2 production rates during glucose exhaustion, at hr 13.5 and hr 20. Production rates have been corrected for solution dynamics. Time zero is the point of glucose exhaustion as determined by measurement of broth glucose concentration. A pulse of nutrient was fed at minute 8 (vertical dashed line). In both cases the average CO_2 production level for the hourly sample was 49.5 mmol.h^{-1} (horizontal dashed line).

6.4.3. Acyl-CoA Profiles

The acyl-CoA levels of the PSF are compared with the CON in Figure 6.8 and Figure 6.9. 3-hydroxybutyryl-CoA datapoints are missing prior to hr 12 because an interfering peak made quantification impossible. The PSF and CON acetyl-CoA profiles are very similar. The PSF profile appears slightly higher for most of the fermentation but this is probably experimental error. Likewise the 3-hydroxybutyryl-CoA profiles match to within experimental error. The acyl-CoA measurements were all taken during glucose-sufficient conditions, generally ten minutes after a nutrient pulse. The graphs demonstrate that there is no substantial long-term effect of repeated glucose exhaustion on the acyl-CoA concentrations.

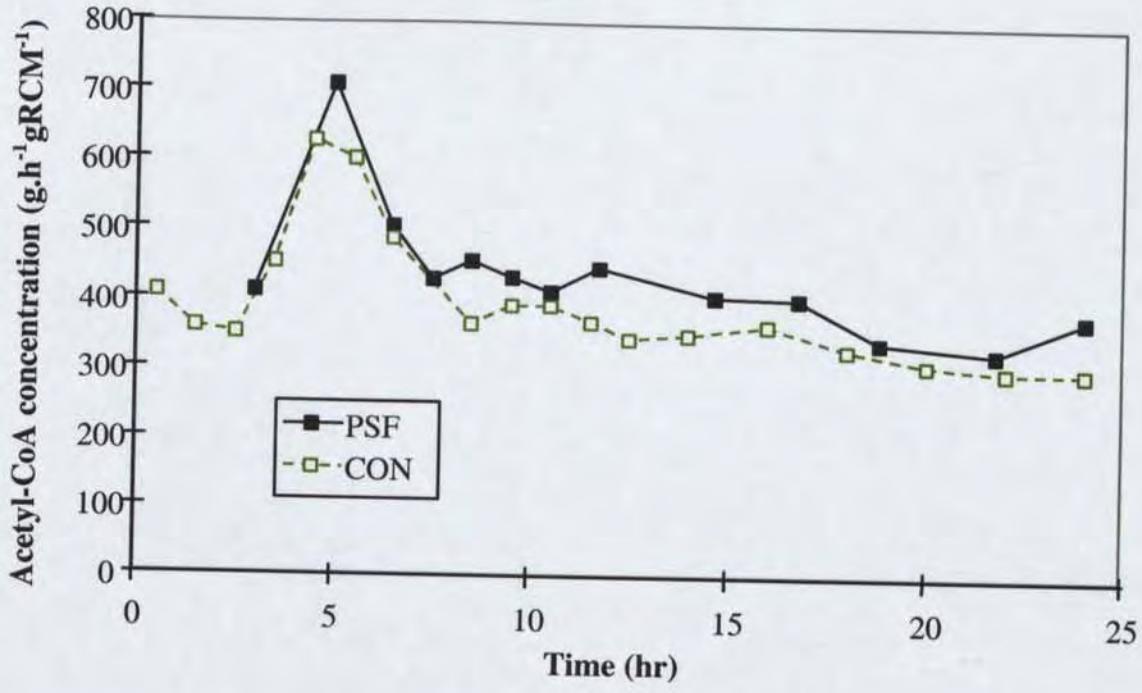

Figure 6.8: Acetyl-CoA levels during the control (CON) and pH-stat (PSF) fermentations.

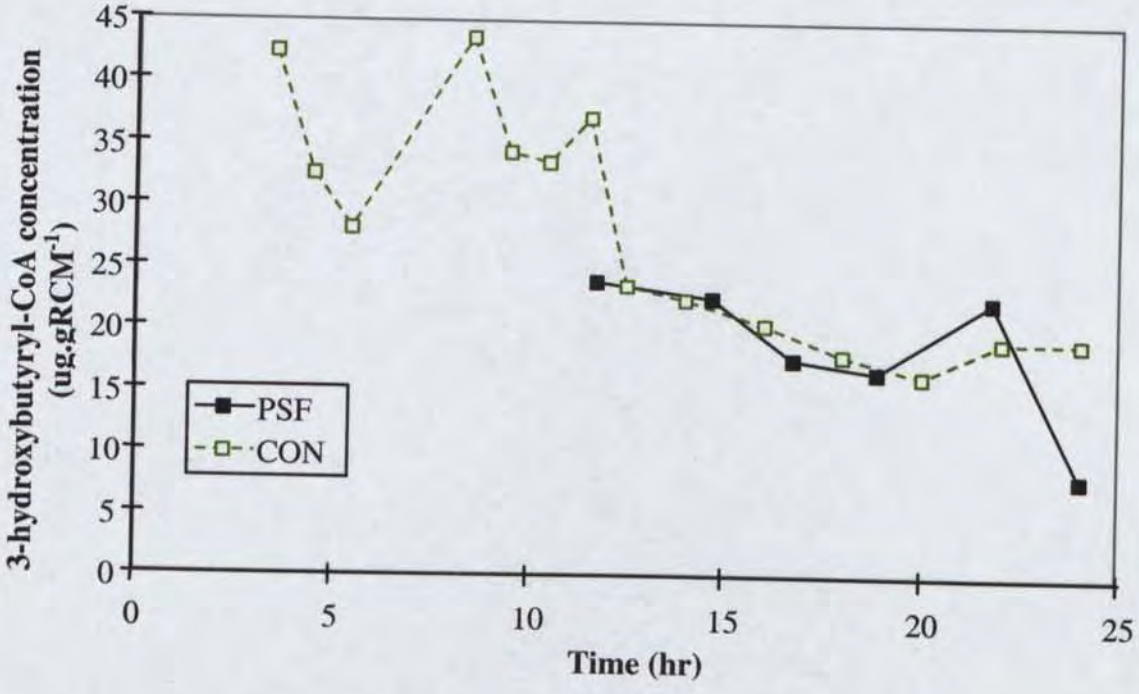

Figure 6.9: 3-hydroxybutyryl-CoA levels during the control (CON) and pH-stat (PSF) fermentations.

6.4.4. Transient Acyl-CoA Measurements

Figure 6.10 shows that acetyl-CoA is essentially unaffected by glucose exhaustion. The hr 20 sample appears to exhibit a slightly elevated acetyl-CoA level during the zero-glucose period, which may be due to reduced PHB synthesis. However the experimental error is too large to be certain.

In contrast Figure 6.11 indicates that 3-hydroxybutyryl-CoA levels are depressed by 20-40% during the period of glucose limitation. This implies that PHB synthesis rate is reduced by a corresponding amount, given the synthase rate equation in Sections 4.6.1 and 4.6.2. The accuracy of the PHB assay is not sufficient to directly determine such a change in rate. Confirmation that PHB production is indeed inhibited during growth on pyruvic acid would require a further experiment, for example allowing glucose exhaustion to continue for several hours.

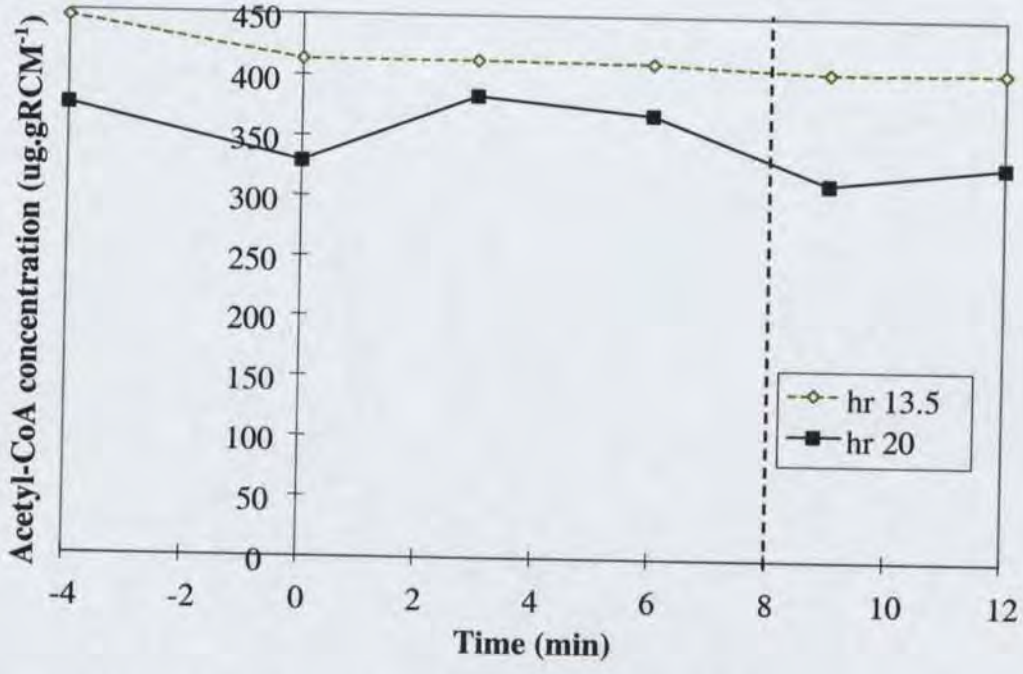

Figure 6.10: Transient acetyl-CoA levels during glucose exhaustion, at hr 13.5 and hr 20. Time zero is the point of glucose exhaustion as determined by measurement of broth glucose concentration. A pulse of nutrient was fed at minute 8 (vertical dashed line).

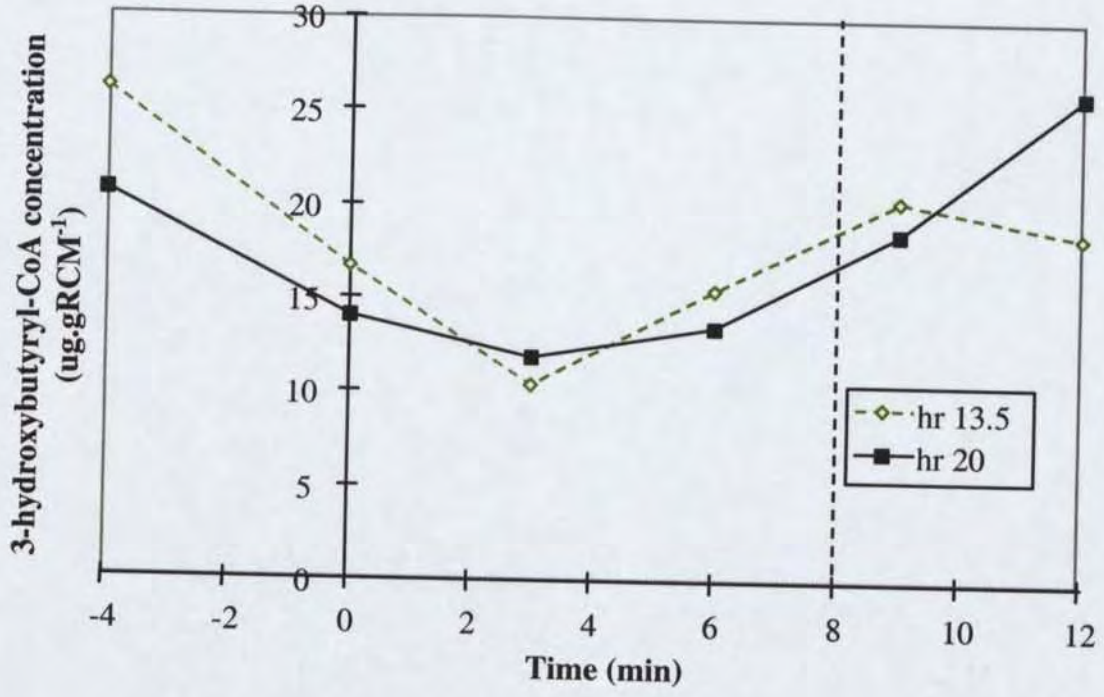

Figure 6.11: Transient 3-hydroxybutyryl-CoA levels during glucose exhaustion, at hr 13.5 and hr 20. Time zero is the point of glucose exhaustion as determined by measurement of broth glucose concentration. A pulse of nutrient was fed at minute 8 (vertical dashed line).

6.5. Flux Analysis and Discussion

Shown below in Table 6.2 is the carbon balance for the PSF. Overall closure is excellent (99%), and closure for each individual sample ranges from 85% - 100%. The redox balance was 95%.

Table 6.2: Overall mass balance on the pH-stat fermentation.

	mol per 100 mol glucose		mol-C per 100 mol-C glucose	
	control	pH-stat	control	pH-stat
carbon dioxide	109	124	18	21
RCM (mol-C-equivalents)	89	96	15	16
PHB	30	35	20	23
acetic acid	32	37	11	12
formic acid	16	13	3	2
lactic acid	33	36	16	18
pyruvic acid	13	8	6	4
succinic acid	6	4	4	3
ethanol	0	0	0	0
Overall closure:			93%	99%

As previously mentioned, most of the PSF profiles closely match the CON. The most significant differences are slightly elevated PHB and CO_2 production, and reduced pyruvic acid production.

Within experimental error, all PSF fluxes match the CON quite closely, apart from pyruvic acid. Figure 6.12 shows that the PSF PHB production per gRCM is possibly slightly elevated from hr 15-20 onwards, as also apparent from Figure 6.1. Similar to the HOF in Chapter 5, the PHB production rate does not appear to decline substantially between hr 10 & 25.

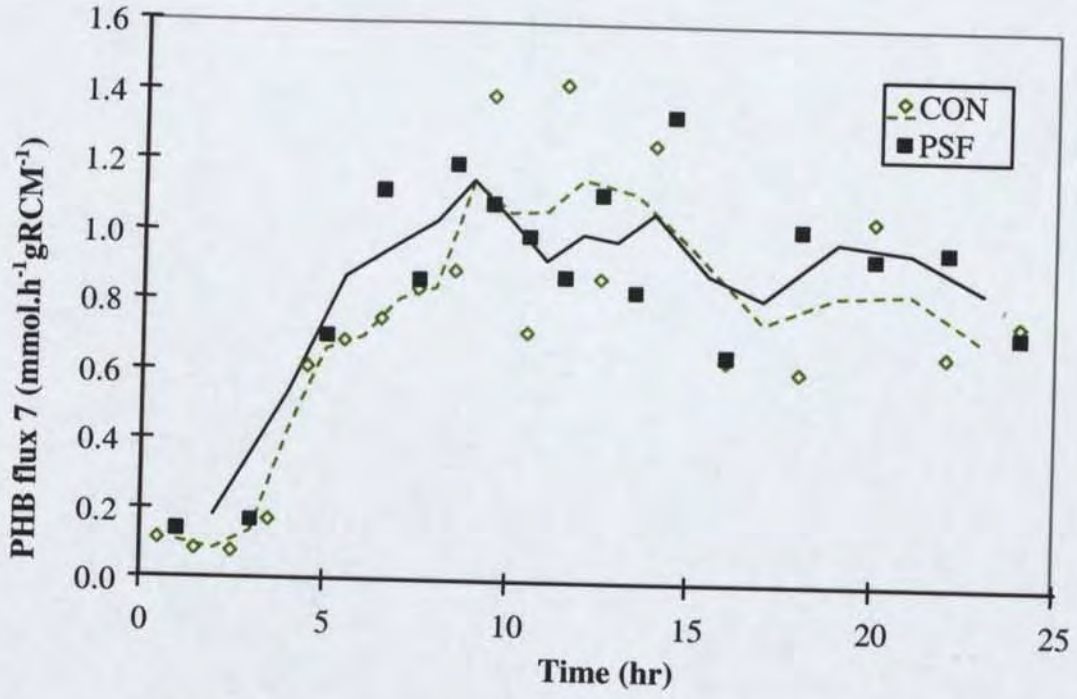

Figure 6.12: PHB production rate (smoothed) on an RCM basis for the control (CON) and pH-stat (PSF) fermentations.

The improved PHB yield on glucose is shown in Figure 6.13, a 16% improvement once pH-stat feeding commenced. This supports the study in Section 5.7.2 which concluded that reducing glucose uptake rate can substantially improve PHB yield on glucose.

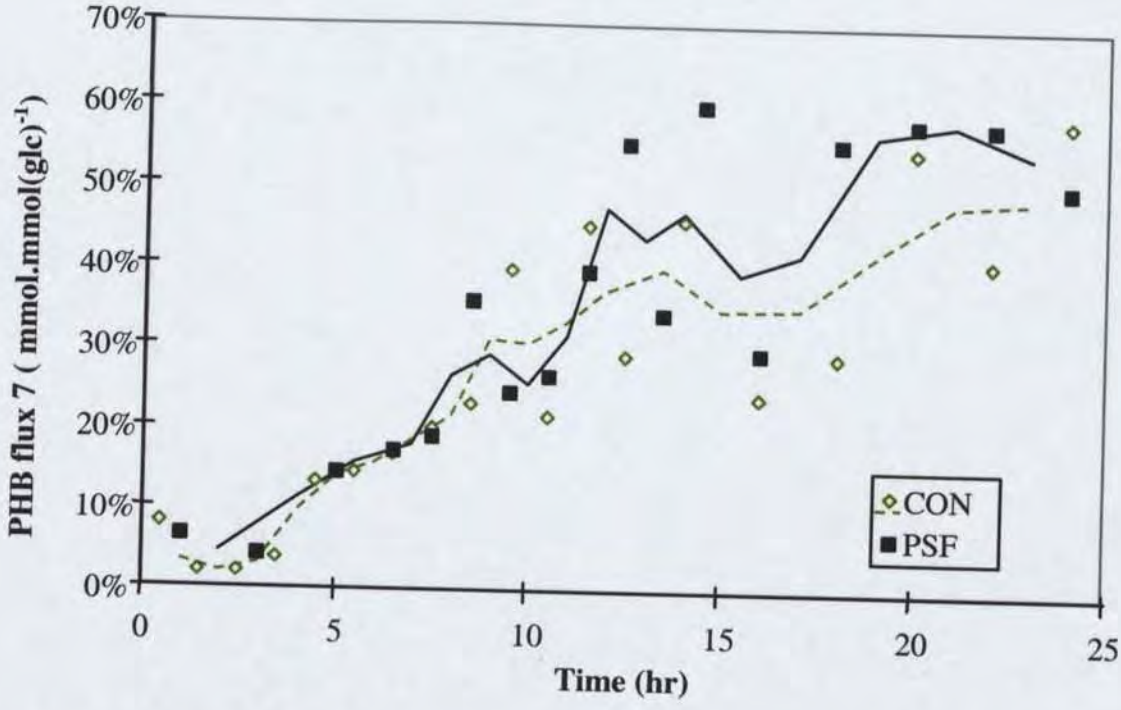

Figure 6.13: PHB yield on glucose (smoothed) for the control (CON) and pH-stat (PSF) fermentations.

It is difficult to tell what happened to the fluxes during the periods of growth on pyruvate, because this occurred for only 10% of the time. Nevertheless the time-averaged effect of brief periods of growth on pyruvate seems to be small. The yield of PHB on glucose was improved due to reduced overall acid excretion and a lower average glucose uptake rate. PHB production rate may have been slightly improved over the long term but this is not certain given the level of experimental error.

6.6. Conclusions and Further Work

The pH-stat feeding method in this fermentation differs somewhat to conventional pH-stat feeding, because pyruvic acid was reutilised in preference to acetic acid. The overall effects of repeated glucose exhaustion and growth on pyruvic acid appear to be small:

- reduced net pyruvic acid excretion (40%);
- reduced glucose consumption (10-15%);
- increased CO_2 production (5-8%).

Metabolic activity may also decline less rapidly, as deduced from overall glucose uptake rate. The effect on PHB production rate appears negligible, however PHB yield on glucose was improved by 16%.

Transient analysis during periods of glucose exhaustion shows that oxygen usage and carbon dioxide production are unchanged from glucose growth. However a 20-40% decline in the PHB production rate can be inferred from measurements of 3-hydroxybutyryl-CoA concentration. This is probably due to a reduced supply of NADPH/NADP during growth on pyruvic acid, since the acetyl-CoA concentrations are unaffected. For this reason, extended growth on pyruvic acid (and probably acetic or lactic acid also) should be avoided.

In conjunction with the high-cell-density fermentation in Chapter 2, this study shows that pH-stat feeding can improve PHB yield on glucose when compared with constant-glucose feeding. Further experiments are necessary to characterise the effects of extended glucose deprivation, for example allowing the pyruvic acid to be completely reutilised and uptake of lactic and acetic acid to commence. The ideal glucose-feeding regime may involve short, frequent nutrient pulses, with feedback control based on pH or glucose measurements. This would feed glucose at a rate just slow enough to avoid acid excretion whilst still maintaining high PHB production rate. Such a strategy has the potential to greatly improve PHB yield on glucose, reduce salt additions, and sustain high PHB production rates for longer periods.

Chapter 7

This chapter's purpose is to summarise the insights and contributions of the thesis.

7.1. Overall Summary

As described in Chapter 1, the aim of this thesis is to improve understanding of PHA production by recombinant *E. coli*, with a view to guiding future developmental work. Such understanding is an important aid to achieving improvements in an economic sense.

The major contributions made by this thesis are:

- Providing an economic description of PHA production by *E. coli*, highlighting areas where significant cost reductions are possible. This was achieved by Chapter 3, utilising preliminary fermentation data provided by Chapter 2.
- Developing a quantitative analytical framework for cellular metabolism during PHA production. A metabolic framework utilising metabolic flux analysis was developed in Chapter 2, then refined in Chapter 4 using more-rigorously-collected fermentation data.
- Adapting the *in-vitro* kinetics of the PHB pathway for use with *in-vivo* fermentation data, which was performed in Chapter 4.
- Designing appropriate experimental techniques and conducting repeatable experiments to verify the suitability of the models. Chapter 4 used the fermentation data in Chapter 2 as a basis for developing the necessary experimental protocol for a quantitative and repeatable control fermentation. The suitability of the protocol was verified in Chapter 4 and again in Chapters 5 and 6.
- Applying the metabolic and kinetic models to address several previously unanswered questions, including:
  - *Which environmental and/or metabolic factors trigger the onset of PHB production in E. coli?* This was addressed by Chapter 4 and studied further in Chapter 5, with the conclusion that oxygen limitation is the primary factor responsible.
  - *What are the underlying metabolic changes that occur during various stages of the fermentation, and how can they be exploited to improve PHA production?* Chapter 4 investigated the general metabolic progress of PHB production by XL1-Blue(pSYL107), and the understanding achieved was extended in Chapters 5 and 6.
  - *What are the short-term and long-term effects of oxygen deprivation on PHB production?* Chapter 5 showed in conjunction with Chapter 2 that oxygen supply is crucial to achieving good PHB production rates with efficient use of glucose. Oxygen limitation causes the onset of PHB production, but when supply drops below a critical level rapid acid excretion occurs. The longer-term effects of this are reduced PHB production rate and impaired yield on glucose.
  - *Does the nutrient-feeding strategy used have an appreciable effect on PHB production?* As shown in Chapter 6, pH-stat nutrient feeding appears to improve PHB yield on glucose without significantly impairing production rate. This confirms the Chapter 5 finding that reducing glucose uptake rate may significantly improve PHB yield on glucose.
  - *What further improvements to PHA production are possible and how can they be implemented?* In the economic context provided by Chapter 3, Chapters 4, 5, and 6 outline a number of areas where changes to fermentation protocol or cellular genetics may provide substantial improvements to PHA production.

7.2. Detailed Summary

The most important specific findings from this thesis are detailed below:

7.2.1. Quantification of Fermentation Performance

Chapters 2, 4, 5, and 6 have accurately quantified a number of aspects of PHB production by XL1-Blue(pSYL107), in particular

- byproduct excretion levels;
- oxygen requirements;
- CO_2 production;
- glucose uptake rate and PHB yield on glucose;
- variation of acetyl-CoA and 3-hydroxybutyryl-CoA concentrations.

Accurate measurements for many of these did not previously exist. Likewise, a protocol for quantitatively repeatable PHB fermentation had not been demonstrated previously.

7.2.2. General Progress of an XL1-Blue(pSYL107) PHB Fermentation

As shown in Chapters 2, 4, 5, and 6, in all cases the fermentation progresses through four phases, approximately divided as follows:

Phase 1 - fully aerobic phase, exponential growth

Cell growth is unrestricted, with all specific production rates constant. The growth rate is near 0.30 - 0.35 $g.gRCM^{-1}h^{-1}$, with PHB production steady at a low rate, approximately 0.008 $gPHB.gRCM^{-1}h^{-1}$. This gives rise to the observed initial PHB content, approximately 2.3% of dry cell weight. There is extensive use of the TCA cycle for ATP generation, despite the fully aerobic conditions.

Phase 2, onset of oxygen limitation

This second phase is initiated by the onset of oxygen limitation. For the fermentations in Chapters 4, 5, and 6 this was comparatively rapid (2-3 h) whereas in the Chapter 2 high-cell-density fermentation it was more gradual (7-10 h). In all cases there was a rapid (six-fold or more) rise in PHB production. This was accompanied by a decline in TCA cycle flux and rapid excretion of formic acid. The low-cell-density fermentations also showed rapid excretion of acetic, lactic, pyruvic and succinic acids. In contrast, the high-cell-density fermentation exhibited production of acetic and lactic acids which were repeatedly reutilised due to the pH-stat nutrient feeding method. In all cases, RCM production begins to decline during Phase 2.

The likely explanation for these events is elucidated by the studies in Chapters 2, 4, and 5. When oxygen availability drops below a certain level, formic acid excretion is triggered. Excretion lasts for several hours, at which point another factor prevents further synthesis. This may be inhibitory concentrations in the medium, or may be related to other metabolic events. In the case of high-cell-density fermentation there is no apparent oxygen limitation, however the data suggest that rapid transient oxygen limitation probably occurs, due to inadequate mixing. This leads to the production of acids despite an apparently high oxygen concentration. Acetic and lactic acid are reutilised upon return to oxygen-sufficient zones, however formic acid is not and hence accumulates in the medium.

The decline in oxygen availability also causes a reduction in RCM synthesis. This is not due to ATP restrictions: a more likely explanation is that the low oxygen tension induces widespread changes in enzyme levels. Possible effectors are the global regulation systems dependent on oxygen tension, viz Arc (aerobic respiration control) and Fnr (fumarate nitrate reduction). The decline in oxygen availability causes a rise in NADH/NAD, which shuts down the TCA cycle. This in turn causes the acetyl-CoA levels to rise, as observed experimentally in Chapters 4, 5, and 6. The kinetic analysis in Chapter 4 demonstrates that the rapid increase in PHB production rate is probably caused by this change in acetyl-CoA levels. A rise in NADPH/NADP may also assist to a lesser degree, potentially coupled through from NADH/NAD by the transhydrogenase.

Accompanying these changes is a rise in intracellular pyruvate, causing excretion of pyruvate in the low-cell-density fermentations. The elevated levels of intracellular pyruvate and NADH/NAD enhance lactic acid production. In wild-type *E. coli*, pyruvate kinase is inhibited by NADH, which would prevent the intracellular accumulation of pyruvate. The observation that this does not occur with XL1-Blue(pSYL107) suggests that it may contain a mutation which prevents NADH inhibition of pyruvate kinase.

Phase 3, gradual metabolic shift phase

Over the next phase (4 - 6 h) the excretion of formic acid ceases. In conjunction with increased PHB synthesis this causes a return of acetic acid flux to a low level. TCA cycle flux drops to zero, probably due to the previously mentioned global regulatory genes. RCM production reaches a low, basal level whereas PHB production rises to its maximum level. The decline in growth rate allows the copy number of pSYL107 to increase, and hence express higher levels of PHB enzymes. This effectively "hijacks" the cellular machinery for synthesis and maintenance of DNA, RNA and proteins. In turn this reduces the synthesis of cellular machinery itself, with the net result that residual cell mass synthesis declines to a low basal level. As shown in Chapters 4 and 5, the concentration of the PHA enzymes also increases over this period, probably for the same reason, giving rise to the observed increase in PHB production rate.

Phase 4, slow decline, hr 10- 25

Over the remainder of the fermentation there is a slow decline in all fluxes on an RCM basis. Fluxes on a glucose basis stabilise, although PHB production utilises an increasing fraction of the glucose, as much as 90% mol/mol. Likewise the ATP dissipation increases on a glucose basis, despite declining overall. The likely cause of these observations is a general metabolic slowdown. Once RCM synthesis drops to too low a level, the cell is no longer able to synthesise sufficient proteins to maintain enzyme levels. Hence the enzymes gradually degrade and are not replaced. Cell lysis may also be occurring. The measured metabolite levels in Chapters 4, 5, and 6 show that the acetyl-CoA concentration, 3-hydroxybutyryl-CoA concentration, and PHA synthase activity are declining on an RCM basis. However on an intracellular volume basis they remain steady or even increase slightly. This suggests that the diminishing PHB production rate may be partially caused by PHB accumulation and increasing medium osmolarity, which reduce intracellular volume.

All fermentations show a sudden rise in dissolved oxygen concentration near the start of phase 4. The rise indicates a slightly reduced consumption of oxygen, despite the fact that supply remains limiting. This is probably due to a change in the enzymes of the respiratory chain, for example a switch from cytochrome bd to cytochrome o.

7.2.3. Byproduct Excretion Characteristics

Based on the fermentations in Chapters 2, 4, 5, and 6, the byproduct-excretion characteristics of XL1-Blue(pSYL107) have been quantified. This gives a greater understanding of the underlying metabolic changes, and will assist in predicting the effects of future modifications to fermentation protocol and/or cellular genotype.

The byproducts can be roughly grouped into 4 categories based on their observed behaviour:

- Pyruvic acid and acetic acid, whose excretion appears controlled mostly by the extracellular concentration. Provided that oxygen limitation has occurred, their excretion does not appear influenced by changes in oxygen supply. Some production of acetic acid via overflow metabolism is observed under oxygen-sufficient conditions. The production of pyruvic acid is unusual and may indicate the presence of a mutation in the central metabolism of XL1-Blue.
- Lactic acid production, which correlates closely with oxygen supply rate on a $gRCM^{-1}$ basis, and appears independent of broth concentration and cell density. Lactic acid generally accounts for the greatest fraction of byproducts excreted.
- Formic acid and succinic acid, whose excretion rates appear independent of broth concentration and inversely related to the well-mixedness of the broth. It is likely that formic acid production occurs due to the formation of local oxygen-deficient zones within the bioreactor. At high levels of oxygen demand and/or conditions of poor mixing, steady accumulation of formic acid occurs. Hence in the Chapter 2 high-cell-density fermentation, the appearance of formic acid indicates that some degree of oxygen stress was occurring several hours before the measured oxygen concentration approached zero. Succinic acid excretion appears to exhibit similar behaviour but the reasons for this are not clear.
- Ethanol excretion was only observed under conditions of extreme oxygen deprivation, and only low levels were produced.

Upon exhaustion of glucose, the Chapter 6 fermentation demonstrated that pyruvic acid is preferentially reutilised. Once pyruvic acid is exhausted, acetic and lactic acids are rapidly reutilised. In contrast, formic acid reutilisation is very slow.

7.2.4. Effects of Oxygen

Chapter 5 investigated the effects of oxygen on PHB production, with the following outcomes:

- Oxygen limitation is shown to be the trigger for PHB production in XL1-Blue(pSYL107). As described in Section 7.2.1, the onset may be rapid or gradual.
- To a first approximation, the production of residual cell mass and PHB (on an RCM basis) is almost independent of the cell density, holding other factors constant. In particular, supplying a greater level of oxygen during the entire fermentation has the effect of delaying the onset of PHB production, without changing the fermentation profile on an RCM basis. However it is likely that the well-mixedness of the fermentation is also important, and improves PHB production. In addition the excretion of acetic acid and pyruvic acid is different, as outlined in Section 7.2.3.
- The effects of a step-decrease in oxygen supply are several:
  - Short term effects include an immediate drop in 3-hydroxybutyryl-CoA concentration, but no effect on acetyl-CoA levels. Lactic acid excretion is increased, ATP dissipation is reduced, and PHB production rate is impaired. No short-term effects on glucose uptake rate or RCM production are observed.

- Over the longer term, glucose uptake, RCM production and PHB production are all impaired as compared to the control fermentation. The activity of PHA synthase appears to decline more rapidly than the control. Significantly greater amounts of lactic acid are produced.

- The observations suggest that the cellular metabolism is strongly regulated and is essentially independent of PHB production. The cell satisfies its own needs first from the available cofactors (e.g. ATP, NADPH) and PHB production is dictated by what remains. Under conditions of reduced oxygen supply, the cell maximises ATP production whilst using lactic acid excretion to eliminate excess NADH, diverting flow away from acetyl-CoA and hence impairing PHB synthesis.
- Chapter 5 also shows that increasing PHB production rate without a corresponding increase in oxygen supply will probably cause excessive lactic acid excretion.
- Linear optimisation shows that considerable opportunity exists for redirecting metabolic fluxes to improve PHB yield, including reducing the glucose uptake rate. The studies also show that the cellular metabolism during PHB production is nearly optimal for ATP production, suggesting that the cells are ATP limited. The major cause of byproduct excretion is to maintain the internal redox balance when insufficient oxygen is available.

7.2.5. Kinetic Analysis

Chapter 4 adapted *in-vitro* kinetic expressions for PHB production to the *in-vivo* fermentation data. In conjunction with acyl-CoA measurements from Chapters 4, 5, and 6 the following outcomes were achieved:

- The likely range of a number of kinetic parameters were established for PHB production by XL1-Blue(pSYL107). In particular estimates were obtained for the acetyl-CoA/CoA ratio, the activities of the three PHA enzymes, the intracellular pH, and the intracellular concentrations of acetyl-CoA, acetoacetyl-CoA, 3-hydroxybutyryl-CoA, NADP, and NADPH.
- Metabolic control analysis was used to quantify the sensitivity of PHB production rate to enzyme activities and metabolite concentrations. This information can be used to set the direction for future genetic manipulation.
- The kinetic and flux models developed can also be readily adapted to synthesis of PHBV or other novel PHAs, which will assist efforts to analyse and improve their production.

7.2.6. Nutrient Feeding

In addition to supplying extra metabolic understanding as outlined above, Chapter 6 also revealed several differences between pH-stat feeding and constant-glucose feeding. During growth on pyruvic acid for short periods, there is little change to central metabolism. In particular, oxygen consumption and acid production are unaffected. CO_2 production is slightly increased, whereas PHB production rate is impaired by 20%. Over the longer term, the PHB production rate is unaffected but the yield on glucose is improved. On the balance, pH-stat feeding appears superior to constant-glucose feeding.

7.2.7. Process Economics

The economic analysis in Chapter 3 provides a useful framework to identify and test potential improvements to the PHB production process. The analysis outcomes include:

- A reasonable estimate of PHB break-even production cost is US1995$4.88 kg^{-1}.
- The production of PHBV should be economically similar to PHB, provided that the control of HV content can be mastered.

- The economics are highly sensitive to several process variables, in particular:
  - downstream PHB recovery;
  - final broth cell density, which is largely constrained by cellular oxygen demand;
  - process scaleup;
  - medium cost. In particular dairy whey is a suitable candidate to partially replace the glucose used, although seasonal availability is a severe constraint.

7.2.8. Opportunities for Improved PHA Production

A number of areas were identified in each chapter where substantial improvements to PHB fermentations are possible:

- Reduction of acid excretion, which represents glucose wastage and metabolic inefficiency. In particular, the production of formic acid may be inhibitory to the cell.
- Improving plasmid control. The low initial growth rates may be due to the metabolic burden imposed by a high copy number plasmid. Use of a vector with controlled copy number may thus improve the fermentation, by reducing the amount of time taken to reach high cell density.
- Reducing oxygen requirements. Chapter 5 showed that reducing the oxygen supply to the cell causes redox balance problems and reduced ATP supply, both of which impair PHB yield and production rate over the long term. Strategies to overcome these problems include:
  - Finding an alternative to pyruvate dehydrogenase which does not produce NADH. Examples of this are pyruvate-formate-lyase in conjunction with formate-hydrogen-lyase, or the aerobic formate dehydrogenase.
  - Reducing glucose uptake rate, by genetic manipulation or use of an appropriate feeding strategy.
- Alleviating the effects of locally oxygen-deficient zones caused by poor mixing. The influence of these zones on the cells might be avoided in several ways, for example:
  - cloning the haemoglobin gene from *Vitreoscilla* into the plasmid;
  - providing an alternative electron acceptor in the broth, such as nitrate.
- Initiating PHB synthesis without the need for oxygen limitation. Data from Chapters 2, 4, and 5 suggest that maintaining a high level of oxygen supply during the first few hours of PHB production leads to increased PHA enzyme levels. Consequently the PHB production rate and yield on glucose are improved. There are several ways that this may be achieved:
  - providing a more gradual onset of oxygen limitation, as shown in Chapter 2;
  - externally inhibiting the TCA cycle, thereby increasing the acetyl-CoA/CoA ratio and triggering PHB production;
  - reducing the growth rate to half of its unrestricted level, hence increasing plasmid copy number and PHA enzyme levels.
- The decay of cellular metabolism during the final phase of PHB production might be reduced by periodically adding small amounts of complex nutrients. This may replenish cellular enzymes and extend PHB production.
- Kinetic analysis suggests several metabolic alterations that may significantly improve PHB production:
  - increasing the ratio of acetyl-CoA to CoA;
  - increasing the total CoA thioester content of the cells;
  - to a lesser degree, increasing the NADPH/NADP ratio;
  - utilising mutants which maintain intracellular pH at low levels;
  - reducing medium osmolarity and hence increasing intracellular volume.

Appendix A Experimental Equipment and Analysis

Appendix A.1 Exhaust Gas Sampling Equipment

In order to obtain the average composition of the exhaust gas stream, an autosampling syringe was set up to fill continuously over the sampling period. This is possible because the total gas flowrate is constant and the mol fraction of argon in the exhaust gas is not appreciably affected by the levels of carbon dioxide production and oxygen consumption. One important feature of the equipment is that diffusion must be negligible, otherwise the sample will not be averaged properly.

The basic sampling syringe design is shown in Figure A.1

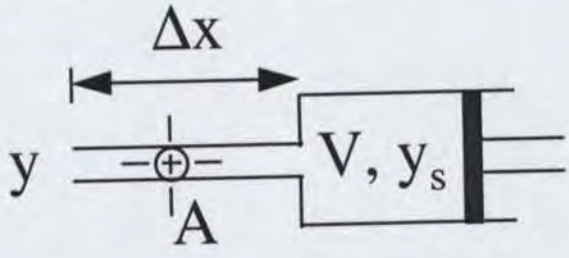

Figure A.1: Schematic diagram of gas-sampling syringe.

The tip of the syringe needle (left) is inserted into the exhaust gas stream and the plunger is smoothly withdrawn over the sampling period. A photograph of the apparatus is shown in Figure A.2.

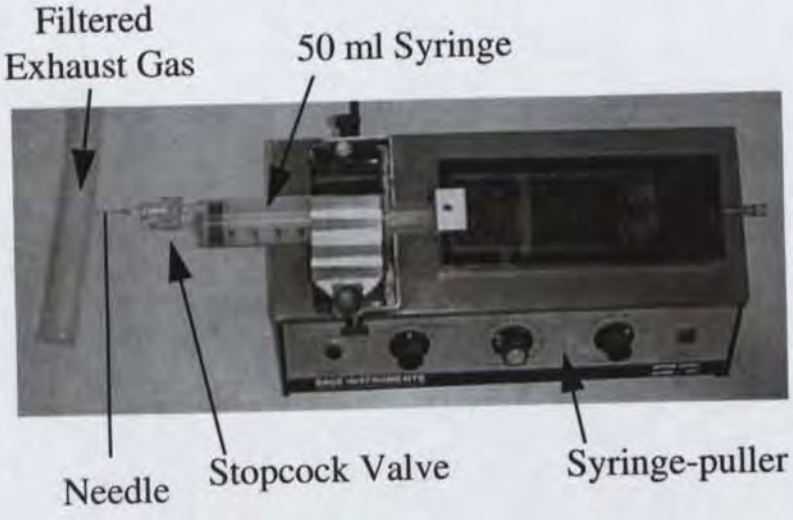

Figure A.2: Photograph of gas-sampling apparatus.

The design can be checked to ensure that diffusion will not results in appreciable error, as follows:

In Figure A.1 above,

y	= CO_2 concentration of sampled gas (mol fraction)
y_s	= bulk CO_2 concentration of syringe gas (mol fraction)
V	= current syringe volume (mm^3)
A	= cross-sectional area of syringe needle (mm^2)
Δx	= length of syringe needle (mm)

A mass balance on the syringe including equimolar counterdiffusion of CO_2 gives:

$$\frac{d(V.y_s)}{dt} = \frac{dV}{dt}y - D_{AB}\frac{(y_s - y)A}{\Delta x} \qquad (A.1)$$

where

D_{AB}	= diffusivity of CO_2 in air (mm^2s^{-1})

which rearranges to

$$V\frac{dy_s}{dt} = (y - y_s)\left(\frac{dV}{dt} + \frac{D_{AB}A}{\Delta x}\right) \qquad (A.2)$$

If we now define $V = mt$ where m is constant, and let

$$C = \left(\frac{dV}{dt} + \frac{D_{AB}A}{\Delta x}\right)$$

then Equation A.2 rearranges to

$$mt\frac{dy_s}{dt} + Cy_s = Cy$$

and solving this differential equation for y_s at time t_1 yields

$$y_s(t_1) = \frac{C}{mt_1^{C/m}}\int_0^{t_1} y(t)t^{C/m-1}.dt$$

i.e.,

$$y_s(t_1) = \frac{\int_0^{t_1} y(t)w(t).dt}{\int_0^{t_1} w(t).dt} \qquad \text{(A.3)}$$

where
$w(t)$ is a "weighting function" for the average composition:

$$w = t^{(C/m)-1} = t^{\frac{D_{AB}A}{\Delta x}\Big/\frac{dV}{dt}} \qquad \text{(A.4)}$$

For the case of no diffusion, w = 1 and hence the final syringe concentration y_s is the true average of y over the time period.
For the worst case with the apparatus in Figure A.1:
50 mL is collected in 2 hours, hence $\frac{dV}{dt} = 6.94\ \text{mm}^3\text{s}^{-1}$
D_{AB}= 16 mm^2s^{-1} at 25 °C (Incropera and deWitt (1996))
A = 0.12 mm^2
Δx = 50 mm

Substituting these values into Equation A.4 gives

$$w = t^{0.005533} \qquad \text{(A.5)}$$

The weighting therefore varies from an initial value of 1 to a final value of 1.050 according to Figure A.3.

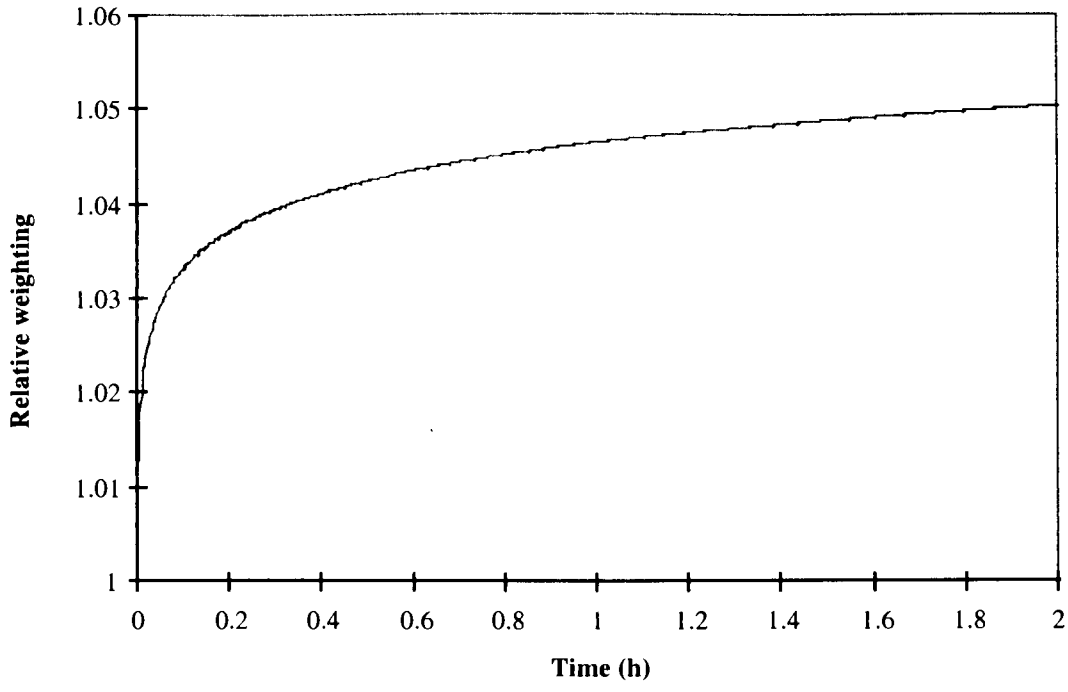

Figure A.3: Weighting function for gas-samples collected by the syringe-puller.

Oxygen and argon have comparable diffusivities to carbon dioxide and give a similar weighting function, hence the averaging error caused by diffusion is negligible.

Appendix A.2 Correction of CO_2 Production for Dynamic Mass-transfer Effects.

CO_2 produced by the respiring cells is excreted into the medium. Under non-steady-state conditions, some of this is transferred to the gas phase and the remainder is converted to carbonate and bicarbonate ions. This reaction scheme is shown pictorially in Figure A.4.

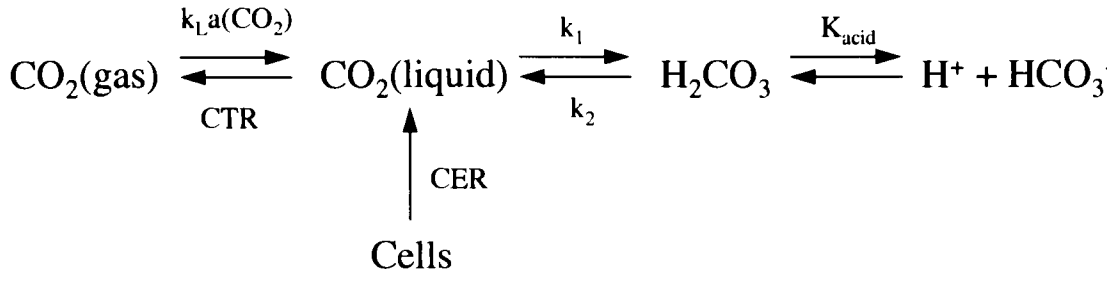

Figure A.4: Possible destinations of CO_2 in the bioreactor. CER = carbon dioxide evolution rate. CTR = carbon dioxide transfer rate to gas phase. $k_La(CO_2)$ is the volumetric mass-transfer coefficient for CO_2. k_1 and k_2 are kinetic constants. K_{acid} is an equilibrium constant.

The value of interest is the CO_2 production by the cells (CER), however analysing the exhaust gas concentration only detects the CO_2 transferred to the gas phase (CTR). Hence the gas measurement must be corrected to account for the solution dynamics.

The first step is a mol balance on CO_2, yielding Equation A.6.

$$CER = CTR + \frac{dm_{CO2(liquid)}}{dt} + \frac{dm_{H2CO3}}{dt} + \frac{dm_{HCO3-}}{dt} \qquad (A.6)$$

where

CER	= carbon dioxide evolution rate by the cells (mmol.s^{-1})
CTR	= carbon dioxide transfer rate to the gas phase (mmol.s^{-1})
m	= total moles (mmol)

At pH near 7, the concentration of H_2CO_3 (and CO_3^{2-}) is negligible, giving Equation A.7:

$$CER = CTR + V_L\left(\frac{dC_{CO2(liquid)}}{dt} + \frac{dC_{HCO3-}}{dt}\right) \qquad (A.7)$$

where

V_L	= broth volume (l)
C	= molar concentration (mmol.l^{-1})

Given that $\frac{dC_{H2CO3}}{dt} \approx 0$, the kinetic equation for production of HCO_3^- from CO_2(liquid) is Equation A.8 (Royce (1992)),

$$\frac{dC_{HCO3-}}{dt} = k_1 C_{CO2(liquid)} - k_2 C_{H2CO3} \qquad \text{(A.8)}$$

The H_2CO_3 dissociation reaction is extremely fast and is therefore assumed to be at equilibrium, giving Equation A.9:

$$C_{H2CO3} = \frac{10^{-pH}.C_{HCO3-}}{K_{acid}} \qquad \text{(A.9)}$$

where
K_{acid} = acid-base equilibrium constant

Finally, an appropriate expression for the CTR is given by Equation A.10,

$$CTR = k_L a(CO_2).V_a.\left(C_{CO2(liquid)} - \frac{P_{CO2}}{H_{CO2}}\right) \qquad \text{(A.10)}$$

where
$k_L a(CO_2)$ = volumetric mass-transfer coefficient for CO_2 (s^{-1})
V_a = aerated broth volume (l)
P_{CO2} = partial pressure of CO_2 in the gas phase (kPa)
H_{CO2} = Henry's law constant for CO_2 ($kPa.l.mmol^{-1}$)

The holdup time of the gas in the fermenter headspace is short (30 s) and has been ignored in this derivation.

The mass-transfer coefficient for CO_2 can be estimated from the coefficient for O_2 using Equation A.11,

$$k_L a(CO_2) = 0.89 k_L a(O_2) \qquad \text{(A.11)}$$

The aerated broth volume is assumed to be 5% higher than the actual broth volume, V_L.

The Henry's law constant for CO_2 at 30 °C can be estimated using Equation A.12 (Royce and Thornhill (1991)),

$$H_{CO2} = \exp\left(11.25 - \frac{395.9}{T - 175.9}\right) \qquad \text{(A.12)}$$

where
T = temperature (K)

Estimates for the parameters (at 30 °C) are obtained from Royce (1992) and Pinsent *et al.* (1956), viz

k_1 = 0.036 s^{-1}

k_2 = 39.05 s^{-1} (Royce (1992) states 0.6 s^{-1} at 37 °C, however this is a mistake arising from the absence of water concentration in their rate equation.)

K_{acid} = 2.5×10^{-4} (M^{-1}) at 28 °C

Equations 6.1 to 6.5 can be numerically integrated to solve for the CER given the measured CTR, pH, oxygen volumetric mass-transfer coefficient, and exhaust-gas composition. For the fermentations in this thesis, steady-state (95% change) CER = CTR is achieved after approximately five minutes. Hence the dynamic correction must be applied for short-term samples where the pH and/or CER are changing. In the case of longer sampling periods (e.g. hourly) the concentration of dissolved forms of CO_2 (typically 2 mM) is negligible with respect to the amount liberated to gas.

Appendix A.3 Acyl-CoA Rapid-sampling Equipment

A prerequisite for obtaining accurate acyl-CoA measurements is rapid sampling and deactivation: the turnover times of acetyl-CoA and 3-hydroxybutyryl-CoA are estimated at 0.7 s and 0.12 s respectively. The apparatus used to perform rapid sampling is shown in Figure A.5 and Figure A.6.

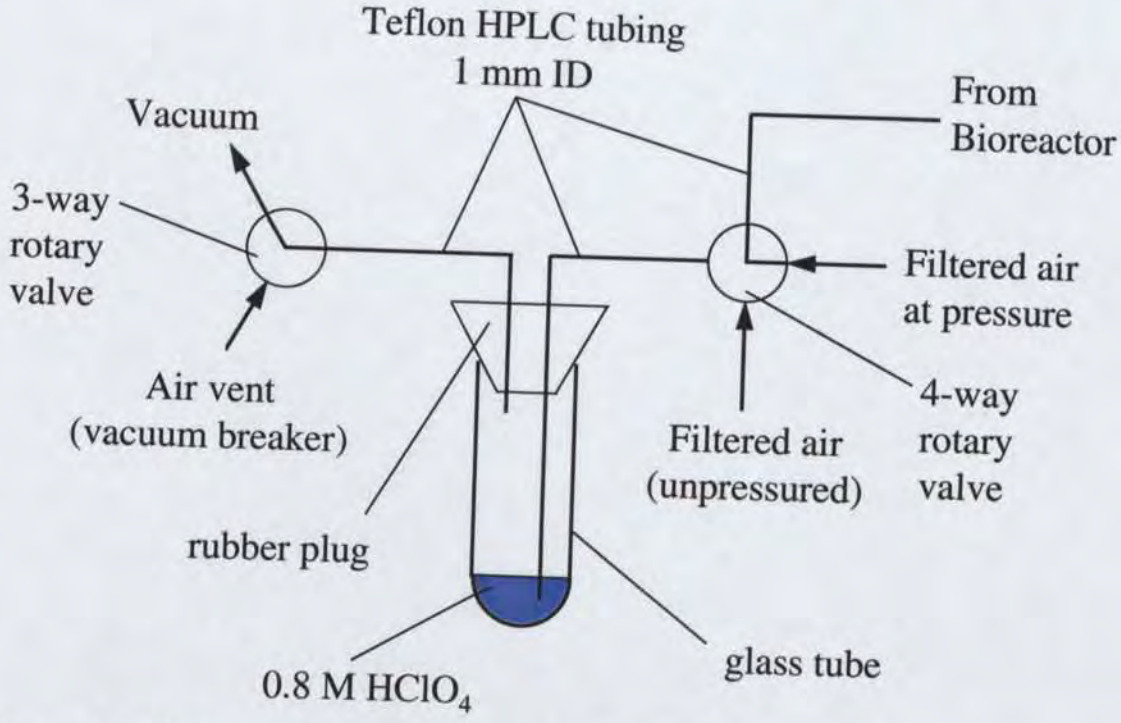

Figure A.5: Design of the rapid-sampling apparatus.

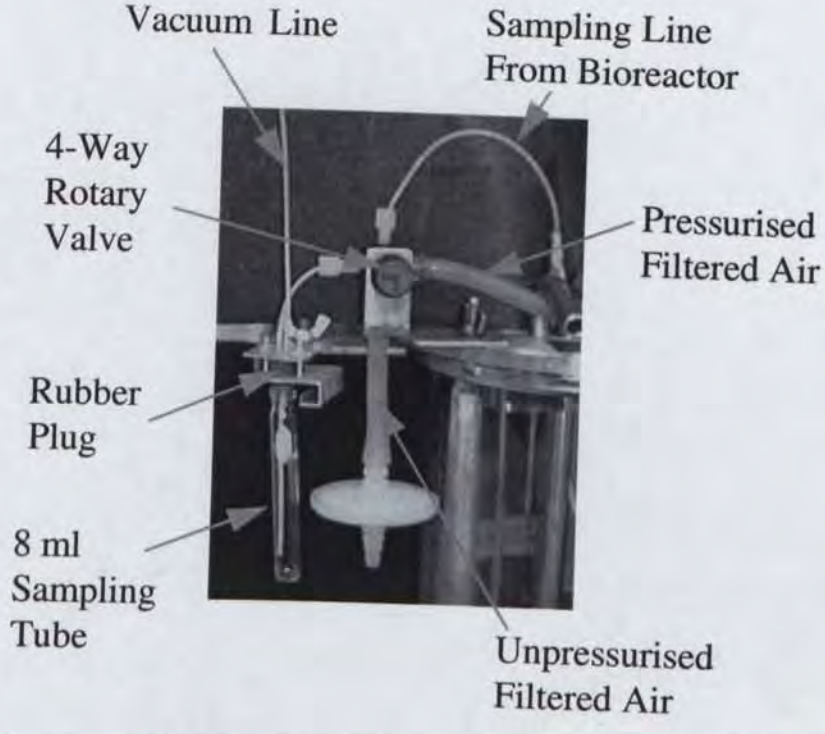

Figure A.6: Photograph of the rapid-sampling apparatus.

The operation of the apparatus is as follows:

1. Initially the 3-way rotary valve is set to connect the glass tube with the air vent, and the 4-way rotary valve is positioned to purge filtered air through the bioreactor sample line.
2. The glass tube containing chilled 0.8 M $HClO_4$ is wedged onto the rubber plug creating an airtight seal.
3. The 3-way valve is rotated to apply vacuum to the tube.
4. Once the tube is evacuated, the 4-way valve is briefly rotated to connect the tube with the bioreactor sample line and broth is drawn up through the lines to mix intimately with the $HClO_4$.
5. The 4-way valve is rotated back to the air-purge position, the tube vacuum is broken using the 3-way valve, and the tube is removed.
6. The sample lines are purged by fitting a waste tube to the plug, rotating the 4-way valve to the unpressured filtered air position and applying vacuum.
7. The valves are returned to their initial configuration (Step 1).

The entrance of the bioreactor sample line is located away from any baffles, at a point approximately 1/4 of the broth height above the bottom of the bioreactor and at a radial position halfway between the centreline and the bioreactor wall.

The measured residence time of broth in the sampling lines is approximately 0.2 s and the flowrate of sample is approximately 2.5 $ml.s^{-1}$.

Appendix B Intracellular Volume Estimation

This section shows the derivation of an expression for the intracellular volume of *E. coli*, used to estimate the volumetric concentration of acetyl-CoA and 3-hydroxybutyryl-CoA.

For the purposes of the analysis, several assumptions have been made

1. Acetyl-CoA and 3HB-CoA are confined to unbound cytoplasmic water.
2. The residual cell mass is composed of two fractions: a wall-associated component (e.g. lipopolysaccharide, associated membrane proteins) and a non-wall-associated component (e.g. RNA, soluble protein).
3. As the cell cytoplasm is filled with PHB granules, the non-wall-associated component is proportionally displaced. i.e. the concentration of the non-wall-associated components does not increase, and the cell shape does not change.
4. Periplasmic volume is not affected by accumulation of PHB.
5. The activity coefficient of the acyl-CoA metabolites is approximately constant.

Given these assumptions we can proceed with the first step, estimating the fraction of RCM which is wall-associated. Neidhardt and Umbarger (1996) give a breakdown of the dry weight of an average *E. coli* cell (*E. coli* B/r at 37, aerobic growth). Also shown is the estimated wall-associated-percentage of each fraction.

Table B.1: Breakdown of *E. coli* into wall-associated and non-wall-associated components.

	% of dry weight	% wall-associated	contribution to wall
protein	55.0%	12.5%	6.9%
RNA	20.5%	0%	0%
DNA	3.1%	100%	3.1%
lipid	9.1%	100%	9.1%
lipopolysaccharide	3.4%	100%	3.4%
peptidoglycan	2.5%	100%	2.5%
(others)		0%	0%
Total			25%

Kadner (1996) indicates that the cytoplasmic membrane contains 6-9% of the total cellular protein and comprises 60% of the protein in the cell envelope. Hence the cell envelope contains 10-15% of the total cellular protein.

Cayley *et al.* (1991) show the cytoplasmic volume of *E. coli* to be a linear function of medium osmolarity. For the control fermentation the osmolarity ranged from 0.3 OSM at the start to approximately 0.9 OSM by termination, giving estimates for cytoplasmic volume of 2.0 $ml.gRCM^{-1}$ and 1.3 $ml.gRCM^{-1}$ respectively. Of these, a constant amount (0.40 $ml.gDCW^{-1}$) is "bound" water, leaving free cytoplasmic water volumes of 1.6 $ml.gRCM^{-1}$ and 0.9 $ml.gRCM^{-1}$ respectively.

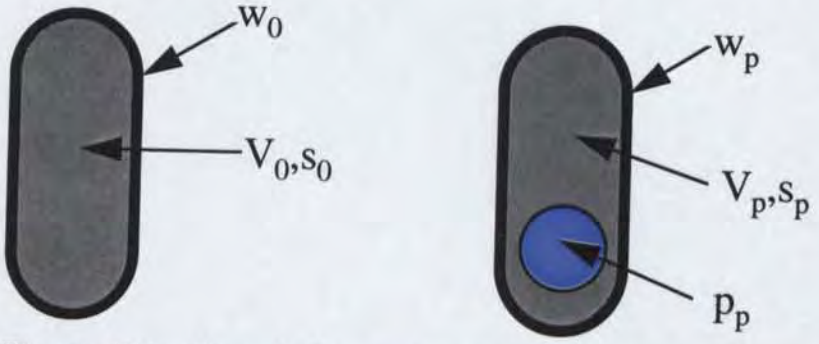

Figure B.1: Mass balance diagram for cells containing PHB granules.

Figure B.1 shows the condition of a cell before (subscript 0) and after (subscript p) the addition of a PHB granule, where

w	= dry weight of wall-associated components (g)
s	= dry weight of non-wall-associated components (g)
p	= weight of PHB granule (g)
V	= cytoplasmic volume (ml)

By a simple mass balance on the cell we obtain

$$r_0 = w_0 + s_0 \tag{B.1}$$

$$r_p = w_p + s_p \tag{B.2}$$

and

$$p_p = \frac{X}{(1-X)} r_p \tag{B.3}$$

where

r	= the total residual cell mass (g)
X	= PHB content of the total cell ($gPHB.gDCW^{-1}$)

Based on the assumption that the cell shape is unaltered and the non-wall-associated components have been proportionally displaced during growth, we obtain

$$V_p = V_0 - \frac{p_p}{\rho} \tag{B.4}$$

and

$$s_p = s_0 \frac{V_p}{V_0} \tag{B.5}$$

where

$$V_0 = \hat{V}_{lit} . r_0 \tag{B.6}$$

and

ρ = density of PHB granules ($g.ml^{-1}$) = 1.18 (Horowitz and Sanders (1995))

$\hat{V}_{lit}$ = literature value of free cytoplasmic water volume ($ml.gRCM^{-1}$)

These equations can be rearranged to give the final result:

$$\hat{V}_p = \hat{V}_{lit} + \frac{X}{\rho.(1-X)}\left(\frac{s_0}{r_0} - 1\right) \tag{B.7}$$

Appendix C Conditional Probability Distributions of Rate Equations

The following derivations show how to obtain the conditional probability distributions of variables in the 3-ketothiolase and 3-ketoacyl-CoA reductase rate equations, given that they must satisfy two constraints:

- PHB production rate is the same for both equations;
- acetoacetyl-CoA concentration is the same for both equations.

The proof is easier to understand if formulated using discrete variables, i.e. where each variable is divided into "bins". By applying the limit of bin size going to zero, the equivalent formulae for continuous variables can be obtained.

The value of each variable in the rate equation is not known with certainty. The best we can do is to assign a probability function for its possible values. When we use the rate equation to solve for acetoacetyl-CoA concentration, we therefore obtain a probability function. However if this is performed for both 3-ketothiolase and 3-ketoacyl-CoA reductase, we obtain two different probability functions. We therefore wish to revise the distributions of each variable, based on the knowledge that the acetoacetyl-CoA concentration must match for both rate equations. In other words, we need an expression for the conditional probability function of each variable given that the constraint is satistified.

We define X as a variable in the 3-ketothiolase rate equation, e.g. acetyl-CoA concentration. X is then partioned into n "bins" according to its probability function, where P(Xi) denotes the probability that X has a value within the i^{th} bin.

In a similar manner we define A as acetoacetyl-CoA concentration calculated using the 3-ketothiolase rate equation, and B as acetoacetyl-CoA concentration calculated using the 3-ketoacyl-CoA reductase equation. Each is partitioned into a number of "bins".

First we obtain an expression for the conditional probability of acetoacetyl-CoA concentration, $P(A_i|Satisfied)$

From the law of conditional probability,

$$P(Satisfied|A_i) = \frac{P(B_i \cap A_i)}{P(A_i)} \tag{C.1}$$

i.e. the probability that the equality condition is satisfied, given that the 3-ketothiolase equation yielded Ai, equals the probability that both 3-ketothiolase and 3-acyl-CoA reductase gave the same acetoacetyl-CoA concentration (Ai = Bi), divided by the probability of obtaining Ai from the 3-ketothiolase equation.

Since A and B are independent variables,

$$P(B_i \cap A_i) = P(A_i)P(B_i)$$

and hence

$$P(Satisfied|A_i) = \frac{P(A_i)P(B_i)}{P(A_i)} = P(B_i) \tag{C.2}$$

Applying the law of conditional probability twice, we observe that

$$P(A_i|Satisfied) = P(Satisfied|A_i)\frac{P(A_i)}{P(Satisfied)}$$

and therefore

$$P(A_i|Satisfied) = \frac{P(A_i)P(B_i)}{P(Satisfied)} \tag{C.3}$$

The partition thereom yields

$$P(Satisfied) = \sum_{k=1}^{n}\left(P(Satisfied|A_k)P(A_k)\right)$$

and substituting from Equation C.2 yields

$$P(Satisfied) = \sum_{k=1}^{n}\left(P(B_k)P(A_k)\right) \tag{C.4}$$

leading to

$$P(A_i|Satisfied) = \frac{P(A_i)P(B_i)}{\sum_{k=1}^{n}\left(P(B_k)P(A_k)\right)} \tag{C.5}$$

This is the "revised" probability distribution for acetoacetyl-CoA, and represents a more accurate estimate of the true acetoacetyl-CoA distribution than do either of the original estimates (A or B). Note that Equation C.5 is symmetrical in B and A, hence

$$P(A_i|Satisfied) = P(B_i|Satisfied)$$

(as of course it must be).

The next step is to obtain a conditional probability distribution for X, viz

$$P(X_i|Satisfied)$$

Once again we start from $P(Satisfied|X_i)$, observing that X and A are related by a joint probability function $P(A_k, X_i)$. (i.e. $P(A_k, X_i)$ is the probability of obtaining both A_k and X_i, as determined by the rate equation for 3-ketothiolase)

The law of conditional probability gives

$$P(Satisfied|X_i) = \frac{P(Satisfied \cap X_i)}{P(X_i)} \tag{C.6}$$

where (by the partition theorem)

$$P(Satisfied \cap X_i) = \sum_{k=1}^{n} \left(P(Satisfied|A_k \cap X_i) P(A_k, X_i) \right) \tag{C.7}$$

The criterion for satisfying the rate equations does not involve Xi, therefore

$$P(Satisfied|A_k \cap X_i) = P(Satisfied|A_k) \tag{C.8}$$

Substituting into Equation C.7 using Equation C.8 and Equation C.2 gives

$$P(Satisfied \cap X_i) = \sum_{k=1}^{n} \left(P(B_k) P(A_k, X_i) \right)$$

and hence

$$P(Satisfied|X_i) = \frac{\sum_{k=1}^{n} \left(P(B_k) P(A_k, X_i) \right)}{P(X_i)} \tag{C.9}$$

By applying the conditional probability theorem twice, we get

$$P(X_i|Satisfied) = P(Satisfied|X_i)\frac{P(X_i)}{P(Satisfied)}$$

and substituting from Equation C.9 and Equation C.4 we therefore obtain the final result:

$$P(X_i|Satisfied) = \frac{\sum_{k=1}^{n}\left(P(B_k)P(A_k, X_i)\right)}{\sum_{k=1}^{n}\left(P(B_k)P(A_k)\right)} \tag{C.10}$$

The joint probability function $P(A_k, X_i)$ is determined by the 3-ketothiolase rate equation. For variables in the 3-ketoacyl-CoA reductase equation the appropriate equation is

$$P(X_i|Satisfied) = \frac{\sum_{k=1}^{n}\left(P(A_k)P(B_k, X_i)\right)}{\sum_{k=1}^{n}\left(P(A_k)P(B_k)\right)} \tag{C.11}$$

Appendix D Derivation of Flux Analysis Equations

Consider the following system of chemical reactions:

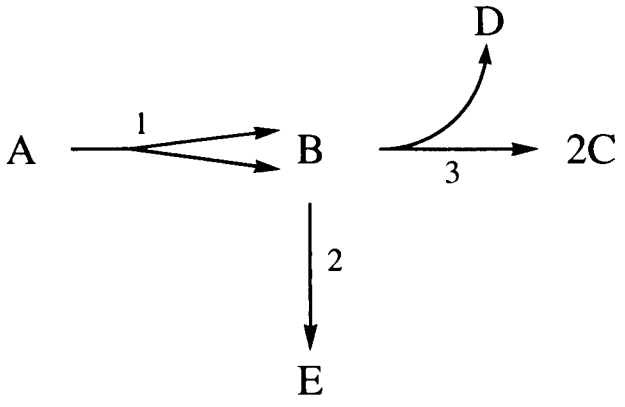

Figure D.1: A simple metabolic network.

This gives us the following mass balance equations:

A: $-x_1 = r_A$
B: $2x_1 - x_2 - x_3 = r_B$
C: $2x_3 = r_C$
D: $x_3 = r_D$
E: $x_2 = r_E$

where:

x	= flux, or rate of reaction ($mol.h^{-1}$)
r	= accumulation rate ($mol.h^{-1}$)

B is an intracellular metabolite. For this example we measure the accumulation rates of A, C, and E, and calculate the accumulation rate of D. The grouping of equations is therefore

Measured:

A: $-x_1 = r_A$
C: $2x_3 = r_C$
E: $x_2 = r_E$
or

$$\begin{bmatrix} -1 & 0 & 0 \\ 0 & 0 & 2 \\ 0 & 1 & 0 \end{bmatrix} \begin{bmatrix} x_1 \\ x_2 \\ x_3 \end{bmatrix} = \begin{bmatrix} r_A \\ r_C \\ r_E \end{bmatrix}$$

or

$$\underline{\mathbf{A}}_m \underline{\mathbf{x}} = \underline{\mathbf{r}}_m \qquad \text{(D.1)}$$

Calculated:

D: $x_3 = r_D$

or

$$\begin{bmatrix} 0 & 0 & 1 \end{bmatrix} \begin{bmatrix} x_1 \\ x_2 \\ x_3 \end{bmatrix} = \begin{bmatrix} r_D \end{bmatrix}$$

or

$$\underline{\mathbf{A}}_c \underline{\mathbf{x}} = \underline{\mathbf{r}}_c \tag{D.2}$$

Pseudo-steady-state:

B: $2x_1 - x_2 - x_3 = r_B$

or

$$\begin{bmatrix} 2 & -1 & -1 \end{bmatrix} \begin{bmatrix} x_1 \\ x_2 \\ x_3 \end{bmatrix} = \begin{bmatrix} 0 \end{bmatrix}$$

or

$$\underline{\mathbf{A}}_p \underline{\mathbf{x}} = \underline{0} \tag{D.3}$$

Row reduction of $\underline{\mathbf{A}}_p$ gives

$$\begin{bmatrix} 1 & -0.5 & -0.5 \end{bmatrix} \begin{bmatrix} x_1 \\ x_2 \\ x_3 \end{bmatrix} = \begin{bmatrix} 0 \end{bmatrix}$$

(For this simple example row-reduction does not eliminate any redundant constraints.) Thus there is one "dependent" variable, arbitirarily set to x_1 in this case.

Hence, writing the equations above in matrix form gives

$$\left[\begin{array}{c|cc} -1 & 0 & 0 \\ 0 & 0 & 2 \\ 0 & 1 & 0 \\ \hline 0 & 0 & 1 \\ \hline 1 & -0.5 & -0.5 \end{array}\right] \left[\begin{array}{c} x_1 \\ \hline x_2 \\ x_3 \end{array}\right] = \left[\begin{array}{c} r_A \\ r_C \\ r_E \\ \hline r_D \\ \hline 0 \end{array}\right]$$

or

$$\begin{bmatrix} \underline{\mathbf{A}}_{md} & \underline{\mathbf{A}}_{mi} \\ \underline{\mathbf{A}}_{cd} & \underline{\mathbf{A}}_{ci} \\ \underline{\mathbf{I}} & \underline{\mathbf{A}}_{pi} \end{bmatrix} \begin{bmatrix} \underline{\mathbf{x}}_d \\ \underline{\mathbf{x}}_i \end{bmatrix} = \begin{bmatrix} \underline{\mathbf{r}}_m \\ \underline{\mathbf{r}}_c \\ \underline{\mathbf{0}} \end{bmatrix} \tag{D.4}$$

The first row of this matrix equation can be written as

$$\underline{\mathbf{A}}_{md}\,\underline{\mathbf{x}}_d + \underline{\mathbf{A}}_{mi}\,\underline{\mathbf{x}}_i = \underline{\mathbf{r}}_m \tag{D.5}$$

and since we have defined

$$\underline{\mathbf{I}}.\underline{\mathbf{x}}_d + \underline{\mathbf{A}}_{pi}\,\underline{\mathbf{x}}_i = \underline{\mathbf{0}} \tag{D.6}$$

or

$$\underline{\mathbf{x}}_d = -\underline{\mathbf{A}}_{pi}\,\underline{\mathbf{x}}_i \tag{D.7}$$

this yields

$$\underline{\mathbf{A}}_{md}\left(-\underline{\mathbf{A}}_{pi}\,\underline{\mathbf{x}}_i\right) + \underline{\mathbf{A}}_{mi}\,\underline{\mathbf{x}}_i = \underline{\mathbf{r}}_m$$
$$\left(\underline{\mathbf{A}}_{mi} - \underline{\mathbf{A}}_{md}.\underline{\mathbf{A}}_{pi}\right)\underline{\mathbf{x}}_i = \underline{\mathbf{r}}_m$$

or

$$\underline{\mathbf{T}}.\underline{\mathbf{x}}_i = \underline{\mathbf{r}}_m \tag{D.8}$$

where

$$\underline{\mathbf{T}} = \underline{\mathbf{A}}_{mi} - \underline{\mathbf{A}}_{md}\,\underline{\mathbf{A}}_{pi} \tag{D.9}$$

Given the vector of measured rates $\underline{\mathbf{r}}_m$, this allows us to solve for $\underline{\mathbf{x}}_i$ using the equation

$$\underline{\mathbf{x}}_i = \left(\underline{\mathbf{T}}^T \underline{\mathbf{F}}_m^{-1} \underline{\mathbf{T}}\right)^{-1} \underline{\mathbf{T}}^T \underline{\mathbf{F}}_m^{-1} \underline{\mathbf{r}}_m \tag{D.10}$$

where

$\underline{\mathbf{F}}_m$ is the variance-covariance matrix of the measured rates.

and since

$$\underline{\mathbf{x}}_{\mathrm{d}} = -\underline{\mathbf{A}}_{\mathrm{pi}}\,\underline{\mathbf{x}}_{\mathrm{i}}$$

we obtain

$$\underline{\mathbf{x}} = \begin{pmatrix} \underline{\mathbf{x}}_{\mathrm{d}} \\ \underline{\mathbf{x}}_{\mathrm{i}} \end{pmatrix} = \begin{pmatrix} -\underline{\mathbf{A}}_{\mathrm{pi}}\left(\underline{\mathbf{T}}^{\mathrm{T}}\underline{\mathbf{F}}_{\mathrm{m}}^{-1}\underline{\mathbf{T}}\right)^{-1}\underline{\mathbf{T}}^{\mathrm{T}}\underline{\mathbf{F}}_{m}^{-1}\underline{\mathbf{r}}_{\mathrm{m}} \\ \left(\underline{\mathbf{T}}^{\mathrm{T}}\underline{\mathbf{F}}_{\mathrm{m}}^{-1}\underline{\mathbf{T}}\right)^{-1}\underline{\mathbf{T}}^{\mathrm{T}}\underline{\mathbf{F}}_{m}^{-1}\underline{\mathbf{r}}_{\mathrm{m}} \end{pmatrix} \tag{D.11}$$

Appendix E Standard Operating Procedures

Appendix E.1 PHB analysis by GC

Equipment used

Specific

- glass reaction tubes (8mL Kimax) with teflon-lined caps
- custom-made plastic "baking box" to enclose the tubes during baking
- Shimadzu GC-17A Gas Chromatograph with Class GC-10 V1.34 software
- Carbowax 20M (Chromosorb W-AW 60/80 mesh) packed column (6 foot by 1/8")

General

- dedicated autopipettes (200 uL, 1 mL, 5 mL)
- vortex mixer
- 100C oven
- freeze dryer
- centrifuge
- blunt needles (11 cm long) with luer-lock connector, 10 mL syringe
- 5 μL liquid syringe
- analytical grade chemicals: chloroform, methyl benzoate, sulphuric acid, methanol, poly-hydroxyalkanoate standards.

Sample Preparation

- Pipette a certain volume of broth into an 8mL GC reaction tube: aim for 4 - 10mg of Dry Cell Weight in the tube but do not use more than 6 mL. Record the volume added.
- Make the volume up to 6 mL using 0.7% w/v NaCl. For example. if 4 mL of sample was added in the previous step, then add 2 mL of 0.7% w/v NaCl.
- Mix thoroughly.
- Using the SM24 rotor, centrifuge the tubes at 1100g (3000 rpm) for 10 minutes.
- Remove the supernatant using an 11cm needle, taking care to avoid dislodging the pellet.
- Add 1 mL of MilliQ water to the tube.
- Repeat steps 1 to 6 for all tubes.
- Make up some standards as described in the Standards Preparation section below.
- Freeze dry the tubes as follows:
  - Tightly cap the tubes.
  - Lay each tube on its side in a foam box. The aim is to produce a 'shell' of ice along the wall of the tube.
  - Place dry ice on top of the tubes and leave until all tubes are frozen (1/2 hour will do it).
  - Loosen each cap: enough so that the tubes are not airtight, but not so much that the cap will lift off. Place a piece of autoclave tape to hold the cap in position but do not make the tube airtight.
  - Place the tubes in a rack, then place the assembly into a container with dry-ice.
  - Place the tubes in the freeze dryer and promptly apply the vacuum to avoid defrosting. For dryers with a chamber simply place the rack directly into the chamber. Other freeze

dryers have only a 'tree' with positions for round-bottom flasks. In this case, remove four GC tubes from the ice, place them into a round bottom flask (using a long-nosed set of pliers helps a lot here), attach to one of the positions on the freeze dryer tree, and apply the vacuum. Repeat for all remaining tubes.

- After a suitable period (varies according to the freeze dryer, generally overnight is enough) the sample pressure should be 0.1 mbar or less. Remove the tubes (using the pliers if necessary) and tightly cap them while storing.

- Preheat the oven to 100 °C.
- In a fume hood: to each GC tube, add 2mL chloroform, 2mL acidified methanol and 200 μL of internal standard. See below for reagent preparation.
- Seal each GC tube TIGHTLY with a cap. DO NOT USE CAPS WHICH ARE VISIBLY WEAKENED. During the baking procedure, the internal pressure of the tubes will reach 3-4 bar.
- Mix well by shaking vigorously.
- Place the GC tubes (broth samples and standard solutions) into the plastic reaction box and tape the lid securely shut. NB the plastic box will not withstand extended exposure to chloroform. Avoid spilling chloroform on it.
- Place the box into an oven at 100 °C for at least three and a half hours. Shake the box two or three times during the incubation.
- At the end of this time, remove the box and allow it (and the GC tubes) to cool to room temperature (an hour or so). DO NOT OPEN THE BOX BEFORE IT HAS COOLED.
- Once cooled, remove the GC tubes from the box. Add 1 mL of high purity reagent water ("Milli-Q") into each tube and agitate it with the vortex mixer for thirty seconds or so. Two phases should form after some settling time, with cell debris accumulating at the interface. Generally overnight is long enough for this to occur. The lower phase contains the PHB.

Reagents Used

1. analytical grade chloroform.
2. methanol containing 3% v/v sulphuric acid. WARNING: do not add the acid to methanol in a measuring cylinder, place the methanol in a beaker first. Otherwise it has a tendency to boil and shoot up the cylinder. This step must be done in a fume hood!
3. internal standard: dissolve methyl benzoate in methanol at a concentration of 5.5 g/kg.

Notes

- Freezing is ok for storing broth samples before PHA assay.
- The washing steps are necessary because several compounds in the medium give peaks that interfere with the butyrate and valerate peaks. In particular the interference is very bad for the valerate peaks. Washing with 0.7% NaCl instead of water is to reduce cell lysis from osmotic pressure, increasing PHA granule retention. The washing and resuspension also reduces the amount of water that must be removed during freeze-drying, which makes it possible to perform overnight.
- DO NOT CENTRIFUGE THE GC TUBES ABOVE 1100g. The tubes will crack if you go too much higher.
- A small amount of cell mass may decant with the supernatant, this is unavoidable unfortunately. Repeatability tests show that it probably does not introduce appreciable error.

- Adding 1mL of water before freeze-drying is necessary to give a more porous freeze-dried pellet. If the cells aren't resuspended then about 15% PHB is undetected and the standard error of measurements increases threefold.
- Freeze drying is necessary- oven drying results in some sample degradation, the samples turn black, and the resultant chromatograms are much messier. Also the freeze-drying method allows better release of PHB from the cells during methanolysis because the pellet is much more porous. It is necessary to pre-freeze the sample tubes because otherwise they boil over and spill sample everywhere when you apply the vacuum.
- The technique of producing an ice 'coating' along the wall of the tube is to prevent sample loss. If you freeze the samples as a solid plug at the bottom of the tube they will tend to boil over. Such plugs can climb their way out of the tube due to sublimating ice underneath the plug, and can also explode and shoot out of the tubes. Quite apart from sample loss this can damage the vacuum pump. The caps are left on the tubes to prevent sample loss, if they are loose then they don't interfere with the drying. It is necessary to tape them open because otherwise the vibrations of the freeze-dryer tend to make the caps tighten themselves shut, which prevents proper drying.
- The reaction box is necessary because the internal pressure of the tubes will reach 3-4 bar during baking. There are no commercially available tubes and caps specifically designed for this, hence the Kimax tubes are used. They seem to stand up to the conditions ok, but occasionally a tube or cap breaks during the procedure. Furthermore, if a tube were going to fail during baking, the most likely time of failure would be when it is picked up & moved. Therefore the purpose of the box is to prevent you being hideously scarred for life by hot acidified methanol and chloroform.
- Milli-Q water is used because even distilled water still contains appreciable quantities of impurities (eg organic compounds) which can potentially interfere with the analysis.

Standards Preparation

You will need four standards: 1mg, 2mg, 3mg and 4mg.

1. Weigh approximately 2 mg of PHA (PHB or PHBV as appropriate) into a sample tube and record the exact weight added.
2. Repeat for the other standards.

For best accuracy with this second method you should use a 5-decimal place mass balance.

GC analysis

1. Ensure that the GC is configured correctly to use the carbowax packed column.
2. Start up the GC, following the instructions next to the computer.
3. Load the appropriate method (eg PHA.met)
4. For each standard solution, inject exactly 2 μL of the bottom phase. See "Correct Injection Technique:" below. Try to avoid drawing any cell material into the syringe.
5. When the run is finished, view the chromatogram using "Post-Run Analysis" - "Single".
6. Calculate the ratio of butyrate (or valerate) peak area to internal std (methyl benzoate) peak area. Occasionally the GC software may have trouble integrating the peaks, you can use the 'manipulate' option to exert greater control over its behaviour.
7. Plot the standards' results to obtain a calibration curve.
8. For the other samples, inject exactly 2 μL of the bottom phase and find the peak area. Use the calibration curve to calculate the mass of PHBV present in the sample.

Notes

- Some syringes will not fit into the small GC tubes, in this case transfer some of the bottom phase to an eppendorf tube first.
- Good injection technique is essential for reproducible results. The syringe must be in good working order. Use the same injection volume for all samples. Although the internal standard can help compensate for injection errors it becomes less accurate if the injection volume ranges too widely.
- Always check correct syringe operation since they fail regularly.
- After you've finished for the day ALWAYS clean the syringe out with hexane 5-10 times. If you don't, then the PHA will deposit on the plunger and inside the barrel. If you're lucky this will only result in the syringe becoming clogged and stuck. If you're unlucky it will result in subtle injection volume errors leading to poor results.
- The standard deviation of your areas should be 2-4% or so. If not, something is wrong (eg leaky joints, leaky syringe, leaky septum, leaky FID nozzle, poor injection technique etc). NB also, after extensive use the column itself degrades: the peaks will start to tail and area calculations will be inaccurate since the GC software has trouble determining the end of a peak.

Correct Injection Technique:

The following example is for a 5 uL syringe. The procedure can of course be applied to other sizes.

1. Wash the syringe with sample by drawing up the full 5 uL then discarding to waste. Repeat 3-5 times. This step removes any residual washing liquid, the volume of which can be appreciable in small volume syringes.
2. Place the tip of the needle in the sample and 'pump' the syringe to remove air bubbles. This means drawing up 0.5 uL of sample and expelling it several times in quick succession.
3. Draw up the required volume of sample. Avoid touching the needle with your fingers because the heat from your hand can cause thermal expansion and lead to injection volume errors.
4. Wipe the needle with a tissue. This removes any sample adhering to the outside of the needle which would otherwise contaminate the septum. With some syringes the plunger is a loose fit in the barrel and you will need to be careful not to let the plunger slide around while you're performing this step.
5. Draw up an extra 0.5 uL of air. This is to prevent sample loss eg during septum puncturing or due to thermal expansion.
6. Insert the needle through the septum. Take care not to bend it! If it gets stuck you have hit the rim of the liner, so withdraw and try again.
7. Promptly inject the sample. The actual injection should be as quick as possible without bending the plunger. There are two reasons for this- firstly to avoid peak spreading which will occur if the sample isn't all loaded at once. Secondly, if the velocity of the liquid coming from the needle isn't high enough, drops will form on the tip of the needle and lead to incorrect volumes and septum contamination.
8. Promptly remove the needle. The needle should not remain in the port for any longer than necessary because the sample will continue to vaporise from the needle. This leads to peak spreading and greater detection of the more volatile components relative to the less volatile components, causing errors.
9. Wash the syringe 3-5 times by drawing up 5 uL of solvent (in this case chloroform) and expelling it to waste.

Appendix E.2 Acyl-CoA Sampling

Equipment used

Specific

- 8mL reaction tubes (Kimax), 2 per sample
- magnetic stirrer beads (micro-spinbars) that fit in the reaction tubes
- micro-peristaltic pump (Masterflex C/L model 77 120-60)
- peristaltic pump tubing (Cole Parmer Tygon 0.01" ID) joined to teflon HPLC tubing with a union piece
- micro-pH probe (Orion 9103 BN)
- sampling device (See Appendix A.3)
- 0.45 μm syringe-tip filters (Alltech 4mm nylon)
- Shimadzu HPLC system (SPD-10A UV detector, CTO-10A temperature-controlled oven, LC-10AD pump unit, FCV-10AL flow control valve unit, GT-102 degassing unit) with Class LC-10 V1.4 software
- Allsphere ODS-2 5U, 250mm x 4.6mm column
- Allsphere ODS-2 5U guard column

General

- a centrifuge that can be chilled to 0 °C
- blunt needles (11 cm long) with luer-lock connector
- several 10 mL luer-lock disposable syringes
- KOH pellets, 70% $HClO_4$
- -50 °C freezer
- 50 μL HPLC liquid-injection syringe

Preparation steps

- For each sample you will take, place 1.5mL of 0.8 molar perchloric acid into a GC reaction tube (8 mL). Weigh each tube with the cap on. Chill the tubes to 4 °C in the fridge. NB 0.8 molar is 6.875% by volume of 70% $HClO_4$.
- For each tube containing perchloric acid, obtain a corresponding empty GC reaction tube. Place a micro stirrer-bead into each empty tube. Store these tubes in the freezer (-20 °C).
- Make up 50 mL of 5 molar KOH and place into the fridge.
- Place a 100 mL container of milli-Q water into the fridge.
- Prechill the SM24 centrifuge rotor to 0 °C.
- Make at least two ice baths. (eg place an open-type tube rack into a beaker and fill with ice)
- Make a dry-ice/Ethanol bath.
- Setup the small peristaltic pump to deliver 5 M KOH.
- Plug in the micro-pH probe to equilibrate, then calibrate it.

Sampling

1. Remove the sampling tube(s) with perchloric acid from the fridge and place into an ice bath.
2. Make sure the vacuum line is correctly connected and the pump is running.

3. Rotate the four-way switch to purge air through the inlet sample line.
4. Remove a tube from the ice bath, undo the lid.
5. Fit the tube onto the sample outlet, ensuring a positive seal between the tube and the rubber stopper.
6. Fit the implosion shield (plastic syringe) over the tube and hang it from the ledge.
7. With your right hand, close the vacuum-breaking valve.
8. Wait a few seconds for vacuum to be achieved in the sample tube.
9. Rotate the sample valve anticlockwise by 90 degrees, to draw sample from the fermenter into the tube.
10. After approximately 2 mL of sample has been collected (1-2 seconds), rotate the valve 90 degrees clockwise, back to the inlet purge position.
11. Break the vacuum by opening the vacuum-breaking valve.
12. Remove the implosion shield, then remove the sample tube.
13. Cap the sample tube then return it to the ice bath. Start the timer.
14. Put the waste GC tube onto the sample outlet.
15. Fit the implosion shield.
16. Close the vacuum breaking hose valve.
17. Rotate the valve CLOCKWISE 180 degrees to the outlet-purge position.
18. After a few seconds, rotate the valve ANTICLOCKWISE 180 degrees to the inlet purge position.
19. Remove the implosion shield and the sample tube, then pour the waste into a kill bucket.
20. Remove the sample tube from the ice bath, wipe it dry, then weigh the tube and record it.
21. Replace the tube in the ice bath.

Neutralisation

1. After 5 minutes in the ice bath, place the sample tube(s) into the SM24 rotor (prechilled to 0 °C).
2. Spin for 5 minutes at 1100 RCF (3000 rpm). Turn the centrifuge brake off.
3. Gently remove the tubes from the rotor, taking care not to dislodge the pellet. Place the tubes into an ice bath.
4. For each tube: Using a syringe with 11cm-long needle attached, withdraw the supernatant and transfer it to a pre-chilled GC tube. (ie the ones containing a stirrer). Try to remove most of the supernatant but avoid sucking up cell mass.
5. Record both tube-numbers.
6. Draw up about 100 uL of cold milli-Q water into the syringe, swirl it gently, then add it to the supernatant from step 4. Do not use too much milli-Q because larger volumes in the test tube impair proper mixing during KOH addition.
7. Place the tube of supernatant into an ice-bath.
8. Place the first supernatant tube above the stirrer plate so that the stirrer bead is spinning freely. (Use the highest speed of the stirrer).
9. Slowly add the initial amount of 5 M KOH using an autopipette. (see notes)
10. Record the time that you added the KOH.
11. Insert the micro-pH probe so that the electrolyte-bridge is just below the surface of the liquid.
12. Insert the HPLC tubing into the tube so that the outlet is a centimetre or two below the surface of the liquid.
13. Using the variable speed control on the pump, adjust the pH of the solution to 3.5 +/- 0.05. DO NOT OVERSHOOT. See the notes section below for more detail.
14. Recap the tube and place into the dry ice/ethanol bath.
15. Repeat steps 8 to 14 for each tube.

16. When the tubes are frozen solid, place into a dry-ice container in the freezer.

Sampling Notes

- Perchloric acid is corrosive. In all steps of the procedures above, wear gloves and other appropriate protective gear. When making up the 0.8 molar solution, use the fume hood.
- Take care during sampling to avoid loss-of-containment of the culture broth.
- The purpose of the implosion shield is to guard against damage should a tube fail under vacuum. An implosion could otherwise badly cut your hand, simultaneously contaminating it with both perchloric acid and bacterial culture.
- When placing GC tubes in the freezer, ensure that they are not wet on the outside otherwise they may become frozen into the tube rack.
- You can reuse the syringes and needles but make sure they are thoroughly rinsed with milli-Q between samples. They do not need to be dried.
- During the sampling and neutralisation procedure, it is important to keep the tubes cold: this minimises degradation of the metabolites.
- Depending on how well buffered the solution is, the approach to pH 3.5 is quite finicky. If the solution overshoots pH 6 during the neutralisation step, the sample will be destroyed. There are a few steps that you should take to avoid this:
  - Do a rough test beforehand on a junk sample to determine the approximate volume required, then use about 80% of this value to add initially using an autopipette. Note that as the fermentation progresses this initial dose will become increasingly less, due to greater buffering action by the excreted acetate and lactate.
  - Do not add the KOH too quickly, because the stirrer bead's mixing is not perfect.
  - To improve mixing & pH meter response time you can gently slide the pH probe up and down within the tube during KOH addition.
  - If you overshoot pH 3.5 by a small amount (up to about pH 5), you can add a little $HClO_4$ solution to reduce it. The easiest way to do this is to place a tiny drop from an autopipette onto the tip of the probe itself, then immerse in the solution. (Individual drops from the autopipette tip are generally too large.)
- The sample is initially neutralised to pH 3.5 (instead of pH 4.0) in order to reduce the pH increase during freeze-drying: during the drying, acetic acid and lactic acid are removed. A solution with acetate ions will liberate acetic acid by removing protons from water to generate OH^-. In contrast, un-ionised acetic acid will not cause a pH change. Hence, the greater the ratio of ionised to un-ionised acid (ie the higher the initial pH), the greater the pH change during drying.
- DO NOT leave KOH sitting in the tubing for days at a time, it will cause blockages and force you to replace the tubing. Flush the tubing with water before storage.

Analysis Pretreatment

1. Freeze-dry the samples to remove all water. See the section on PHB analysis by GC for info on how to freeze-dry samples properly.
2. Store in the -70 °C freezer until ready to analyse (as soon as possible).

For each sample:

1. Add 1 mL of room-temperature MilliQ water to the tube.
2. Vortex the tube to remove any deposits adhering to the walls.
3. Insert the micro-pH probe and adjust the sample's pH back to 4.00 +/-0.05 using either KOH or $HClO_4$ as appropriate. (See the section on Neutralisation, above)
4. Centrifuge at 3000 rpm (1111 RCF) for 5 mins, in the SM24 rotor (prechilled to 0 °C).

5. Using a syringe with 11mm-long needle attached, withdraw the supernatant. Avoid sucking up any precipitate.
6. Pull a small bubble of air into the syringe, remove the needle, and filter the solution through a 0.45 μm syringe filter (low-dead volume type) into an eppendorf tube.
7. Place the eppendorf into a container of dry ice.

HPLC Analysis

1. Five minutes before the sample is due, remove the eppendorf from the dry ice and defrost using body heat (ie holding in your hand).
2. Inject 20 μL of sample, rinsing the syringe twice beforehand.
3. Wash the syringe five times with MilliQ.
4. Immediately replace the eppendorf in the dry ice container.

Method details:

- 40 °C oven
- flowrate 0.5 mL/min
- gradient = linear: 0 min = 100%A, 8 min = 94.9%A, 14 min = 82.1%A, 20 min = 64.1%A, 32 min = 0%A, 42 min = 0%A, 45 min = 100%A, 55 min = 100%A and end of run.
- UV detection at 254 nm

HPLC Notes

- At the end of each day, flush the column with 20 column volumes of aqueous wash (10% Methanol) then flush with 5 column volumes of 90% Methanol. (Do not use pure water, this will repel the C18 chains causing them to lie flat and trap salts.)
- Do not switch directly from KH_2PO_4 buffer to organic solvent: the KH_2PO_4 will precipitate out and cause blockages.
- After each run, flush a small quantity of water through the washing tube: this will remove any leaked salts from behind the pump seals, prolonging their life.

HPLC Buffers

Depending on the analytes you wish to measure, one (or both) of the following buffer types will be required:

Buffer Type 1
Buffer A1: 6%v/v of (98%v/v Methanol + 2%v/v Chloroform) + 94% water. 100 mM KH_2PO_4 + 10 mM formate, pH 4
Buffer B1: 45%v/v of (98%v/v Methanol + 2%v/v Chloroform) + 55% water. 70 mM KH_2PO_4 + 10 mM formate, pH 4

Buffer Type 2
Buffer A2: 6%v/v of (98%v/v Methanol + 2%v/v Chloroform) + 94% water. 250 mM KH_2PO_4 + 10 mM formate, pH 4
Buffer B2: 45%v/v of (98%v/v Methanol + 2%v/v Chloroform) + 55% water. 95 mM KH_2PO_4 + 10 mM formate, pH 4

Recipes:
Make up organic solution, 98%v/v Methanol + 2%v/v Chloroform, equivalent to 96.3%w/w Methanol + 3.7%w/w Chloroform.

Then make up buffers according to the following table

	KH_2PO_4 (w/w)	water (w/w)	formic acid (μL/kg)	5M KOH	organic solution (w/w)
A1	1.358%	93.80%	376	Adjust pH to 4.0	4.843%
B1	1.031%	59.55%	409	Adjust pH to 4.0	39.42%
A2	3.327%	91.93%	369	Adjust pH to 4.0	4.747%
B2	1.395%	59.33%	407	Adjust pH to 4.0	39.27%

Adjust the pH to 4.0 BEFORE adding organic solution.
Filter each buffer before use and store in an airtight bottle. The buffers will last almost indefinately.
Use only HPLC grade chemicals.

Appendix E.3 Measuring Offgas CO_2 & O2 using GC-MS

This SOP is written for a Hewlett-Packard GC-MS (6890 GC, 5973 MS).

GC-MS setup:

Almost any column packing is suitable, the current column in use is an AT1000 25m x 0.25 mm. Column flow is 1.2 mL He/min, split ratio is 50:1. Column temperature is 60 °C. A 50 μL gas-sampling syringe is used. The MS is tuned for maximum sensitivity and operated in SIM mode for ions 32 (O_2), 40 (Ar), and 44 (CO_2), with a 20 ms dwell time. The method length is 30 minutes.

Sample measurement (for sampling-valve injection)

Setup

1. Mount the sampling valve assembly on the GC-MS, inserting the needle through the septum.
2. Connect the Helium line to the regulator.
3. Connect the other end of the helium line to the valve assembly but do not tighten the nut yet.
4. Adjust the regulator to approximate 225 kPa.
5. Crack open the valve next to the regulator. Allow gas to purge through the line for a few seconds.
6. Shut the valve, tighten the nut holding the helium line to the valve assembly.
7. Open the valve and thoroughly check for leaks in the sampling valve assembly, using soapy water. If you neglect this step you could find your entire supply of He gone in two days.
8. Turn the sample-valve to the "inject" position (ie the gas flows through the valve into the GC injection port. Allow to purge through for a couple of hours. (If you neglect this step, residual air in the helium line will cause baseline problems.)

Injection

1. Click on the large green "start" arrow.
2. Type an appropriate filename under Data File Name.
3. Click OK
4. Attach the sample syringe to the loading port (luer lock fitting)
5. Rotate the sample valve 90 degrees to the "load" position, then push about 10 mL of gas through.
6. Rotate the sample valve 90 degrees to the "inject" position.
7. Wait for about 20 seconds.
8. Rotate the sample valve 90 degrees to the "load" position. Push a few mL of gas through.
9. Rotate the sample valve 90 degrees to the "inject" position.
10. Wait about 20 seconds.
11. Repeat steps 8 to 10 another 4 times.
12. Repeat steps 4 to 11 for each sample you're analysing.
13. Press the Stop button to finish the run.

Notes:

- The peak heights should be no larger than $1x10^6$, else nonlinearity occurs. However if your injection volume is too small, the CO_2 and/or Ar areas may become inaccurate. Adjust the

regulator pressure (or the needle valve if necessary) to give you a peak height of approximately 1×10^6.
- Do not inject more frequently than every 20 seconds, else the peaks will tend to run together.

Standards:

There are several standards you should use:
- fermenter inlet gas, one for each sample. This is critical, because oxygen usage is very sensitive to small changes in inlet gas composition. Measuring inlet gas also compensates for calibration drift (the MS does tend to drift by 0.1% or so over a few hours).
- (ambient air, for O_2 calibration)
- a CO_2 standard. This can be made up as follows:
  - Obtain the 5.36 L bottle with the rubber-septum in the lid.
  - Purge the bottle with compressed air for 15 minutes or more.
  - Zero the 0.000g balance with an eppendorf tube on it.
  - Place a small chunk of dry ice (approx 200 mg) into the eppendorf, close the lid, weigh, then place into the bottle and seal the lid. You have about 20 s until the eppendorf lid is popped off by the CO_2 pressure.
  -Shake the bottle around to mix up the gas, then allow to reach thermal equilibrium (10 mins or so)

Peak analysis

1. Load the "Enhanced Data Analysis" program.
2. Under the Chromatogram menu, choose Select Integrator then click the ChemStation Integrator.
3. Chromatogram_Display-Ion-Chromatograms-In-Merged-Format
4. Open the appropriate datafile (File-Open)
5. Chromatogram_Extract Ion-Chromatograms. Enter ions 32, 40, 44.
6. Chromatogram_Integrate
7. Chromatogram_Integration Results
8. Copy the table to a text file. Click Done
9. Repeat step 8 for m/z = 40 and 44.

The ratios 32/40 and 44/40 for each sample should have a std deviation of 0.2% or better.
If the data analysis doesn't detect small peaks (eg CO_2 in inlet gas) you will need to adjust the integration parameters until it does. Integration parameters that seem to work well are:
Initial Area Reject = 0
Initial Peak Width = 0.020
Shoulder Detection = Off
Initial Threshold = 13.0

Shutdown

When leaving the GC-MS unused for any length of time, it **must** either remain switched on or be shut down as described below. The MS can be damaged (by air and water) if it is not properly shut down.

1. Switch to the Diagnostics/Vacuum Control view. (View_Diagnostics/Vacuum Control).
2. Select Vent from the Vacuum menu. Allow the MS to cool.
3. Crack open the vent valve on the MS, allow to vent completely, then close again.

4. Remove the column from the MS transfer line by undoing the interface nut.
5. Cap the column using a glass capillary cap.
6. Use a capping ferrule (no hole) with an interface nut to seal the MS transfer line.
7. Select Pump Down from the Vacuum menu. Wait for vacuum to be achieved.

Select Vacuum_Vent again, but do not open the vent valve.

Appendix F Nomenclature

Abbreviations

3HB-CoA	= 3-hydroxybutyryl-CoA
AccoA	= acetyl-CoA
CON	= control fermentation (Chapter 4)
EtOH	= ethanol
GLC	= glucose
Hac	= acetic acid
HCDF	= "high cell density" fermentation (Chapter 2)
HLA	= lactic acid
HOF	= "high oxygen" fermentation (Chapter 5)
LOF	= "low oxygen" fermention (Chapter 5)
PHA	= poly(hydroxyalkanoate)
PHB	= poly(3-hydroxybutyrate)
PHBV	= poly(3-hydroxybutyrate-co-3-hydroxyvalerate)
PHV	= poly(3-hydroxyvalerate)
PSF	= "pH-stat" fermentation (Chapter 6)
PYR	= pyruvic acid

Greek Symbols

α_C	= coefficient of CO_2 in the biomass-generation flux equation
$\underline{\delta}$	= vector of residuals for flux analysis
$\underline{\Delta}$	= residual-calculation matrix for flux analysis
$\Delta\hat{H}_c^\circ$	= standard heat of combustion (kJ.(mol-C)$^{-1}$)
ΔH_i	= heat of combustion of the ith compound at 30 °C, approximately equal to the standard heat of combustion (kJ.mol^{-1})
Δr	= mass of analyte produced (g)
ΔT_1	= temperature difference of entering cooling water (K)
ΔT_2	= temperature difference of exiting cooling water (K)
ΔT_{lm}	= log mean temperature driving force (K)
Δx	= length of syringe needle (mm)
γ	= average mass-sampling factor over a given sample period
γ_A	= coefficient of ATP in the biomass-generation flux equation
γ_k	= mass -sampling factor at sample k.
γ_N	= coefficient of NADH in the biomass-generation flux equation
γ_P	= coefficient of NADPH in the biomass-generation flux equation
κ^*	= "degree of reduction" of analyte
ρ_{PHB}	= density of PHB granules (g.ml^{-1})
ρ_{solids}	= density of solids (kg.m^{-3})
ρ_{water}	= density of water (kg.m^{-3})
$v_{synthase}$	= rate of reaction (mM.h^{-1})

Alphanumeric Symbols

A = heat-exchanger area ($m^2.kl^{-1}$)

$\underline{\mathbf{A}}$ = the stoichiometric matrix embodying a mass balance on each metabolite

A = cross-sectional area of syringe needle (mm^2)

$\underline{\mathbf{A}}_{pi}$ = the matrix relating the "dependent" and "independent" fluxes

C = concentration of analyte ($g.kg(broth)^{-1}$)
or glucose concentration ($kg.kl^{-1}$)
or molar concentration ($mmol.l^{-1}$)

$\underline{\mathbf{C}}_d = \begin{pmatrix} \underline{\mathbf{I}} \\ \underline{\mathbf{0}} \end{pmatrix}$

CER = carbon dioxide evolution rate by the cells ($mmol.s^{-1}$)

$\underline{\mathbf{C}}_i = \begin{pmatrix} \underline{\mathbf{0}} \\ \underline{\mathbf{I}} \end{pmatrix}$

$C_{O2,broth}$ = molar concentration of oxygen in the broth ($mmol.l(broth)^{-1}$)

$C_{supernatant-basis}$ = concentration of analyte ($g.kg(supernatant)^{-1}$)

$C_{total-broth-basis}$ = concentration of analyte ($g.kg(broth)^{-1}$)

CTR = carbon dioxide transfer rate to the gas phase ($mmol.s^{-1}$)

D_{AB} = diffusivity of CO_2 in air (mm^2s^{-1})

f = fraction of inlet oxygen which is utilised.

$flux$ = flux through a metabolite pool ($\mu mol.gRCM^{-1}.s^{-1}$)

$\underline{\mathbf{F}}_m$ = variance-covariance matrix of the measured accumulation rates.

$\underline{\mathbf{F}}_{Xi}$ = variance-covariance matrix of the independent fluxes

G = extra glucose imported and converted to acetic acid, ethanol and formic acid ($mmol.gRCM^{-1}h^{-1}$)

H_{CO2} = Henry's law constant for CO_2 ($kPa.l.mmol^{-1}$)

h_δ = error statistic for flux analysis

H_{O2} = Henry's law constant for oxygen ($kPa.l(broth).mmol^{-1}$)

k = ratio of gas specific heat at constant pressure to gas specific heat at constant volume

K_{acid} = acid-base equilibrium constant

k_La = volumetric mass transfer coefficient of oxygen (h^{-1})

$k_La(CO_2)$ = volumetric mass-transfer coefficient for CO_2 (s^{-1})

K_m = effective Michaelis-Mention kinetic constant (μM).

m = mass of broth on a no-sampling basis (kg)
or total moles (mmol)

m_{actual} = actual mass of broth in bioreactor (g)

$\dot{m}_{solids}$ = mass flowrate of solids to dryer ($kg.s^{-1}$)

$\hat{m}_{supernatant}$ = mass of supernatant per mass of broth ($kg.kg(broth)^{-1}$)

m_{total} = per-batch mass of glucose used during fermentation (kg)

$\dot{m}_{water}$ = water evaporation rate ($kg.s^{-1}$)

N_a = molar flow of air ($mol.s^{-1}$)

n_{air} = molar flow of gas ($mol.s^{-1}$)

N_e = molar flow of enriched air with 85% oxygen content ($mol.s^{-1}$)

N_i = molar flow of gas to bioreactor ($mol.s^{-1}$)

$\dot{n}_i$ = net consumption rate of the ith analyte ($mol.s^{-1}kl(broth)^{-1}$)

N_{O2} = consumption rate (=mass transfer rate) of oxygen (mmol.l(broth)$^{-1}$h^{-1})

P = PHB production rate (mmol.gRCM^{-1}h^{-1})

$P(A, X)$ = joint relative frequency distribution for the variable and the original acetoacetyl-CoA concentration, as determined from the rate equation for 3-ketothiolase

$P(B, X)$ = joint relative frequency distribution for the variable and acetoacetyl-CoA concentration, as determined from the rate equation for 3-ketoacyl-CoA reductase

$P(X_i | Satisfied)$ = relative frequency of the ith bin of the X variable's revised histogram

P_1 = intake gas pressure (bar) = 1 bar

P_2 = delivery gas pressure (bar)

$P_{bioreactor}$ = operating pressure (kPa)

P_{CO2} = partial pressure of CO_2 in the gas phase (kPa)

P_{O2} = average partial pressure of oxygen in the gas phase (kPa)

$P_{O2,inlet}$ = partial pressure of oxygen in the gas phase (kPa)

p = weight of PHB granule (g)

q = heat removal rate (kW.kl^{-1})

Q_C = centrifuge flowrate (m^3.h^{-1})

Q_{Cref} = reference flowrate (m^{3}h^{-1}) = 1.6 m^{3}h^{-1}

Q_{dryer} = flowrate to dryer (m^3.s^{-1})

$Q_{transfer}$ = heat removal via exchanger surfaces (kW.kl(broth)$^{-1}$)

r = the total residual cell mass (g)
or reaction velocity (mM.h^{-1})

$\underline{\mathbf{r}}$ = column vector of metabolite accumulation rates.

$\dot{r}$ = external addition of analyte (g), for example glucose feed

R = gas constant (8.314 J.K^{-1}mol^{-1})

r_{max} = maximum forward reaction rate (mM.h^{-1})

R_X^Y = response coefficient of Y to X

s = dry weight of non-wall-associated components (g)

$\frac{s_0}{r_0}$ = ratio of non-wall-associated residual cell mass to total residual cell mass

S_{actual} = actual mass withdrawn from bioreactor between samples n and n+1 (g)

$\underline{\mathbf{T}}$ = solution matrix for flux analysis

T = temperature (K)

t_t = turnover time (s)

U = overall heat transfer coefficient, assumed 2.4 kW.m^{-2}K^{-1}

V = volume per batch (kl)
or current syringe volume (mm^3)
or cytoplasmic volume (mL)

V_a = aerated broth volume (l)

V_L = broth volume (l)

$\hat{V}_{lit}$ = literature value of free cytoplasmic water volume (ml.gRCM^{-1})

$\hat{V}_{nominal}$ = literature intracellular volume (ml.gRCM^{-1}), a function of medium osmolarity

$\hat{V}_{true}$ = true intracellular volume (ml.gRCM^{-1})

w	= dry weight of wall-associated components (g)
W_{air}	= ideal power (W)
W_C	= centrifuge power requirement (kW)
W_{Cref}	= reference power requirement (kW) = 27 kW
$w(t)$	= a "weighting function" for the average composition obtained by gas sampling
$\underline{\mathbf{x}}$	= vector of fluxes
X	= input variable (e.g. acetyl-CoA/CoA ratio) **or** oxygen consumption rate (mmol.gRCM^{-1}h^{-1}) **or** PHB content of the total cell (gPHB.gDCW^{-1})
$[x]$	= acyl-CoA concentration or PHB rate, on an intracellular-volume basis (μM or μM.h^{-1} respectively)
$\hat{x}$	= acyl-CoA concentration or PHB rate, on an RCM basis (μmol.gRCM^{-1} or μmol.gRCM^{-1}h^{-1} respectively)
x_i	= molar composition of gas to bioreactor
$X_{O2,inlet}$	= oxygen mole fraction in inlet air
X_{PHB}	= mass fraction PHB in cell
y	= CO_2 concentration of sampled gas (mol fraction)
Y	= system response to a perturbation
y_s	= bulk CO_2 concentration of syringe gas (mol fraction)
Y_{xATP}	= molar requirement of ATP per g RCM of biomass
Y_{xNAD}	= molar requirement of NADH per g RCM of biomass
Y_{xNADPH}	= molar requirement of NADPH per g RCM of biomass

Appendix G References

H. Abe, I. Matsubara, Y. Doi and Y. Hori (1994), "Physical properties and enzymatic degradability of Poly(3-hydroxybutyrate) stereoisomers with different stereoregularites" *Macromolecules*, **27**(21):6018.

H. Abe, I. Matsubara and Y. Doi (1995), "Physical properties and enzymatic degradability of polymer blends of bacterial poly [(R)-3-hydroxybutyrate] and poly [R,S)-3-hydroxybutyrate] stereoisomers" *Macromolecules*, **28**(4):844-853.

A.J. Anderson and E.A. Dawes (1990), "Occurrence, metabolism, metabolic role, and industrial uses of bacterial polyhydroxyalkanoates" *Microbiological Reviews*, **54**(4):450-472.

A.J. Anderson, G.W. Haywood and E.A. Dawes (1990), "Biosynthesis and composition of bacterial poly(hydroxyalkanoates)" *International Journal of Biological Macromolecules*, **12**(April):102-105.

A.A. Aristidou, K.Y. San and G.N.Bennett (1995), "Metabolic engineering of *Escherichia coli* to enhance recombinant protein production through acetate reduction." *Biotechnology Progress*, **11**(4):475-478.

B. Atkinson and F. Mavituna (1987), "Biochemical Engineering and Biotechnology Handbook", 2nd Edition, Macmillan, England.

J.E. Bailey (1991), "Toward a science of metabolic engineering" *Science*, **252**:1668-1675.

P.J. Barham (1990), "Physical properties of poly(hydroxybutyrate) and poly(hydroxybutyrate-co-hydroxyvalerate)" *in* E.A. Dawes (ed), "Novel Biodegradable Microbial Polymers", Kluwer Academic Publishers, Dordrecht.

P.J. Barham, P. Barker and S.J. Organ (1992), "Physical properties of poly(hydroxybutyrate) and copolymers of hydroxybutyrate and hydroxyvalerate" *FEMS Microbiology Reviews*, **103**(2-4):289-298.

M.V. Bartow (1999), "Supersizing the aerobic fermentor" *Chemical Engineering*, **1999**(July):70-75.

C. Bastioli (1995), "Starch-polymer composites" *in* G. Scott and D. Gilead (eds), "Degradable Polymers: Principles & Applications", 1st Edition, Chapman & Hall, Cambridge, England, Chapter 6.

C. Bastioli, F. Degli Innocenti, I. Guanella and G. Romano (1995), "Compostable films of Mater-Bi Z grades" *in* A.C. Albertsson and S.J. Huang, "Degradable Polymers, Recycling, and Plastics Waste Management", 1st Edition, Marcel Dekker, New York.

E. Berger, B.A. Ramsey, J.A. Ramsay, C. Chavarie and G. Braunegg (1989), "PHB recovery by hypochlorite digestion of non-PHB biomass" *Biotechnology Techniques*, **3**:227-232.

A. Bock and G. Sawers (1996), "Fermentation" *in* F.C. Neidhardt *et al.*, "*Escherichia coli* and *Salmonella Typhimurium*", 2nd Edition, ASM Press, Washington DC, Chapter 18.

H.P.J. Bonarius, G. Schmid and J. Tramper (1997), "Flux analysis of underdetermined metabolic networks: the quest for the missing constraints" *Trends in Biotechnology*, **15**:308-314.

K.M. Bonthrone, J. Clauss, D.M. Horowitz B.K. Hunter and J.K.M. Sanders (1992), "The biological and physical chemistry of polyhydroxyalkanoates as seen by NMR spectroscopy" *FEMS Microbiology Reviews*, **103**:269-278.

H. Brand and P. Puchner (1990), "Degradation of shampoo bottles in a lake" *in* E.A. Dawes (ed), "Novel Biodegradable Microbial Polymers", Kluwer Academic Publishers, Dordrecht.

H. Brandl, R. Bachofen, J. Mayer and E. Wintermantel (1995), "Degradation and applications of polyhydroxyalkanoates" *Canadian journal of microbiology*, **41**(Supp 1):143-153.

G. Braunegg, B. Sonnleitner and R.M. Lafferty (1978), "A rapid gas chromatographic method for the determination of poly-beta-hydroxybutyric acid in microbial biomass" *European Journal of Applied Microbiology and Biotechnology*, **6**:29-37.

V. Brendel and A.S. Perelson (1993), "Quantitative model of ColE1 plasmid copy number control." *Journal of Molecular Biology*, **229**(4):860-872.

T.D.K. Brown, M.C. Jones-Mortimer and H.L. Kornberg (1977), "The enzymic interconversion of acetate and acetyl-coenzyme A in *Escherichia coli*" *Journal of General Microbiology*, **102**:327-336.

D. Byrom (1987), "Polymer synthesis by microorganisms: technology and economics" *Trends in Biotechnology*, **5**:246-250.

D. Byrom (1990), "Industrial production of copolymer from *Alcaligenes eutrophus*" *in* E.A. Dawes (ed), "Novel Biodegradable Microbial Polymers", Kluwer Academic Publishers, Dordrecht.

D. Byrom (1992), "Production of poly-B-hydroxybutyrate:poly-β-hydroxyvalerate copolymers" *FEMS Microbiology Reviews*, **103**:247-250.

D. Byrom (1994), "Poly-hydroxyalkanoates" *in* D.P. Mobley, "Plastics from Microbes-Microbial Synthesis of Polymers & Polymer Precursors", 1st Edition, Hanser/Gardner Publications Ltd., Cincinnati, Ohio, Chapter 2.

A. Cayley, B.A. Lewis, H.J. Guttman and M.T. Record (1991), "Characterisation of the cytoplasm of *Escherichia coli* K-12 as a function of external osmolarity." *Journal of Molecular Biology*, **222**:281-300.

S. Chohnan, H. Izawa, H. Nishihara and Y. Takamura (1998), "Changes in size of intracellular pools of coenzyme A and its thioesters in *Escherichia coli* K-12 cells to various carbon sources and stresses." *Bioscience, biotechnology, and biochemistry*, **62**(6):1122-1128.

J.I. Choi and S.Y. Lee (1997), "Process analysis and economic evaluation for poly(3-hydroxybutyrate) production by fermentation." *Bioprocess Engineering*, **17**(6):335-342.

J.I. Choi and S.Y. Lee (1999), "High-level production of Poly(3-hydroxybutyrate-co-3-hydroxyvalerate) by fed-batch culture of recombinant *Escherichia coli*" *Applied & Environmental Microbiology*, **65**(10):4363-4368.

J.I. Choi, S.Y. Lee and K. Han (1998), "Cloning of the *Alcaligenes latus* polyhydroxyalkanoate biosynthesis genes and use of these genes for enhanced production of Poly(3-hydroxybutyrate) in *Escherichia coli*." *Applied & Environmental Microbiology*, **64**(12):4897-4903.

D.P. Clark and J.E. Cronan (1996), "Two-carbon compounds and fatty acids as carbon sources" *in* F.C. Neidhardt *et al.*, "*Escherichia coli* and *Salmonella Typhimurium*", 2nd Edition, ASM Press, Washington DC, Chapter 21.

B.E. Corkey (1988), "Analysis of Acyl-Coenzyme A esters in biological samples" *in* "Methods in Enzymology", **166:**55-70.

M.K. Cox (1993), "The effect of material parameters on the properties and biodegradation of 'BIOPOL'" *in* Y. Doi and K. Fukuda, "Biodegradable Plastics & Polymers", Elsevier, New York.

J.E. Cronan and D. LaPorte (1996), "Tricarboxylic acid cycle and glyoxylate bypass" *in* F.C. Neidhardt *et al.*, "*Escherichia coli* and *Salmonella Typhimurium*", 2nd Edition, ASM Press, Washington DC, Chapter 16.

J.M. Cutayar and D. Poillon (1989), "High cell density culture of *Escherichia coli* in a fed-batch system with dissolved oxygen as substrate feed indicator." *Biotechnology Letters*, **11**(3):155-160.

J.B. Davis (1964), "Cellular lipids of a Nocardia grown on propane and n-butane" *Applied Microbiology*, **12**:301-304.

E.A. Dawes (1990), "Novel microbial polymers: an introductory review" *in* E.A. Dawes (ed), "Novel Biodegradable Microbial Polymers", Kluwer Academic Publishers, Dordrecht.

E.A. Dawes and P.J. Senior (1973), "The role & regulation of energy reserve polymers in micro-organisms" *Advances in Microbial Physiology*, **10**:203.

G. de Koning (1995), "Physical properties of bacterial poly((R)-3-hydroxyalkanoates)" *Canadian journal of microbiology*, **41**(Supp 1):303-309.

G.J.M. de Koning, M. Kellerhals, C. van Meurs and B. Witholt (1997), "A process for the recovery of poly(hydroxyalkanoates) from Pseudomonads Part 2: Process development and economic evaluation" *Bioprocess Engineering*, **17**:15-21.

M.S. Debuysere and M.S. Olson (1983), "Analysis of acyl-coenzyme A derivatives by reverse-phase high-performance liquid chromatography" *Analytical Biochemistry*, **133**(2):373-379.

G.J.M. Dekoning, H.M.M. Vanbilsen, P.J. Lemstra, W. Hazenberg, B. Witholt, H. Preusting, J.G. Vandergalien, A. Schirmer and D. Jendrossek (1994), "A biodegradable rubber by crosslinking poly(hydroxyalkanoate) from *Pseudomonas* oleovorans" *POLYMER*, **35**(10):2090-2097.

J. Delgado and J.C. Liao (1997), "Inverse flux analysis for reduction of acetate excretion in *Escherichia coli*" *Biotechnology Progress*, **13**:361-367.

D.E. Dennis (1991), "Improved production of poly-beta-hydroxybutyrate in transformed *Escherichia coli*" *patent*, **WO91/18993**.

T S. Dhir, K.J. Morrow, R.R. Rhinehart and T. Wiesner (2000), "Dynamic optimization of hybridoma growth in a fed-batch bioreactor." *Biotechnology and Bioengineering*, **67**(2):197-205.

F. Diez-Gonzalez and J.B. Russell (1997), "The ability of *Escherichia coli* O157:H7 to decrease its intracellular pH and resist the toxicity of acetic acid." *Microbiology*, **143**:1175-1180.

C.C. DiRusso and W.D. Nunn (1985), "Cloning and characterisation of a gene (fadR) involved in regulation of fatty acid metabolism in *Escherichia coli*" *Journal of Bacteriology*, **161**:583-588.

Y. Doi (1990a), "Production of biodegradable copolyesters by *Alcaligenes eutrophus*" *in* E.A. Dawes (ed), "Novel Biodegradable Microbial Polymers", Kluwer Academic Publishers, Dordrecht.

Y. Doi (1990b), "Microbial Polyesters", VCH publishers, New York.

Y. Doi, A. Segawa and M. Kunioka (1989), "Biodegradable poly(3-hydroxybutyrate-co-4-hydroxybutyrate) produced from gamma-butyrolactone and butyric acid by *Alcaligenes eutrophus*" *Polymer Communications*, **30**:169-171.

Y. Doi, Y. Kumagai, N. Tanahashi and K. Mukai (1993), "Structural effects on biodegradation of microbial and synthetic poly(hydroxyalkanoates)" *in* Y. Doi and K. Fukuda, "Biodegradable Plastics & Polymers", Elsevier, New York.

P.M. Doran (1997), "Bioprocess Engineering Principles", 1st Edition, Harcourt Brace & Co, London, UK.

Editor (1998), *The Chemical Engineer*, **Issue 699**.

G. Eggink, P. de Waard and G.N.M. Huijberts (1992), "The role of fatty acid biosynthesis & degradation in the supply of substrates for poly(3-hydroxyalkanoate) formation in *Pseudomonas putida*" *FEMS Microbiology Reviews*, **103**:159-164.

B. Engberg and K. Nordstrom (1975), "Replication of R-factor R1 in *Escherichia coli* K-12 at different growth rates." *Journal of Bacteriology*, **123**(1):179-186.

US Environmental Protection Agency (1991), "Plastic Wastes- Management, Control, Recycling and Disposal", Noyes data corp, United States.

D.A. Fell (1992), "Metabolic control analysis: a survey of its theoretical and experimental development" *Biochemical Journal*, **286**:313-330.

R.C. Fuller (1990), "Bacterial Polyesters: past, present & future" *in* E.A. Dawes (ed), "Novel Biodegradable Microbial Polymers", Kluwer Academic Publishers, Dordrecht.

R.B. Gennis and V. Stewart (1996), "Respiration" *in* F.C. Neidhardt *et al.*, "*Escherichia coli* and *Salmonella Typhimurium*", 2nd Edition, ASM Press, Washington DC, Chapter 17.

K Gerdes (1988), "The parB (hok/sok) locus of plasmid R1: a general purpose plasmid stabilization system" *Bio/technology*, **6**:1402-1405.

A. Goel, M.M Domach, W. Hanley, J.W. Lee and M.M. Ataai (1995a), "Coordination of glycolysis and TCA cycle reaction networks" *Annals of the New York Academy of Sciences*, **782**:2.

A. Goel, J. Lee, M.M. Domach and M.M. Ataai (1995b), "Suppressed acid formation by cofeeding of glucose and citrate in Bacillus cultures: emergence of pyruvate kinase as a potential metabolic engineering site." *Biotechnology Progress*, **11**(4):380-385.

J. Guillet (1995), "Plastics and the environment" *in* G. Scott and D. Gilead (eds), "Degradable Polymers: Principles & Applications", 1st Edition, Chapman & Hall, Cambridge, Chapter 12.

R.P. Hafner, G.C. Brown and M.D. Brand (1990), "Analysis of the control of respiration rate, phosphorylation rate, proton leak rate and protonmotive force in isolated mitochondria using the 'top-down' approach of metabolic control theory" *European Journal of Biochemistry*, **188**:313-319.

S.K. Hahn, Y.K. Chang, B.S. Kim, K.M. Lee and H.N. Chang (1994), "Optimisation of microbial poly(3-hydroxybutyrate) recovery using dispersions of sodium hypochlorite solution and chloroform" *Biotechnology & Bioengineering*, **44**:256-261.

T.A. Hammelman, G.A. O'Toole, J.R. Trzebiatowski, A.W. Tsang, D. Rank and J.C. Escalante-Semerena (1996), "Identification of a new prp locus required for propionate catabolism in *Salmonella typhimurium* LT2" *FEMS Microbiology Letters*, **137**:233-239.

G. Harlan and C. Kmiec (1995), "Ethylene-carbon monoxide copolymers" *in* G. Scott and D. Gilead (eds), "Degradable Polymers: Principles & Applications", 1st Edition, Chapman & Hall, Cambridge, Chapter 8.

F.M. Harold and P.C. Maloney (1996), "Energy transduction by ion currents" *in* F.C. Neidhardt *et al.*, "*Escherichia coli* and *Salmonella Typhimurium*", 2nd Edition, ASM Press, Washington DC, Chapter 19.

S.T. Harrison (1990), "The extraction and purification of poly-B-hydroxybutyrate from *Alcaligenes eutrophus*.", PhD dissertation, University of Cambridge, U.K.

G.W. Haywood, A.J. Anderson, L. Chu and E.A. Dawes (1988), "The role of NADH & NADPH-linked acetoacetyl-CoA reductases in the poly-3-hydroxybutyrate synthesizing organism *Alcaligenes eutrophus*" *FEMS Microbiology Letters*, **52**:259-264.

G.W. Haywood, A.J. Anderson and E.A. Dawes (1989), "The importance of PHB-synthase substrate specificity in polyhydroxyalkanoate synthesis by *Alcaligenes eutrophus*" *FEMS Microbiology Letters*, **57**:1-6.

M. Hiramitsu and Y. Doi (1993), "Microbial Synthesis & Characterisation of Poly-3-hydroxybutyrate-co-3-hydroxypropionate" *POLYMER*, **34**(22):4782.

P.J. Hocking, M.R. Timmins, T.M. Scherer, R.C. Fuller, R.W. Lenz and R.H. Marchessault (1995), "Enzymatic degradation of Poly(B-hydroxybutyrate) as a function of tacticity" *Journal of macromolecular science. Pure and applied chemistry*, **A32**(4):889-894.

P.A. Holmes (1988), "Biologically produced (R)-3-hydroxyalkanoate polymers and copolymers" *in* D.C. Bassett, "Developments in Crystalline Polymers-2", Elsevier Applied Science, London.

D.M. Horowitz and J.K.M Sanders (1995), "Biomimetic, amorphous granules of polyhydroxyalkanoates: composition, mobility, and stabilisation in vitro by proteins" *Canadian journal of microbiology*, **41**(Supp 1):115-123.

A.R. Horswill and J.C. Escalante-Semerena (1997), "Propionate catabolism in *Salmonella typhimurium* LT2: two divergently transcribed units comprise the prp locus at 8.5 centisomes, prpR encodes a member of the sigma-54 family of activators, and the prpBCDE genes constitute an operon" *Journal of Bacteriology*, **179**(3):928-940.

S.T. Hsu and S.T. Yang (1991), "Propionic acid fermentation of lactose by *Propionibacterium acidipropionici*. Effects of pH." *Biotechnology & Bioengineering*, **38**(6):571-578.

F.P. Incropera and D.P. deWitt (1996), "Fundamentals of heat and mass transfer", 4th Edition, John Wiley & Sons, New York.

J.L. Ingraham, O. Maaloe and F.C. Neidhardt (1983), "Growth of the Bacterial Cell", Sinauer Associates, Sunderland, USA.

S. Jackowski (1996), "Biosynthesis of pantothenic acid and Coenzyme A" *in* F.C. Neidhardt *et al.*, "*Escherichia coli* and *Salmonella Typhimurium*", 2nd Edition, ASM Press, Washington DC, Chapter 44.

S. Jackowski and C.O. Rock (1986), "Consequences of reduced intracellular coenzyme A content in *Escherichia coli*" *Journal of Bacteriology*, **166**(3):866-871.

B. Janes, J. Hollar and D. Dennis (1990), "Molecular characterisation of the poly-beta-hydroxybutyrate biosynthetic pathway of *Alcaligenes eutrophus* H16" *in* E.A. Dawes (ed), "Novel Biodegradable Microbial Polymers", Kluwer Academic Publishers, Dordrecht.

D. Jendrossek, A. Schirmer and H.G. Schlegel (1996), "Biodegradation of Polyhydroxyalkanoic Acids [Review]" *Applied microbiology and biotechnology*, **46**(5-6):451-463.

H. Jorgensen, J. Nielsen and J. Villadsen (1995), "Metabolic flux distributions in Penicillium chrysogenum during fed-batch cultivations" *Biotechnology & Bioengineering*, **46**:117-131.

R.J. Kadner (1996), "Cytoplasmic membrane" *in* F.C. Neidhardt *et al.*, "*Escherichia coli* and *Salmonella Typhimurium*", 2nd Edition, ASM Press, Washington DC, Chapter 7.

J.P. Kalk and A.F. Langlykke (1986), "Cost Estimation for Biotechnology Projects" *in* A.L. Demain and N.A. Solomon, "Manual of Industrial Microbiology and Biotechnology", American Society for Microbiology, Washington DC, Chapter 26.

S. Kalousek and W. Lubitz (1995), "High-level poly(beta-hydroxybutyrate) production in recombinant *Escherichia coli* in sugar-free, complex medium" *Canadian journal of microbiology*, **41**(Supp 1):216-221.

S. Karlsson and A.C. Albertsson (1995), "Techniques and mechanisms of polymer degradation" *in* G. Scott and D. Gilead (eds), "Degradable Polymers: Principles & Applications", 1st Edition, Chapman & Hall, Cambridge,Chapter 3.

Keey (1978), "Introduction to Industrial Drying Operations", 1st Edition, Pergamon Press, Sydney.

D. Kessler and J. Knappe (1996), "Anaerobic dissimilation of pyruvate" *in* F.C. Neidhardt *et al.*, "*Escherichia coli* and *Salmonella Typhimurium*", 2nd Edition, ASM Press, Washington DC, Chapter 15.

J. Kidwell, H.E. Valentin and D. Dennis (1995), "Regulated expression of the *Alcaligenes eutrophus* pha biosynthesis genes in *Escherichia coli*" *Applied & Environmental Microbiology*, **61**(4):1391-1398.

B.S. Kim, S.Y. Lee and H.N. Chang (1992), "Production of polyhydroxybutyrate by fed-batch culture of recombinant *Escherichia coli*" *Biotechnology Letters*, **14**(9):811.

B.S. Kim, S.C. Lee, S.Y. Lee and H.N. Chang (1994), "Production of Poly(3-hydroxybutyric-co-3-hydroxyvaleric acid) by fed-batch culture of *Alcaligenes eutrophus* with substrate control using on-line glucose analyser" *Enzyme and microbial technology*, **16**(7):556.

A.R. Kleinig, C.J. Mansell, Q.D. Nguyen, A. Badalyan and A.P.J. Middelberg (1995), "Influence of broth dilution on the disruption of *Escherichia coli*." *Biotechnology Techniques*, **9**:759-762.

Y.F. Ko, W.E. Bentley and W.A. Weigand (1993), "An integrated metabolic modeling approach to describe the energy efficiency of *Escherichia coli* fermentations under oxygen-limited conditions: cellular energetics, carbon flux, and acetate production." *Biotechnology & Bioengineering*, **42**:843-853.

R.G. Kroll and I.R. Booth (1983), "The relationship between intracellular pH, the pH gradient, and potassium transport in *Escherichia coli*" *Biochemical Journal*, **216**:709-716.

T.A. Leaf and F. Srienc (1998), "Metabolic modeling of polyhydroxybutyrate biosynthesis" *Biotechnology & Bioengineering*, **57**(5):557-570.

S.Y. Lee (1994), "Suppression of filamentation in recombinant *Escherichia coli* by amplified FtsZ activity" *Biotechnology Letters*, **16**(12):1247.

S.Y. Lee (1996a), "Poly(3-hydroxybutyrate) extrusion by cells of recombinant *Escherichia coli*" *Journal of Microbiology and Biotechnology*, **6**(2):147-149.

S.Y. Lee (1996b), "High cell-density culture of *Escherichia coli*" *Trends in Biotechnology*, **14**(3):98.

S.Y. Lee (1996c), "Bacterial polyhydroxyalkanoates" *Biotechnology & Bioengineering*, **49**:1-14.

S.Y. Lee (1996d), "Plastic bacteria? Progress and prospects for polyhydroxyalkanoate production in bacteria" *Trends in Biotechnology*, **14**:431-438.

S.Y. Lee and H.N. Chang (1994), "Effect of complex nitogen source on the synthesis and accumulation of poly(3-hydroxy-butyric acid) by recombinant *Escherichia coli* in flask and fed-batch cultures." *Journal of Environmental Polymer Degradation*, **2**:169-176.

S.Y. Lee and H.N. Chang (1995), "Production of poly(3-hydroxybutyric acid) by recombinant *Escherichia coli* strains: genetic and fermentation studies" *Canadian journal of microbiology*, **41**(1):207-215.

S.Y. Lee, K.S. Yim, H.N. Chang and Y.K Chang (1994a), "Construction of plasmids, estimation of plasmid stability, and use of stable plasmids for the production of poly(3-hydroxybutyric acid) by recombinant *Escherichia coli*" *Journal of Biotechnology*, **32**:203-211.

J. Lee, A. Goel, M.M. Ataai and M.M. Domach (1994b), "Flux adaptions of citrate synthase-deficient *Escherichia coli*" *Annals of the New York Academy of Sciences*, **745**:35.

S.Y. Lee, H.N. Chang and Y.K. Chang (1994c), "Production of Poly(B-Hydroxybutyric Acid) by Recombinant *Escherichia coli*" *Annals of the New York Academy of Sciences*, **721**:43-53.

S.Y. Lee, K.M. Lee, H.N. Chang and A. Steinbuchel (1994d), "Comparison of Recombinant *Escherichia coli* strains for synthesis and accumulation of poly-3-hydroxybutyric acid & morphological changes" *Biotechnology & Bioengineering*, **44**:1337-1347.

I.Y. Lee, H.N. Chang and Y.H. Park (1995a), "A simple method for recovery of microbial poly-B-hydroxybutyrate by alkaline solution treatment" *Journal of Microbiology and Biotechnology*, **5**(4):238-240.

S.Y. Lee, Y.K. Lee and H.N. Chang (1995b), "Stimulatory Effects of Amino Acids & Oleic Acid on Poly(3-hydroxybutyric acid) Synthesis by Recombinant *Escherichia coli*" *Journal of Fermentation and Bioengineering*, **79**(2):177-180.

A.L. Lehninger, D.L. Nelson and M.M. Cox (1993), "Principles of Biochemistry", 2nd Edition, Worth Publishers, New York.

V.P. Lewis and S.T. Yang (1992), "A novel extractive fermentation process for propionic acid production from whey lactose" *Biotechnology Progress*, **8**:104-110.

Y. Ling (1999), "Extraction and recovery process of poly-B-hydroxybutyrate from recombinant *Escherichia coli*", PhD dissertation, University of Adelaide, Adelaide.

Y. Ling, D.R.G. Williams, C.J. Thomas and A.P.J. Middelberg (1997), "Recovery of poly-3-hydroxybutyrate from recombinant *E. coli* by homogenization and centrifugation" *Biotechnology Techniques*, **11**(6):409-412.

F. Liu, W. Li, D. Ridgway, T. Gu and Z. Shen (1998), "Production of poly-beta-hydroxybutyrate on molasses by recombinant *Escherichia coli*." *Biotechnology Letters*, **20**(4):345-348.

J.L. Lu and J.C. Liao (1997), "Metabolic engineering and control analysis for production of aromatics - role of transaldolase" *Biotechnology & Bioengineering*, **53**(2):132-138.

A.S. Lynch and E.C.C. Lin (1996), "Responses to molecular oxygen" *in* F.C. Neidhardt *et al.*, "*Escherichia coli* and *Salmonella Typhimurium*", 2nd Edition, ASM Press, Washington DC, Chapter 95.

R.M. Macrae and J.F. Wilkinson (1958), "Poly-B- hydroxybutyrate metabolism in washed suspensions of Bacillus cereus and Bacillus megaterium" *Journal of General Microbiology*, **19**:210-222.

W.J. Maddever (1992), "Starch-based degradable plastics" *in* S.H. Hamid, M.B. Amin and A.G. Maadhah (eds), "Handbook of Polymer Degradation", 1st Edition, Marcel Dekker, New York.

S.R. Maloy and W.D. Nunn (1981), "Role of gene fadR in *Escherichia coli* acetate metabolism" *Journal of Bacteriology*, **148**:83-90.

D.A. Mansfield, A.J. Anderson and L.A. Naylor (1995), "Regulation of PHB metabolism in *Alcaligenes eutrophus*" *Canadian journal of microbiology*, **41**(Supp 1):44-49.

K. Mauch, S. Arnold and M. Reuss (1997), "Dynamic sensitivity for metabolic systems" *Chemical Engineering Science*, **52**(15):2589-2598.

J.M. Mayer, G.R. Elion, C.M. Buchanan, B.K. Sullivan, S.D. Pratt and D.L. Kaplan (1995), "Biodegradable blends of cellulose acetate and starch: production and properties" *in* A.C. Albertsson and S.J. Huang, "Degradable Polymers, Recycling, and Plastics Waste Management", 1st Edition, Marcel Dekker, New York.

F. Mayer, M.H. Madkour, U. Pieperfurst, R. Wieczorek, M.L. Gesell and A. Steinbuchel (1996), "Electron microscopic observations on the macromolecular organization of the boundary layer of bacterial pha inclusion bodies" *Journal of General and Applied Microbiology*, **42**(6):445-455.

C.M. Melbourne (1995), "Production of Poly(hydroxyalkanoate) in recombinant *Escherichia coli*", Honours Thesis, Faculty of Science, University of Adelaide, Adelaide, Australia.

J. Mergaert, C. Anderson, A. Wouters, J. Swings and K. Kersters (1992), "Biodegradation of polyhydroxyalkanoates" *FEMS Microbiology Reviews*, **103**:317-322.

J. Mergaert, A. Wouters, C. Anderson and J. Swings (1995), "In situ biodegradation of poly(3-hydroxybutyrate) and poly(3-hydroxybutyrate-co-3-hydroxyvalerate) in natural waters" *Canadian journal of microbiology*, **41**(Supp 1):154-159.

A.P.J Middelberg (1996), "The influence of protein refolding strategy on cost for competing reactions" *The Biochemical Engineering Journal*, **61**:41-52.

A.P.J. Middelberg, S.Y. Lee, J. Martin, D.R.G. Williams and H.N. Chang (1995), "Size analysis of poly(3-hydroxybutyric acid) granules produced in recombinant *Escherichia coli*." *Biotechnology Letters*, **17**(2):205-210.

F.C. Neidhardt and H.E. Umbarger (1996), "Chemical composition of *Escherichia coli*" *in* F.C. Neidhardt *et al.*, "*Escherichia coli* and *Salmonella Typhimurium*", 2nd Edition, ASM Press, Washington DC, Chapter 3.

O.M. Neijssel, M.J.T. de Mattos and D.W. Tempest (1996), "Growth yield and energy distribution." *in* F.C. Neidhardt *et al.*, "*Escherichia coli* and *Salmonella Typhimurium*", 2nd Edition, ASM Press, Washington DC,Chapter 107.

J. Nielsen and J. Villadsen (1994), "Bioreaction Engineering Principles", 1st Edition, Plenum Press, New York and London.

W.D. Nunn (1986), "Two-carbon compounds and fatty acids as carbon sources" *in* F.C. Neidhardt, J.L Ingraham, K.B. Low, B. Magasanik, M. Schaechter and H.E. Umbarger (eds), "*Escherichia coli* and *Salmonella typhimurium*: cellular and molecular biology", American Society for Microbiology, Washington D.C.

V. Oeding and H.G. Schlegel (1973), "B-Ketothiolase from Hydrogenomonas eutropha H16 and its significance in the regulation of poly-B-hydroxybutyrate metabolism" *Biochemical Journal*, **134**:239-248.

W.J. Page (1995), "Bacterial polyhydroxyalkanoates, natural biodegradable plastics with a great future." *Canadian journal of microbiology*, **41**(Supp 1):1-3.

J.S. Park, H.C. Park, T.L. Huh and Y.H. Lee (1995), "Production of poly-beta-hydroxybutyrate by *Alcaligenes eutrophus* transformants harbouring cloned phbCAB genes" *Biotechnology Letters*, **17**:735-740.

T. Penfound and J.W. Foster (1996), "Biosynthesis and recycling of NAD" *in* F.C. Neidhardt *et al.*, "*Escherichia coli* and *Salmonella Typhimurium*", 2nd Edition, ASM Press, Washington DC,Chapter 48.

O.P. Peoples and A.J. Sinskey (1989a), "Poly-beta-hydroxybutyrate biosynthesis in *Alcaligenes eutrophus* H16: Identification and characterization of the PHB polymerase gene (phbC)" *The Journal of biological chemistry*, **264**:15298-15303.

O.P. Peoples and A.J. Sinskey (1989b), "Poly-beta-hydroxybutyrate biosynthesis in *Alcaligenes eutrophus* H16: Characterization of the genes encoding beta-ketothiolase and acetoacetyl-CoA reductase." *The Journal of biological chemistry*, **264**:15293-15297.

R.H. Perry, D.W. Green and J.O. Maloney (eds) (1984), "Perry's chemical engineers' handbook", 6th Edition, McGraw-Hill, New York, p25-64.

M.G. Peter (1995), "Applications and environmental aspects of chitin and chitosan" *in* A.C. Albertsson and S.J. Huang, "Degradable Polymers, Recycling, and Plastics Waste Management", 1st Edition, Marcel Dekker, New York.

M.S. Peters and K.D. Timmerhaus (1991), "Plant Design and Economics for Chemical Engineers", 4th Edition, McGraw-Hill, New York.

D. Petrides, C.L Cooney, L.B. Evans, R.P Field and M. Snoswell (1989), "Bioprocess simulation: an integrated approach to process development" *Computers in Chemical Engineering*, **13**(4/5):553-561.

D. Petrides, E. Sapidou and J. Calandranis (1995), "Computer-aided process analysis and economic evaluation for biosynthetic human insulin production - a case study" *Biotechnology & Bioengineering*, **48**:529-541.

B.R. Pinsent, L. Pearson and F. Roughton (1956), "The kinetics of combination of carbon dioxide with hydroxide ions." *Transactions of the Faraday Society*, **52**:1512-1520.

Y Poirier, C Newrath and C Somerville (1995), "Production of polyhydroxyalkanoates, a family of biodegradable plastics and elastomers, in Bacteria and Plants." *Bio/technology*, **13**(Feb):142-150.

P.A. Quant (1993), "Experimental application of top-down control analysis to metabolic systems" *Trends in biochemical sciences*, **18**:26-30.

H.G. Rhie and D. Dennis (1995a), "The function of ackA and pta genes is necessary for Poly(3-hydroxybutyrate-co-3-hydroxyvalerate) synthesis in recombinant pha+ *Escherichia coli*" *Canadian journal of microbiology*, **41**(1):200.

H.G. Rhie and D. Dennis (1995b), "Role of fadR and atoC(Con) mutations in Poly(3-hydroxybutyrate-co-3-hydroxyvalerate) synthesis in recombinant pha+ *escherichia coli*" *Applied & Environmental Microbiology*, **61**(7):2487.

P.N. Royce (1992), "Effect of changes in the pH and carbon dioxide evolution rate on the measured respiratory quotient of fermentations." *Biotechnology & Bioengineering*, **40**(10):1129-1138.

P.N.C. Royce and N.F. Thornhill (1991), "Estimation of dissolved carbon dioxide concentrations in aerobic fermentations" *AICHE Journal*, **37**:1680-1686.

D. Rusendi and J.D. Sheppard (1995), "Hydrolysis of potato processing waste for the production of poly-beta-hydroxybutyrate" *Bioresource Technology*, **54**(2):191-196.

U. Sauer, V. Hatzimanikatis, J.E. Bailey, M. Hochuli, T. Szyperski and K. Wuthrich (1997), "Metabolic fluxes in riboflavin-producing Bacillus subtilis." *Nature Biotechnology*, **15**(5):448-452.

P. Schubert, A. Steinbuchel and H.G. Schlegel (1988), "Cloning of the *Alcaligenes eutrophus* genes for synthesis of poly-B-hydroxybutyric acid (PHB) and synthesis of PHB in *Escherichia coli*" *Journal of Bacteriology*, **170**:5837-5847.

G. Scott and D. Gilead (1995), "Degradable polymers in waste and litter control" *in* G. Scott and D. Gilead (eds), "Degradable Polymers: Principles & Applications", 1st Edition, Chapman & Hall, Cambridge, Chapter 13.

H. Shi, J. Nikawa and K. Shimizu (1999), "Effect of modifying metabolic network on poly-3-hydroxybutyrate biosynthesis in recombinant *Escherichia coli*" *Journal of Bioscience and Bioengineering*, **87**(5):666-677.

E. Shimamura, M. Scandola and Y. Doi (1994a), "Microbial synthesis and characterisation of Poly(3-hydroxybutyrate-co-3-hydroxypropionate)" *Macromolecules*, **27**(16):4429.

E. Shimamura, K. Kasuya, G. Kobayashi, T. Shiotani, Y. Shima and Y. Doi (1994b), "Physical properties and biodegradability of microbial poly (3-hydroxybutyrate-co-3-hydroxyhexanoate)" *Macromolecules*, **27**(3):878-880.

S.J. Sim, K.D. Snell, S.A. Hogan, J. Stubbe, C. Rha and A.J. Sinskey (1997), "PHA synthase activity controls the molecular weight and polydispersity of polyhydroxybutyrate in vivo" *Nature Biotechnology*, **15**(Jan):63.

S.C. Slater, W.H. Voige and D.E. Dennis (1988), "Cloning and expression in *Escherichia coli* of the *Alcaligenes eutrophus* H16 poly-B-hydroxybutyrate biosynthetic pathway" *Journal of Bacteriology*, **170**:4431-4436.

S. Slater, T. Gallaher and D. Dennis (1992), "Production of Poly(3-hydroxybutyrate-co-3-hydroxyvalerate) in a recombinant *Escherichia coli* strain" *Applied & Environmental Microbiology*, **58**(4):1089-1094.

S Slater, K.L. Houmiel, M. Tran, T.A. Mitsky, N.B. Taylor, S.R. Padgette and K.J. Gruys (1998), "Multiple beta-ketothiolases mediate poly(beta-hydroxyalkanoate) copolymer synthesis in *Ralstonia eutropha*." *Journal of Bacteriology*, **180**(8):1979-1987.

J.L. Slonczewski and J.W. Foster (1996), "pH-regulated genes and survival at extreme pH" *in* F.C. Neidhardt *et al.*, "*Escherichia coli* and *Salmonella Typhimurium*", 2nd Edition, ASM Press, Washington DC, Chapter 96.

J.J.G. Soest and J.F.G. Vliegenthart (1997), "Crystallinity in starch plastics: consequences for material properties" *Trends in Biotechnology*, **15**:208-213.

A. Steinbuchel (1991), "Polyhydroxyalkanoic acids" *in* D Byrom, "Biomaterials. Novel materials from biological sources", Macmillan Press, United Kingdom.

A. Steinbuchel and H.G. Schlegel (1991), "Physiology and molecular genetics of poly(beta-hydroxyalkanoic acid) synthesis in *Alcaligenes eutrophus*" *Molecular Microbiology*, **5**:535-542.

A. Steinbuchel and H.E. Valentin (1995), "Diversity of bacterial polyhydroxyalkanoates" *FEMS Microbiology Letters*, **128**:219-228.

A. Steinbuchel, K. Aerts, W. Babel, C. Follner, M. Liebergesell, M.H. Madkour, F. Mayer, U. Pieper-Furst, A. Pries, H.E. Valentin and R. Wieczorek (1995), "Considerations on the structure and biochemistry of bacterial polyhydroxyalkanoic acid inclusions" *Canadian journal of microbiology*, **41**(Supp 1):94-105.

G. Stephanopolous and T.W. Simpson (1997), "Flux amplification in complex metabolic networks" *Chemical Engineering Science*, **52**(15):2607-2627.

G Stephanopolous and J.J. Vallino (1991), "Network rigidity and metabolic engineering in metabolite overproduction" *Science*, **252**:1675-1681.

E.S. Stuart, R.W. Lenz and R.C. Fuller (1995), "The ordered macromolecular surface of polyester inclusion bodies in *Pseudomonas* oleovorans" *Canadian journal of microbiology*, **41**(Supp 1):84-93.

P.S. Tsai, V. Hatzimanikatis and J.E. Bailey (1996), "Effect of Vitreoscilla hemoglobin dosage on microaerobic *Escherichia coli* carbon and energy metabolism" *Biotechnology & Bioengineering*, **49**:139-150.

J.J. Vallino and G. Stephanopolous (1993), "Metabolic flux distributions in Corynebacterium glutamicum during gorwth and lysine overproduction" *Biotechnology & Bioengineering*, **41**:633-646.

R.T.J.M. van der Heijden, B. Romein, J.J. Heijnen, C. Hellinga and K.Ch.A.M Luyben (1994a), "Linear constraint relations in biochemical reaction systems: I. Classification of the calculability and balanceability of conversion rates." *Biotechnology & Bioengineering*, **43**:3-10.

R.T.J.M. van der Heijden, B. Romein, J.J. Heijnen, C. Hellinga and K.Ch.A.M Luyben (1994b), "Linear constraint relations in biochemical reaction systems: II. Diagnosis and estimation of gross errors." *Biotechnology & Bioengineering*, **43**:11-20.

F.R. van der Leij and B. Witholt (1995), "Strategies for the sustainable production of new biodegradable polyesters in plants: a review" *Canadian journal of microbiology*, **41**(Supp 1):222-238.

W.M. van Gulik and J.J. Heijnen (1995), "A metabolic network stoichiometry analysis of microbial growth and product formation." *Biotechnology & Bioengineering*, **48**(6):681-698.

R.J. van Wegen, Y. Ling and A.P.J. Middelberg (1998), "Industrial production of polyhydroxyalkanoates using *Escherichia coli*: an economic analysis" *Transactions of the Institute of Chemical Engineers*, **3**(3):417-426.

Various (1995), "Economic Indicators" *Chemical Engineering*.

A. Varma and B.O. Palsson (1993a), "Metabolic capabilities of *Escherichia coli*: I. Synthesis of biosynthetic precursors and cofactors" *Journal of Theoretical Biology*, **165**:477-502.

A. Varma and B.O. Palsson (1993b), "Metabolic capabilities of *Escherichia coli*: II. Optimal growth patterns" *Journal of Theoretical Biology*, **165**:503-522.

A. Varma, B.W. Boesch and B.O. Palsson (1993a), "Stoichiometric interpretation of *Escherichia coli* glucose catabolism under various oxygenation rates." *Applied & Environmental Microbiology*, **59**(8):2465-2473.

A. Varma, B.W. Boesch and B.O. Palsson (1993b), "Biochemical Production Capabilities of *Escherichia coli*" *Biotechnology & Bioengineering*, **42**:59-73.

M. Vert, G. Schwarch and J. Coudane (1995), "Present and future of PLA polymers" *in* A.C. Albertsson and S.J. Huang, "Degradable Polymers, Recycling, and Plastics Waste Management", 1st Edition, Marcel Dekker, New York.

L.L. Wallen and W.K. Rohwedder (1974), "Poly-B-hydroxyalkanoate from activated sludge" *Environmental Science & Technology*, **8**:576-579.

F. Wang and S.Y. Lee (1997), "Production of poly(3-hydroxybutyrate) by fed-batch culture of filamentation-suppressed recombinant *Escherichia coli*" *Applied & Environmental Microbiology*, **63**:4765-4769.

J.W.T. Wimpenny and A. Firth (1972), "Levels of nictoinamide adenine dinucleotide and reduced nicotinamide adenine dinucleotide in facultative bacteria and the effect of oxygen." *Journal of Bacteriology*, **111**(1):24-32.

H.H. Wong (1996), "Modelling studies of the interaction between homogenisation, centrifugation, and inclusion body dissolution", PhD Dissertation, The University of Adelaide, Australia.

H.H. Wong and S.Y. Lee (1998), "Poly-(3-hydroxybutyrate) production from whey by high-density cultivation of recombinant *Escherichia coli*." *Applied microbiology and biotechnology*, **50**(1):30-33.

B. Xu, M. Jahic, G. Blomsten and S. O. Enfors (1999), "Glucose overflow metabolism and mixed-acid fermentation in aerobic large-scale fed-batch processes with *Escherichia coli*" *Applied microbiology and biotechnology*, **51**:564-571.

M.F. Yagmurlu, F. Korkusuz, I. Gursel, P. Korkusuz, U. Ors and V. Hasirci (1999), "Sulbactam-cefoperazone polyhydroxybutyrate-co- hydroxyvalerate (PHBV) local antibiotic delivery system: In vivo effectiveness and biocompatibility in the treatment of implant-related experimental osteomyelitis." *Journal of Biomedical Materials Research*, **46**(4):494-503.

T. Yamane (1993), "Yield of Poly-D(-)-3-hydroxybutyrate from various carbon sources: a theoretical study" *Biotechnology & Bioengineering*, **41**(1):165-170.

S.T. Yang, Y. Huang and G. Hong (1995), "Novel recycle batch immobilized cell bioreactor for propionate production from whey lactose" *Biotechnology & Bioengineering*, **45**(5):379-386.

L. Yee and H.W. Blanch (1992), "Recombinant protein expression in high cell density fed-batch cultures of *Escherichia coli*" *Bio/technology*, **10**:1550-1556.

K.S. Yim, S.Y. Lee and H.N. Chang (1995), "Effect of acetic acid on poly-(3-hydroxybutyrate-co-3-hydroxyvalerate) synthesis in recombinant *Escherichia coli*" *Korean Journal of Chemical Engineering*, **12**(2):264-268.

K.S. Yim, S.Y. Lee and H.N. Chang (1996), "Synthesis of Poly-(3-hydroxybutyrate-co-3-hydroxyvalerate) by recombinant *Escherichia coli*" *Biotechnology & Bioengineering*, **49**:495-503.

J.G. Zadow (1992), "Review and Report on Whey Utilisation", Dairy Research and Development Corporation.

R.R. Zall (1992), "Sources and composition of whey and permeate" *in* J.G. Zadow, "Whey & Lactose Processing", 1st Edition, Elsevier Applied Science, London & New York, Chapter 1.

S. Zhang (2000), PhD dissertation, University of Adelaide, Adelaide, Australia.

C. Zupke and G. Stephanopolous (1995), "Intracellular flux analysis in Hybridomas using mass balances and in vitro 13C NMR" *Biotechnology & Bioengineering*, **45**:292-303.

Appendix H Publications List

Conference Papers:

R.J. van Wegen, S.Y. Lee, A.P.J. Middelberg (1997) "Production of PHB, a biodegradable plastic, from dairy whey using recombinant *Escherichia coli*" Chemeca Conference Paper

R.J. van Wegen, S.Y. Lee, C.J. Thomas, D.R.G. Williams, A.P.J. Middelberg (1997) "Using recombinant *Escherichia coli* and dairy whey to produce Poly(3-hydroxybutyrate)" Asia-Pacific Biochemical Engineering Conference Paper.

Journal Papers:

R.J. van Wegen, Y. Ling, A.P.J. Middelberg (1998) "Industrial production of polyhydroxyalkanoates using Escherichia coli: an economic analysis" *Trans IChemE* Vol 76 p417-426.

H.H. Wong, R.J. van Wegen, J.I. Choi, S.Y. Lee, A.P.J. Middelberg (1999) "Metabolic analysis of Poly(3-hydroxybutyrate) production by recombinant *Escherichia coli*" *J. Microbiol. Biotechnol.* Vol 9(5):593-603. (I wrote this paper after analysing raw data which H.H. Wong had collected.)

R.J. van Wegen, S.Y. Lee, A.P.J. Middelberg (2001) "Metabolic and kinetic analysis of poly(3-hydroxybutyrate) production by recombinant *Escherichia coli*" *Biotech. Bioeng.* Accepted but not yet published.